

Synthesis and Characterisation of Polypyridyl Metal Complexes for New Fuels



**This thesis is presented for the degree of
Doctor of Philosophy**

By

Avishek Paul, MSc.

Under the Supervision of

Prof. Johannes G. Vos & Dr. Mary T. Pryce

School of Chemical Sciences

Dublin City University

2012

Authors' declaration

I hereby certify that this material, which I now submit for assessment on the programme of study leading to the award of PhD is entirely my own work, that I have exercised reasonable care to ensure that the work is original, and does not to the best of my knowledge breach any law of copyright, and has not been taken from the work of others save and to the extent that such work has been cited and acknowledged within the text of my work.

Signed: _____ (AVISHEK PAUL)

Student ID No.: 58120424

Date: _____

*To my wife Nive
and
the memory of Mr. Asish Das*

Acknowledgement

I am extremely grateful and thankful to my supervisors Prof. Johannes G. Vos (Han) and Dr. Mary T. Pryce (Mary) for their continuous expert guidance, suggestions, support and motivation throughout my research work. It has been a great pleasure and privilege for me to have invaluable research experience during this period. I would also like to thank Dr. Damian Connolly for helping me all the way for ion chromatography. I have learnt many things from him. I can say from bottom of heart that Han and Mary are the best supervisors in the world, I believe that everybody will love to work with them, they are just superb, perfect personality and very friendly. Mary, I do not know how to express my (our) thanks to you for everything. I am really and personally thankful to Han for his great offer. I can say that Han is the game changer of my life; I convey my heartiest regards and respect and honour for his greatness. I believe that everybody can make a significant contribution to the society if they are trusted and given an opportunity to dream; Han is the person who gave me that right opportunity and changed my life. Thank you very much Han, I will never forget you, I will be there for you whenever you need.

I express my heartiest thanks to all my group members (Nikki, Emma, Jen, Dan, Hamid, Jane, Laura, Martin, Rob, Evan, Gurmeet, Suraj, Declan, Nive) and many more friends for their love, help and friendly co-operation. Huge thanks to DCU chemical science technical team, Veronica, John, Damien, Brandan, Ambrose, Vinnie, Mary and Cathrine for their great service. I really want to acknowledge and appreciate all of your cooperation and help.

My special thanks go to all my family members and especially to my wife Nive (one of our group members) for their unconditional support, encouragement to pursue my research interest. I feel deeply indebted to them for whatever I achieved so far. My wife Nive is my true inspiration. She has supported me from all aspects, and she suffered a lot for me. I truly appreciate her sacrifices and the unconditional love she provides me. I salute you Mr. Asish Das. You are my role model. I truly respect your views and rules of life. It's most unfortunate that you left us very early. But, I still feel you're around and seeing us from the heaven. I will always miss you.

Table of Contents

Title Page	i
Declaration	ii
Dedication	iii
Acknowledgements	iv
Table of Contents	v
Abstract	x
Abbreviations	xi
1. Chapter 1: Introduction	1
1.1. Energy issue of earth and global warming	2
1.2. Possible solutions of energy requirement and global warming	3
1.3. Ruthenium in solar hydrogen evolution	6
1.4. Iridium in solar hydrogen evolution	16
1.5. Rhenium in solar hydrogen evolution	24
1.6. Metal complexes in photocatalytic CO ₂ reduction	25
1.7. Aim of this thesis	32
1.8. References	34
2. Chapter 2: Synthesis and characterisation of ruthenium(II) based mononuclear precursors	
2.1. Introduction	41
2.2. Synthetic procedures for organic ligands	44
2.2.1. Synthetic procedure for the esterification of 2,2'-bipyridine	44
2.2.2. Synthetic procedure for 3,5-bis(2-pyridyl)-4-hydro-1,2,4-triazole(Hbpt)	45
2.2.3. Synthetic procedures for 5-bromo-2,2'-bipyridine(5Brbpy) and 2,2':5',2''-terpyridine (bpp)	45
2.2.4. Synthetic procedure for 2,2':5',3'':6'',2'''-quaterpyridine (bisbpy)	51
2.3. Synthetic procedures for metal complexes	52
2.3.1. Synthetic procedures for [Ru(dceb) ₂ Cl ₂]	52
2.3.2. Stability of ester groups in [Ru(dceb) ₂ Cl ₂]	57
2.3.3. Synthesis of [Ru(bpy) ₂ (L)] ²⁺ and [Ru(dceb) ₂ (L)] ²⁺ type compounds	63

2.4. Characterisation of compounds using NMR spectroscopy	66
2.4.1. Bridging ligands	66
5-bromo-2,2'-bipyridine(5Brbpy)	66
2,2':5',2''-terpyridine (bpp)	69
2,2':5',3'':6'',2'''-quaterpyridine (bisbpy)	72
2.4.2. Metal complexes	75
¹ H NMR of N719	75
NMR interpretation for[Ru(bpy) ₂ (bisbpy)](PF ₆) ₂ using	
[Ru(d ₈ -bpy) ₂ (bisbpy)](PF ₆) ₂	76
NMR interpretation for [Ru(bpy) ₂ (bpp)](PF ₆) ₂ using	
[Ru(d ₈ -bpy) ₂ (bpp)](PF ₆) ₂	78
NMR interpretation for [Ru(bpy) ₂ (2,5-dpp)](PF ₆) ₂ using	
[Ru(d ₈ -bpy) ₂ (2,5-dpp)](PF ₆) ₂	81
[Ru(dceb) ₂ (bisbpy)](PF ₆) ₂	84
[Ru(dceb) ₂ (bpp)](PF ₆) ₂	85
[Ru(dceb) ₂ (Hbpt)](PF ₆) ₂	87
[Ru(dceb) ₂ (2,5-dpp)](PF ₆) ₂	89
2.5. Absorption and emission spectra of mononuclear complexes	91
2.6. Conclusion	97
2.7. Experimental	98
2.7.1. Materials and instrumental techniques	98
2.7.2. Organic ligands	99
3,5-bis(2-pyridyl)-4-hydro-1,2,4-triazole(Hbpt)	99
5-bromo-2,2'-bipyridine (5Brbpy)	100
2,2':5',3'':6'',2'''-quaterpyridine (bisbpy)	100
2,2':5',2''-terpyridine (bpp)	100
2,5-di(pyridin-2-yl)pyrazine (2,5-dpp)	101
2.7.3. Metal complexes	101
[Ru(dceb) ₂ Cl ₂]	101
[Ru(dceb) ₂ (NCS) ₂].2H ₂ O	102
[Ru(dceb) ₂ (Hbpt)](PF ₆) ₂	102
[Ru(bpy) ₂ (bisbpy)](PF ₆) ₂ .2H ₂ O	103
[Ru(d ₈ -bpy) ₂ (bisbpy)](PF ₆) ₂ .3H ₂ O	103
[Ru(dceb) ₂ (bisbpy)](PF ₆) ₂ .2H ₂ O	104
[Ru(bpy) ₂ (bpp)](PF ₆) ₂	104
[Ru(d ₈ -bpy) ₂ (bpp)](PF ₆) ₂ .H ₂ O	105
[Ru(dceb) ₂ (bpp)](PF ₆) ₂ .H ₂ O	105
[Ru(bpy) ₂ (2,5-dpp)](PF ₆) ₂	105
[Ru(d ₈ -bpy) ₂ (2,5-dpp)](PF ₆) ₂ .H ₂ O	106
[Ru(dceb) ₂ (2,5-dpp)](PF ₆) ₂ .2H ₂ O	106
2.8. References	107

3. Chapter 3: Synthesis and characterisation of ruthenium(II) /rhenium(I) complexes

3.1. Introduction	111
3.2. Synthetic procedures for organic ligands	114
3.2.1. 4,4'-diphosphonato-2,2'-bipyridine (dpb)	114
3.3. Synthetic procedures for Ru(II)/Re(I) metal complexes	115
3.4. Infrared spectroscopy	117
3.5. Characterisation of compounds using NMR spectroscopy	123
3.5.1. Organic ligands	123
4,4'-Bis(hydroxymethyl)-2,2'-bipyridine	123
4,4'-Bis(bromomethyl)-2,2'-bipyridine	124
4,4'-Bis(diethylmethylphosphonato)-2,2'-bipyridine (dpb)	125
3.5.2. NMR spectra of $[(X_2bpy)Re(CO)_3Cl]$ type complexes; X= COOEt and $CH_2PO(OCH_2CH_3)_2$	126
3.5.3. Ru-Re heterodinuclear metal complexes	128
3.6. Absorption and emission spectroscopy of Ru(II)/Re(I) complexes	142
3.6.1. Absorption and emission spectra of mononuclear complexes	142
3.6.2. Absorption and emission spectra of Ru(II)-Re(I) heterodinuclear complexes	144
3.7. Immobilisation of carboxy ester containing Ru(II)/Re(I) complexes on nickel oxide surface	154
3.8. Conclusion	156
3.9. Experimental	158
3.9.1. Material and instrumental	158
3.9.2. Organic ligands	159
4,4'-Bis(hydroxymethyl)-2,2'-bipyridine	159
4,4'-Bis(bromomethyl)-2,2'-bipyridine	159
4,4'-Bis(diethylmethylphosphonato)-2,2'-bipyridine (dpb)	159
3.9.3. Metal complexes	160
$[Re(dceb)(CO)_3Cl]$	160
$[Re(dpb)(CO)_3Cl]$	160
$[Ru(dceb)_2(\mu-bisbpy)Re(CO)_3Cl](PF_6)_2$	160
$[Ru(bpy)_2(\mu-bisbpy)Re(CO)_3Cl](PF_6)_2$	161
$[Ru(dceb)_2(\mu-Hbpt)Re(CO)_3Cl](PF_6)_2$	161
$[Ru(bpy)_2(\mu-2,5-dpp)Re(CO)_3Cl](PF_6)_2$	162
$[Ru(d_8-bpy)_2(\mu-2,5-dpp)Re(CO)_3Cl](PF_6)_2$	162
$[Ru(dceb)_2(\mu-2,5-dpp)Re(CO)_3Cl](PF_6)_2$	162
3.10. References	163

4. Chapter 4: Synthesis and characterisation of iridium(III) mononuclear complexes

4.1. Introduction	169
4.2. Synthetic procedures of organic ligands	172
4.2.1. Synthesis of ethyl 4-(2-pyridyl)benzoate	173
4.3. Synthetic procedures for metal complexes	174
4.3.1. Synthesis of $[\text{Ir}(\text{ppy-COOEt})_2(\mu\text{-Cl})]_2$	174
4.3.2. Synthesis of $[\text{Ir}(\text{ppy-COOEt})_2(\text{L})](\text{PF}_6)$ type complexes	175
4.4. ^1H NMR spectroscopy of organic ligands	177
4.4.1. 4-(2-pyridyl)benzoic acid (ppy-COOH)	177
4.4.2. Ethyl 4-(2-pyridyl)benzoate (ppy-COOEt)	178
4.5. NMR spectroscopy of metal complexes	179
4.5.1. $[\text{Ir}(\text{ppy-COOEt})_2(\text{dceb})](\text{PF}_6)$	181
4.5.2. $[\text{Ir}(\text{ppy-COOEt})_2(\text{bpy})](\text{PF}_6)$	184
4.5.3. $[\text{Ir}(\text{ppy-COOEt})_2(\text{dpb})](\text{PF}_6)$	187
4.5.4. $[\text{Ir}(\text{py-COOEt})_2(5\text{Brbpy})](\text{PF}_6)$	191
4.5.5. $[\text{Ir}(\text{py-COOEt})_2(\text{bpp})](\text{PF}_6)$	194
4.5.6. $[\text{Ir}(\text{py-COOEt})_2(\text{bisbpy})](\text{PF}_6)$	198
4.6. Photophysical properties of monomeric iridium complexes	201
4.6.1. Absorption spectra	201
4.6.2. Emission spectra and life time data	204
4.7. Conclusion	207
4.8. Experimental	208
4.8.1. Materials and instrumental	208
4.8.2. Organic ligands	209
4-(2-pyridyl)benzoic acid (ppy-COOH)	209
Ethyl 4-(2-pyridyl)benzoate (ppy-COOEt)	210
4.8.3. Metal complexes	210
$[\text{Ir}(\text{ppy-COOEt})(\mu\text{-Cl})]_2 \cdot 2\text{H}_2\text{O}$	210
$[\text{Ir}(\text{ppy-COOEt})_2(\text{bpp})](\text{PF}_6)$	211
$[\text{Ir}(\text{ppy-COOEt})_2(\text{bisbpy})](\text{PF}_6)$	211
$[\text{Ir}(\text{ppy-COOEt})_2(\text{bpy})](\text{PF}_6)$	212
$[\text{Ir}(\text{ppy-COOEt})_2(5\text{Br bpy})](\text{PF}_6) \cdot \text{H}_2\text{O}$	212
$[\text{Ir}(\text{ppy-COOEt})_2(\text{dpb})](\text{PF}_6)$	212
$[\text{Ir}(\text{ppy-COOEt})_2(\text{dceb})](\text{PF}_6)$	213
4.9. References	213

5.	Chapter 5: The effect of water during the quantitation of formate in photocatalytic studies on CO₂ reduction in dimethylformamide	
5.1.	Introduction	221
5.2.	Experimental	222
5.2.1.	Materials and sample preparation	222
5.2.2.	Instrumentation	222
5.3.	Ion chromatography and method validation	223
5.3.1.	Precision	224
5.3.2.	Sensitivity	225
5.3.3.	Linearity	225
5.3.4.	Selectivity	227
5.4.	Result and discussion	228
5.4.1.	Ion chromatography	228
5.4.2.	NMR Spectroscopy	236
5.4.3.	FTIR spectroscopy	239
5.5.	Possible mechanism for formation of formate	240
5.6.	Conclusion	241
5.7.	References	242
6.	Chapter 6: Future work	244
7.	Appendix A	
8.	Appendix B	

Abstract

Chapter 1 serves as a general introduction to the thesis, and describes how a combination of sunlight and photocatalysts may help elevate our energy crisis and climate change. This chapter describes how sunlight can be used to split water, producing hydrogen, as the ultimate green fuel. Recent research on photocatalysis involving different metal complexes as photo-catalysts is included. Particularly, an overview and a detailed discussion of recent developments on ruthenium, iridium and rhenium metal complex mediated photocatalytic systems are included.

Chapter 2 introduces derivatisation at the 4 and 4' positions of the 2,2'-bipyridine ligand and different synthetic procedures for ruthenium(II) dichloride complex containing bis-4,4'-diethoxycarbonyl-2,2'-bipyridine. This chapter describes the stability of these ester groups under different conditions by performing a series of experiments. This chapter also introduces some novel bridging ligands, their synthesis and optimisation of the reaction conditions employed in their synthesis. Different synthetic paths have been investigated to prepare these bridging ligands and their corresponding mononuclear ruthenium complexes. This chapter also shows how deuteration is an important tool when interpreting complex NMR spectra for polypyridyl complexes.

Chapter 3 covers the synthesis and characterisation of Ru(II)-Re(I) heterodinuclear complexes which contain carboxy functionalised peripheral ligands and different bridging ligands. Various reaction conditions for the synthesis of the carboxy-functionalised ruthenium-rhenium heterodinuclear complexes are discussed. This chapter tries to understand the different isomerism pattern for Ru(II)-Re(I) heterodinuclear complexes with the help of NMR and IR spectroscopy. The absorption and emission spectra of these complexes were recorded and described. This chapter also introduces a preliminary surface immobilisation study for Ru(II)/Re(I) heterodinuclear and mononuclear Re(I) complexes containing carboxy and phosphonate ester groups.

Chapter 4 introduces a series of monomeric cyclometallated iridium(III) complexes. These monomeric Ir(III) complexes contain carboxy ester functionalised cyclometallated phenylpyridine ligands and different bpy based ancillary ligands. Synthetic modifications are discussed in detail. These iridium complexes were characterised using ^1H , 2D COSY NMR spectroscopy and CHN analysis. Photophysical data for these Ir(III) complexes are also reported.

Chapter 5 describes the use of ion-chromatography to quantify the reduction products of CO_2 reduction following photocatalysis. A series of time and water concentration dependent experiments were carried out to investigate the formation of formate from 5:1 dimethylformamide (DMF)/triethylamine (TEA) and 5:1 dimethylformamide (DMF)/triethanolamine (TEOA) solutions. The experimental results suggest that aqueous solutions of DMF formed a significant amount of formate in the presence of organic bases like triethylamine and triethanolamine. Production of formate was further confirmed by IR and ^{13}C NMR spectroscopy.

Chapter 6 involves the future work for this thesis.

Abbreviations

bpy	2,2'-bipyridine
dcb	4,4'-dicarboxylate-2,2'-bipyridine
dceb	4,4'-diethylcarboxylate-2,2'-bipyridine
BL	Bridging ligand
bisbpy	2,2':5',3":6",2'''-quaterpyridine
bpp	2,2':5',2"-terpyridine
5Brbpy	5-bromo-2,2'-bipyridine
6Brbpy	6'-bromo-2,3'-bipyridine
COSY	Correlation Spectroscopy
CT	Charge transfer
DCM	Dichloromethane
DMA	Dimethylamine
dmb	4,4'-dimethyl-2,2-bipyridine
DMF	N,N-dimethylformamide
DMSO	Dimethylsulphoxide
2,5-dpp	2,5-dipyridyl-pyridine
DSSC	Dye sensitised solar cell
eV	Electron volt
<i>fac</i> -	Facial
HAT	benzo[1,2-b:3,4-b':5,6-b']tripyrazine
hbpt	3,5-bis(2-pyridyl)-4-hydro-1,2,4-triazole
HOMO	Highest occupied molecular orbital
ILET	Inter ligand energy transfer
ISC	Inter-system crossing
¹ LC	Ligand centred singlet excited state
³ LC	Ligand centred triplet excited state
LUMO	Lowest unoccupied molecular orbital
<i>mer</i> -	Meridional
MLCT	Metal-ligand charge transfer
MV	Methyl viologen
NMR	Nuclear magnetic resonance

OD	Optical density
OEA	Oxygen evolving complex
OER	One electron reduction
OLED	Organic light emitting device
Ph	Phenyl
Py	Pyridine
PV	Photovoltaic
RT	Room temperature
TEOA	Triethanolamine
THF	Tetrahydrofuran
TLC	Thin layer chromatography
TON	Turn over number
tpphz	Tetrapyridylphenazine
UV	Ultra violet
λ_{max}	Maximum wavelength
ε	Extinction co-efficient

Chapter 1

Introduction

Chapter 1 serves as a general introduction to the thesis, and describes how a combination of sunlight and photocatalysts may help elevate our energy crisis and climate change. This chapter describes how sunlight can be used to split water, producing hydrogen, as the ultimate green fuel. Recent research on photocatalysis involving different metal complexes as photocatalysts is included. Particularly, an overview and a detailed discussion of recent developments on ruthenium, iridium and rhenium metal complexes which mediate photocatalytic systems are included.

1.1. Energy issues of earth and global warming

Global energy demands are projected to increase up to 50% by 2035.¹⁻³ Continuous use of carbon-based coal and fossil fuel contributes to global warming, which will get worse, and will cause even more extreme droughts, storms, other climatic disruptions and will adversely affect our health. Outcomes from the UN Climate Change Conference 2009 held in Copenhagen, included a reduction in CO₂, phasing out of carbon-based fossil fuels and innovative energy policies for renewable resources that are greener and mostly carbon free. The prices of coal and natural gas have also increased by 20% from 2008 to 2010 and it is expected to increase further in the near future. The survey (see **Figure 1.1**) suggests, increasing the use of renewable sources from 4% to 37%. Currently 46% of our energy requirement depends upon natural gas sources which are not only unreliable but also one of the main causes of the green-house gas effect.^{4,5}

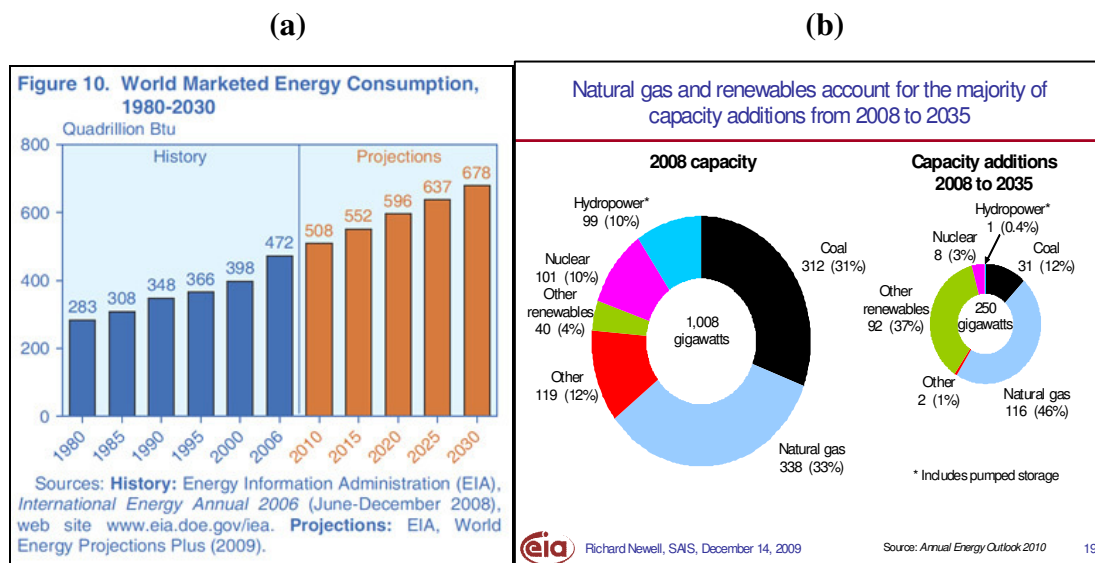


Figure 1.1: (a) Estimated calculation of world's energy consumption up to 2030. (b) The proposed strategy to fulfil the energy requirement from the renewable resources.¹

1.2. Possible solutions of energy requirement and global warming

Renewable green energy production has become one of the most profound challenges of the 21st century to fulfil the looming energy requirements.⁶⁻¹² We can choose new paths that use the practical and long-lasting solutions of efficiency and renewable energy sources like wind, solar and sustainable biomass to reduce global warming, pollution and reduce the pain of rising energy costs.^{3,13} Among the entire renewable energy sources solar energy is the greenest, is zero cost and is also the most powerful. The sun generates an enormous amount of energy approximately 1.1×10^{20} kWh every second (1 kWh is the amount of energy needed to power a 100 watt light bulb for ten hours).¹⁴ The earth's outer atmosphere intercepts about 12-billionth of the energy generated by the sun, or about 1500 quadrillion (1.5×10^{18}) kWh per year. The solar energy distribution map is provided in **Figure 1.2**.

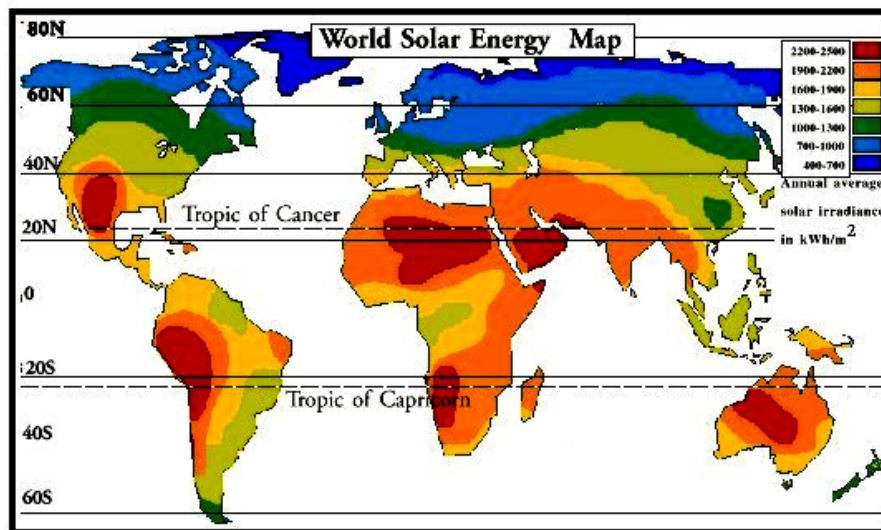


Figure 1.2: Solar energy distribution map on the surface of earth.

Because of reflection, scattering, and absorption by gases and aerosols in the atmosphere, only 47% of this, or approximately 700 quadrillion (7×10^{17}) kWh reaches the surface of the earth. The United States consume roughly 25 trillion (2.5×10^{13}) kWh per year. This translates to more than 260 kWh per person per day.⁷

Based on solar energy, several approaches are possible with the photovoltaic solar cell producing electricity which can be further used for commercial water electrolysis (**Figure 1.3**).^{9,15,16} One approach is to store this solar energy as a fuel by splitting water into hydrogen and oxygen because of the hydrogen's attraction as an instant fuel. The theoretical efficiency for the Si-based solar cell is 33% and the best reported lab-based solar cell efficiency is 24% but commercially available Si-solar cell are in the 12-16% range. Water oxidation requires a greater driving force than the theoretical voltage -1.23 V at normal room temperature and a reasonable rate. Water electrolysis energy efficiencies are 60% for such type of Si-based PV cell. So 10% of efficiency is desirable from a Si-solar cell for solar hydrogen generation. The cost of such a system will be more expensive than that produced chemically from coal or natural gas. Durability of this type of system is also an issue.

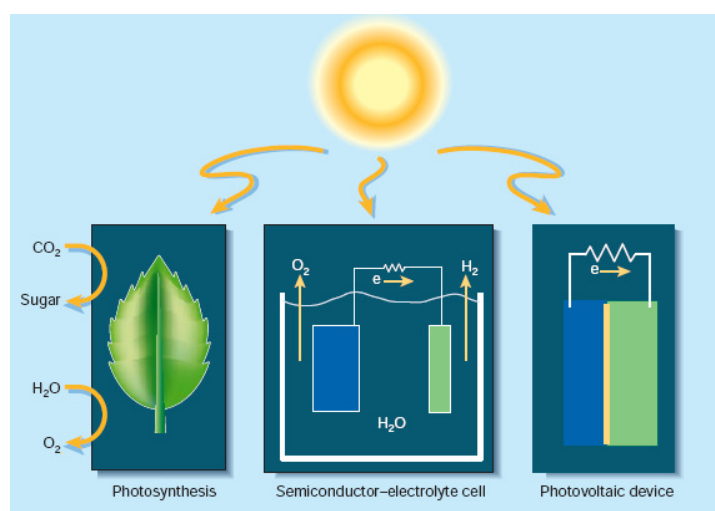


Figure 1.3: Energy-conversion strategies for creating fuel or electricity from sunlight.¹⁷

A number of strategies are being developed for light driven splitting of water and these are all based on artificial photosynthesis.^{11,18-22} In natural photosynthesis, light is absorbed by an antenna array (photo system-II), which transfers the energy to a chlorophyll molecule in a neighbouring protein complex, known as the reaction centre.²³ The excitation of the chlorophyll is quenched by transferring electrons to acceptor molecules elsewhere in the photosystem. Electron deficient molecules (oxidants) are thus created and can accept electrons from neighbours. The electron

donating centre is known as the oxygen evolving complex (OEA) which obtains an electron from a water molecule and generates oxygen. The synthetic chemist needs to mimic this photosynthetic system and design a model system which will be equally efficient towards splitting water into hydrogen and oxygen.²⁴ A schematic diagram of artificial water splitting system is shown below (**Figure 1.4**).

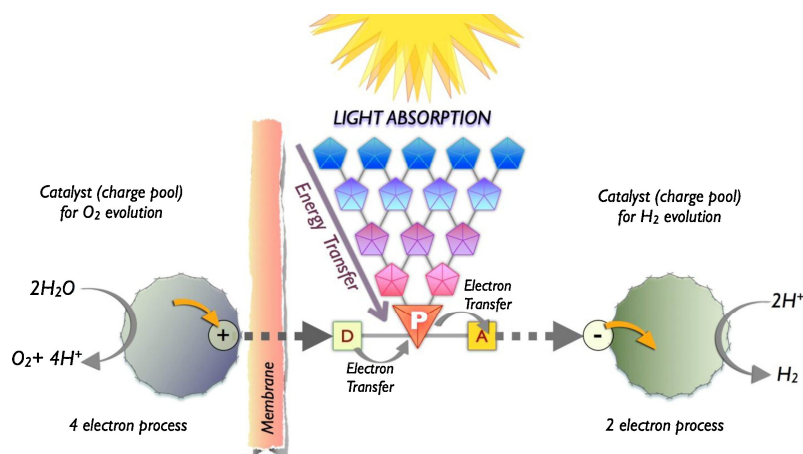


Figure 1.4: Schematic representation of an artificial photosynthetic system.²⁴

Much current research is focused on the harvesting of solar energy for chemical fuels. Solar energy can be harvested for two more important energy issues, production of hydrogen from water and reduction of CO₂ to chemical fuel.

1. **Production of hydrogen from water:** Hydrogen is considered as the next generation environmentally friendly clean fuel. Production of H₂ from water using solar energy requires two successive electrons transfer processes to two protons. Metal complexes as molecular photocatalysts are potentially useful in H₂ production from water, due to their ability to absorb visible light and to enhance the rate of the electron transfer.^{9,25-28}
2. **Reduction of carbon dioxide:** Photochemical carbon dioxide reduction is not a straight forward process and poses a number of difficulties. One of the difficulties with CO₂ reduction is its low solubility. Another factor is the stability of CO₂. Transition-metal complexes are used as catalysts since they can absorb in the visible region, poses long-lived excited states, and can promote the activation of

small molecules.^{29,30} Examples of the reduction products of CO₂ include carbon monoxide, formic acid and methanol. Many of the reduction products may be useful starting materials for the chemical industry.

1.3. Ruthenium in solar hydrogen evolution

Ruthenium polypyridyl complexes have been extensively studied for their long lived excited states which were further investigated as light harvesters in photocatalysis.^{20,21,31-34} Photocatalytic hydrogen production from water using an intermolecular catalytic system is based on a light harvesting unit (mainly ruthenium polypyridyl complexes) and an external catalyst. In 1977, Lehn *et al.* reported the first example of such an intermolecular photocatalytic system which involved [Ru(bpy)₃]Cl₂ as the photosensitiser, triethylamine (TEA) as a sacrificial electron donor, a Rh bipyridine complex as the proton and electron storage system and colloidal platinum (Adams' catalyst, PtO₂) as an external catalyst.³⁵ They reported that the catalytic system was remarkably pH dependent (highest efficiency was observed at pH 7.5) and suggested that the TEA/TEA⁺H⁺ buffer acted as both a proton and electron source. The turn-over number (TON) for Ru was several hundred, whereas the TON for the Rh complex was only 20. In 1978, Kalyanasundaram *et al.* also used a ruthenium-based photosensitiser [Ru(bpy)₃]²⁺ for photocatalytic hydrogen evolution where methylviologen (MV²⁺) was used as an electron acceptor and triethanolamine as a sacrificial electron donor.³⁶ Under these catalytic conditions, MV²⁺ forms a stable radical cation MV^{•+} which is reoxidised by water by successive hydrogen evolution in the presence of Adam's catalyst, PtO₂. DeLaive *et al.*³⁷ used [RuL₃]²⁺ (where L = 4,4'-dicarboxy-2,2'-bipyridine isopropyl ester) as a hydrophobic photosensitiser. Adam's catalyst PtO₂ was also used as an active catalyst and triethylamine as an electron donor. The electron acceptor MV²⁺ was not used in this case. The hydrogen evolution mechanism was described as water reduction by photochemically generated [RuL₃]²⁺ in the presence of PtO₂ to give [RuL₃]²⁺ and hydrogen. It was also suggested that the catalytically formed triethylamine radical cation can act as an active reductant to produce hydrogen from water. The above mixture produced hydrogen in 25% aqueous acetonitrile solution, however no hydrogen was produced when the catalysis was carried out in non-aqueous acetonitrile and without PtO₂. Based on that observation, it was suggested that the

source of protons was water. Kiwi *et al.* in 1979 studied the suitability of finely dispersed Pt particles as mediators in photocatalytic hydrogen evolution.³⁸ They investigated the reaction (**Equation 1**) in an aqueous medium containing $[\text{Ru}(\text{bpy})_3]^{2+}$ as the photosensitiser and EDTA as an electron donor.



(Where MV^+ stands for reduced methylviologen)

Investigations on the above reaction revealed that a reduced form of methylviologen required 15 μs time to reoxidise in the presence of 10^{-3} M Pt catalyst. The catalytic hydrogen evolution from water is shown in **Figure 1.5**.

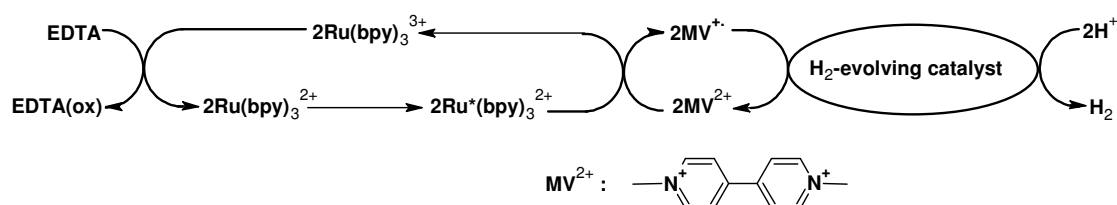


Figure 1.5: A photochemical model system for H_2 evolution, which consists of $[\text{Ru}(\text{bpy})_3]^{2+}$ as a photosensitiser, MV^{2+} (methylviologen) as an electron relay, and either colloidal platinum or a platinum(II) catalyst as an H_2 evolving catalyst. The overall reaction can be understood as a visible light-induced reduction of water into molecular hydrogen using EDTA as a sacrificial electron donor.^{36,38}

Brown *et al.* used $[\text{Ru}(\text{bpy})_3]^{2+}$ as a photosensitiser in an intermolecular hydrogen evolution catalytic system where a Co(II) macrocycle complex were used as the active catalyst and ascorbic acid as the sacrificial electron donor.³⁹ Flash photolysis of a catalytic mixture of $[\text{Ru}(\text{bpy})_3]^{2+}$, a Co(II) macrocycle and ascorbic acid in acetonitrile, confirmed the reduction of Co(II) to Co(I). The pH of the catalytic mixture was maintained at 4 with NaOH. The catalytic hydrogen evolution mechanism suggests the successive oxidative addition of two hydronium ions to the Co(I) metal centre and formation of hydrogen. The catalytic process is shown in **Figure 1.6**.

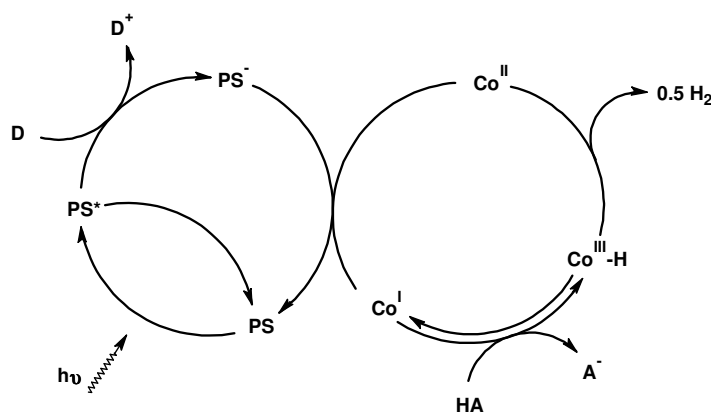


Figure 1.6: Hydrogen evolution by a inter-molecular catalytic system involving $[Ru(bpy)_3]^{2+}$ as photosensitiser (PS), electron donor ascorbic acid (D) and a Co(II) catalyst.³⁹

In 1980, Amouyal *et al.* reported an inter-molecular catalytic system for hydrogen generation which also consisted of $[Ru(bpy)_3]^{2+}$ as the photosensitiser.⁴⁰ They tested RuO_2 as the catalyst in the above mentioned catalytic process instead of colloidal Pt catalyst. They showed catalytic activity at pH 8 with RuO_2 as catalyst whereas no hydrogen was formed above pH 7 with colloidal Pt catalyst. They observed a maximum value of hydrogen production at pH 5, and nearly same value at pH 6 upon visible light radiation (λ 400 – 600 nm) for 2 h. They also reported that no hydrogen production was observed if any of the catalytic components is absent from the system. Fisher and Cole-Hamilton studied a catalytic hydrogen production using $[Ru(bpy)_3]^{2+}$ as a photosensitiser, ascorbic acid as an electron donor and $[PdH(PEt_3)_3]$ as the catalyst. They investigated the formation of the Pd(I) radical during the catalytic process, which facilitated the formation of hydrogen from water. The catalytic process was terminated because of substantial oxidation of the Pd(I) radical by dihydroascorbic acid which was generated from ascorbic acid due to sacrificial electron donation to the ruthenium complex.

Wang *et al.* reported a hydrogen production photocatalytic system with a bio-inspired catalyst $[2Fe_2S]$ (see **Figure 1.7**), $[Ru(bpy)_3]^{2+}$ as a photosensitiser and without any electron transferring relay.⁴¹ Ascorbic acid was used as a sacrificial electron donor. It has been suggested that $[Ru(bpy)_3]^{2+}$ can act as an electron transfer relay in this system. They have also suggested that using an intermolecular catalysis

approach, the reverse electron transfer can be avoided by the formation of a $\text{Fe}^{\text{I}}\text{Fe}^{\text{II}}\text{-H}$ species, as an intermediate for H-H bond formation.

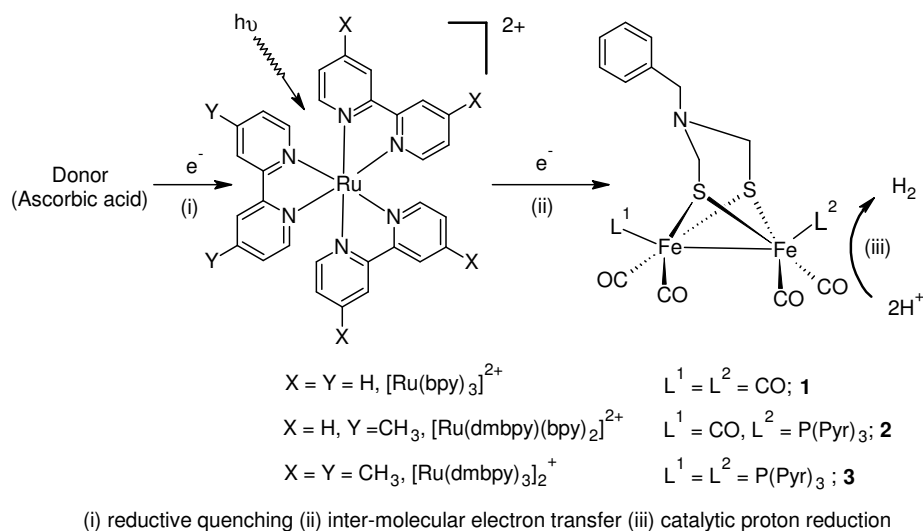


Figure 1.7: Photocatalytic hydrogen production using ruthenium metal complex as photosensitiser and $[2\text{Fe}2\text{S}]$ model bio molecule as catalyst.⁴¹

Photocatalytic intermolecular hydrogen production systems have been widely studied, however there are many interfacial parameters that are difficult to influence. An *intramolecular* electron transfer approach was introduced by Rau *et al.* in 2006 using a conjugated bridging ligand.⁴² In *intramolecular* hydrogen production, neither intermolecular collisions or a self assembled system for electron transfer from the photosensitiser to the catalytic centre are required. As the light harvesting unit and catalytic metal centre are both coordinated to a bridging ligand, the electrons are transferred through the bridge.⁴³ The schematic diagram for *intramolecular* hydrogen production is provided in **Figure 1.8**.

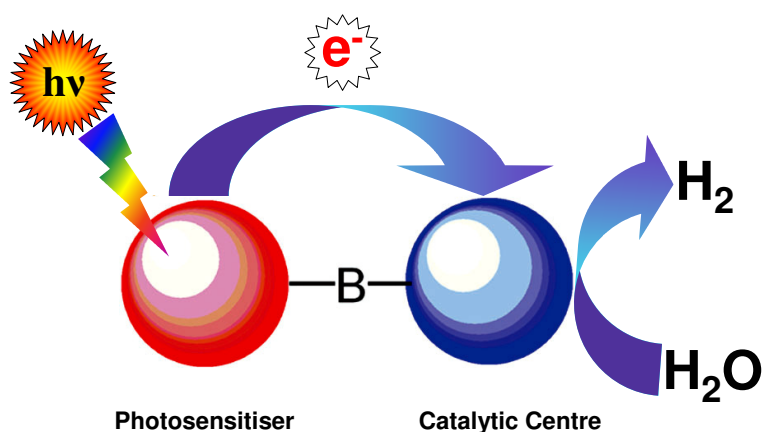


Figure 1.8: Light driven intramolecular homogeneous catalysis for hydrogen generation from water. The red ball represents ruthenium (Ru)-based polypyridyl complexes as photosensitiser, **B** represents an organic bridging ligand and the blue ball represents a catalytic centre ($M = Pd$ or Pt).^{42,43}

Based on the above working principle, many heterodinuclear photocatalysts and their efficiency towards hydrogen production in a solution were reported.⁴³ These heterodinuclear photocatalysts contain three parts. Firstly, the photosensitiser, which is mainly based on ruthenium polypyridyl complexes. Secondly, the bridging ligand which is based on conjugated polypyridyl ligands and helps transferring the photo excited electrons to the catalytic metal centre. The third part is the catalytic metal centre which reduces water to hydrogen. By altering the ligand architecture and catalytic metal centres, a wide range of heterodinuclear photocatalysts can be synthesised creating a library of photocatalysts. Several research groups have used ruthenium polypyridyl complexes as photosensitisers because of their well studied long lived excited state and interesting electrochemical properties. These properties can be altered by derivatisation of the peripheral bipyridine rings with different functional groups and bridging ligands so that the electron transfer process can be controlled more efficiently. A number of heterodinuclear photocatalysts and the hydrogen production processes are discussed below.

Rau and co-workers reported a Ru-Pd heterodimetallic *intramolecular* catalytic system which produced visible light (at $\lambda = 470$ nm) induced hydrogen.⁴² The molecular structure of the Ru-Pd heterodimetallic complex is shown in **Figure**

1.9. The peripheral bpy ligands bound to the ruthenium moiety were functionalised with tert-butyl groups. Tetrapyridophenazine (tpphz) was used as the bridging ligand for electron transfer. The Ru-Pd bimetallic complex produces hydrogen with TON = 56 in acetonitrile solution using visible light ($\lambda = 470$ nm).

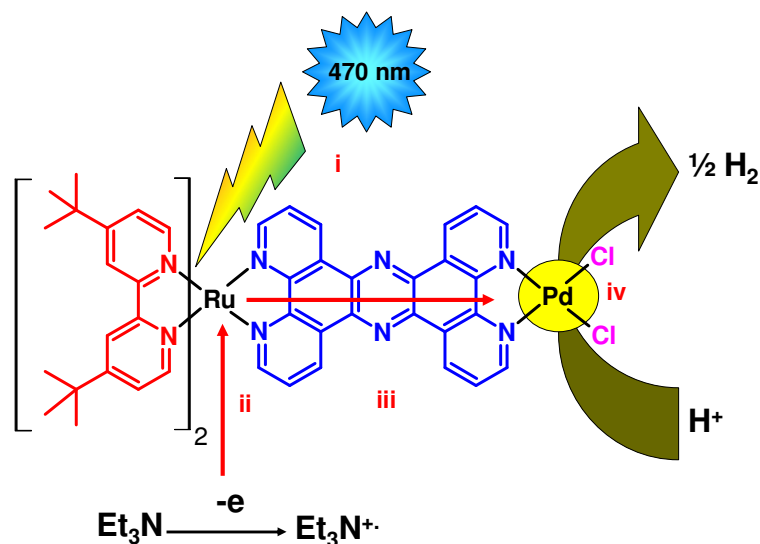


Figure 1.9: Ru-Pd heterodimetallic photocatalysts for photo driven hydrogen production.⁴² i) photo excitation of ruthenium metal centre ii) electron donation by Et_3N to ruthenium centre iii) electron transfer from ruthenium to palladium metal centre iv) reduction of H^+ to $\frac{1}{2} \text{H}_2$.

In the above case, triethylamine was used as a sacrificial electron donor. Step (i) involves photo excitation of the ruthenium centre. The second step (ii) involves electron donation from Et_3N to ruthenium. The third step (iii) involves transferring of the excited state electrons to the catalytic palladium site through a conjugated organic bridging ligand (tpphz) leading to the production of hydrogen from water in the fourth step (iv). In a further study, they reported the effect of water content on the catalytic process and an increase in the TON was observed with an increase in water concentration. The maximum amount of hydrogen was produced with 10% of water present in the catalytic solvent system and a turn-over number of 161.⁴⁴

A number of heterodinuclear photocatalysts with various organic bridging ligands and different catalytic metal centres are shown in **Figure 1.10**.

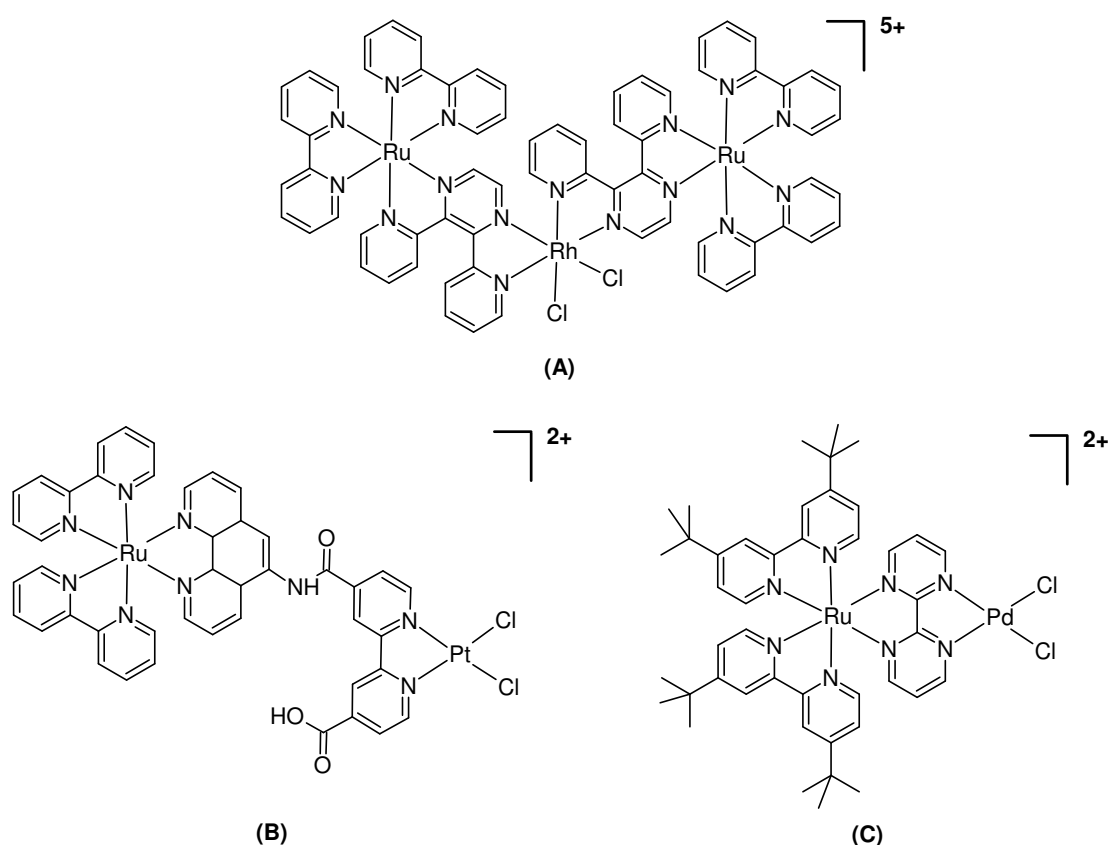


Figure 1.10: Example of a number of heterodimetallic photocatalysts for hydrogen evolution.

Rau *et al.* also published a Ru-Pd type heterodinuclear complex (**C**) in which 2,2'-bipyrimidine was used as a bridging ligand and ruthenium as the photosensitiser but no hydrogen evolution was reported in a non-aqueous acetonitrile/triethylamine catalytic medium.⁴² No further photocatalytic study has been reported on the complex “**C**” yet so far. Brewer and co-workers reported a Ru-Rh-Ru type heterotrimetallic photocatalyst (**A**) for solar driven hydrogen production, in which they have used 2,3-di(2-pyridyl)pyrazine (2,3-dpp) as the bridging ligand and two ruthenium photosensitiser units (**Figure 1.10**). They studied photocatalysis in acetonitrile/water solution and used dimethylamine (DMA) as an electron donor. The maximum turn-over reported was 38.^{45,46} The research carried out by Sakai involved a ruthenium-platinum heterodimetallic system (**B**) in which ethylenediaminetetraacetic acid (EDTA) was used as a sacrificial electron donor and the measured turn-over number (TON) for hydrogen production was 2.4.²⁸ The results obtained for H₂ production

using photo-catalysts **A-C** (see **Figure 1.10**) indicate that the bridging ligand has an inherent influence in photocatalytic hydrogen production from water, considering the π^* level of different bridging ligands and suitable overlapping with the metal's $d\pi$ -orbital.

In 2008, Fihri *et al.* reported a Ru-Co heterodimetallic photocatalyst (see **Figure 1.11**) in which cobalt was used as the catalytic centre. They studied the catalytic process using different solvents and with different sacrificial agents. The maximum TON of 165 was obtained over 15 hours of irradiation with a wavelength greater than 350 nm.⁴⁷ These Ru-Co catalysts were found equally efficient as the Ru-Pd catalysts (TON = 161). Using cobalt as a catalytic centre, the efficiency of the photocatalysts was enhanced and the cost of the overall catalytic system was reduced compared to Ru-Pd or Ru-Pt heterodimetallic photocatalysts.

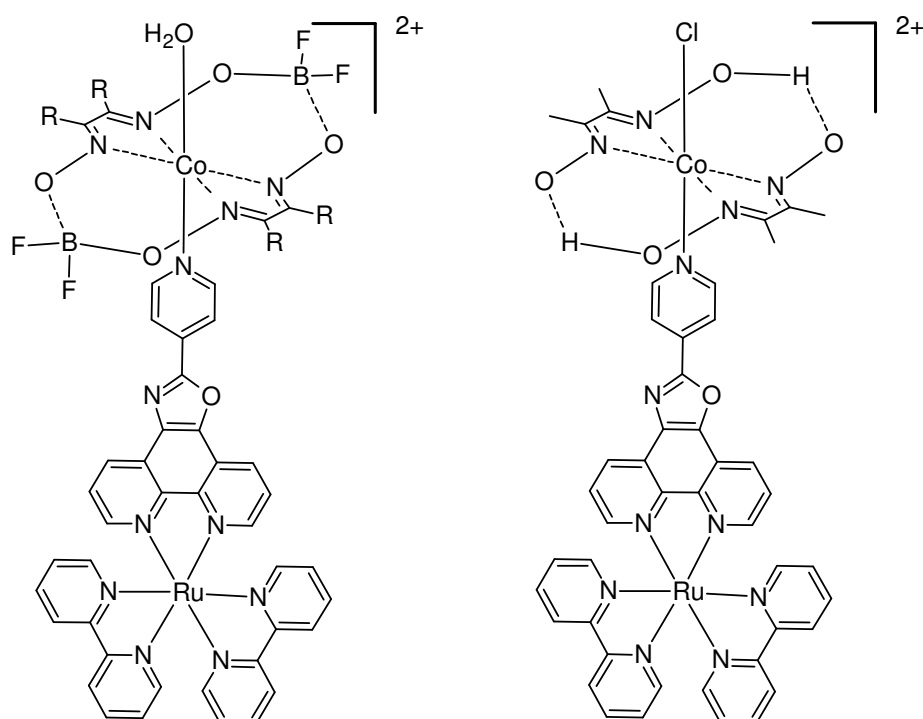


Figure 1.11: Ru-Co heterodimetallic photocatalysts.⁴⁷

In 2009, Mallouk *et al.*⁴⁸ reported a water splitting catalytic system involving a ruthenium complex as the photosensitiser which was bound to a TiO_2 semiconductor. Also, colloidal $\text{IrO}_2 \cdot n\text{H}_2\text{O}$ particles present in the solution acted as the catalyst

(**Figure 1.12**). The working principle is based on Gratzels' solar cell. A platinum cathode and a ruthenium dye immobilised TiO_2 surface as anode were used. The $[\text{Ru}(\text{bpy})_3]^{2+}$ sensitizer was modified with both phosphonate and malonate ligands in the 4-positions of the 2,2'-bipyridine ligands in order to adsorb strongly to TiO_2 and $\text{IrO}_2 \cdot n\text{H}_2\text{O}$, respectively. Oxygen and hydrogen was produced by water splitting at two different electrodes. No organic solvent was used in this catalytic system. The diagram of this heterogeneous catalytic system is shown below in **Figure 1.12**. This catalytic system was highly efficient for oxygen production however the turn-over number for catalytic hydrogen production on the Pt-electrode was reported to be less than 20. The reason for the low turn-over number is associated with the instability of $\text{Ru}(\text{III})$ in water.

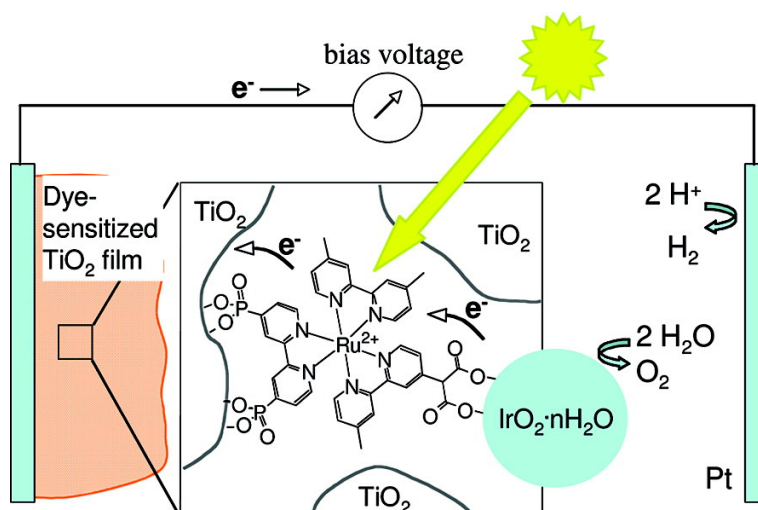


Figure 1.12: A Heterogeneous water-splitting system based on dye-sensitized solar cell. The inset illustrates a sensitizer-capped $\text{IrO}_2 \cdot n\text{H}_2\text{O}$ catalyst particle in the mesopores of the TiO_2 electrode film.⁴⁸

More recently, Armstrong⁴⁹⁻⁵¹ and Lakadamyali⁵² have reported a different approach of efficient hydrogen production on the surface of nanocrystalline TiO_2 . Both the photosensitizer and catalytic centre have been attached to the surface of the semiconductor. The approach demonstrates a new research field for next generation hydrogen production by heterogeneous catalysis in an environmentally sustainable manner (see **Figure 1.13**). The working mechanism is based on three consecutive

steps, excitation of metal $d\pi$ electrons with the help of sunlight, transferring excited state electrons to the conduction band of the TiO_2 and finally electron transfer from TiO_2 to the catalytic site. Armstrong used a biological system $[\text{NiFeSe}]$ -hydrogenase (see **Figure 1.3**) as the catalytic centre whereas Lakadamyali *et al.* used a cobalt oxime pyridyl complex as the catalytic centre.

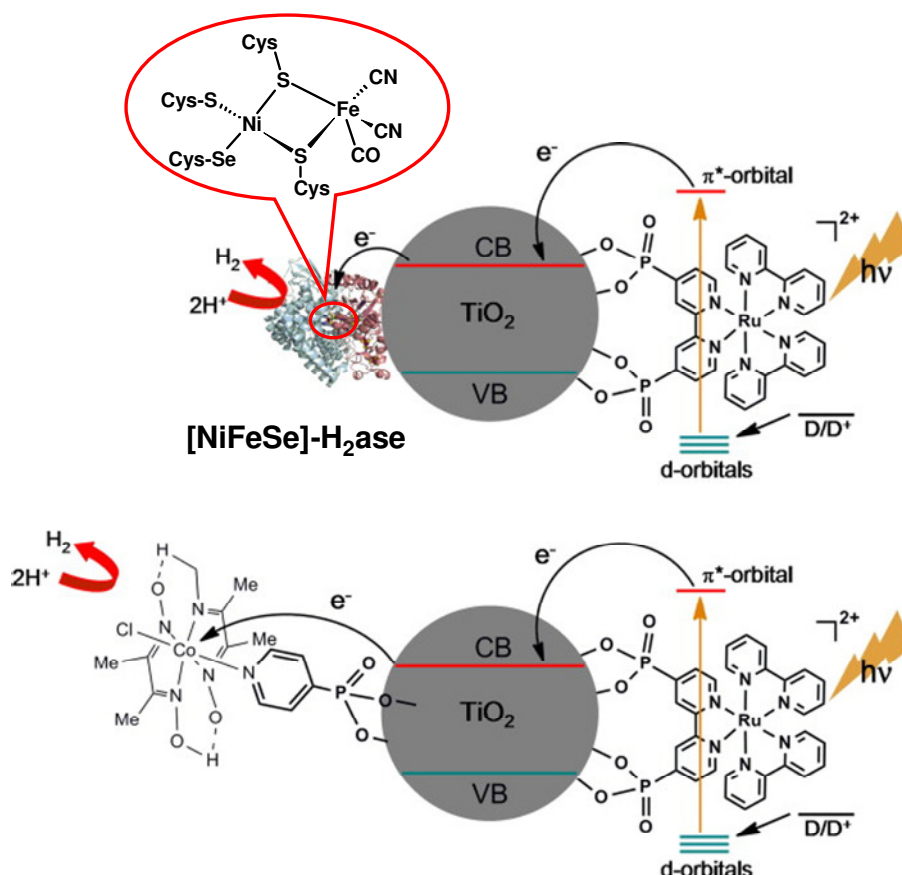


Figure 1.13: Catalytic hydrogen production on the surface of TiO_2 .^{49,50,52}

From the above, the trend of hydrogen production from water using ruthenium metal complexes is highly progressive. The ongoing research is moving forward from homogeneous catalysis to heterogeneous (to the surface of semiconductor) catalysis for greater efficiency and economic feasibility. Understanding catalytic hydrogen generation from water requires more development in terms of catalytic efficiency of such photocatalytic systems with molecular modifications of the metal catalysts and only then can hydrogen be available for commercial and domestic purposes.

1.4. Iridium in solar hydrogen evolution

Cyclometallated iridium(III) complexes have been investigated as photosensitisers for their long lived excited states.^{53,54} The electronic absorption and emission properties of iridium complexes are somewhat different from ruthenium complexes. Iridium complexes have more intense electronic transitions in the UV region which are basically ligand centred charge transfer (LC) transitions. Due to the long lived excited state lifetime and strong emissive properties, iridium complexes were also used as photosensitisers over the last three decades. Many research groups reported that the emissive properties of iridium complexes are highly tuneable based on ligand architecture which are discussed below.

In 1987, King *et al.* first reported a heteroleptic iridium complex $[\text{Ir}(\text{ppy})_2(\text{bpy})]^+$ (**A**, **Figure 1.14**). This complex showed an emission band at 580 nm.⁵⁵ A detailed history of synthesising different iridium complexes has been reported by Dixon *et al.*⁵⁶

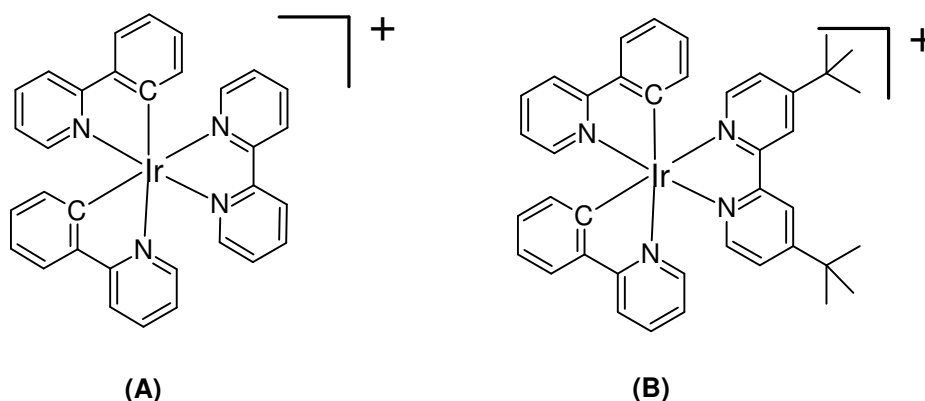


Figure 1.14: Molecular structure of (A) $[\text{Ir}(\text{ppy})_2(\text{bpy})]^+$ and (B) $[\text{Ir}(\text{ppy})_2(\text{tbpy})]^+$

In 2004, Slinker *et al.* reported a $[\text{Ir}(\text{ppy})_2(\text{N}^{\wedge}\text{N})](\text{PF}_6)$ type complex where the $\text{N}^{\wedge}\text{N}$ bpy-based ancillary ligand was functionalised. They showed that the emission of such iridium complexes does not change significantly when the bpy-based ancillary ligand was functionalised with tertiary butyl groups at the 4 and 4' positions (**B**, **Figure 1.14**). Based on the strong emission from the iridium complexes, the group suggested that these complexes can not only be used in organic light emitting devices

(lowest emission wavelength obtained was 531 nm) but also can be used for TiO₂-based photovoltaic cells, photoinduced water-splitting, biomolecular probes and as chiral luminophores in artificial photosynthesis.⁵⁷

Neve *et al.* reported a series of iridium complexes where they observed a variation in the emission wavelength for [Ir(ppy)₂(HL-X)][PF₆] depending on different ancillary ligands (HL-X), where ppy is the monoanion of 2-phenylpyridine; HL-X = hpbpy (**1**), clpbpy (**2**), tpbpy (**3**), cpbpy (**4**), and ttpy (**5**) (see **Figure 1.15**).⁵⁸ For example, compound (**1**) shows emission at 620 nm, compound (**2**) at 645nm, (**3**) at 630 nm, (**4**) at 660 nm and (**5**) at 625 nm at room temperature.

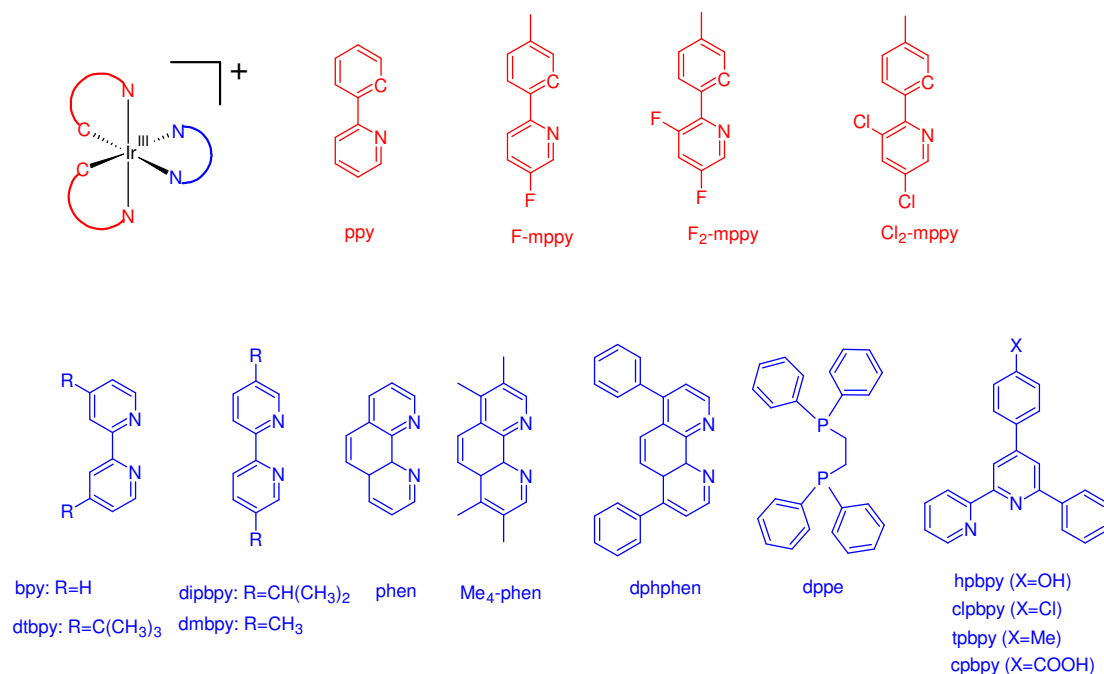


Figure 1.15: Iridium complexes based on different *N*²*N* based ancillary ligands.⁵⁸⁻⁶⁰

Goldsmith *et al.* first showed the use of iridium complexes as an active photosensitiser in photocatalytic hydrogen generation from water. They studied ruthenium and iridium-based photosensitisers (see **Figure 1.15** and **Table 1.1**) under homogeneous catalytic conditions and observed an increased in TON for H₂ production when iridium was used as the photosensitiser as opposed to ruthenium. The turn-over number (TON) for the iridium photosensitiser was found to exceed 900 whereas the turn-over number for the ruthenium photosensitiser had a maximum of

580. The catalytic hydrogen generation process was carried out in 50:50 acetonitrile: water solution. TEOA was used as the sacrificial electron donor and $[\text{Co}(\text{bpy})_3]^{2+}$ as electron the relay as well as the active catalyst. The experimental details, photosensitisers and catalytic centres are provided below in **Table 1.1**.⁶⁰

Table 1.1 Photoinduced hydrogen production^{a 60}

Photosensitiser	H ₂ evolved (μmol)	PS turn-overs
$[\text{Ru}(\text{bpy})_3]^{2+}$	50	100
$\text{Ru}(\text{dmphen})_3^{2+}$	290	580
$\text{Ir}(\text{ppy})_2(\text{bpy})^+$	400	800
$\text{Ir}(\text{ppy})_2(\text{phen})^+$	430	860
$\text{Ir}(\text{ppy})_2(\text{dphphen})^+$	420	840
$\text{Ir}(\text{F-mppy})_2(\text{bpy})^+$	460	920
$\text{Ir}(\text{F-mppy})_2(\text{phen})^+$	430	860
$\text{Ir}(\text{F-mppy})_2(\text{dphphen})^+$	430	860

*a All samples have a total volume of 20 cm³ and contain 50 μM photosensitiser, 2.5 mM $[\text{Co}(\text{bpy})_3]^{2+}$ (electron relay/catalyst), 0.57 M TEOA, and 0.27 M LiCl in 50:50 water:acetonitrile. The pH was adjusted by the addition of 0.4 cm³ of 12 M HCl.*⁶⁰

Tinker *et al.* have investigated the effect of catalyst concentration on hydrogen production.⁶¹ They used $[\text{Ir}(\text{ppy})_2(\text{bpy})]^{2+}$ as the photosensitiser (PS), a cobalt-based electron relay and $\text{K}_2[\text{PtCl}_4]$ as the catalyst. They studied the effect of different concentrations of $\text{K}_2[\text{PtCl}_4]$ in the catalytic process and reported a maximum turn-over number (TON) for the modified catalytic system of 3400 over 20 hours of irradiation when the catalytic system contained 0.3 μmol of $\text{K}_2[\text{PtCl}_4]$. However, with increased concentrations of the iridium photosensitiser (PS), the catalytic efficiency did not increase. A range of different concentrations of PS in solution were applied with a variation in catalyst concentration. 25 μmol of PS and 0.3 μmol catalyst, yielded the highest turn-over number of 3400. Actually the catalytic efficiency was drastically diminished with an increase in PS and catalyst concentration. A dark solid was generated in such photocatalytic process, which were tentatively assigned to aggregated Pt-catalysts. Mass spectroscopy and absorption spectroscopy results suggest degradation of the iridium complex by 2, 2-bipyridine dissociation, which directly correlates to the decreased catalytic activity of the system. Lack of charge separation was created in the excited state photoproducts by the termination of the

$^3\text{MLCT}$ excited state ($t_{2g} \rightarrow \pi^*_{\text{N}^{\wedge}\text{N}}$). This resulted in limited excitations on the cyclometallating ligands and therefore, generated an inactive PS molecule. 2,2'-bipyridine (0.5 mmol) was added to regenerate the original PS molecule, but a decrease in the photocatalytic efficiency was observed compared to the concentration of the original PS.

Cline *et al.* reported an intermolecular homogeneous catalytic system that consists of $[\text{Ir}(\text{C}^{\wedge}\text{N})_2(\text{N}^{\wedge}\text{N})]^+$ as the photosensitiser and $[\text{Rh}(\text{N}^{\wedge}\text{N})_3]^{3+}$ as the water reduction catalyst.⁶² Photophysical and electrochemical investigations reveal formation of $[\text{Rh}(\text{N}^{\wedge}\text{N})_2]^0$ as the active catalytic species, formed by a reductive quenching pathway. The system is the most effective reported photocatalytic system at present. A series of peripheral $\text{C}^{\wedge}\text{N}$ ligands and ancillary $\text{N}^{\wedge}\text{N}$ ligands have been tested in acetonitrile/water solution. The catalytic system consisting of $[\text{Ir}(\text{f-mppy})_2(\text{dtbbpy})](\text{PF}_6)$ (PS) and the water reduction catalyst $[\text{Rh}(\text{dtbbpy})_3](\text{PF}_6)_3$ was found to be the most efficient for hydrogen generation, with a turn-over number (TON) of 5000. A list of iridium and rhodium complexes used for catalytic hydrogen production is provided in **Figure 1.16**.

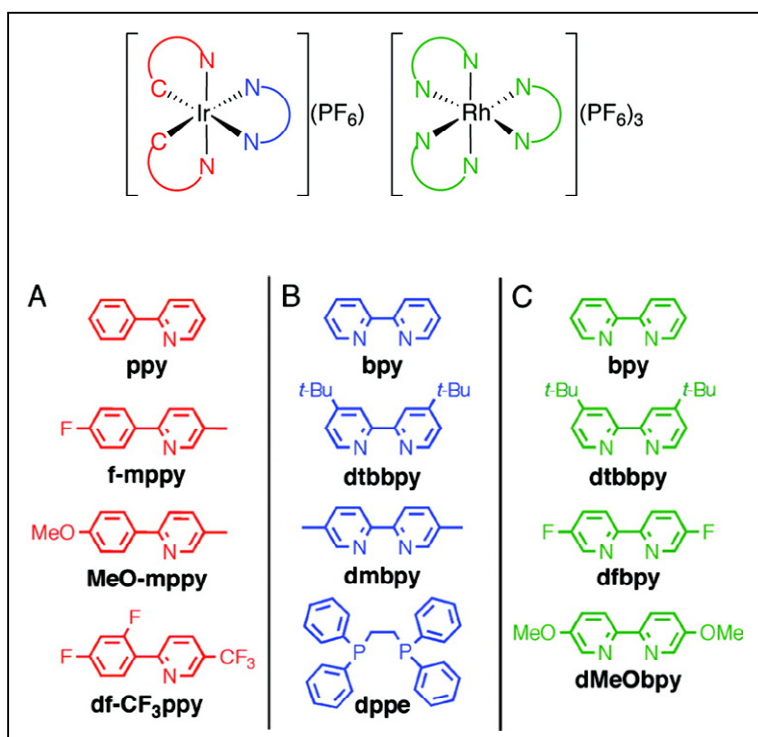


Figure 1.16: List of iridium and rhodium complexes used for catalysis.⁶²

Curtin *et al.*⁶³ studied the effect of varying catalytic conditions such as, solvents, ligand substitutions at the iridium centre along with different catalytic metal centres. They have compared the catalytic hydrogen production with Pt and Pd as the water reduction catalyst (WRC) and with different sacrificial electron donors (TEA and TEOA). The first stage of photocatalysis was carried out with 10 cm³ of 1 mM [Ir(ppy)₂(bpy)](PF₆), 30 µM catalyst and 0.5 M sacrificial electron donor (SR) in 4:1 ACN/H₂O solution. The initial photocatalytic hydrogen evolution rate observed was dependent on the nature of catalyst used. For example, faster initial catalytic hydrogen evolution was found with K₂[PtCl₄] despite the reductive quenching rate of the SRs (TEA ($k_q = 1.9 \times 10^7 \text{ M}^{-1} \text{ s}^{-1}$) and TEOA ($k_q = 6.4 \times 10^6 \text{ M}^{-1} \text{ s}^{-1}$)). However, the TEA system was found to be the longer lived photocatalytic system, however with a slower decay of the hydrogen evolution rate. The acetonitrile/water solvent system was the main cause of dissociation of the N^N ligands from the PS molecule and formation of [Ir(ppy)₂(ACN)]⁺ complex.⁶¹ As an alternative solvent system, DMF/water and THF/water were employed and showed superior performance in the catalytic hydrogen evolution compared to the ACN/water system (see **Figure 1.17**). DMF and THF presented both higher catalytic activity and enhanced stability of the catalytic systems. The weaker ligand strength of DMF and THF ligands resulted in slower dissociation of the N^N ligand from the PS (i. e., decomposition of the PS) and hence enhanced system stability. Studies on different photosensitisers revealed an increase of catalytic activity with the photosensitisers containing bulky groups in C^N and N^N ligands. For example, [Ir(F-ppy)₂(5,5'-dipbpy)]⁺ (TOF = 148) and [Ir(MeO-ppy)₂(5,5'-dipbpy)]⁺ (TOF = 121) showed greater catalytic activity than [Ir(ppy)₂(5,5'-dipbpy)]⁺ (TOF = 104). The increased catalytic activity for these photosensitisers was attributed to less solvent interaction with the iridium metal centre due to bulky groups and stabilisation of the PS by hindering ligand substitution. The study also suggests a unique non-accessible interaction between catalyst and [Ir(F-ppy)₂(dFbpy)]⁺ photosensitiser for the highest TON (312) for hydrogen production. This indicates iridium photosensitisers containing ligands with more electron withdrawing groups (i.e., fluoride in this case) are more efficient photocatalysts for hydrogen evolution from water.

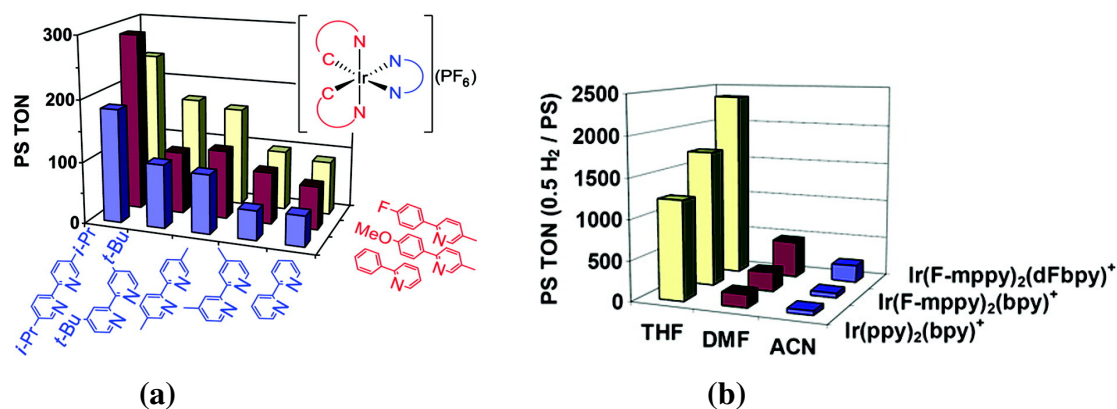


Figure 1.17: (a) Turn-over numbers for different iridium photosensitisers. (b) Solvent effect in homogeneous catalysis.⁶²

Metz *et al.*⁶⁴ reported cyclometallated Ir(III) 4-vinyl-2,2'-bipyridine complexes as superior photosensitisers than the non-vinyl derivate 2,2'-bipyridine containing iridium complexes (see **Figure 1.18**). They performed the catalytic experiment in a sealed vial with a 16-well LED light photoreactor ($\lambda_{\text{em}} = 460 \text{ nm}$) on an orbital shaker with a thermostated block (25 °C). Each sample contained 0.5 μmol of the respective photosensitiser and 0.375 μmol catalyst ($\text{K}_2[\text{PtCl}_4]$ or $[\text{Rh}(\text{bpy})_2\text{Cl}_2]\text{Cl}$) in THF (8 cm^3), triethylamine (sacrificial reductant, 1 cm^3) and H_2O (1 cm^3). The turn over number for hydrogen evolution exceeded 8500 over 18 hours of irradiation. The increased turn-over number is due to the interaction of the vinyl moieties with the *in situ* formed colloidal Pt catalyst.

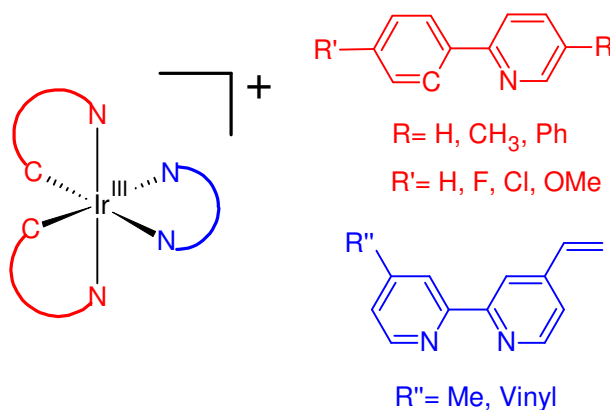
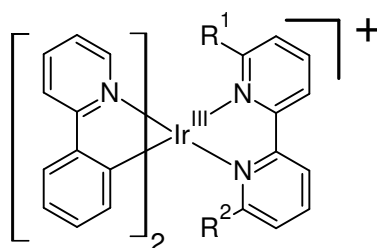


Figure 1.18: Vinyl derivated iridium complexes.⁶⁴

More recently, Gärtner *et al.* reported a number of iridium complexes (see **Figure 1.19**), their suitability and uses as photosensitisers.⁶⁵ THF/water/Et₃N solvent systems were used for homogeneous catalysis.



PS13: R₁ = H, R₂ = H

PS1: R₁ = ⁱPr, R₂ = H

PS2: R₁ = ^tBu, R₂ = H

Figure 1.19: Iridium complexes based on different bpy based ancillary ligands.⁶⁵

They found **PS1** the most efficient photosensitiser. First, they studied the catalytic hydrogen production using different PSs (see **Figure 1.19**) with the water reduction catalyst [HNEt₃][HFe₃(CO)₁₁]. The maximum TON for hydrogen was more than 1800 after 15 hours of irradiation (λ >390 nm). After that they checked the catalytic activity of these iridium photosensitisers with different water reduction catalysts ([HNEt₃][HFe₃(CO)₁₁], [HNEt₃][HFe₃(CO)₁₁]/P[C₆H₃-3-5-(CF₃)₂]₃, [Mn₂(CO)₁₀], Co(BF₄)₂/dmg, K₂[PtCl₆] and RhCl₃). K₂[PtCl₆] was found the most efficient water reduction catalyst (WRC) with a TON reaching a maximum 4200 over 20 hours of irradiation. Apparently, the group did not study any Pd metal based catalyst, whereas Bernhard's group already shown an increased efficiency of Pd based catalysts over Pt based catalysts.⁶³

Fihri *et al.*⁶⁶ reported the photocatalytic behaviour of Ir-Co heterodinuclear complex. In these studies, triethylamine (TEA) was used as a sacrificial electron donor and acetone as a solvent. The hydrogen production efficiency was higher for the Ir-Co heterodinuclear photocatalyst compared to the analogous Ru-Co heterodinuclear complex. Ir-Co complex produced hydrogen with TONs of 210 whereas Ru-Co complex showed TONs of 165. The molecular structure of the Ir-Co complex is shown in **Figure 1.20**.

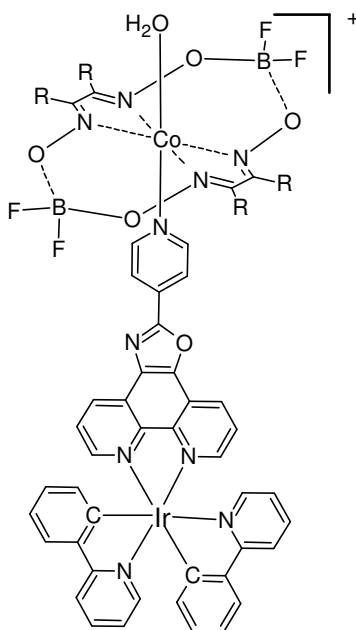


Figure 1.20: Molecular structure of Ir-Co heterodimetallic photocatalyst.⁶⁶

DiSalle and Bernhard reported a number of iridium mononuclear complexes which were immobilised on a Pt solid surface instead of using colloidal Pt as catalyst⁶⁷ and found increased turn-over number for hydrogen production.⁶⁷ Especially, the iridium complex $[\text{Ir}(\text{C}^{\wedge}\text{N})_2(\text{N}^{\wedge}\text{N})]^+$, where the $\text{C}^{\wedge}\text{N}$ ligand is **tolpy** and $\text{N}^{\wedge}\text{N}$ bpy based ligand is **dethqpy** (see **Figure 1.21**), which showed a TON for hydrogen production of over 10,000. To determine the origin of the H_2 , a catalytic experiment using D_2O instead of H_2O provided identical turn-over number and the formation of D_2 .

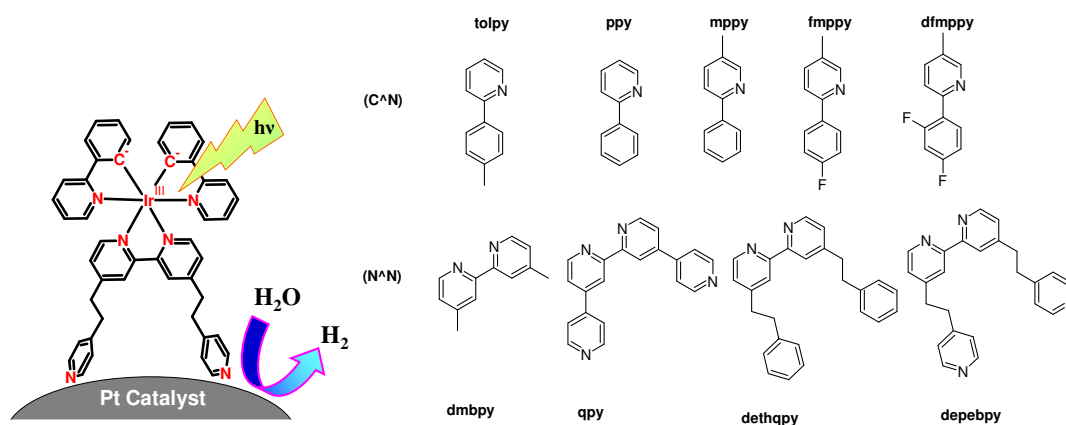


Figure 1.21: Photocatalysis on the surface of Pt using different iridium complexes.⁶⁷

Ruthenium has been used as photosensitisers in *intramolecular* photocatalysis and showed greater catalytic efficiency compared to intermolecular photocatalysis.^{63,64,67,68} Investigations of similar types of *intramolecular* as well as intermolecular photocatalytic systems consisting of different iridium photosensitisers with a variety of catalytic sites are worth studying in homogeneous and in heterogeneous systems because of their better efficiency as a photosensitiser compared to ruthenium.

1.5. Rhenium in solar hydrogen evolution

Fihri *et al.* reported a rhenium-based complex (**A**) as photosensitiser for light induced hydrogen evolution (see **Figure 1.22**).⁴⁷ In addition to this rhenium carbonyl complex, a Co(II) oxime complex was used as an active catalyst. The catalytic hydrogen evolution experiment was powered using $\lambda > 350$ nm. The reported turn-over number (TON) reached a maximum of 273 with a turn over frequency (TOF) of 50. In this catalytic experiment, Et_3NH^+ (300 equivalents) was used as the proton source instead of water and 600 equivalents of triethylamine was used as the sacrificial electron donor. The whole catalytic process was carried out in acetone solution.

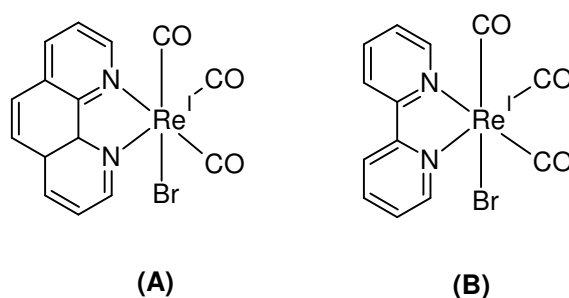


Figure 1.22: Rhenium metal based photosensitisers. (A) $[(\text{Phen})\text{Re}(\text{CO})_3\text{Br}]$, (B) $[(\text{bpy})\text{Re}(\text{CO})_3\text{Br}]$

Another bpy-based rhenium carbonyl complex (**B**) was used as photosensitiser for hydrogen production by Probst *et al.* (see **Figure 1.22**).⁶⁹ This time, the catalyst was a Co(II) glyoxime complex, and TEOA was used as the electron donor. The catalytic process was carried out in DMF solution using $\lambda \geq 400$ nm. Turn-over

numbers obtained for the Co centre after 9 hours of irradiation was 75 and the turnover number for the rhenium photosensitiser was measured as 150.

The recent results on rhenium based complexes hold much promise in the field of photocatalysis and therefore, should be further developed.

1.6. Metal complexes in photocatalytic CO₂ reduction

Increasing atmospheric CO₂ levels has become a real problem in recent years, mostly caused by the combustion of carbon based fossil fuels. There is a need for smart solutions to reduce the CO₂ levels in the atmosphere. Artificial photosynthesis is one such approach towards the reduction of CO₂.^{16,22,70-72} CO₂ reduction is more difficult than the reduction of water, since, CO₂ is a very stable molecule. Electrochemical reduction of CO₂ (one electron reduction) to generate the unstable CO₂^{•-} intermediate requires -1.9 V.²⁹ This process can be improved by multi-electron transfer to CO₂, coupled with proton transfer which will lead to more favourable reduced products such as CO and HCOOH. The reduction potential for multi-electron transfer requires less energy compared to one electron transfer (see **Scheme 1.1**).^{30,73,74}

CO ₂	+ 2H ⁺	+ 2e ⁻	—————>	CO + H ₂ O	E ⁰ = -0.53 V
CO ₂	+ 2H ⁺	+ 2e ⁻	—————>	HCO ₂ H	E ⁰ = -0.61 V
CO ₂	+ 4H ⁺	+ 4e ⁻	—————>	HCHO + H ₂ O	E ⁰ = -0.48 V
CO ₂	+ 6H ⁺	+ 6e ⁻	—————>	CH ₃ OH + H ₂ O	E ⁰ = -0.38 V
CO ₂	+ 8H ⁺	+ 8e ⁻	—————>	CH ₄ + H ₂ O	E ⁰ = -0.24 V
CO ₂		+ e ⁻	—————>	CO ₂ ^{•-}	E ⁰ = -1.90 V

Scheme 1.1: Multi-electron transfer process for CO₂ reduction, required redox potentials for each step and reduced products at pH 7.^{29,73-75}

The main concern about artificial photosynthesis is the design of photocatalysts. There are many examples of photocatalysts for CO₂ reduction which require UV light.⁷⁶ However, it is important to design new photocatalysts that absorb in the visible region of the solar spectrum. Many research groups have worked on the

artificial photosynthetic principle for the reduction of CO₂, and the catalytic conditions with reduced products are listed in **Table 1.2**.

Table 1.2: List of photosensitisers and sacrificial electron donors used for photocatalytic CO₂ reduction and reduced products.

Photosensitisers(PS)	Catalysts	Electron donor	Final Products	Ref
1. [Ru(bpy) ₃] ²⁺	[Co(bpy) _n] ²⁺	R ₃ N	CO, H ₂	77,78
2. [Ru(bpy) ₃] ²⁺	[Co(macrocyclic)] ²⁺	Ascorbic acid	CO, H ₂	79
3. [Ru(bpy) ₃] ²⁺	[Ni(cyclam)] ²⁺	Ascorbic acid	CO, H ₂	80-83
4. [Ru(bpy) ₃] ²⁺	[Ru(bpy) ₂ (CO) ₂] ²⁺	R ₃ N or BNAH	CO, HCOOH	84-86
5. [Ru(bpy) ₃] ²⁺	MV/ formate dehydrogenase	Cysteine	HCOOH	71
6. [Ru(bpy) ₃] ²⁺	MV/Ru, Os colloids	R ₃ N	CH ₄ , H ₂	71,87
7. [Ru(bpy) ₃] ²⁺	Ru colloid	R ₃ N	CH ₄	87,88
8. [Re(X ₂ bpy)(CO) ₃ (Cl)]	*	R ₃ N or BNAH	CO	77,78,89-91

* [Re(X₂bpy)(CO)₃(Cl)] also acted as active catalyst.

In 1983, Hawecker *et al.* reported visible light reduction of CO₂ where they used [Re(bpy)(CO)₃Cl] as the catalyst and observed a maximum TON for CO of 48 (see **Figure 1.23**).⁷⁷ Ziessel *et al.*⁷⁸ reported the reduction of water and CO₂ simultaneously to H₂ and CO using [Ru(bpy)₃]²⁺ as a photosensitiser and a Co(II) complex as an active catalyst.

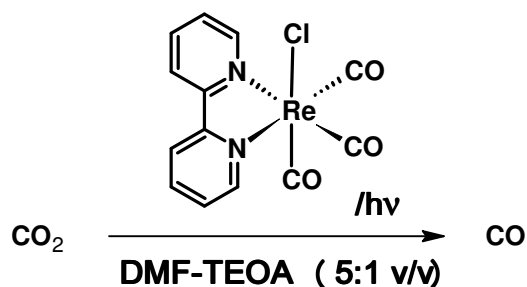
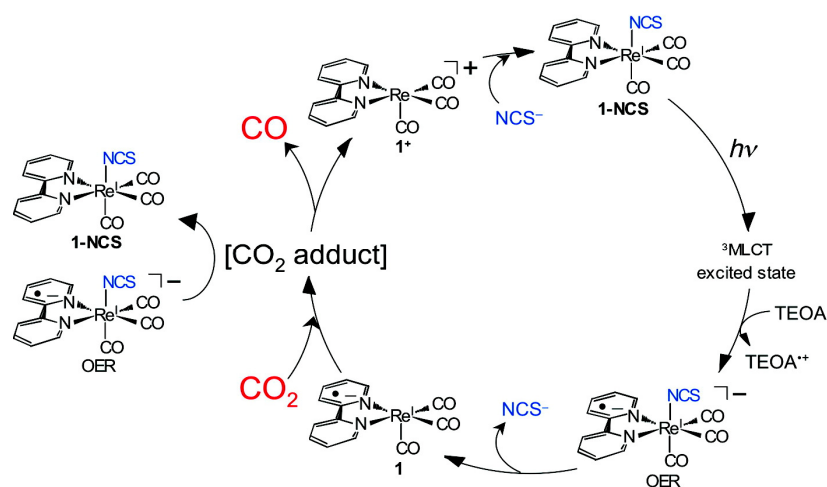


Figure 1.23: Reduction of CO₂ using [Re(bpy)(CO)₃Cl]; DMF was used as solvent and TEOA was used as the sacrificial electron donor.^{30,77}

The main issue with rhenium mononuclear complexes is where they absorb in the UV-Vis spectrum. Rhenium mononuclear complexes show a maximum MLCT around 350 nm (higher in energy). Therefore, mononuclear Re-complexes are only photolytically active for the reduction of CO₂ when irradiated with the light $\lambda \geq 350$ nm. Lehn *et al.*⁸⁹ also reported the reduction of CO₂ using a mixture of [Ru(L)₃]²⁺ (L = bpy derivatives or 1,10-phenanthroline (phen)) as photosensitiser and *cis*-[Ru(bpy)₂(CO)(X)]ⁿ⁺ (X = Cl, H, *n* = 1 or X = CO, *n* = 2) or *cis*-Ru(bpy)(CO)₂(Cl)₂ as the homogeneous catalyst. The investigation of catalytic formation of hydrogen and CO revealed two catalytic cycles and the formation of formate as the ultimate reduced product. The catalytic study also suggested that the formation of formate is dependent on the water content and was not dependent on the CO₂ pressure. The mechanism for the formation of formate from CO₂ was suggested as reductive quenching of the [Ru^{II}(L)₃]²⁺ excited state by a tertiary amine (electron donor) to a Ru^I complex that reduces CO₂.

Ishitani *et al.* proposed a multi-electron reduction mechanism for CO₂ molecule to CO (see **Scheme 1.2**).^{30,92} In this mechanism, it was suggested that the ³MLCT state was quenched by TEOA which generated a one electron reduced species (OER). A key step in this mechanism is the elimination of the NSC⁻ group to form the OER. After that the OER reacts with CO₂ forming the CO₂ adduct. The mechanistic study revealed that [Re(bpy)(CO)₃(NCS)] is a better photocatalyst than [Re(bpy)(CO)₃Cl] for CO₂ reduction.⁹²



Scheme 1.2: Photocatalytic reaction mechanism by [Re(bpy)(CO)₃(NCS)]⁹²

Rhenium carbonyl complexes can not only be used for CO₂ reduction but also as catalysts for synthesising useful chemical materials by converting CO₂ into other forms. Wong *et al.* recently reported a rhenium carbonyl complex which was used in converting organic epoxides to the corresponding cyclic carbonates in the presence of CO₂ and ionic liquids.⁹³ The chemical conversion was reported as up to 98% for certain epoxides. The catalytic process (not light driven catalytic process) and the rhenium carbonyl complex are shown in **Figure 1.24**.

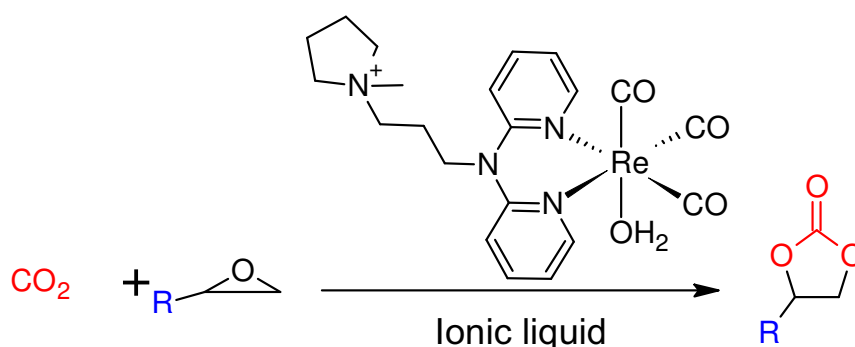
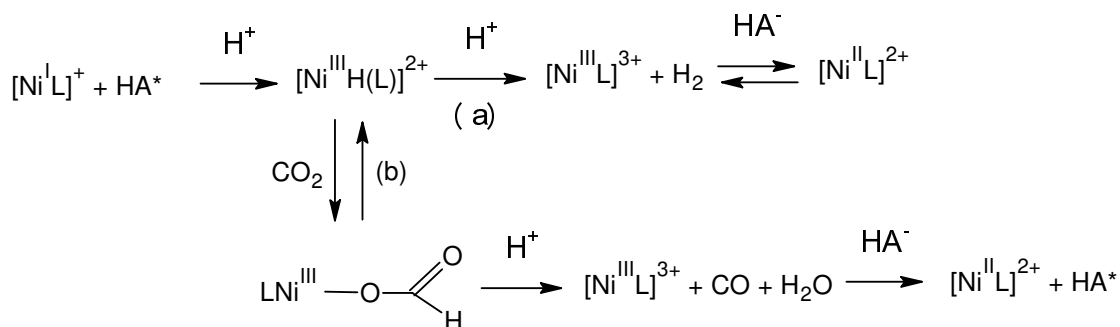


Figure 1.24: Rhenium carbonyl catalyst and conversion of epoxides to cyclic carbonates in the presence of CO₂.⁹³

CO₂ reduction using a [Ni(cyclam)]²⁺ catalyst has been reported by a number of groups in the last two decades. In 1987, Spreer *et al.* reported a intermolecular system for photochemical CO₂ reduction where they used [Ru(bpy)₃]²⁺ as a photosensitiser and [Ni(cyclam)]²⁺ as a catalyst.⁸² The turn-over number for CO was reported as 4.8. A number of experiments were carried out by replacing the catalytic components (PS, catalyst and buffer). Ascorbate buffer (pH 4) was added and the highest catalytic efficiency observed was a TON of 4.8. The suggested mechanism for CO₂ reduction is shown below in **Scheme 1.3** for this system. The excited state of [Ru(bpy)₃]²⁺ was quenched by ascorbate (HA⁻) to produce [Ru(bpy)₃]⁺. The [Ru(bpy)₃]⁺ therefore facilitates the reduction of [Ni^{II}L]²⁺ to unstable [Ni^{III}H(L)]²⁺ by reacting with H₂O⁺ or H₂O. The mechanism suggests that the formation of the intermediate [Ni^{III}H(L)]²⁺ has two possibilities, reacting with another hydronium ion (step **a**) or alternatively reacting with CO₂ (step **b**). Insertion of CO₂ to the Ni-H bond leads to the formation of [LNi^{III}-OOCH]³⁺. Therefore, CO and H₂O were eliminated

followed by the decomposition of the Ni-formate intermediate species. $[\text{Ni}^{\text{II}}\text{L}]^{2+}$ is regenerated from $[\text{Ni}^{\text{III}}\text{L}]^{3+}$ reacting with HA^- to complete the catalytic cycle.



Scheme 1.3: Mechanism of CO₂ reduction by [Ni(cyclam)]²⁺ complex.⁸²

Mochizuki *et al.* reported a photochemical system that consists of three components, $[\text{Ru}^{\text{II}}(\text{bpy})_3]^{2+}$ as the photosensitiser, ascorbic acid as the sacrificial electron donor, and the bimakrocyclic Ni(II) complex, $[\text{6,6'-bi(5,7-dimethyl-1,4,8,11-tetraazacyclotetradecane)}]$ dinickel(II) triflate as the catalyst.⁸³ The catalytic reduction process was performed at pH 4, and H_2 and CO were reported as catalytic products. More recently, homogeneous photocatalysis in aqueous media were reported by Mendez *et al.*⁸⁰ They used a reaction mixture which consists of a water soluble ruthenium tris-bipyridine complex as the light harvester, TEOA as the sacrificial electron donor and $[\text{Ni}^{\text{II}}(\text{cyclam})]^{2+}$ as the catalytic metal centre (see **Figure 1.25**). In this mechanism, direct metal- CO_2 bond formation was suggested, to form $[\text{L-Ni(I)}]^+$ instead of forming the metal-hydride bond as suggested by Spreer *et al.* $[\text{L-Ni(III)-CO}_2]^+$ further reacts with H^+ and forms the Ni(III)-formate intermediate. Ni(II)-CO was generated by the elimination of OH^- from the Ni(II)-formate intermediate. Ni(II)-CO further releases CO and regenerates $[\text{L-Ni(II)}]^{2+}$. Mendez *et al.* also used super critical CO_2 as the reaction medium for the reduction of CO_2 , where water was used as an electron and proton donor. The catalysis was carried out at elevated pressure and the highest turn-over number for CO obtained was 3.6. They reported the production of a significant amount of hydrogen in this system but no new mechanism was suggested.

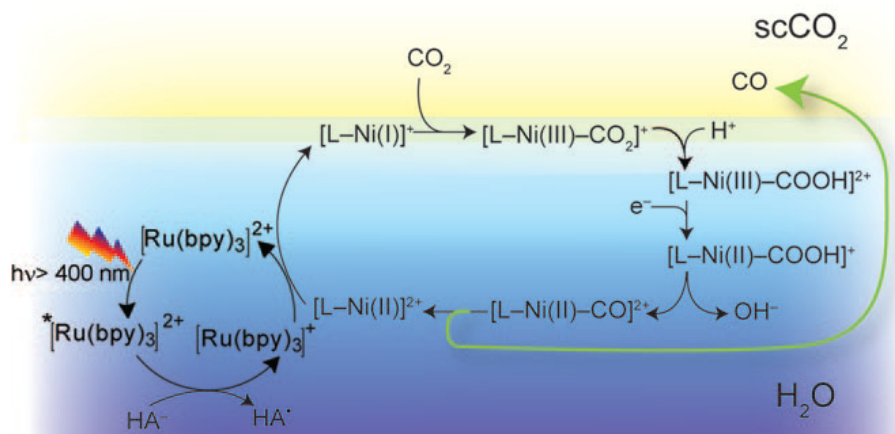


Figure 1.25: A $[Ru(bpy)_3]^{2+}$ and $[Ni^{II}(cyclam)]^{2+}$ based photo-catalytic system for the reduction of CO_2 in aqueous medium.⁸⁰

Recently, Ishitani *et al.* reported visible light driven reduction of CO_2 using heterodinuclear ruthenium-rhenium photocatalysts where ruthenium acted as the photosensitiser and the rhenium moiety acted as the catalytic centre. Turn-over numbers of more than 240 for CO_2 reduction have been reported by Ishitani (see **Figure 1.26**).^{30,94,95} N,N-dimethylformamide (DMF) was used as the solvent for homogeneous catalysis, triethanolamine (TEOA) and 1-benzyl-1,4-dihydronicotinamide (BNAH) were used as sacrificial electron donors. The group reported Ru-Re type heterodinuclear complexes based on different bridging ligands and varied the free site at the rhenium centre from chloride to $P(OEt)_3$. It has been investigated that the efficiency of Ru-Re catalysts with $P(OEt)_3$ ($\Phi_{CO} = 0.21$, TON = 232) is more efficient than the catalyst with chloride ($\Phi_{CO} = 0.12$, TON = 171) (see **Figure 1.26**). The quantum efficiency and the turn-over number for *intramolecular* photocatalysis are higher than *intermolecular* photocatalysis. For example, complex **1a**, a Ru-Re heterodinuclear complex has a quantum yield of 0.12 for CO and a turn-over number of 170. On the other hand, an inter-molecular system which consists of $[Ru(dmb)_3]^{2+}$ as a photosensitiser and *fac*- $[Re(dmb)(CO)_3Cl]$ as the catalyst has a quantum yield of 0.06 for CO and a TON_{CO} of 101. The catalytic efficiency of Ru-Re heterodimetallic photocatalysts is dependent on the nature of the peripheral bpy ligands coordinated to ruthenium centre and the attached ligands to the rhenium centre. For example, compound **1b** ($Y = H$) and **1c** ($Y = CF_3$) have low catalytic efficiency. On the other hand, compound **1a** ($H = CH_3$) is more efficient compared to

1b and **1c** for CO₂ reduction. These results indicate an excited state on the bridging ligand and the catalytic process is dependent on how fast the electron transfer process takes place. The non-conjugated organic bridging ligands possibly have an advantage for rapid electron transfer between the Ru and Re units opposed to a conjugated bridging ligands, however the Ru-Re heterodinuclear complexes with nonconjugated bridging ligands found more efficient opposed to Ru-Re complex with bridging ligands having π -conjugation. For example, compounds **4a** and **4b** were less efficient than the compounds **1a** and **3** (see **Figure 1.26**). As previously discussed above, OER species of rhenium complexes require high reduction potentials (< -1.40 V) for the reduction of CO₂. The bridging ligand in compounds **1a** and **3** have higher reduction potentials (-1.77 V) than the bridging ligand in the compounds **4a** and **4b** (-1.10 V) therefore higher catalytic efficiency was observed for **1a** and **3**. Variation of the ligand at the rhenium centre also makes a significant difference in catalytic efficiency. For example, compound **2** (X = P(OEt)₃) gives a higher TON for CO ($\Phi_{\text{CO}} = 0.21$, TON = 232) compared to compound **1a** ($\Phi_{\text{CO}} = 0.12$, TON = 171).

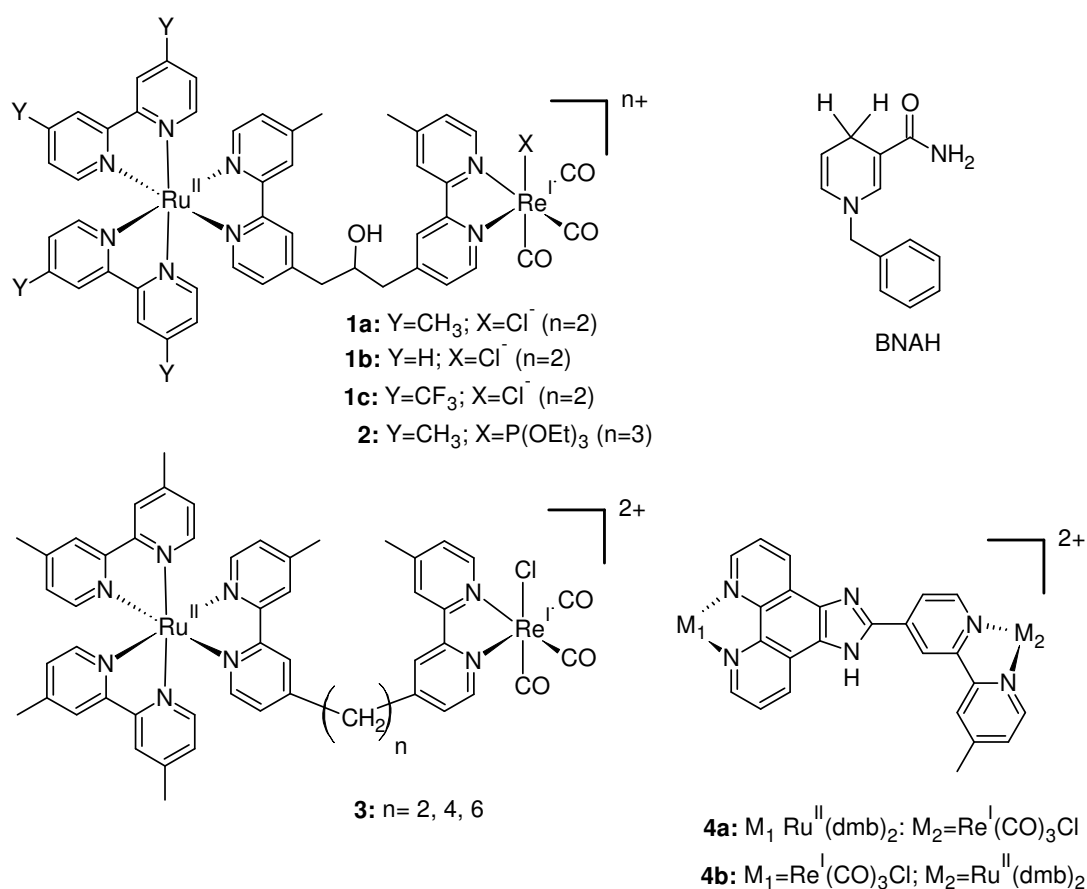


Figure 1.26: List Ru-Re heterodinuclear complexes for CO₂ reduction.³⁰

Considering the above discussion on photocatalysts for CO₂ reduction, more efficient photocatalysts are required. The reduction process is difficult and not straight forward considering the low solubility of CO₂ in many solvents and the potential required (-1.90 eV) for the one electron reduction. There are few heterodinuclear photocatalysts reported to date. There is scope for developing more efficient Ru-Re heterodinuclear photocatalysts for CO₂ reduction. The study can also be extended to include different bridging ligands, considering the energy level overlap between the bridging ligand and metal centres. This crucial research is worth pursuing to understand the photocatalytic activity of different catalysts for the reduction of CO₂, which will lead to more efficient photocatalytic systems for CO₂ reduction.

1.7. Aim of this thesis

The theories established so far for catalytic hydrogen generation^{43,45,47} and CO₂ reduction^{30,92,94-96} in homogeneous medium involves photo-excitation of the ruthenium(II) moiety to ruthenium(III) moiety, regeneration of ruthenium(II) with the help of sacrificial electron donor like tertiary amines, electron transfer to the conjugated organic bridging ligand and finally to the catalytic centre (based on Re, Pt or Pd). The reduced transition state of the catalytic metal centre then transfers the extra electron to two H⁺ ions to form a single molecule of H₂, and CO₂ to CO using the same electron transfer principle. Therefore, the catalytic system needs two electrons for the production of a single molecule of H₂ from water. Homogeneous catalytic systems have many limitations such as stability of the catalysts in homogeneous solvent systems is the major problem. Certain sacrificial electron donors used in all the above mentioned catalytic systems for hydrogen generation and CO₂ reduction processes, such as triethylamine and the organic solvent (e.g., acetonitrile) are the main reasons behind the decomposition of the catalysts.⁹⁷⁻¹⁰⁰ These sacrificial electron donors are also expensive and corrosive in nature (pH > 9). A semiconductor can replace the corrosive sacrificial electron donor.

The research aim is to develop heterodimetallic photocatalysts which can be bound to the surface of semiconductors. Therefore, the idea of homogeneous photocatalysis for the production of H₂ and for CO₂ reduction can be moved to heterogeneous catalytic system. The novelty of this work is the removal of organic

solvents and sacrificial electron donors currently used. The model system for photocatalytic production of hydrogen on a semiconductor is shown in **Figure 1.27**.

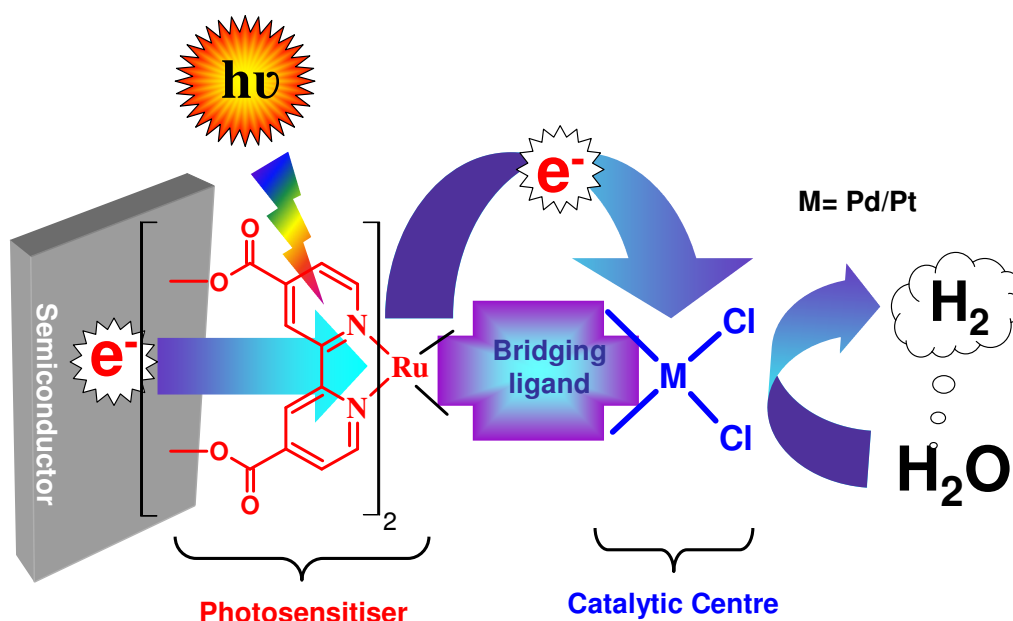


Figure 1.27: Model of novel photocatalyst bound to the surface of semiconductor and photo driven hydrogen production.

Heterodinuclear photocatalysts for hydrogen production reported so far have no surface binding capability. Based on the Gratzel's cell,^{11,19} one option is derivatisation of the photocatalyst with a carboxy group. Carboxy groups are well known for binding to the surface of semiconductors.^{32,101} However, there are potential synthetic problems when working with carboxy groups, in particular the difficulty in purification of the materials. Furthermore, the solubility of these carboxy functionalised precursors may be another issue. Hence, a number of heterodinuclear complexes were designed for binding to the surface of semiconductors where the peripheral bpy ligands were functionalised with carboxy ester groups. One of the aims of this thesis is to synthesise carboxy derivatised heterodinuclear photocatalysts and further bind these photocatalysts to a semiconductor surface. Bridging ligands also play an important role in this type of *intramolecular* photocatalytic molecule.¹⁰²⁻¹⁰⁴ Conjugated organic ligands help in electron transfer from the light absorber to the catalytic centre through efficient orbital energy overlap which permits a long lived charge separation between two units. Therefore, the development of novel bridging

ligands is essential. Another aim in this thesis is to synthesise a number of novel bridging ligands for more favourable electron transfer¹⁰⁵⁻¹⁰⁸ from photosensitiser to the catalytic metal centre.

The approach of heterogeneous photocatalysis on the surface of semiconductors is expected to render a promising result in hydrogen production from water. The same heterogeneous catalytic process can also be entailed for the photo-reduction of CO₂. The approach is more environmentally sustainable than homogenous catalysis.

1.8. References

-
- (1) Energy Information Administration, I. E. O. In www.eia.doe.gov/oiaff/ieo (U.S. Department of Energy, Washington, DC), 2008 and 2010.
 - (2) Lewis, N. S.; Nocera, D. G. *PNAS* **2006**, *103*, 15729-15735.
 - (3) Hoffert, M. I.; Caldeira, K.; Jain, A. K.; Haites, E. F.; Harvey, L. D. D.; Potter, S. D.; Schlesinger, M. E.; Schneider, S. H.; Watts, R. G.; Wigley, T. M. L.; Wuebbles, D. J. *Nature* **1998**, *395*, 881-884.
 - (4) *Climate Change 2007: Mitigation of Climate Change; IPCC Working Group III Fourth Assessment Report*; Intergovernmental Panel on Climate Change: Geneva, 2007.
 - (5) Barber, J. *Chem. Soc. Rev.* **2009**, *38*, 185-196.
 - (6) Chow, J.; Kopp, R. J.; Portney, P. R. *Science* **2003**, *302*, 1528-1531.
 - (7) Cook, T. R.; Dogutan, D. K.; Reece, S. Y.; Surendranath, Y.; Teets, T. S.; Nocera, D. G. *Chem. Rev.* **2010**, *110*, 6474-6502.
 - (8) Esswein, A. J.; Nocera, D. G. *Chem. Rev.* **2007**, *107*, 4022-4047.
 - (9) Eisenberg, R. *Science* **2009**, *324*, 44-45.
 - (10) Du, P.; Knowles, K.; Eisenberg, R. *J. Am. Chem. Soc.* **2008**, *130*, 12576-12577.
 - (11) Kalyanasundaram, K.; Grätzel, M.; Pelizzetti, E. *Coord. Chem. Rev.* **1986**, *69*, 57-125.
 - (12) Dempsey, J. L.; Brunschwig, B. S.; Winkler, J. R.; Gray, H. B. *Acc. Chem. Res.* **2009**, *42*, 1995-2004.
 - (13) Smalley, R. E. *Mater. Res. Soc. Bull.* **2005**, *30*, 412-421.

- (14) *Electric Power Monthly*, U.S. Energy Information Administration **Oct. 2011**.
- (15) Walter, M. G.; Warren, E. L.; McKone, J. R.; Boettcher, S. W.; Mi, Q.; Santori, E. A.; Lewis, N. S. *Chem. Rev.* **2010**, *110*, 6446-6473.
- (16) Bard, A. J.; Fox, M. A. *Acc. Chem. Res.* **1995**, *28*, 141-145.
- (17) Lewis, N. S. *Nature* **2001**, *414*, 589-590.
- (18) Grätzel, M. *J. Photochem. Photobiol. C: Photochem. Rev.* **2003**, *4*, 145-153.
- (19) O'Regan, B.; Gratzel, M. *Nature* **1991**, *353*, 737-740.
- (20) Kalyanasundaram, K.; Grätzel, M. *Coord. Chem. Rev.* **1998**, *177*, 347-414.
- (21) Polo, A. S.; Itokazu, M. K.; Murakami Iha, N. Y. *Coord. Chem. Rev.* **2004**, *248*, 1343-1361.
- (22) McConnell, I.; Li, G.; Brudvig, G. W. *Chem. Biol.* **2010**, *17*, 434-447.
- (23) Herrero, C.; Lassalle-Kaiser, B.; Leibl, W.; Rutherford, A. W.; Aukauloo, A. *Coord. Chem. Rev.* **2008**, *252*, 456-468.
- (24) Puntoriero, F.; Sartorel, A.; Orlandi, M.; La Ganga, G.; Serroni, S.; Bonchio, M.; Scandola, F.; Campagna, S. *Coord. Chem. Rev.* **2011**, *255*, 2594-2601.
- (25) Lazarides, T.; McCormick, T.; Du, P.; Luo, G.; Lindley, B.; Eisenberg, R. *J. Am. Chem. Soc.* **2009**, *131*, 9192-9194.
- (26) McCormick, T. M.; Han, Z.; Weinberg, D. J.; Brennessel, W. W.; Holland, P. L.; Eisenberg, R. *Inorg. Chem.* **2011**, *50*, 10660-10666.
- (27) Sakai, K.; Ozawa, H. *Coord. Chem. Rev.* **2007**, *251*, 2753-2766.
- (28) Ozawa, H.; Haga, M.-a.; Sakai, K. *J. Am. Chem. Soc.* **2006**, *128*, 4926-4927.
- (29) Fujita, E. *Coord. Chem. Rev.* **1999**, *185-186*, 373-384.
- (30) Takeda, H.; Ishitani, O. *Coord. Chem. Rev.* **2009**, *254*, 346-354.
- (31) Hammarström, L.; Johansson, O. *Coord. Chem. Rev.* **2010**, *254*, 2546-2559.
- (32) Nazeeruddin, M. K.; Klein, C.; Liska, P.; Grätzel, M. *Coord. Chem. Rev.* **2005**, *249*, 1460-1467.
- (33) Spiccia, L.; Deacon, G. B.; Kepert, C. M. *Coord. Chem. Rev.* **2004**, *248*, 1329-1341.
- (34) Keyes, T. E.; Weldon, F.; Muller, E.; Pechy, P.; Gratzel, M.; Vos, J. G. *J. Chem. Soc., Dalton Trans.* **1995**, 2705-2706.
- (35) Lehn, J. M.; Sauvage, J. P. *Nouv. J. Chem.* **1977**, *1*, 449-450.
- (36) Kalyanasundaram, K.; Kiwi, J.; Grätzel, M. *Helv. Chim. Acta* **1978**, *61*, 2720-2730.

- (37) DeLaive, P. J.; Sullivan, B. P.; Meyer, T. J.; Whitten, D. G. *J. Am. Chem. Soc.* **1979**, *101*, 4007-4008.
- (38) Kiwi, J.; Gratzel, M. *Nature* **1979**, *281*, 657-658.
- (39) Brown, G. M.; Brunschwig, B. S.; Creutz, C.; Endicott, J. F.; Sutin, N. *J. Am. Chem. Soc.* **1979**, *101*, 1298-1300.
- (40) Amouyal, E.; Keller, P.; Moradpour, A. *J. Chem. Soc., Chem. Commun.* **1980**, 1019-1020.
- (41) Na, Y.; Wang, M.; Pan, J.; Zhang, P.; A. Kermark, B. R.; Sun, L. *Inorg. Chem.* **2008**, *47*, 2805-2810.
- (42) Rau, S.; Schäfer, B.; Gleich, D.; Anders, E.; Rudolph, M.; Friedrich, M.; Görls, H.; Henry, W.; Vos, J. G. *Angew. Chem. Int. Ed.* **2006**, *45*, 6215-6218.
- (43) Rau, S.; Walther, D.; Vos, J. G. *Dalton Trans.* **2007**, 915-919.
- (44) Tschierlei, S.; Karnahl, M.; Presselt, M.; Dietzek, B.; Guthmüller, J.; González, L.; Schmitt, M.; Rau, S.; Popp, J. *Angew. Chem. Int. Ed.* **2010**, *49*, 3981-3984.
- (45) Arachchige, S. M.; Brown, J.; Brewer, K. J. *J. Photochem. Photobiol. A: Chem.* **2008**, *197*, 13-17.
- (46) Elvington, M.; Brown, J.; Arachchige, S. M.; Brewer, K. J. *J. Am. Chem. Soc.* **2007**, *129*, 10644-10645.
- (47) Fihri, A.; Artero, V.; Razavet, M.; Baffert, C.; Leibl, W.; Fontecave, M. *Angew. Chem. Int. Ed.* **2008**, *47*, 564-567.
- (48) Youngblood, W. J.; Lee, S.-H. A.; Maeda, K.; Mallouk, T. E. *Acc. Chem. Res.* **2009**, *42*, 1966-1973.
- (49) Reisner, E.; Fontecilla-Camps, J. C.; Armstrong, F. A. *Chem. Commun.* **2009**, 550-552.
- (50) Reisner, E.; Powell, D. J.; Cavazza, C.; Fontecilla-Camps, J. C.; Armstrong, F. A. *J. Am. Chem. Soc.* **2009**, *131*, 18457-18466.
- (51) Armstrong, F. A.; Belsey, N. A.; Cracknell, J. A.; Goldet, G.; Parkin, A.; Reisner, E.; Vincent, K. A.; Wait, A. F. *Chem. Soc. Rev.* **2009**, *38*, 36-51.
- (52) Lakadamyali, F.; Reisner, E. *Chem. Commun.* **2011**, *47*, 1695-1697.
- (53) Ulbricht, C.; Beyer, B.; Friebe, C.; Winter, A.; Schubert, U. S. *Adv. Mat.* **2009**, *21*, 4418-4441.
- (54) Tinker, L. L.; McDaniel, N. D.; Bernhard, S. *J. Mater. Chem.* **2009**, *19*, 3328-3337.

- (55) King, K. A.; Watts, R. J. *J. Am. Chem. Soc.* **1987**, *109*, 1589.
- (56) Dixon, I. M.; Collin, J.-P.; Sauvage, J.-P.; Flamigni, L.; Encinas, S.; Barigelletti, F. *Chem. Soc. Rev.* **2000**, *29*, 385-391.
- (57) Slinker, J. D.; Gorodetsky, A. A.; Lowry, M. S.; Wang, J.; Parker, S.; Rohl, R.; Bernhard, S.; Malliaras, G. G. *J. Am. Chem. Soc.* **2004**, *126*, 2763-2767.
- (58) Neve, F.; Crispini, A.; Campagna, S.; Serroni, S. *Inorg. Chem.* **1999**, *38*, 2250-2258.
- (59) Slinker, J. D.; Gorodetsky, A. A.; Lowry, M. S.; Wang, J.; Parker, S.; Rohl, R.; Bernhard, S.; Malliaras, G. G. *J. Am. Chem. Soc.* **2004**, *126*, 2763-7.
- (60) Goldsmith, J. I.; Hudson, W. R.; Lowry, M. S.; Anderson, T. H.; Bernhard, S. *J. Am. Chem. Soc.* **2005**, *127*, 7502-7510.
- (61) Tinker, L. L.; McDaniel, N. D.; Curtin, P. N.; Smith, C. K.; Ireland, M. J.; Bernhard, S. *Chem. Eur. J.* **2007**, *13*, 8726-8732.
- (62) Cline, E. D.; Adamson, S. E.; Bernhard, S. *Inorg. Chem.* **2008**, *47*, 10378-10388.
- (63) Curtin, P. N.; Tinker, L. L.; Burgess, C. M.; Cline, E. D.; Bernhard, S. *Inorg. Chem.* **2009**, *48*, 10498-10506.
- (64) Metz, S.; Bernhard, S. *Chem. Commun.* **2010**, *46*, 7551-7553.
- (65) Gärtner, F.; Cozzula, D.; Losse, S.; Boddien, A.; Anilkumar, G.; Junge, H.; Schulz, T.; Marquet, N.; Spannenberg, A.; Gladiali, S.; Beller, M. *Chem. Eur. J.* **2011**, *17*, 6998-7006.
- (66) Fihri, A.; Artero, V.; Pereira, A.; Fontecave, M. *Dalton Trans.* **2008**, 5567-5569.
- (67) DiSalle, B. F.; Bernhard, S. *J. Am. Chem. Soc.* **2011**, *133*, 11819-11821.
- (68) Tinker, L. L.; Bernhard, S. *Inorg. Chem.* **2009**, *48*, 10507-10511.
- (69) Probst, B.; Kolano, C.; Hamm, P.; Alberto, R. *Inorg. Chem.* **2009**, *48*, 1836-1843.
- (70) Alstrum-Acevedo, J. H.; Brennaman, M. K.; Meyer, T. J. *Inorg. Chem.* **2005**, *44*, 6802-6827.
- (71) Mandler, D.; Willner, I. *J. Chem. Soc., Perkin Trans. 2* **1988**, 997-1003.
- (72) Wenger, O. S. *Coord. Chem. Rev.* **2009**, *253*, 1439-1457.
- (73) Morris, A. J.; Meyer, G. J.; Fujita, E. *Acc. Chem. Res.* **1982**, *42*, 1983-1994.
- (74) Grills, D. C.; Fujita, E. *J. Phys. Chem. Lett.* **1982**, *1*, 2709-2718.
- (75) Morris, A. J.; Meyer, G. J.; Fujita, E. *Acc. Chem. Res.* **1992**, *42*, 1983-1994.

- (76) Coleman, A.; Brennan, C.; Vos, J. G.; Pryce, M. T. *Coord. Chem. Rev.* **2008**, 252, 2585-2595.
- (77) Hawecker, J.; Lehn, J.-M.; Ziessel, R. *J. Chem. Soc., Chem. Commun.* **1983**, 536-538.
- (78) Ziessel, R.; Hawecker, J.; Lehn, J.-M. *Helv. Chim. Acta* **1986**, 69, 1065-1084.
- (79) Tinnemans, A. H. A.; Koster, T. P. M.; Thewissen, D. H. M. W.; Mackor, A. *Recueil des Travaux Chimiques des Pays-Bas* **1984**, 103, 288-295.
- (80) Méndez, M. A.; Voyame, P.; Girault, H. H. *Angew. Chem.* **2011**, 123, 7529-7532.
- (81) Kimura, E.; Bu, X.; Shionoya, M.; Wada, S.; Maruyama, S. *Inorg. Chem.* **1992**, 31, 4542-4546.
- (82) Grant, J. L.; Goswami, K.; Spreer, L. O.; Otvos, J. W.; Calvin, M. *J. Chem. Soc., Dalton Trans.* **1987**, 2105-2109.
- (83) Mochizuki, K.; Manaka, S.; Takeda, I.; Kondo, T. *Inorg. Chem.* **1996**, 35, 5132-5136.
- (84) Ishida, H.; Terada, T.; Tanaka, K.; Tanaka, T. *Inorg. Chem.* **1990**, 29, 905-911.
- (85) Matsuoka, S.; Kohzuki, T.; Pac, C.; Ishida, A.; Takamuku, S.; Kusaba, M.; Nakashima, N.; Yanagida, S. *J. Phys. Chem.* **1992**, 96, 4437-4442.
- (86) Ishida, H.; Tanaka, K.; Tanaka, T. *Organometallics* **1987**, 6, 181-186.
- (87) Willner, I.; Maidan, R.; Mandler, D.; Duerr, H.; Doerr, G.; Zengerle, K. *J. Am. Chem. Soc.* **1987**, 109, 6080-6086.
- (88) Maidan, R.; Willner, I. *J. Am. Chem. Soc.* **1986**, 108, 8100-8101.
- (89) Lehn, J.-M.; Ziessel, R. *J. Organomet. Chem.* **1990**, 382, 157-173.
- (90) Ishitani, O.; George, M. W.; Ibusuki, T.; Johnson, F. P. A.; Koike, K.; Nozaki, K.; Pac, C.; Turner, J. J.; Westwell, J. R. *Inorg. Chem.* **1994**, 33, 4712-4717.
- (91) Hori, H.; P. A. Johnson, F.; Koike, K.; Takeuchi, K.; Ibusuki, T.; Ishitani, O. *J. Chem. Soc., Dalton Trans.* **1997**, 1019-1024.
- (92) Takeda, H.; Koike, K.; Inoue, H.; Ishitani, O. *J. Am. Chem. Soc.* **2008**, 130, 2023-2031.
- (93) Wong, W.-L.; Cheung, K.-C.; Chan, P.-H.; Zhou, Z.-Y.; Lee, K.-H.; Wong, K.-Y. *Chem. Commun.* **2007**, 2175-2177.
- (94) Bian, Z.-Y.; Sumi, K.; Furue, M.; Sato, S.; Koike, K.; Ishitani, O. *Dalton Trans.* **2009**, 983-993.

- (95) Bian, Z.-Y.; Sumi, K.; Furue, M.; Sato, S.; Koike, K.; Ishitani, O. *Inorg. Chem.* **2008**, *47*, 10801-10803.
- (96) Morris, A. J.; Meyer, G. J.; Fujita, E. *Acc. Chem. Res.* **2009**, *42*, 1983-1994.
- (97) Thompson, D. T. *Coord. Chem. Rev.* **1996**, *154*, 179-192.
- (98) Macyk, W.; Franke, A.; Stochel, G. *Coord. Chem. Rev.* **2005**, *249*, 2437-2457.
- (99) Mägerlein, W.; Dreisbach, C.; Hugl, H.; Tse, M. K.; Klawonn, M.; Bhor, S.; Beller, M. *Catal. Today* **2007**, *121*, 140-150.
- (100) Oyama, S. T.; Oyama, S. T. In *Mechanisms in Homogeneous and Heterogeneous Epoxidation Catalysis*; Elsevier: Amsterdam, 2008.
- (101) Pellegrin, Y.; Le Pleux, L.; Blart, E.; Renaud, A.; Chavillon, B.; Szuwarski, N.; Boujtita, M.; Cario, L.; Jobic, S.; Jacquemin, D.; Odobel, F. *J. Photochem. Photobiol. A: Chem.* **2011**, *219*, 235-242.
- (102) Coates, C. G.; Keyes, T. E.; McGarvey, J. J.; Hughes, H. P.; Vos, J. G.; Jayaweera, P. M. *Coord. Chem. Rev.* **1998**, *171*, 323-330.
- (103) Kim, M.-J.; Konduri, R.; Ye, H.; MacDonnell, F. M.; Puntoriero, F.; Serroni, S.; Campagna, S.; Holder, T.; Kinsel, G.; Rajeshwar, K. *Inorg. Chem.* **2002**, *41*, 2471-2476.
- (104) Fagalde, F.; Katz, N. E. *Polyhedron* **1995**, *14*, 1213-1220.
- (105) Ardo, S.; Sun, Y.; Staniszewski, A.; Castellano, F. N.; Meyer, G. J. *J. Am. Chem. Soc.* **2010**, *132*, 6696-6709.
- (106) Hoertz, P. G.; Staniszewski, A.; Marton, A.; Higgins, G. T.; Incarvito, C. D.; Rheingold, A. L.; Meyer, G. J. *J. Am. Chem. Soc.* **2006**, *128*, 8234-8245.
- (107) Whitten, D. G. *Acc. Chem. Res.* **1980**, *13*, 83-90.
- (108) Tschierlei, S.; Presselt, M.; Kuhnt, C.; Yartsev, A.; Pascher, T.; Sundström, V.; Karnahl, M.; Schwalbe, M.; Schäfer, B.; Rau, S.; Schmitt, M.; Dietzek, B.; Popp, J. *Chem. Eur. J.* **2009**, *15*, 7678-7688.

Chapter 2

Synthesis and characterisation of ruthenium(II) based mononuclear precursors

Chapter 2 introduces derivatisation at the 4 and 4' positions of the 2,2'-bipyridine ligand and different synthetic procedures for ruthenium(II) dichloride complex containing bis-4,4'-diethoxycarbonyl-2,2'-bipyridine. This chapter describes the stability of these ester groups under different conditions by performing a series of experiments. This chapter also introduces some novel bridging ligands, their synthesis and optimisation of the reaction conditions employed in their synthesis. Different synthetic paths have been investigated to prepare these bridging ligands and their corresponding mononuclear ruthenium complexes. This chapter also shows how deuteration is an important tool when interpreting complex NMR spectra for polypyridyl complexes.

2.1. Introduction

Ruthenium mononuclear complexes containing different types of polypyridyl ligands hold much interest because of their interesting photo-physical properties.¹⁻⁷ The results obtained in this thesis show that the MLCT transition can be tuned by introducing derivatised polypyridyl ligands. Such polypyridyl ruthenium mononuclear precursors are used as building blocks in light harvesting units in solar energy transfer,⁷⁻¹¹ photo splitting of water,¹²⁻¹⁴ DSSC solar cells,¹¹ generation of solar hydrogen from water¹⁴⁻¹⁷ and photo reduction of CO₂.^{18,19} These types of photocatalysis are sub divided into two types, i) intermolecular photocatalysis and ii) *intramolecular* photocatalysis. In both cases catalytic metal centres are involved. A detailed discussion about these photocatalytic processes is provided in **Chapter 1**. The ultimate aim was to synthesis hetero di-nuclear photo-catalysts which can be bound to the surface of semiconductors as was previously discussed in **Chapter 1**.

Ruthenium precursors are an important part of heterodinuclear photocatalysts. In this study, bpy ligands need to be derivatised with an anchoring group such that the whole heterodinuclear catalyst will be bound to the surface of semiconductor. To follow this principle, the carboxy group was considered as a good anchoring group based on Gratzel's cell.^{20,21} There are some crucial steps involved in the synthesis of these types of mononuclear units; **a)** derivatisation of the 2,2'-bipyridine ligand, **b)** synthesis of different types of [Ru(L)₂Cl₂] ; L = 2,2'-bipyridine (bpy), (d₈)-2,2'-bipyridine (d₈-bpy) and diethyl 2,2'-bipyridine-4,4'-dicarboxylate (dceb) (**Figure 2.1**) **c)** synthesis of bis-(bidentate) bridging ligands (**Figure 2.2**) and **d)** synthesis of mononuclear complexes which involves a reaction between [Ru(L)₂Cl₂] and a bridging ligand.

¹H NMR spectra of these mononuclear complexes are complex in nature. The NMR peaks can't be assigned without 2D H-H COSY NMR or without the aid of partially deuteriated complexes in which the peripheral 'bpy' ligands are deuteriated. The idea behind the deuteriation in this particular example is the assignment of the protons of the coordinated bridging ligand. Hence, each proton in the mononuclear complex can be assigned by comparing the ¹H NMR spectrum of the partially deuteriated mononuclear complex. These partially mononuclear complexes can be

studied further for their photo-physical and photo-catalytic properties. Few examples of the $[\text{Ru}(\text{L})_2\text{Cl}_2]$ type complexes are shown in **Figure 2.1** where L = 2,2'-bipyridine (bpy), (d_8)-2,2'-bipyridine (d_8 -bpy) and diethyl 2,2'-bipyridine-4,4'-dicarboxylate (dceb)

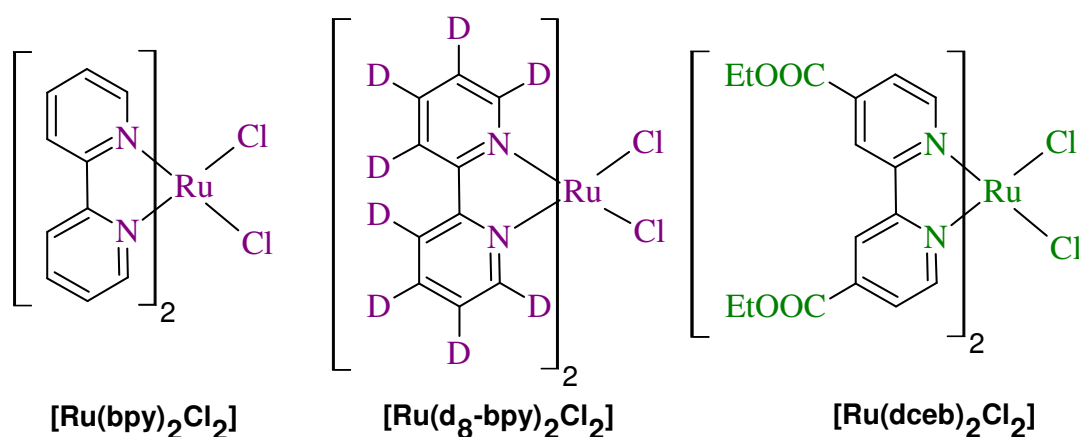


Figure 2.1: Molecular structure of different types of $[\text{Ru}(\text{L})_2\text{Cl}_2]$ where L = 2,2'-bipyridine (bpy), (d_8)-2,2'-bipyridine (d_8 -bpy) and diethyl 2,2'-bipyridine-4,4'-dicarboxylate (dceb)

Bridging ligands play an important role in these types of intra-molecular photo-catalytic systems. Four different bridging ligands are introduced in this Chapter. The structures and abbreviations for the ligands cited in this chapter are shown in **Figure 2.2**.

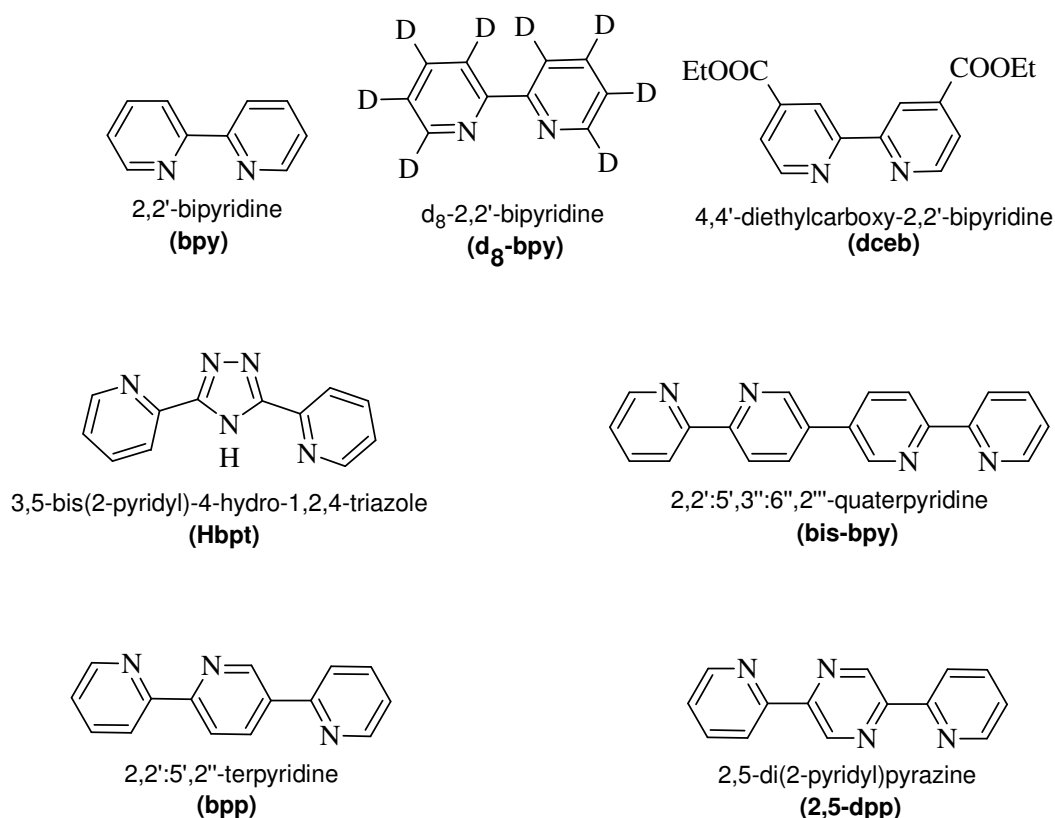


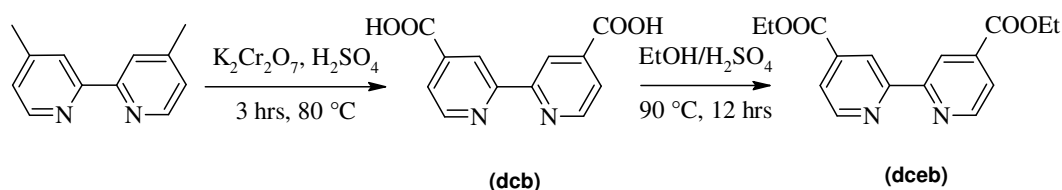
Figure 2.2: List of ligands and their abbreviations as cited in this thesis.

Considering the bridging ligands, bpp is a specific kind of bridging ligand which has both $N^{\wedge}N$ and $N^{\wedge}C$ coordination sites. This combination of coordinating sites is unique compared to the other three bridging ligands containing two $N^{\wedge}N$ coordinating sites (2,5-dpp and bisbpy). The formation of Ru-Ru dinuclear complexes is reduced to 0% since ruthenium does not form cyclometallated complexes under normal ethanol/water/reflux conditions, and thereby only the desired mononuclear complex is obtained. Compared to the three other bridging ligands, bpp may behave differently when it is bound to the catalytic metallic site. The catalytic metal is cyclometallated, which introduces a negatively charged carbon.

2.2. Synthetic procedures for organic ligands

2.2.1. Synthetic procedure for the esterification of 2,2'-bipyridine

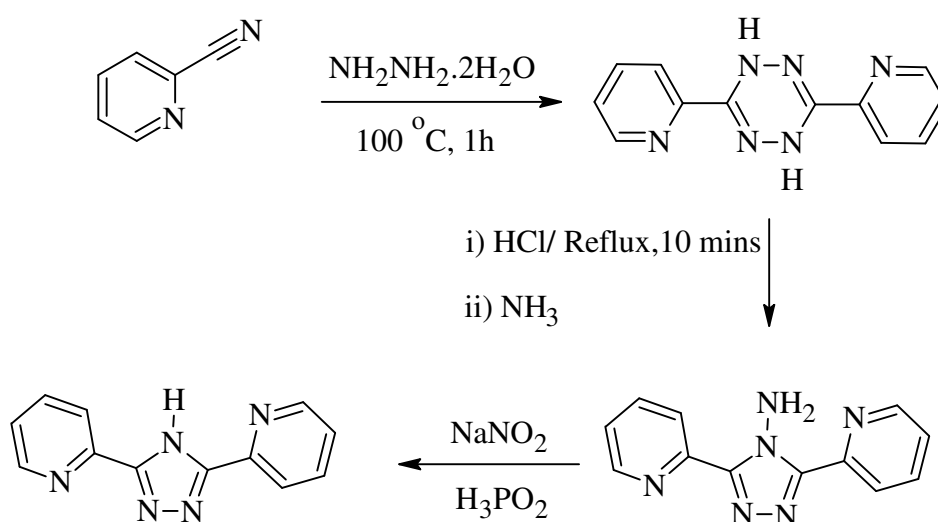
There are several general synthetic procedures for derivatising the 2,2'-bipyridine ligand at its different positions.^{22,23} Synthesis of 4,4'-diethoxycarbonyl-2,2'-bipyridine(dceb) is already reported.^{24,25} It can be synthesised from pyridine or the 4-methylpyridine molecule. There are several synthetic procedures to synthesise 2,2'-bipyridine and 4,4'-dimethyl-2,2'-bipyridine. 4,4'-dimethyl-2,2'-bipyridine was synthesised from 4-picoline following a coupling reaction with Pd/C. The next step is oxidation of 4,4'-dimethyl-2,2'-bipyridine to form 4,4'-dicarboxy-2,2'-bipyridine (dcb) and finally esterification of these carboxylic groups. Oxidation of the methyl group can be carried out by KMnO_4 ²⁶ and by $\text{K}_2\text{Cr}_2\text{O}_7$.²⁷ All these oxidation processes are well known but the most efficient process is the oxidation using $\text{K}_2\text{Cr}_2\text{O}_7/\text{H}_2\text{SO}_4$ as high yields (up to 98%)^{28,29} are obtained. There is however an issue from the safety point of view. $\text{K}_2\text{Cr}_2\text{O}_7$ is known as a very strong oxidising agent and potentially carcinogenic in nature, and needs careful handling. 4,4'-dicarboxylato-2,2'-bipyridine (dcb) has poor solubility characteristics. The dcb obtained after the reaction is slightly yellowish because of remaining Cr(III). So the yellowish crude product was heated at reflux with 50% HNO_3 to remove Cr(III) from the crude product and a white product was obtained. Removal of Cr(III) can also be done by dissolving the crude product in aq. NaOH solution and then reprecipitation by dilute HCl. Esterification was performed by the well known acid catalysed procedure, EtOH/ H_2SO_4 .³⁰ The work-up process needs careful balancing of pH as the ester dissolves quickly if the pH goes slightly higher than 8. The reaction scheme is shown in **Scheme 2.1**.



Scheme 2.1: Synthetic procedure of 4,4'-diethoxycarboxy-2,2'-bipyridine(dceb)

2.2.2. Synthetic procedure for 3,5-bis(2-pyridyl)-4-hydro-1,2,4-triazole(Hbpt)

Hbpt was synthesised following the literature procedure. One change was performed in an attempt to improve the yield, but unfortunately the yield was the same as that reported in the literature.^{31,32} H_3PO_2 was introduced in the last step of the synthesis instead of reacting with HCl .³³ The synthetic sequence for synthesising Hbpt is shown below in **Scheme 2.2**. ^1H NMR data of Hbpt is provided in the experimental part (**Section 2.6**).



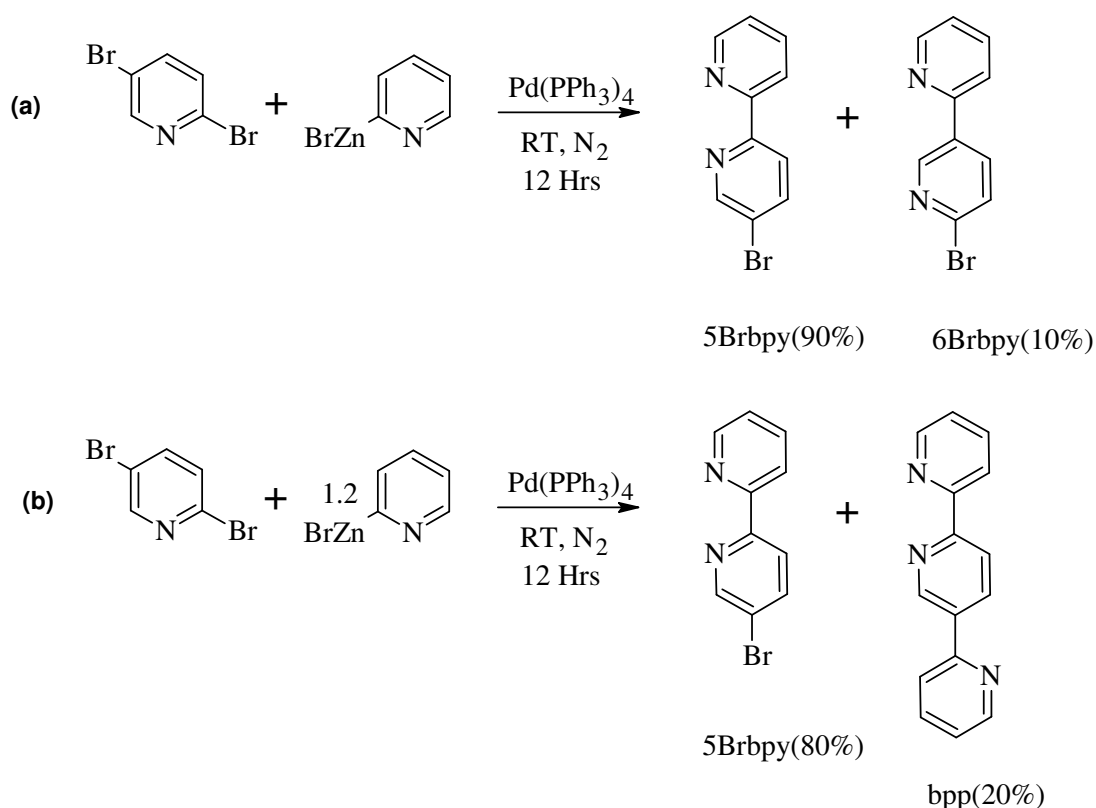
Scheme 2.2: Synthetic route for 3,5-bis(2-pyridyl)-4-hydro-1,2,4-triazole(Hbpt)

2.2.3. Synthetic procedures for 5-bromo-2,2'-bipyridine(5Brbpy) and 2,2':5',2''-terpyridine (bpp)

5-bromo-2,2'-bipyridine (5Brbpy) was obtained by Negishi coupling which is a $\text{Pd}(0)$ catalysed reaction.^{23,34-37} 2-Pyridylzincbromide and 2,5-dibromopyridine were reacted to obtain 5Brbpy. The literature procedure was modified to increase the yield of the product. The modification involves keeping the reaction flask between 0-4 °C after adding $\text{Pd}(\text{PPh}_3)_4$ and 2,5-dibromopyridine. Then, 2-pyridylzincbromide (in THF) was added slowly to the reaction mixture (which was kept in an ice bath) because 2-pyridylzincbromide has a flash point of -17 °C. After the addition of the 2-pyridylzincbromide solution the ice bath was removed. A nitrogen atmosphere was

maintained throughout the reaction since $\text{Pd}(\text{PPh}_3)_4$ is easily oxidised by air. The reaction was carried out for 12 hours under a nitrogen atmosphere. The yield of the reaction was reduced if fresh catalyst was not used. The reaction mixture was then added to an aqueous solution of EDTA/ NaCO_3 to remove ZnBr_2 which forms a water soluble Zn/EDTA complex. The product was extracted with DCM. This reaction produces two isomers, 5Brbpy (Yield-90 %) and 6'-bromo-2,3'-bipyridine(6Brbpy) (Yield-10%) (See **Scheme 2.3**) as determined by TLC and NMR spectroscopy. 5Brbpy was further purified using a neutral alumina column. The yield obtained was 80-85%.

A third spot was observed on the TLC plate when the above reaction was carried out with a slight excess of 2-pyridylzincbromide. The ^1H NMR showed a product with 11 protons that was identified as 2,2':5',2''-terpyridine(bpp). The reason for the formation of bpp is related to 6'-bromo-2,3'-bipyridine(6Brbpy) which is more reactive than 5-bromo-2,2'-bipyridine(5Brbpy) since the bromine is ortho to the nitrogen atom of the pyridyl ring in 6Brbpy. Based on this observation the reaction was carried out with an excess of 2-pyridylzincbromide which further reacts with 6Brbpy by a second catalytic cycle producing 2,2':5',2''-terpyridine(bpp).

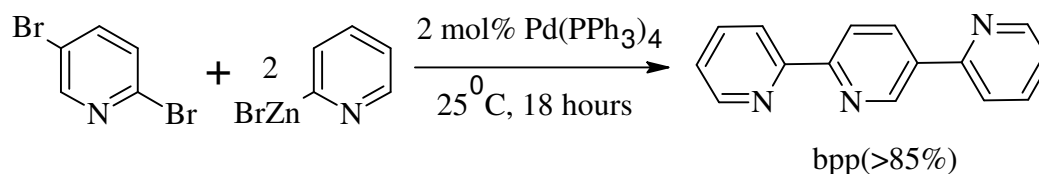


Scheme 2.3: The first reaction (a) introduces the synthesis of 5-bromo-2,2'-bipyridine(5Brbpy). Reaction (b) shows the different products obtained if a slight excess of pyridylzincbromide was reacted with 2,5-dibromopyridine.

Interestingly 2,2':5',2''-terpyridine(bpp) itself can be a very useful bridging ligand for synthesizing Ru-Pd, Ru-Pt, Ir-Pd and Ir-Pt hetero dinuclear catalysts. Therefore, 2,2':5',2''-terpyridine(bpp) was synthesised using two synthetic procedures to understand the mechanism and optimise the reaction conditions. The synthetic paths are as follows.

Method 1:

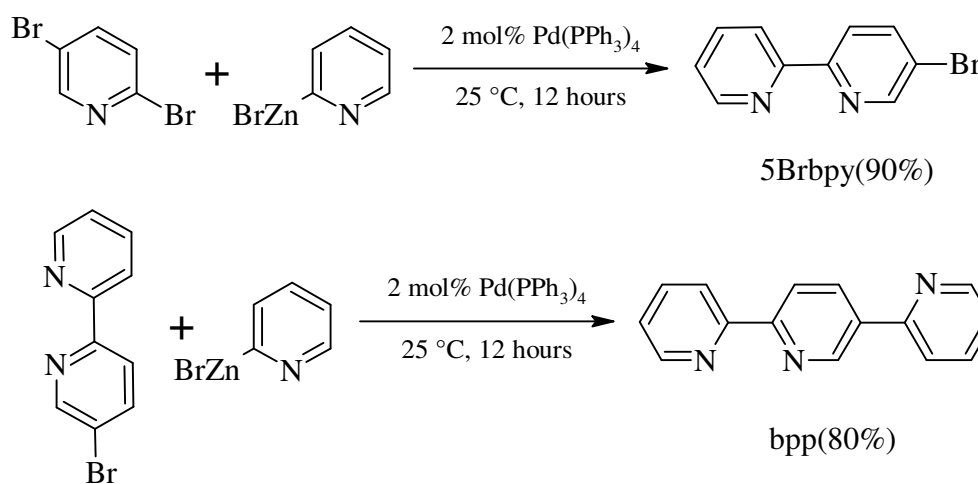
In this approach bpp was synthesised in one step procedure. Two equivalents of 2-pyridylzincbromide were reacted with one equivalent of 2,5-dibromopyridine. The product forms via two catalytic cycles. In the first catalytic cycle, 90% 5Brbpy and 10% of 6Brbpy were formed. In the second catalytic cycle both the isomers acted as aryl halides and coupled with the remaining 2-pyridylzincbromide and yielded more than 85% of the final product 2,2':5',2''-terpyridine(bpp).



Reaction 2.1: Method 1 reaction scheme for synthesising 2,2':5',2''-terpyridine(bpp)

Method 2

In this approach bpp was prepared in a two step procedure. In the first step 5-bromo-2,2'-bipyridine(5Brbpy) was synthesised by reacting one equivalent of 2,5-dibromopyridine with one equivalent of 2-pyridylzincbromide. The yield for this step was ~90%. 5Brbpy was then purified by column chromatography. In the second step, one equivalent of 5Brbpy was further reacted with one equivalent of 2-pyridylzincbromide to obtain the final product as bpp. The yield for the second step was ~80%. The over all yield of bpp using Method 2 is 75%.



Scheme 2.4: Method 2 reaction schemes for synthesising 2,2':5',2''-terpyridine(bpp) in a 2 step procedure.

The product 2,2':5',2''-terpyridine(bpp) obtained by two methods were identified by ^1H NMR, 2D H-H COSY NMR and CHN analysis. It can be therefore

concluded that the overall yield of 2,2':5',2''-terpyridine(bpp) obtained in Method 2 is less than the product obtained in Method 1. Also Method 2 consumes twice the amount of catalyst and requires a longer reaction time, as opposed to Method 1 where a greater yield was obtained, with the use of half the amount of catalyst. So the preferred synthetic route was Method 1 which is a one step procedure producing better yields in less time.

The above investigation suggests that bpp was formed by a two step catalytic process. The catalyst used in Method 1 acted twice in the catalytic process to form 2,2':5',2''-terpyridine(bpp). Therefore, it can be concluded that the reaction pathway in Method 1 contains two catalytic cycles. A proposed reaction pathway for Method 1 is shown in **Figure 2.3**.

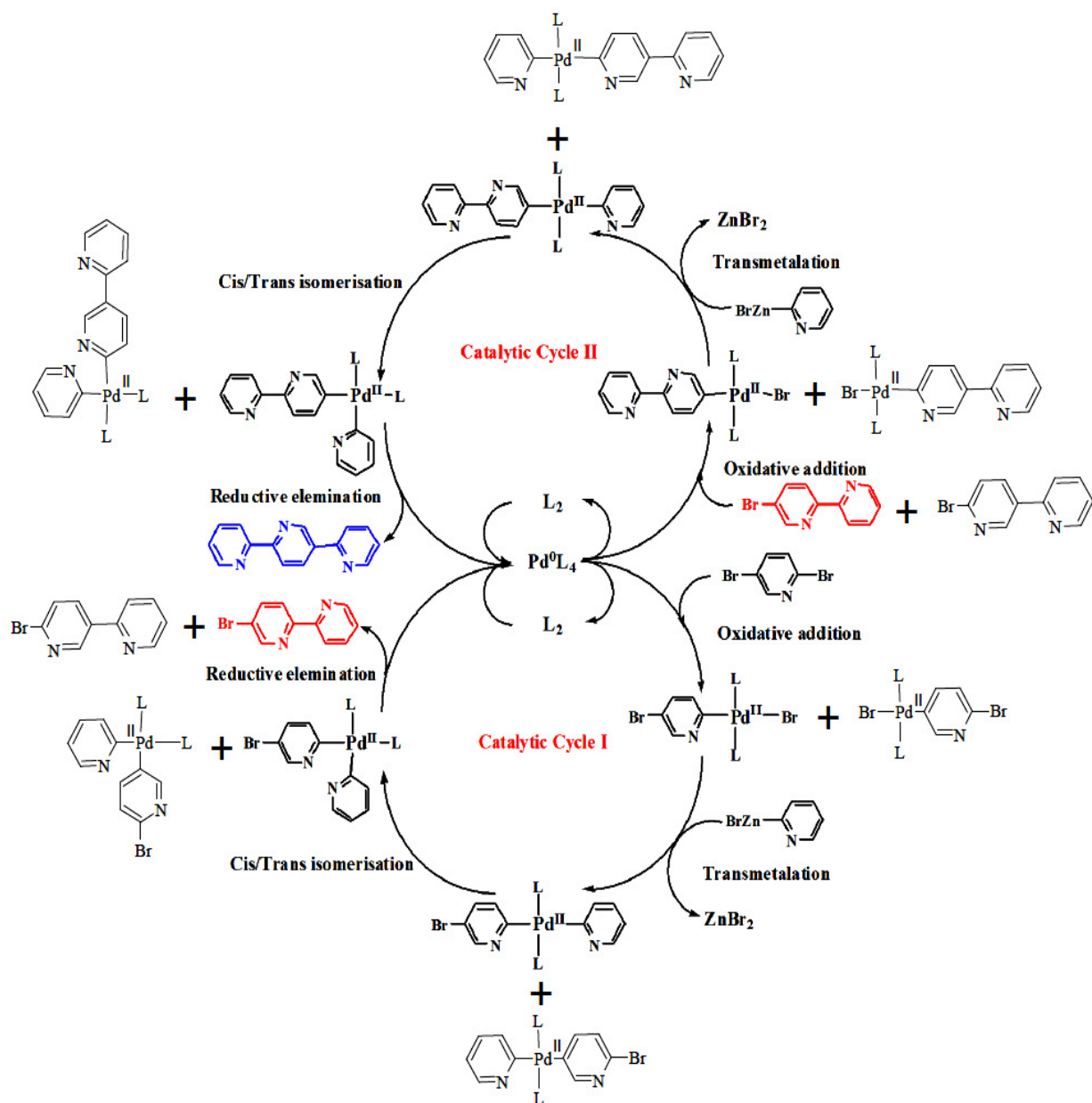
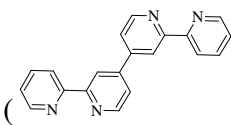
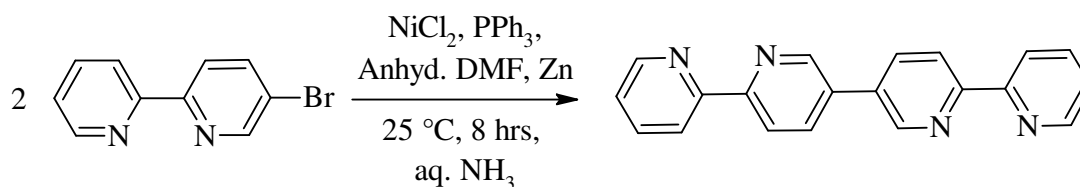


Figure 2.3: The proposed reaction pathway for Method 1.

2.2.4. Synthetic procedure for 2,2':5',3'':6'',2'''-quaterpyridine (bisbpy)

The reported synthesis for the related 2,2':4',4'':2'',2'''-quaterpyridine ligand () requires expensive starting materials (boronic acid derivative of 2,2'-bipyridine) and catalysts ($[\text{Pd}(\text{PPh}_3)_4]$).³⁸ An alternative procedure was therefore developed. This approach describes the synthetic route for synthesising Ru-Ru and Ru-Os dinuclear complexes with 2,2':5',3'':6'',2'''-quaterpyridine(bisbpy) as the bridging ligand. Here, 2,2':5',3'':6'',2'''-quaterpyridine(bisbpy) based complexes were obtained using a Ni(0) catalysed homo-coupling¹⁴⁻¹⁵ reaction.



Reaction 2.2: Synthesis of 2,2':5',3'':6'',2'''-quaterpyridine(bisbpy) using Ni(0) catalysed Ullman type homo coupling.

Ni(0) catalysed Ullman type coupling^{39,40} generally requires anhydrous conditions. Anhydrous DMF was therefore used as solvent. The reaction was completed in 8 hours at room temperature and followed by TLC. 20% of triphenylphosphine oxide ($\text{Ph}_3\text{P}=\text{O}$) was found as an impurity in the product, formed during the work up carried out in aqueous NH_3 . It was difficult to remove this impurity as it was sticky in nature. A low yield was obtained after the purification which involved column chromatography using hexane/ethylacetate solvents (9:1) (yield 35%). So, two alternative procedures were performed to purify the product.

- 1) Careful recrystallisation from a DCM/hexane solution.
- 2) Washing with hexane.

If both the above purification procedures are compared, procedure **2** was better than the procedure **1** as the purification performed by procedure **1** always had an impurity which can be seen in ^1H NMR at 7.5-7.65 ppm due to the oxidative product of tri-phenylphosphine. However, this impurity was removed by several washing with hexane following procedure **2**. The overall yield of the product obtained by washing with hexane was greater than that obtained with the recrystallisation procedure (procedure **1**).

The NMR data of all ligands prepared are shown in the experimental part (Section 2.7). All ligands were characterised by ^1H NMR, H-H 2D COSY NMR and CHN analysis.

2.3. Synthetic procedures for metal complexes

2.3.1. Synthetic procedures for $[\text{Ru}(\text{dceb})_2\text{Cl}_2]$

The synthesis of the light harvesting ruthenium moiety with bpy ligands having two carboxylate groups is not straightforward. The traditional synthetic procedure for $[\text{Ru}(\text{bpy})_2\text{Cl}_2] \cdot 2\text{H}_2\text{O}$ in DMF with LiCl at reflux temperature for 8 hours³² was found not to be suitable for the carboxylate ester groups. Matthias *et al.* have reported a microwave assisted synthesis of $[\text{Ru}(\text{dcmb})_2\text{Cl}_2]$ (dcmb = 4,4'-dimethylcarboxy-2,2'-bipyridine) in good yields (95%) and high purity where the methyl group was introduced for the protection of the carboxy group.⁴¹ The stickiness and solubility problems of these ruthenium complexes containing carboxy groups can be avoided by protecting the carboxy groups by esterification.¹⁷ Hou *et al.* have also reported a synthetic procedure to synthesise $[\text{Ru}(\text{dceb})_2\text{Cl}_2]$ (dceb = 4,4'-diethylcarboxy-2,2'-bipyridine) which involved refluxing in ethanol under a nitrogen atmosphere for 3 days⁴². In this thesis a new synthetic route has been developed for synthesising $[\text{Ru}(\text{dceb})_2\text{Cl}_2]$ in 1 hour with a yield of 70%.

The first trial reaction for $[\text{Ru}(\text{dceb})_2\text{Cl}_2]$ was performed in anhydrous DMF at reflux temperature under a nitrogen atmosphere for 8 hours in the presence of LiCl. The reaction mixture turned dark green when the addition of ligand was completed. This reaction was not completed in 8 hours because un-reacted dceb ligand was found

in the ^1H NMR spectrum. A large amount of a greenish brown impurity (may be side products) was formed which was insoluble in most of the organic solvents e.g. ethanol, DCM, acetone and acetonitrile so it was not possible to identify. The ^1H NMR spectra of the product recrystallised from acetone solution also contained many impurities which may be due to the presence of hydrolysed products. It is possible that the ester groups may undergo hydrolysis at high temperature for long reaction times. It was difficult to check if the reaction was completed by simple TLC as the reaction mixture was in DMF. IR data showed a band around $1900\text{--}2000\text{ cm}^{-1}$ which clearly indicated the presence of $[\text{Ru}(\text{dceb})_2(\text{CO})\text{Cl}]$ in the product because of the decomposition of DMF to CO at high temperature. Modified reaction conditions were desirable so as to improve the yield. Furthermore at high temperatures in DMF, ester groups may also undergo hydrolysis. LiCl may be another cause of hydrolysis of the ester groups because of the basic reaction conditions. So two changes were made in the above procedure:

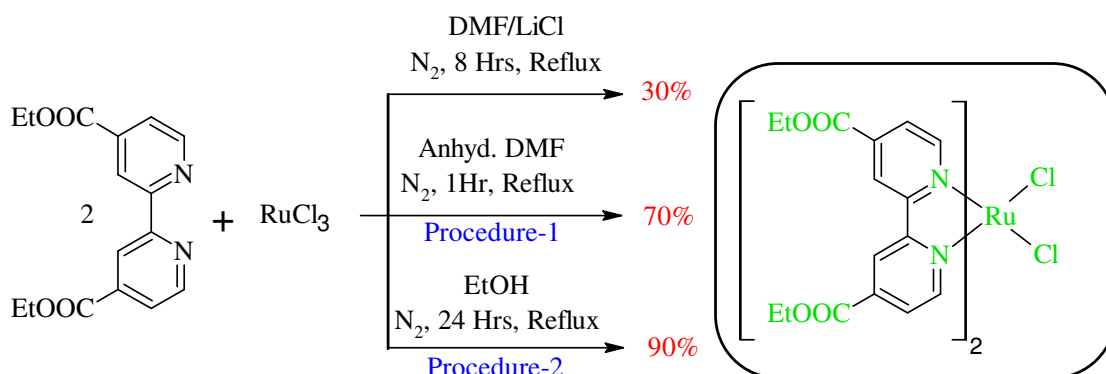
1. The use of anhydrous DMF instead of using reagent-grade normal DMF.
2. No LiCl was used

The reaction was again performed strictly under inert conditions. The temperature of the reaction is an important parameter. It had been observed that if the reaction was carried out at $>150\text{ }^\circ\text{C}$ the reaction mixture turned slightly brown and less product was obtained.

RuCl_3 was first dissolved completely in anhydrous DMF for 10 minutes under a nitrogen atmosphere. The decb was dissolved in anhydrous DMF and carefully added to the reaction mixture slowly over 30 minutes. The reaction was carried out for another 30 minutes after the addition of the dceb and there was no indication of the formation of the ruthenium carbonyl complex (checked by IR). Direct recrystallisation from acetone solution gave a high yield ($\sim 70\%$). From the ^1H NMR spectra (**Figure 2.4**) it can be inferred that no free ligand was present in the product.

One of the reported synthetic procedures to prepare $[\text{Ru}(\text{dceb})_2\text{Cl}_2]$ involves 3 days heating at reflux temperature in ethanol.⁴² In our hands the reaction was completed within 24 hours using more solvent and yielded $\sim 90\%$ of product with

high purity. From the ^1H NMR spectra (**Figure 2.4** and **Figure 2.5**) it was confirmed that the product obtained from the aforesaid two procedures was the same. The procedure involving ethanol as a solvent has lots of advantages. The percentage yield obtained was higher than when the experiment carried out in anhydrous DMF.



Scheme 2.5: Reaction Schemes for synthesising $[\text{Ru}(\text{dceb})_2\text{Cl}_2]$

There was no evidence for the formation of a ruthenium carbonyl complex as a by-product. From the yield (~90%), it can be concluded that the ester groups are highly stable under these conditions and only a small amount of the product (~10%) may be hydrolysed or forms $[\text{Ru}(\text{dceb})_2(\text{Cl})(\text{H}_2\text{O})]$. The work up for this procedure (in ethanol) was considerably easy. First, the solvent was removed by rotary evaporation and the product was washed with diethyl ether to remove the unreacted dceb and then with water to remove water soluble side products and impurities. In the ^1H NMR there was no sign of unreacted dceb ligand, but a small peak for the DMF proton at 7.95 ppm (in procedure 1, see **Figure 2.4**) which could be removed by repeated washing with diethyl ether. ^1H NMR spectra of the products obtained from both procedures (DMF, EtOH as solvent) were found to be identical in nature.

From the above discussion it can be concluded that $[\text{Ru}(\text{dceb})_2\text{Cl}_2]$ can be synthesised using two different synthetic procedures.

1. Using anhydrous DMF as solvent (**Procedure-1**)
2. Using EtOH as solvent (**Procedure-2**)

Procedure-2 is a comparatively better procedure than **Procedure-1**. **Procedure-1** involves DMF (boiling point 151 °C) as solvent which is a known mutagen whereas EtOH has a comparatively low boiling point (78 °C) and not harmful. Even though **Procedure-2** requires long reaction times than **Procedure-1**, superior yields were obtained with a less complicated work up procedure.

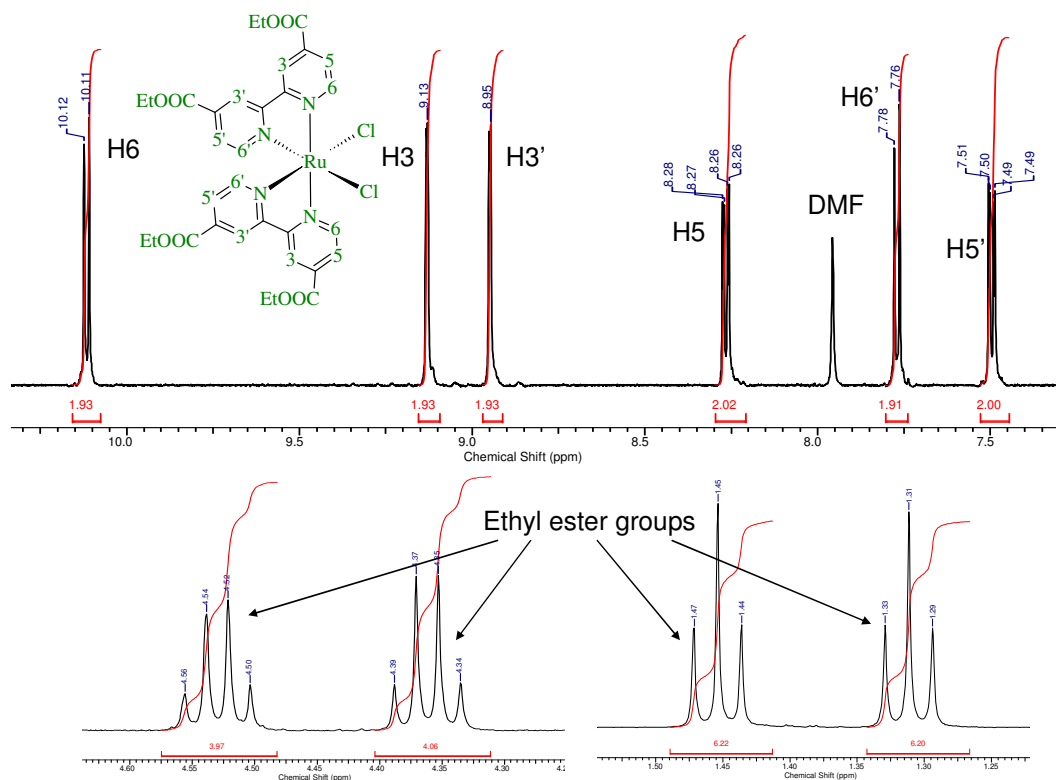


Figure 2.4: ^1H NMR (400 MHz, DMSO-d_6) of $[\text{Ru}(\text{dceb})_2\text{Cl}_2]$ obtained from the reaction in which anhydrous DMF was used as solvent.

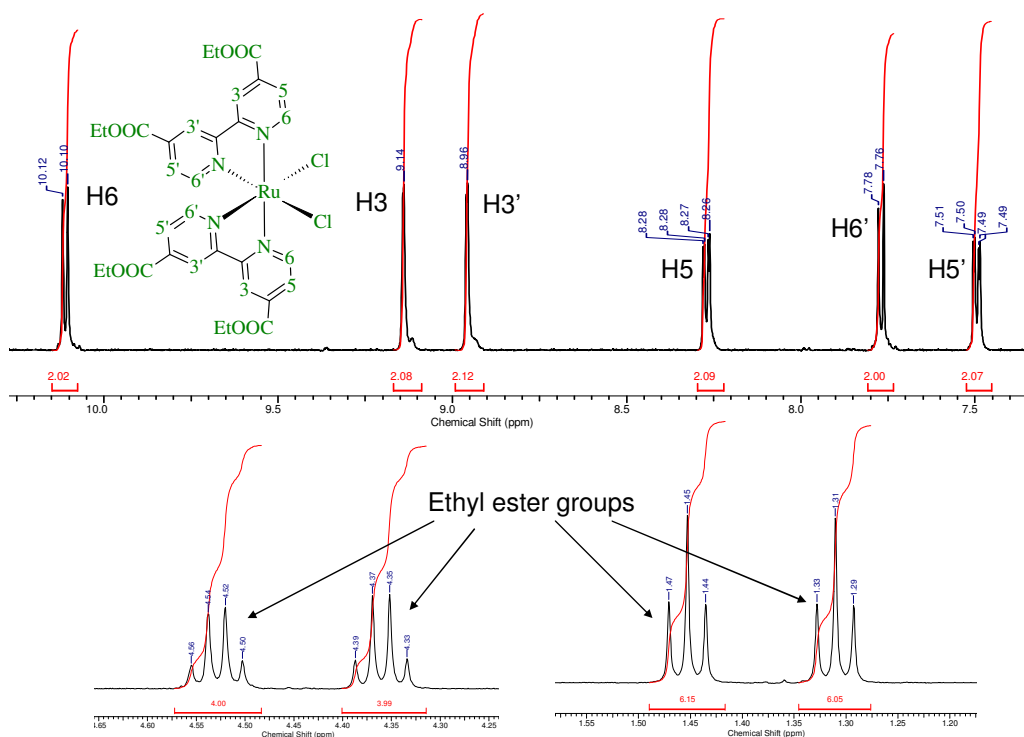
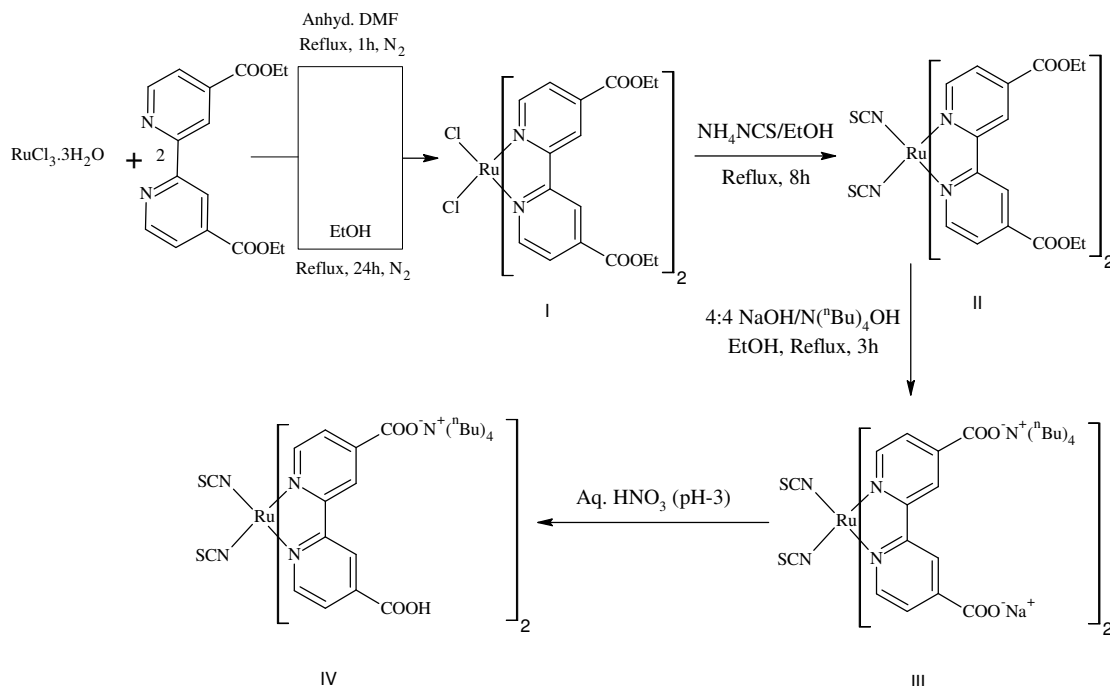


Figure 2.5: ^1H NMR (400 MHz, DMSO-d_6) of $[\text{Ru}(\text{dceb})_2\text{Cl}_2]$ obtained from the reaction in which ethanol was used as solvent.

2.3.2. Stability of ester groups in $[Ru(dceb)_2Cl_2]$

In the last section an improved (See **Scheme 2.6**) synthesis for $[Ru(dceb)_2Cl_2]$ was discussed.



Scheme 2.6: Complete optimised reaction scheme for synthesising IV (N719) from $[Ru(dceb)_2Cl_2]$

This compound was used as a precursor for the synthesis of the heterodinuclear complexes. For the synthetic pathway to be successful, it is necessary to have synthetic routes where the ester groups remain intact. Deprotection of the carboxy groups may lead to the formation of a range of complexes which would be difficult to purify. Also, Cl^- ligand is considered a weak field ligand in the spectrochemical series thus loosely bound to the ruthenium and can be replaced by other ligands. The NCS group, a strong field ligand, and will not be replaced by either with H_2O or OH^- ligands when working in acidic or basic environments. A number of experiments are discussed below which are concerned with this issue. The results obtained in these studies are compared by 1H NMR spectra. The spectra for the material as prepared from the synthesis are shown in **Figure 2.6-2.10**. Different studies were carried out so as to investigate the stability of ester groups with respect to acids, base and temperature.

Experiment 1:

1 equivalent of $[\text{Ru}(\text{dceb})_2(\text{NCS})_2]$ and a 4 mol equivalent of NaOH were stirred in ethanol at room temperature under a N_2 atmosphere for 12 hours. Ethanol was removed by rotary evaporation. A 4.5 mole (excess) equivalent of aq. $\text{N}(\text{nBu})_4\text{OH}$ solution was added and stirred for another 30 minutes at room temperature. Here $\text{N}(\text{nBu})_4\text{OH}$ acted as a weak base. This experiment was carried out to check whether the ester groups are resistant to weak bases at room temperature or not. No precipitation was observed from the red colour solution. The pH of the solution was then maintained between 3 and 4 using a dilute aq. HCl solution. A very dark purple coloured precipitate was observed after few minutes which was collected by filtration. A ^1H NMR (see **Figure 2.6**) of the precipitate was identified as $[\text{Ru}(\text{dceb})_2(\text{NCS})_2]$. No hydrolysis had taken place. The above experiment proved that the ester groups are stable under acidic or basic conditions at room temperature.

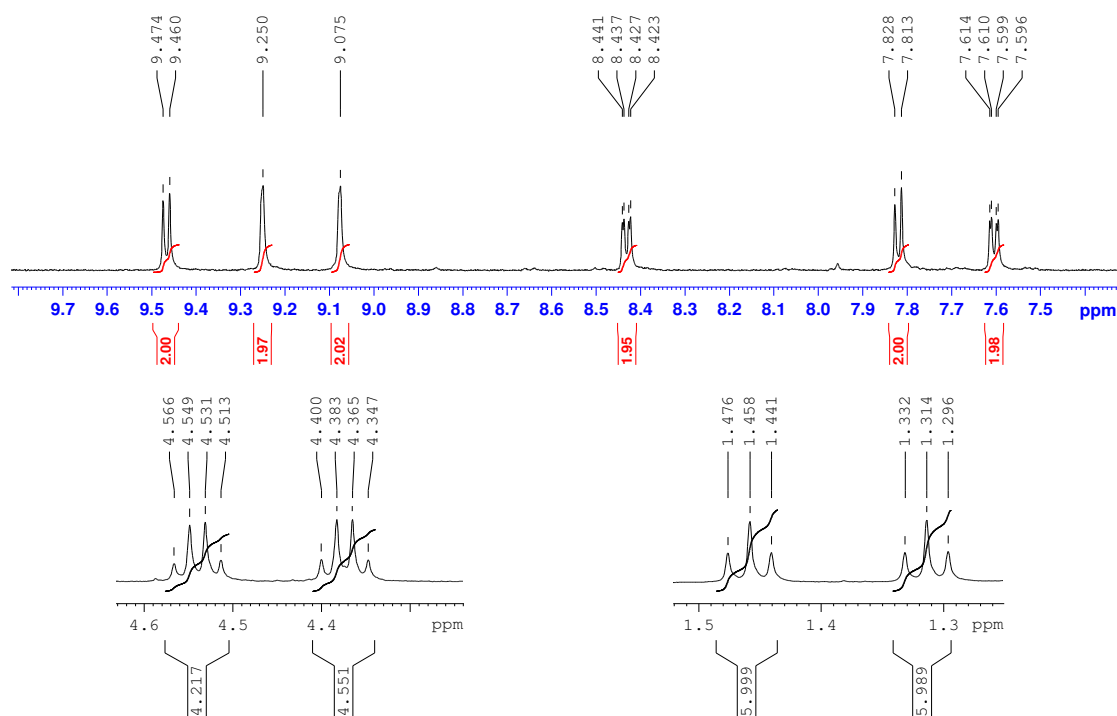


Figure 2.6: ^1H NMR($\text{DMSO}-d_6$, 400 MHz) of the material obtained from experiment 1.

Experiment 2:

$[\text{Ru}(\text{dceb})_2(\text{NCS})_2] \cdot 2\text{H}_2\text{O}$ was stirred with an excess of CH_3COOH at room temperature for 3 hours. Here CH_3COOH acted as a weak acid. This experiment was carried out to check if a weak acid is effective to hydrolyse the ester groups or not at room temperature. The solid material that formed was collected by filtration. The aromatic region in the ^1H NMR (see **Figure 2.7**) was the same as that of $[\text{Ru}(\text{dceb})_2(\text{NCS})_2]$. The ester groups also remained unhydrolysed under weak acidic conditions.

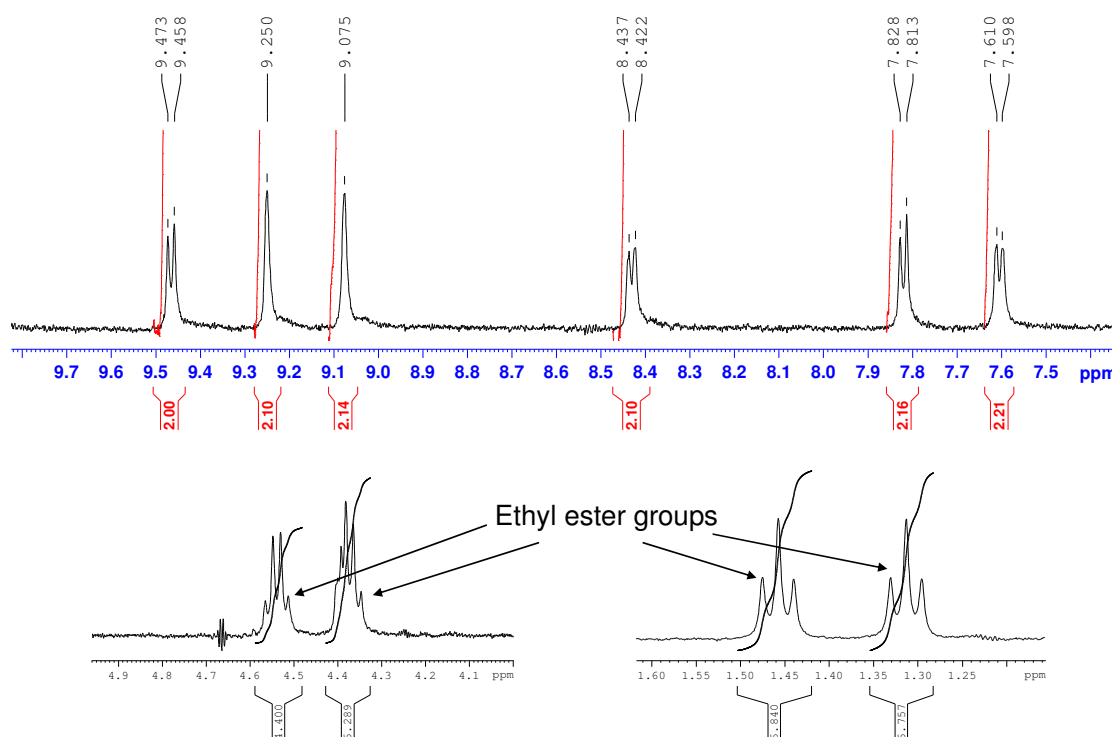


Figure 2.7: ^1H NMR($\text{DMSO}-d_6$, 400 MHz) of compound obtained from experiment 2.

Experiment 3:

One equivalent of $[\text{Ru}(\text{dceb})_2(\text{NCS})_2]$ and four equivalent of $\text{N}(\text{tBu})_4\text{OH}$ were taken up to in ethanol and stirred for 12 hours at room temperature. This experiment was carried out to check if the ester groups were resistant to weakly basic conditions for 12 hours at room temperature. The ethanol was removed by rotary evaporation. A ^1H NMR spectrum of the crude product was found to be the same as that of $[\text{Ru}(\text{dceb})_2(\text{NCS})_2]$. The ester groups were not hydrolysed under these conditions.

Experiment 4:

One equivalent of $[\text{Ru}(\text{dceb})_2(\text{NCS})_2] \cdot 2\text{H}_2\text{O}$ was heated at reflux with excess of $\text{N}(\text{tBu})_4\text{OH}$ in ethanol for 3 hours. Ethanol was removed by rotary evaporation. The crude product was then dissolved in a small amount of acetone and kept between 0–4 °C for two hours. The solution was filtered thereafter but no precipitate was collected. The acetone was then removed by rotary evaporation. Four characteristic multiplets were observed in the ^1H NMR spectrum in the aliphatic region which indicated the compound contains $\text{N}(\text{tBu})_4$. The aromatic protons underwent different chemical shifts following hydrolysis of the ester groups. Peaks for the ester groups were identified but integration of those ester groups indicated that the number of protons were lower than the starting material $[\text{Ru}(\text{dceb})_2(\text{NCS})_2]$. The aromatic region in the ^1H NMR spectrum (**Figure 2.8**) shows unidentified peaks which may be from the partially hydrolysed product of $[\text{Ru}(\text{dceb})_2(\text{NCS})_2]$.

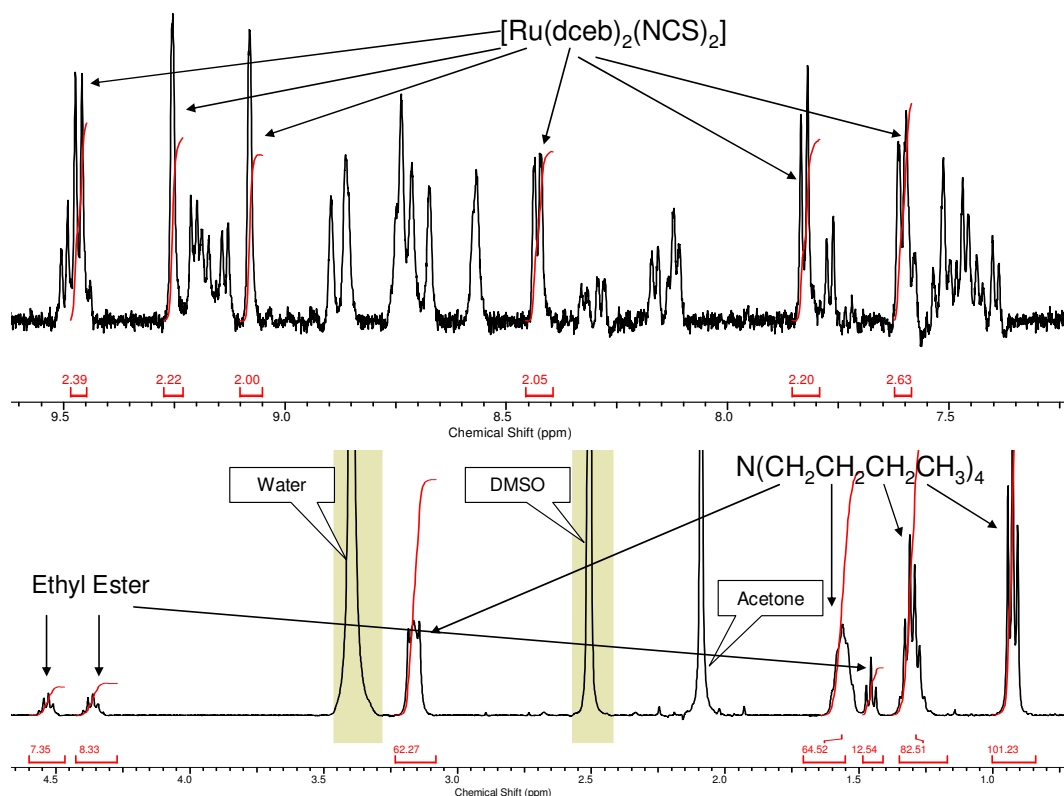


Figure 2.8: ^1H NMR(DMSO-d_6 , 400 MHz) of the product obtained from experiment 4

Experiment 5:

One equivalent of $[\text{Ru}(\text{dceb})_2(\text{NCS})_2] \cdot 2\text{H}_2\text{O}$, two equivalents of NaOH and two equivalents of $\text{N}^+(\text{nBu})_4\text{OH}$ were heated at reflux in ethanol for 3 hours. Ethanol was removed by rotary evaporation. The crude product was dissolved in 20 cm³ of acetone and was kept at 0–4 °C for two hours. The cold solution was filtered but no precipitate was formed. The acetone was then removed from the filtrate by rotary evaporation, and the product was dissolved in water. The pH of the solution was maintained at pH 3 using a dilute aqueous HNO_3 solution. A dark red precipitate was collected by filtration and air dried. All ester groups were found to be hydrolysed in the NMR spectra. ¹H NMR spectra (**Figure 2.9**) also confirmed the presence of two $\text{N}^+(\text{nBu})_4$ groups in the product.

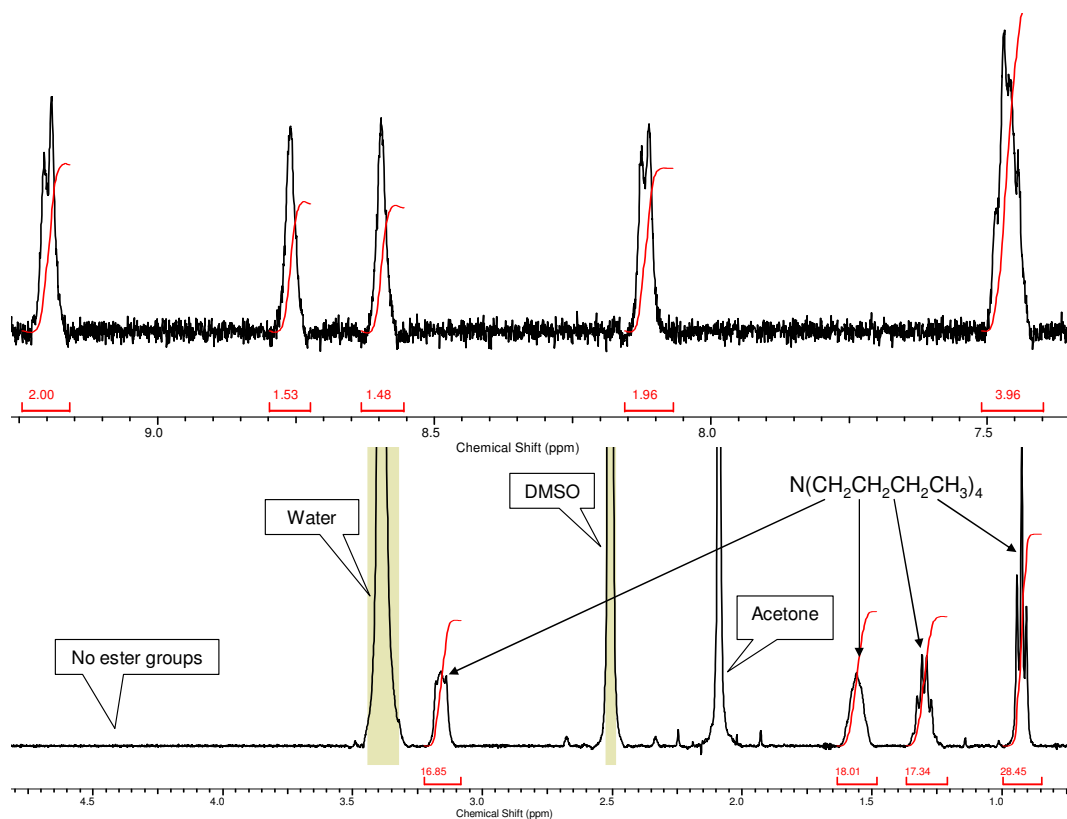


Figure 2.9: ¹H NMR(DMSO-*d*₆, 400 MHz) of the product obtained from experiment 5.

Experiment 6:

One equivalent of $[\text{Ru}(\text{dceb})_2(\text{NCS})_2] \cdot 2\text{H}_2\text{O}$, two equivalents of NaOH and five equivalents of $\text{N}^+(\text{nBu})_4\text{OH}$ were refluxed in ethanol for 3 hours. The ethanol was removed by rotary evaporation. The crude product was dissolved in 20 cm³ of acetone

and was kept at 0-4 °C for two hours. The cold solution was filtered and acetone was removed from the filtrate by rotary evaporator. A ^1H NMR spectrum (**Figure 2.17**) of this crude product confirmed the presence of four $\text{N}^+(\text{nBu})_4$ groups and no ester groups. The product was then dissolved in water and the pH of the solution was maintained at pH 3 using a dilute aq. HNO_3 solution. A dark red precipitate was collected by filtration and air dried. ^1H NMR spectra of the product were broad as the NMR of the compound obtained in experiment number 5.

The -NSC groups were further confirmed by IR spectra (2105 cm^{-1}) (see **Figure 2.10**). Assignment of $\nu(\text{N-C})$ band was made with reference to reported data.⁴³⁻⁴⁵

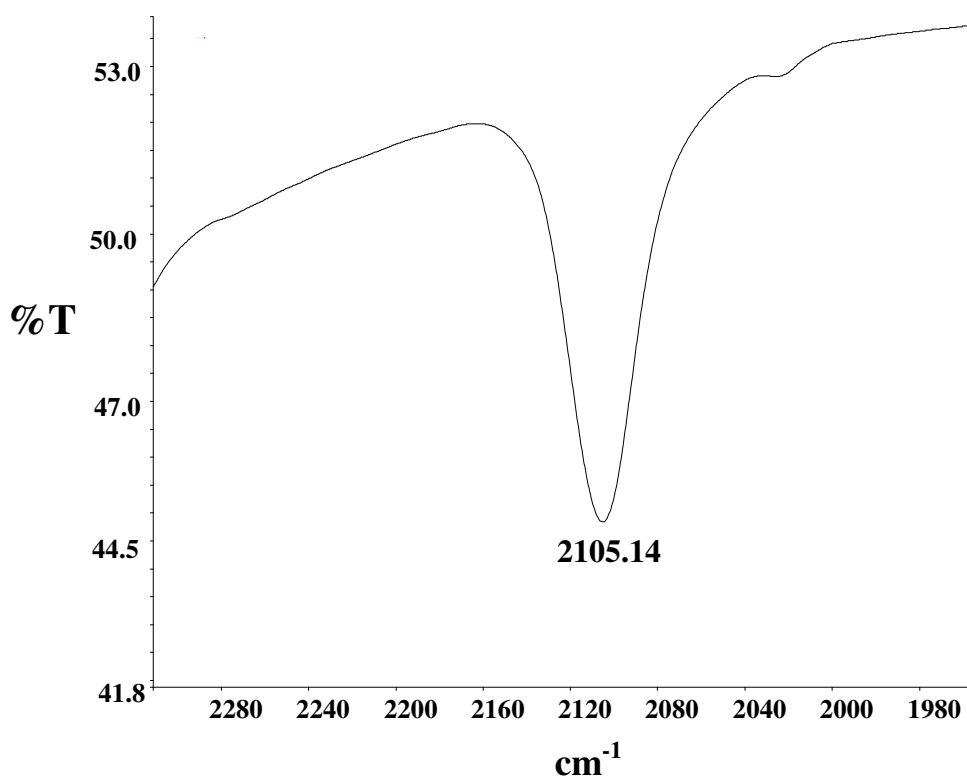


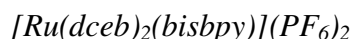
Figure 2.10: IR(KBr) spectra of the compound obtained from experiment 6.

The ester groups are resistant to acids and bases at room temperature but not resistant to bases at higher temperature above 50 °C. This group of experiments was performed to check the stability of these ester groups. Following the above experiments, a new route was devised for the preparation of the N719 dye. The experimental results also provide a better understanding of reaction conditions (acidic

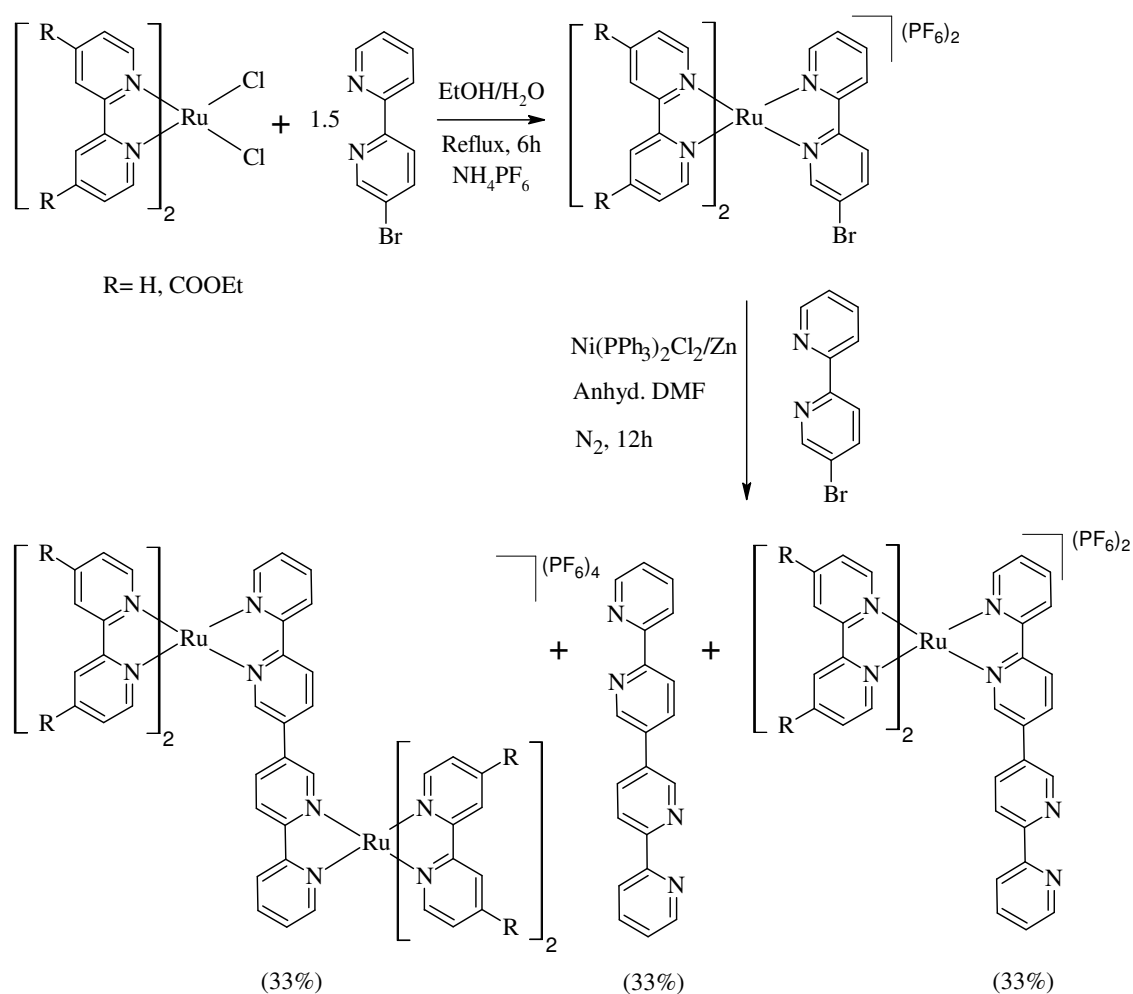
or basic medium at ≤ 50 °C) by which the ester groups can be hydrolysed. These conditions can be further utilised to hydrolyse the ester groups for binding the hetero-bimetallic photocatalysts to the surface of semiconductors.

2.3.3. Synthesis of $[Ru(bpy)_2(L)]^{2+}$ and $[Ru(dceb)_2(L)]^{2+}$ type compounds

The synthesis of $[Ru(bpy)_2(L)]^{2+}$ and $[Ru(dceb)_2(L)]^{2+}$ were carried out in a 3:1 methanol/water at reflux temperature as reported before for similar type compounds.³⁹ Other ruthenium mononuclear precursors were synthesised using analogous synthetic procedures.

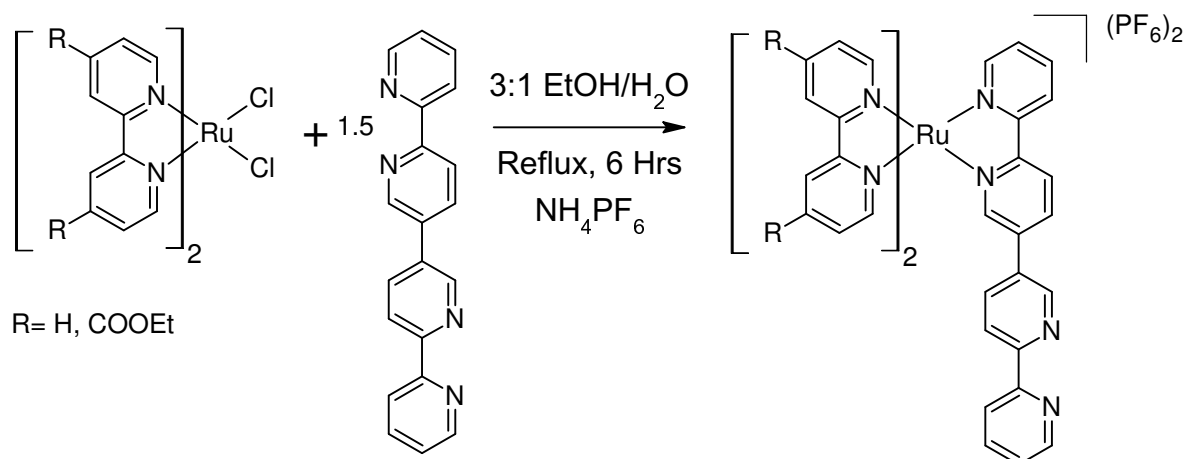


To obtain $[Ru(dceb)_2(bisbpy)](PF_6)_2$ a hetero coupling reaction (Ullmann type coupling reaction) was carried out using $[Ru(dceb)_2(5Brbpy)](PF_6)_2$ and 5Brbpy at 90 °C under a nitrogen atmosphere. The yield of the product obtained was very low which may be due to the evaporation of 5Brbpy from the system under the above mentioned reaction conditions. Instead of the formation of the desired product, three different products were formed due to the coupling reaction between two different molecules having the same halide group (see **Scheme 2.7**). Another reason for obtaining a very low yield than expected was due to the complicated work up procedure.



Scheme 2.7: Reaction scheme and side products for the coupling reaction.

As a result, a different synthetic route was taken. First the synthesis of the bisbpy bridging ligand was carried out and then the monomer was synthesised. Using this synthetic route, a higher yield was obtained and less complexity in the synthetic procedure was observed. The monomer was synthesised using a 3:1 ethanol/water mixture and a yield in excess of 70% was obtained (See **Reaction 2.3**).



Reaction 2.3: Reaction for $[\text{Ru}(\text{dceb})_2(\text{bisbpy})](\text{PF}_6)_2$

Because of the poor solubility of bisbpy bridging ligand in the reaction solvent there is a tendency for the formation of a Ru-Ru dimer. But this can be avoided by carrying out the reaction with an excess of the bridging ligand (1.5 equivalents) and solvent. Because of the poor solubility of the bisbpy, the bridging ligand is less available to the $[\text{Ru}(\text{L})_2\text{Cl}_2]$ in solution and as a result, the excess $[\text{Ru}(\text{L})_2\text{Cl}_2]$ reacts with the bridging ligand in the monomer and forms the Ru-Ru dimer. The product was recrystallised from an acetone/toluene solution. The correct number of protons was observed in the aromatic region (30 protons) and aliphatic region (8 protons at 4.5 and 12 protons at 1.5 for the four ester groups) which agreed with the ^1H NMR of the expected product.

All the compounds obtained were fully characterised using elemental analysis, ^1H NMR and electronic spectroscopy.

2.4. Characterisation of compounds using NMR spectroscopy

2.4.1. Bridging ligands

5-bromo-2,2'-bipyridine(5Brbpy)

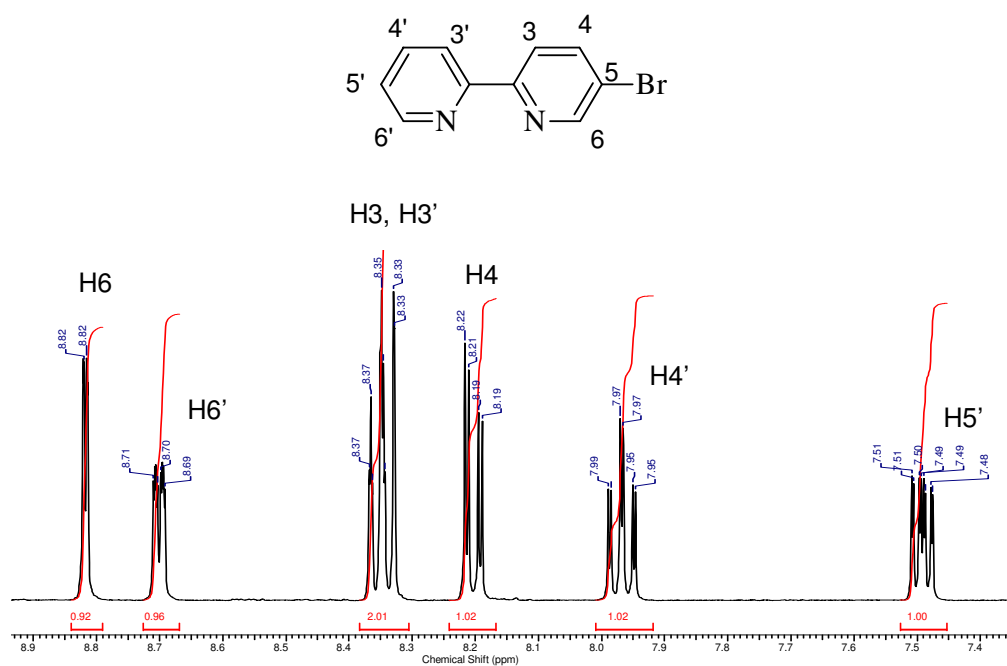


Figure 2.11: ^1H NMR ($\text{DMSO}-d_6$, 400 MHz) of 5-bromo-2,2'-bipyridine(5Brbpy)

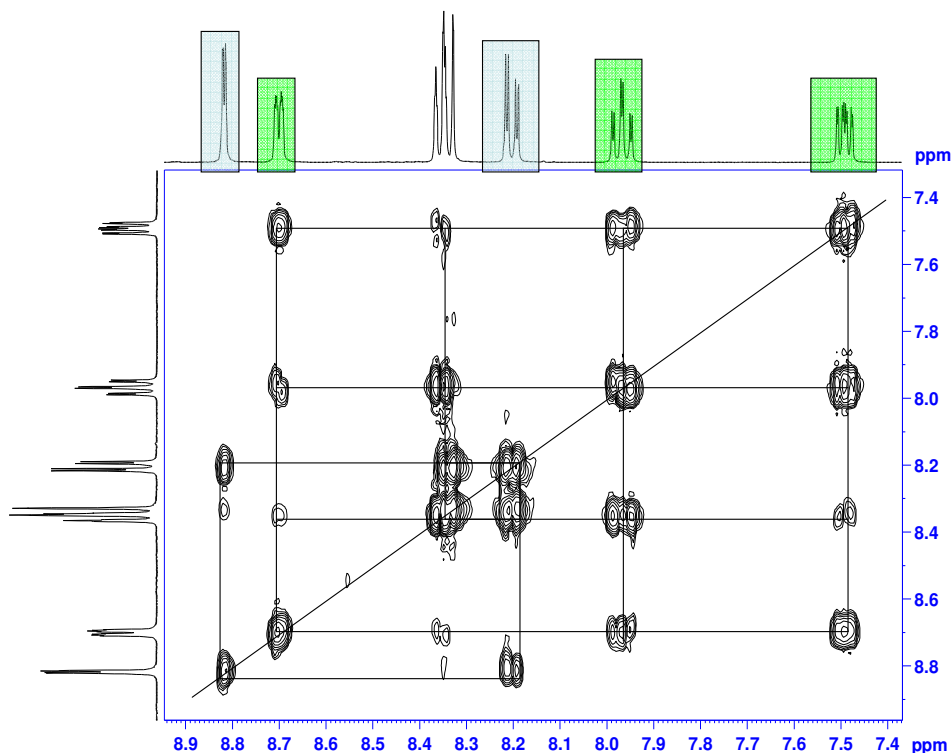


Figure 2.12: COSY NMR ($\text{DMSO-}d_6$, 400 MHz) of 5-bromo-2,2'-bipyridine (5Brbpy)

The ^1H NMR for 5-bromo-2,2'-bipyridine (5Brbpy) is displayed in **Figure 2.11**. The COSY spectrum obtained for this compound is shown in **Figure 2.12**. The signal at 8.82 ppm belongs to H6 ($^3J = 4.67$ Hz) and has long range coupling with H4 (8.20 ppm, $^4J = 1.77$ Hz). The proton H4 at 8.20 ppm couples with the proton H3 (8.35 ppm). Hence H7, H6 and H5 protons are assigned using COSY NMR. The doublet at 8.70 ppm corresponds to H6'. This H6' proton couples with H5' ($^3J = 4.80$ Hz, 7.49 ppm). H6' also undergoes long range coupling with H4' and couple with H3'. As other doublets are assigned for the compound, The H3' doublet overlaps with the multiplet at 8.35 ppm. The remaining resonance assigned to the H4' couples with H5' ($^3J = 7.71$ Hz), H3' (8.35 ppm) and H6' ($^4J = 2.65$ Hz). The assignment and coupling constant data are tabulated in **Table 2.1**.

Table 2.1: Correlation ^1H NMR data for the assigning the protons containing in 5-bromo-2,2'-bipyridine (5Brbpy)

No.	Shift (ppm)	H's	Type	J (Hz)
H5'	7.49	1	dd	7.71, 4.80
H4'	7.97	1	td	7.71, 7.71
H4	8.20	1	dd	8.46, 2.40
H3', H3	8.35	2	m	-
H6'	8.70	1	dd	4.67, 2.65
H6	8.82	1	d	1.77

2,2':5',2''-terpyridine (bpp)

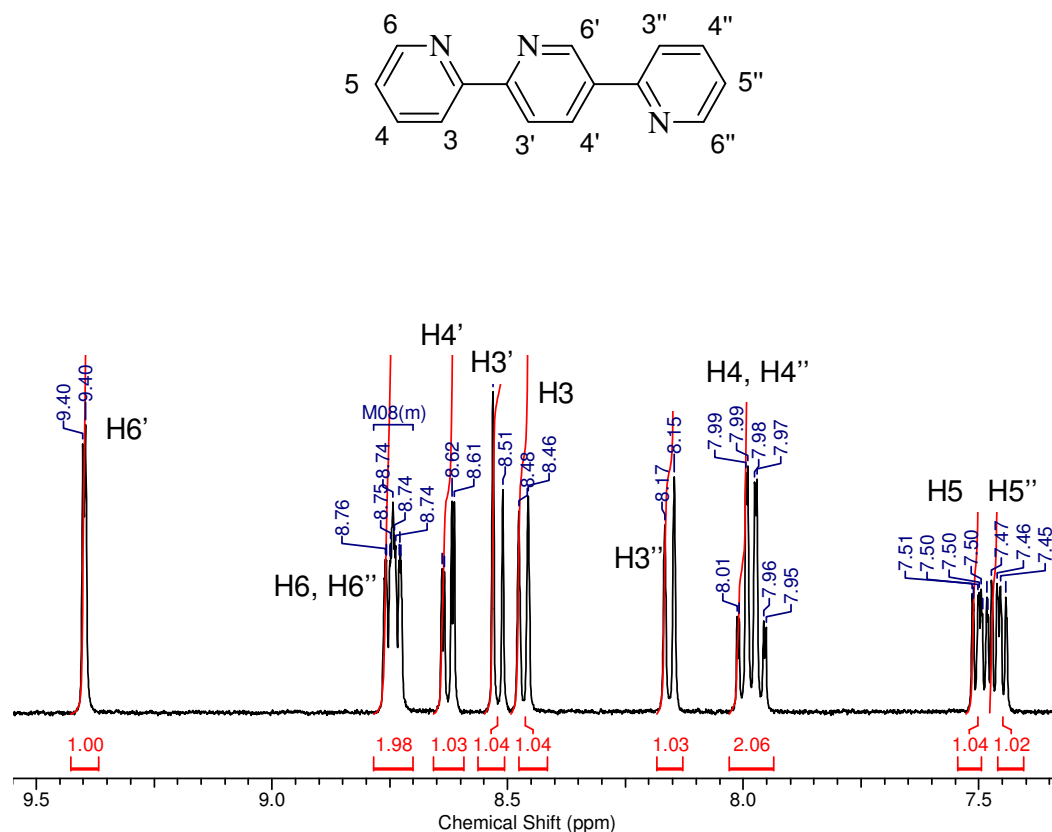


Figure 2.13: ^1H NMR ($\text{DMSO}-d_6$, 400 MHz) of 2,2':5',2''-terpyridine (bpp)

The ^1H NMR spectrum corresponding to 2,2':5',2''-terpyridine (bpp) is displayed in **Figure 2.13** and contains a total of 11 protons. 2,2':5',2''-terpyridine (bpp) has two pyridyl rings attached at the 2' and 5' position (not equivalent) of the middle pyridyl ring. Integration of the proton NMR gives the total number of expected protons. Difficulty in assigning the protons in the two external pyridyl rings is due to their almost identical environments. The coupling constants are very similar for the two outer pyridyl rings. The peaks obtained in the ^1H NMR were assigned using COSY NMR data. One of the outer pyridyl rings attached at the 2' position of the central pyridyl ring will be slightly affected by the electron withdrawing effect of the nitrogen atom of the central ring. This nitrogen atom is nearer to the pyridyl ring at the 2' position than the pyridyl ring attached at the 5' position. This suggests that the chemical shifts of the protons in the outer pyridine attached at 2' position will be slightly downfield shifted than the protons in the outer pyridine ring at 5' position of the central ring. A more detailed discussion regarding assignment of the protons using the COSY NMR (**Figure 2.14**) is provided below.

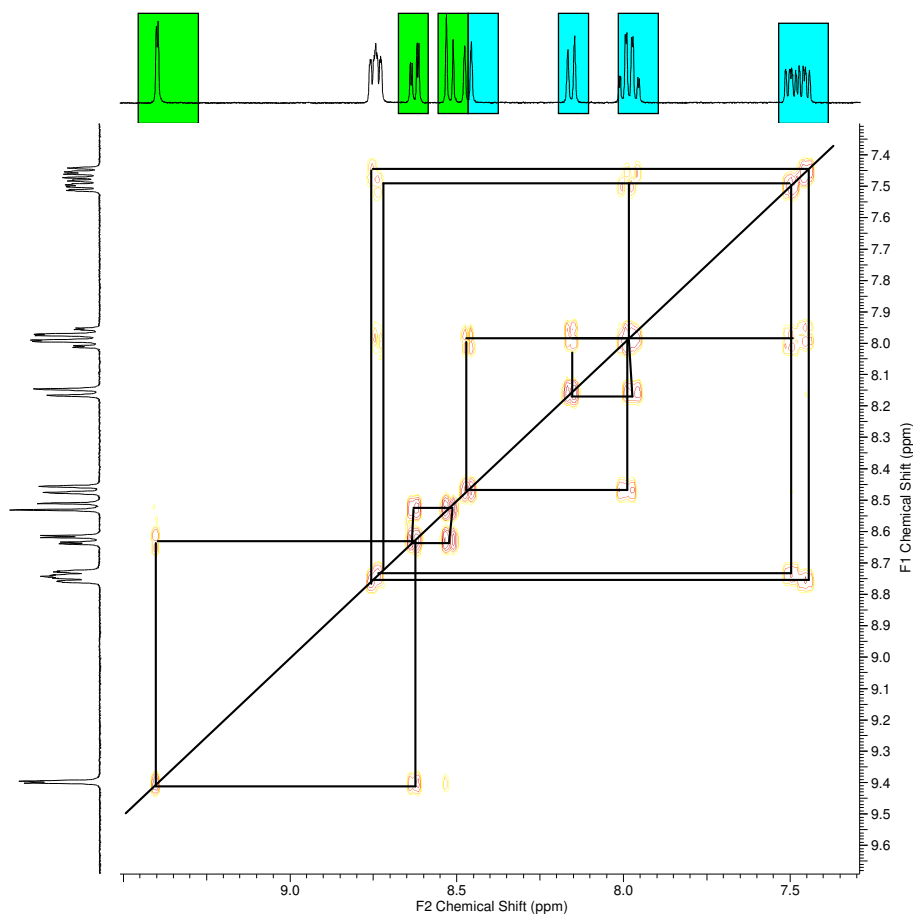


Figure 2.14: COSY NMR(DMSO- d_6 , 400 MHz) of 2,2':5',2''-terpyridine (bpp)

According to the above discussion, the H6' proton (d, 9.40 ppm) is long range coupled with H4' ($^4J = 2.27$ Hz). H6' is also long range coupled with H5 which is weak in the COSY NMR hence H3' and H4' can be assigned using COSY NMR. H4' appeared at 8.54 ppm which is long range coupled with H6' and with H3'. The protons in the two outer pyridyl rings are difficult to distinguish. Based on the above, protons contained in the pyridyl ring attached at the 2' position will show a slightly downfield shift. There is a multiplet at 8.74 ppm which actually contains two doublets. One doublet is slightly downfield shifted and is coupled with H5 (dd, 7.46 ppm). This indicates that another proton signal (inside the multiplet at 8.74 ppm) belongs to H6'' and couples with H5'' proton at 7.50 ppm. H5 and H5'' are both found correlated to the multiplet at 7.98 ppm. This multiplet is supposed to contain H4 and H4'' proton signals. The coupling pattern was not visible in the NMR as H4 overlaps with the H4'' signal. There is another doublet (suggested as H6'') inside the multiplet at 8.74 ppm which couples with H4'' at 7.50 ppm. So H6', H5', H4, H4',

H6, H6', H5, H5' are assigned. Now two more protons are left to assign which are H3 and H3''. The electron withdrawing effect of nitrogen atom of the central pyridine ring will be greater on the H3 proton than the H3'' as the nitrogen is closer to the H3 proton than the H3''. So the H3 proton is expected to be further downfield shifted than H3''. This assumption can be confirmed with COSY NMR. The multiplet at 7.94 ppm is correlated with the doublet at 8.16 ppm and 8.46 ppm. So the doublet at 8.16 ppm can be assigned to the H3'' and the doublet at 8.46 is assigned to the H3 proton.

Table2.2: Correlation ^1H NMR data for the assigning the protons containing in 2,2':5',2''-terpyridine (bpp)

No.	Shift (ppm)	H's	Type	J (Hz)
H5''	7.46	1	dd	7.58, 4.80
H5	7.50	1	dd	7.59, 5.43
H4	7.98	2	m	-
H4''				
H3''	8.16	1	d	8.08
H3	8.47	1	d	8.08
H3'	8.52	1	d	8.34
H4'	8.63	1	dd	8.34, 2.27
H6	8.74	2	m	-
H6''				
H6'	9.40	1	d	2.27

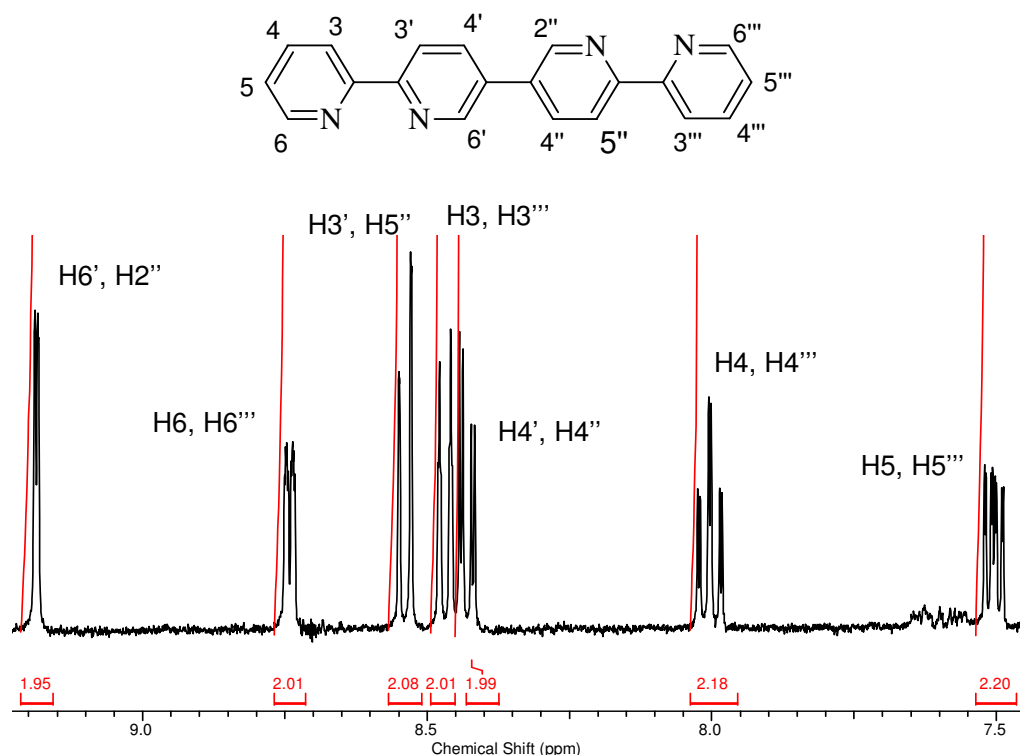
2,2':5',3'':6'',2'''-quaterpyridine (bisbpy)

Figure 2.15: ¹H NMR (DMSO-d₆, 400 MHz) of 2,2':5',3'':6'',2'''-quaterpyridine(bisbpy)

Figure 2.15 shows the ¹H NMR spectra of 2,2':5',3'':6'',2'''-quaterpyridine (bisbpy). The integration shows fourteen protons in the compound as expected. Bisbpy has two bipyridine rings which are attached by a single bond. So it can be suggested that both the bipyridine units have the same environment as the outside rings are identical as the two inside ones, hence will show the same chemical shift. Above the NMR spectrum satisfies the expected number of protons. According to above assumption, H6' and H2'' have identical chemical shifts. Similarly, H4', H3', H6, H5, H4, H3 have identical chemical shifts as H4'', H5'', H6'', H5'', H4''' and H3''' respectively. A more specific assignment can be made from an H-H COSY NMR spectrum, which is shown in **Figure 2.16**. A chemical shift data for all the protons are tabulated in **Table 2.3**. A detail assignment of the protons is discussed below.

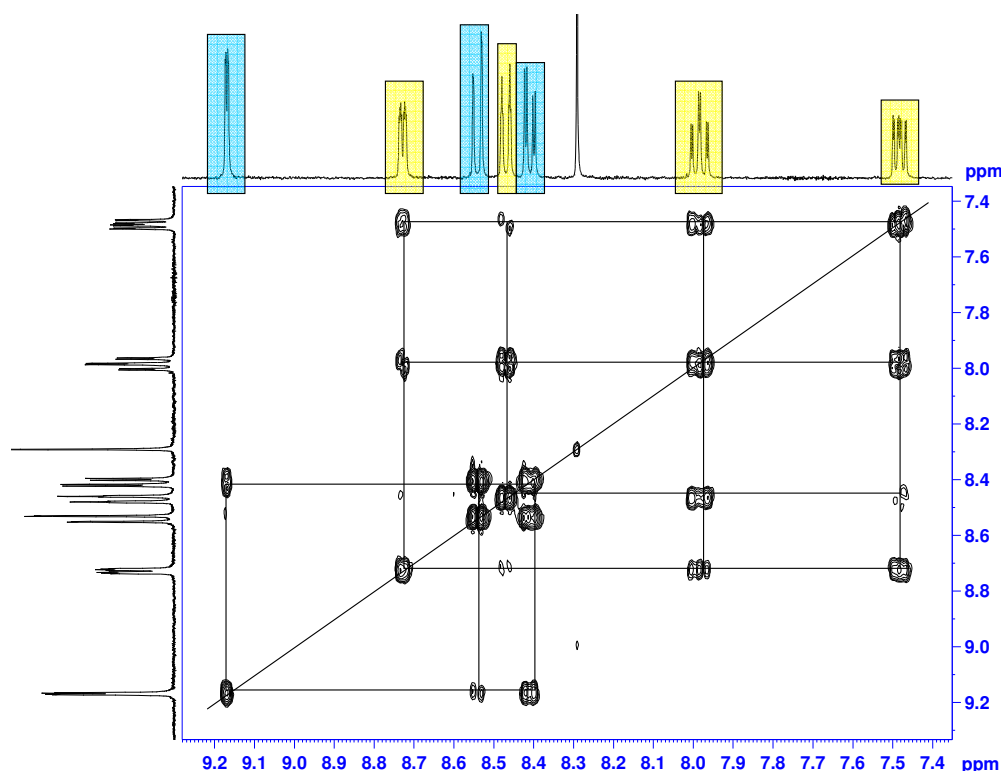


Figure 2.16: COSY NMR ($\text{DMSO-}d_6$, 400 MHz) of 2,2':5',3'':6'',2'''-quaterpyridine (bisbpy)

According to above discussion, bisbpy has two identical bpy units. So the assignment of protons for one bpy unit will also be identical for the other bpy unit. The most downfielded signal at 9.19 ppm is assigned to the the $\text{H6}'(\text{H2}'')$ proton. Further, $\text{H6}'$ couples with $\text{H4}'$ (Similarly $\text{H2}''$ couples with $\text{H4}''$). From the COSY NMR spectra $\text{H4}'(\text{H4}'')$ is assigned to the doublet at 8.43 ppm which also couples with $\text{H3}'(\text{H5}'')$ appearing at 8.54 ppm. The doublet at 8.74 ppm is assigned to the $\text{H6}(\text{H6}'')$ because this proton is ortho to the nitrogen atom in the pyridine ring and will be more deshielded. H6 couples with H5 (similarly $\text{H6}''$ with $\text{H5}''$) which appears at 7.50 ppm. It can be seen that $\text{H5}(\text{H5}'')$ couples with H4 (similarly $\text{H5}''$ and $\text{H4}''$) and assigned to the the 'dd' signal at 8.00 ppm. So, there is only one proton left to assign which is $\text{H3}(\text{H3}'')$. The doublet signal at 8.47 couples with H3 (at 8 ppm) and is assigned to the $\text{H3}(\text{H3}'')$. Chemical shifts and coupling constant data for all the protons are provided in **Table 2.3**.

Table2.3: Correlation NMR data for the assigning the protons containing in 2,2':5',3'':6'',2'''-quaterpyridine (bisbpy)

No.	Shift (ppm)	H's	Type	J (Hz)
H5, H5'''	7.50	2	dd	7.52, 4.74
H4, H4'''	8.00	2	td	7.83, 7.83
H4', H4''	8.43	2	d	8.34
H3, H3'''	8.47	2	d	7.83
H3', H5''	8.54	2	d	8.08
H6, H6'''	8.74	2	d	4.11
H6', H2''	9.19	2	d	1.77

2.4.2. Metal complexes

NMR is a powerful tool to characterise ruthenium polypyridyl complexes. Although the protons NMR of these ruthenium complexes are complicated, the NMR spectral data can be interpreted using 2D COSY NMR and partially deuteriated complexes. All the ruthenium mononuclear precursors were characterised by ^1H NMR and CHN analysis. The 2D COSY NMR is also complicated and difficult to understand. But the product was clearly identified from the exact numbers of protons (in aromatic region) observed in the NMR and presence of multiplets for the expected number of protons at 4.5 ppm (8H) and 1.5 ppm (12H) for the ester groups. The product was further confirmed by CHN analysis and UV-Vis spectra.

^1H NMR of N719

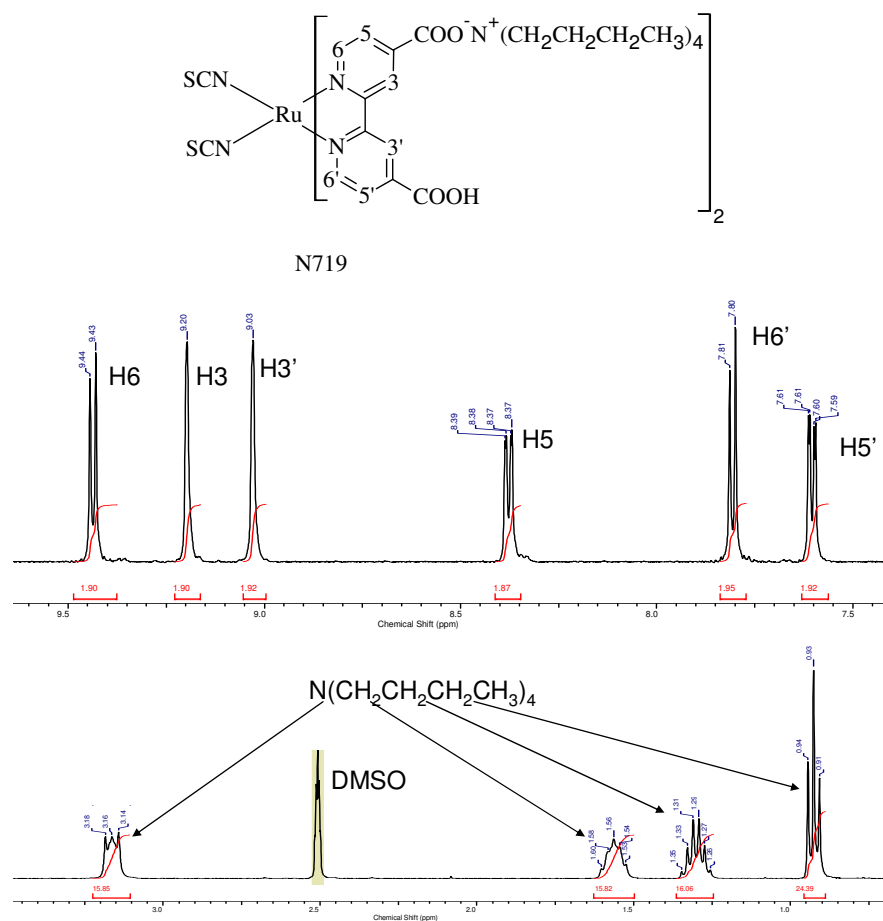


Figure 2.17: ^1H NMR(DMSO- d_6 , 400 MHz) of N719 with a drop of HNO_3

A better resolution ^1H NMR of N719 (**Figure 2.17**) was recorded with a drop of HNO_3 . The NMR spectrum showed six distinguished and clear peaks in the aromatic region which correspond to the bipyridine rings. The NMR spectrum also showed the presence of three multiplets which are at 1.30, 1.56 and 3.15 ppm (3×16 H) and another multiplet at 0.93 ppm (24H). From the integration of the aromatic and aliphatic regions in the ^1H NMR it is confirmed that the compound has two $\text{N}^+(\text{n-But})_4$ groups and two carboxy acid groups.

NMR interpretation for $[\text{Ru}(\text{bpy})_2(\text{bisbpy})](\text{PF}_6)_2$ using $[\text{Ru}(d_8\text{-bpy})_2(\text{bisbpy})](\text{PF}_6)_2$

Proton NMR spectra of ruthenium(II) polypyridyl complexes are complex in nature. This issue can be resolved by synthesising partially deuteriated complexes. The simplest way is deuteration of the peripheral bipyridine ligands. This will help to interpret the protons on the bridging ligand without ‘interference’ from the protons on the peripheral bipyridine ligands. The partially deuteriated complex and non-deuteriated complex are compared here and the protons are assigned using H-H 2D COSY NMR. Molecular structures of the complexes, ^1H NMRs and 2D COSY NMR spectra are displayed in **Figure 2.18**, **2.29** and **2.20** respectively.

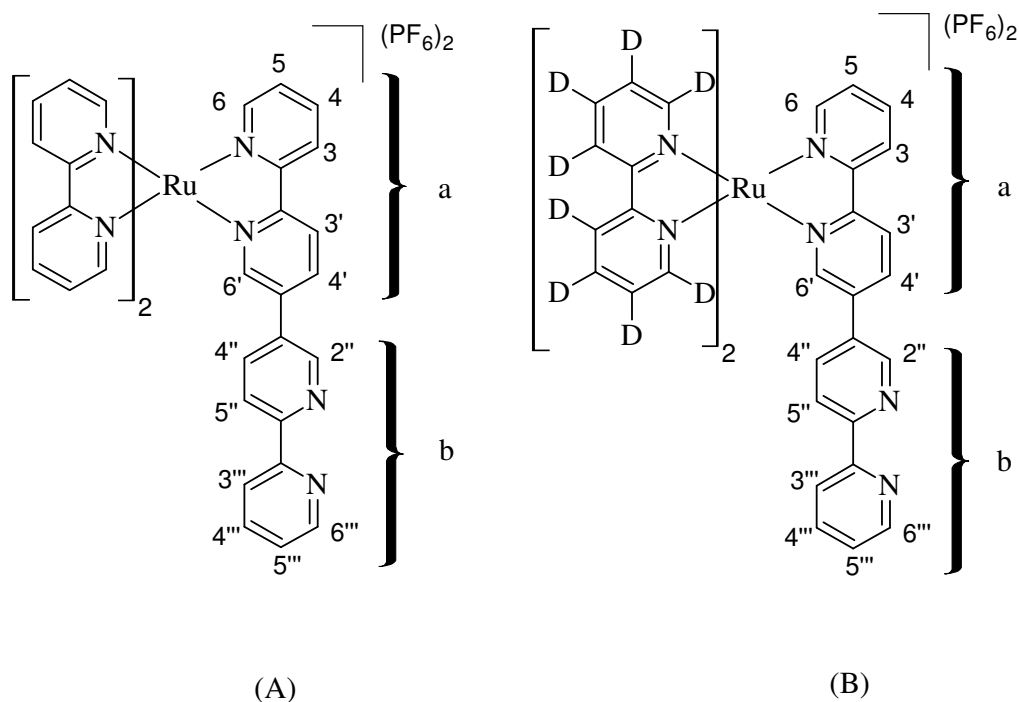


Figure 2.18: Molecular structure of (A) $[\text{Ru}(\text{bpy})_2(\text{bisbpy})](\text{PF}_6)_2$, (B) $[\text{Ru}(d_8\text{-bpy})_2(\text{bisbpy})](\text{PF}_6)_2$

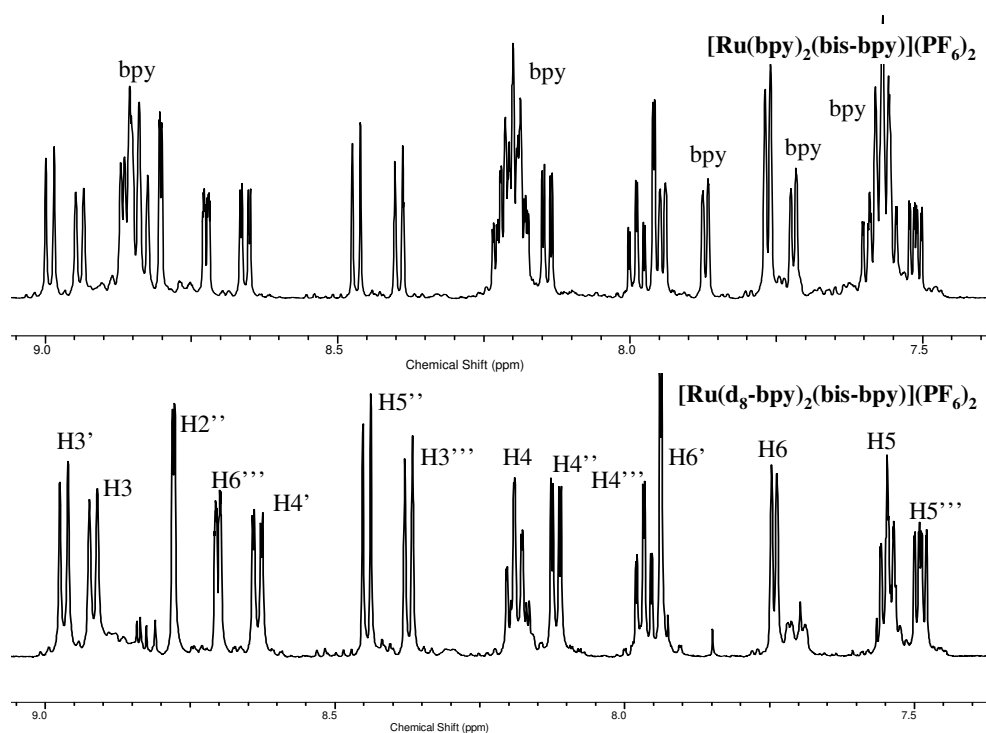


Figure 2.19: ^1H NMR ($\text{DMSO-}d_6$, 400 MHz) of (A) $[\text{Ru}(\text{bpy})_2(\text{bisbpy})](\text{PF}_6)_2$, (B) $[\text{Ru}(d_8\text{-bpy})_2(\text{bisbpy})](\text{PF}_6)_2$

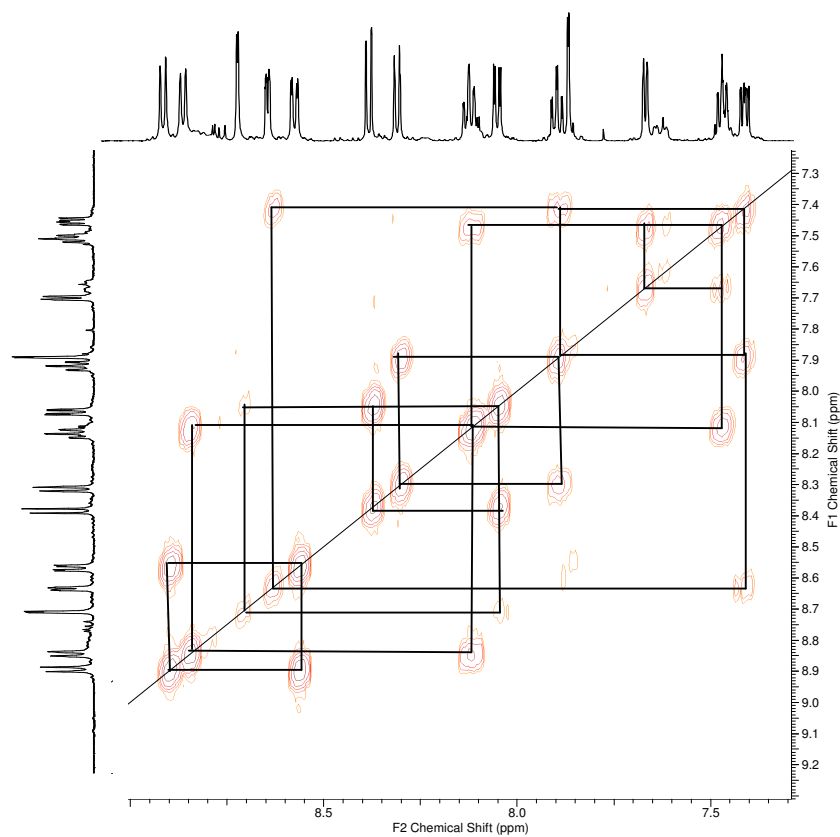


Figure 2.20: 2D COSY NMR ($\text{DMSO-}d_6$, 400 MHz) of $[\text{Ru}(d_8\text{-bpy})_2(\text{bisbpy})](\text{PF}_6)_2$

Table 2.4: Difference in the chemical shift between the free bisbpy and complexed bisbpy with metal centre.

Assignment of proton signals with respect to chemical shift (ppm)			
		Free ligand	Complexed ligand
(a)	H5	7.50	7.55
	H4	8.00	8.17
	H4'	8.43	8.63
	H3	8.47	8.92
	H3'	8.54	8.97
	H6	8.74	7.74
	H6'	9.19	7.94
(b)	H5'''	7.50	7.49
	H4'''	8.00	7.97
	H4''	8.43	8.12
	H3'''	8.47	8.37
	H5''	8.54	8.44
	H6'''	8.74	8.70
	H2''	9.19	8.70

NMR interpretation for $[Ru(bpy)_2(bpp)](PF_6)_2$ using $[Ru(d_8-bpy)_2(bpp)](PF_6)_2$

The environment of the free bridging ligand and the coordinated bridging ligand to the metal centre are entirely different. When the bridging ligand is bound to the metal centre, the neighbouring protons of the nitrogen atom (on the bound side of the bridging ligand, 'a') will be slightly up-fielded as the electronegative effect of nitrogen atom is lowered due to coordination. There is another end (ring 'b') of the bridging ligand which is not bound to the metal centre. This will have almost the identical environments as uncomplexed ligand and therefore no change in the chemical shift of the protons occurs. More precisely assigned proton NMR spectra of both non deuteriated and partially deuteriated complexes are provided below (**Table**

2.5). Chemical shifts of both free ligands and bridging ligand coordinated to metal centre are also provided below.

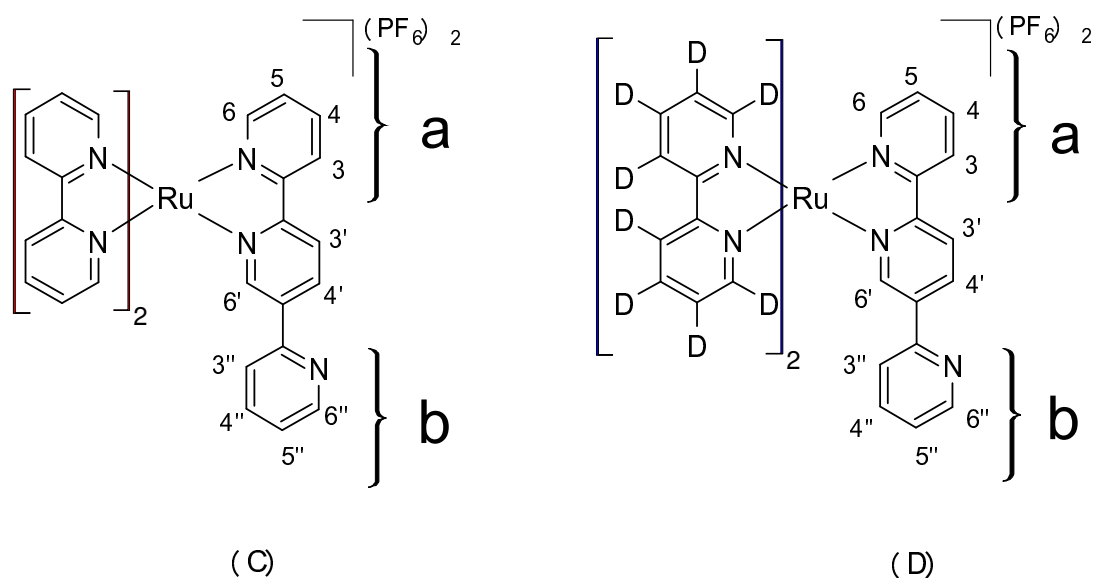


Figure 2.21: Molecular structure of $[Ru(bpy)_2(bpp)](PF_6)_2$ and $[Ru(d_8-bpy)_2(bpp)](PF_6)_2$

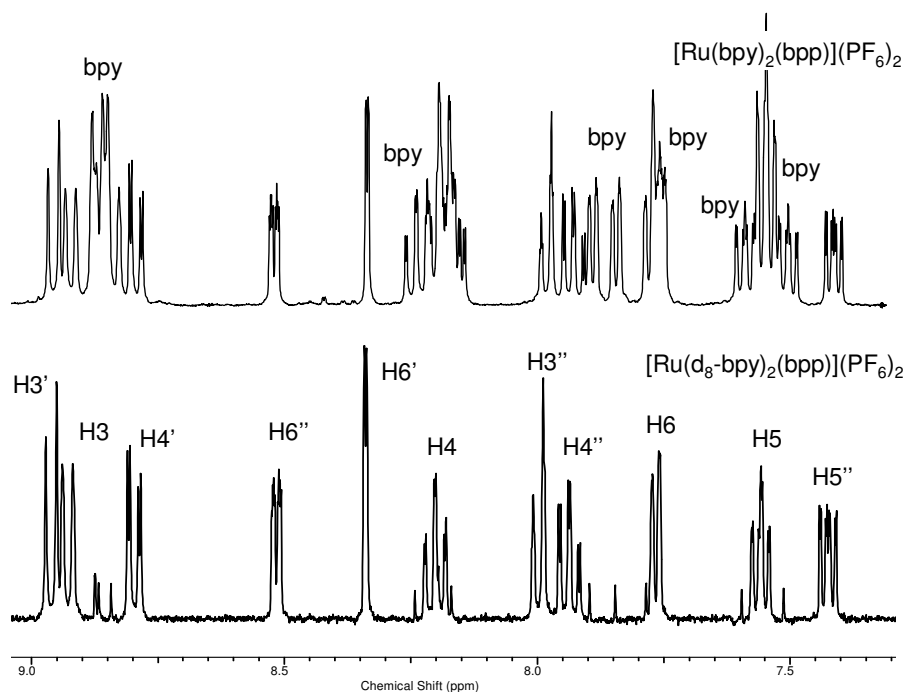


Figure 2.22: The 1H NMR ($DMSO-d_6$, 400 MHz) of $[Ru(bpy)_2(bpp)](PF_6)_2$ and $[Ru(d_8-bpy)_2(bpp)](PF_6)_2$

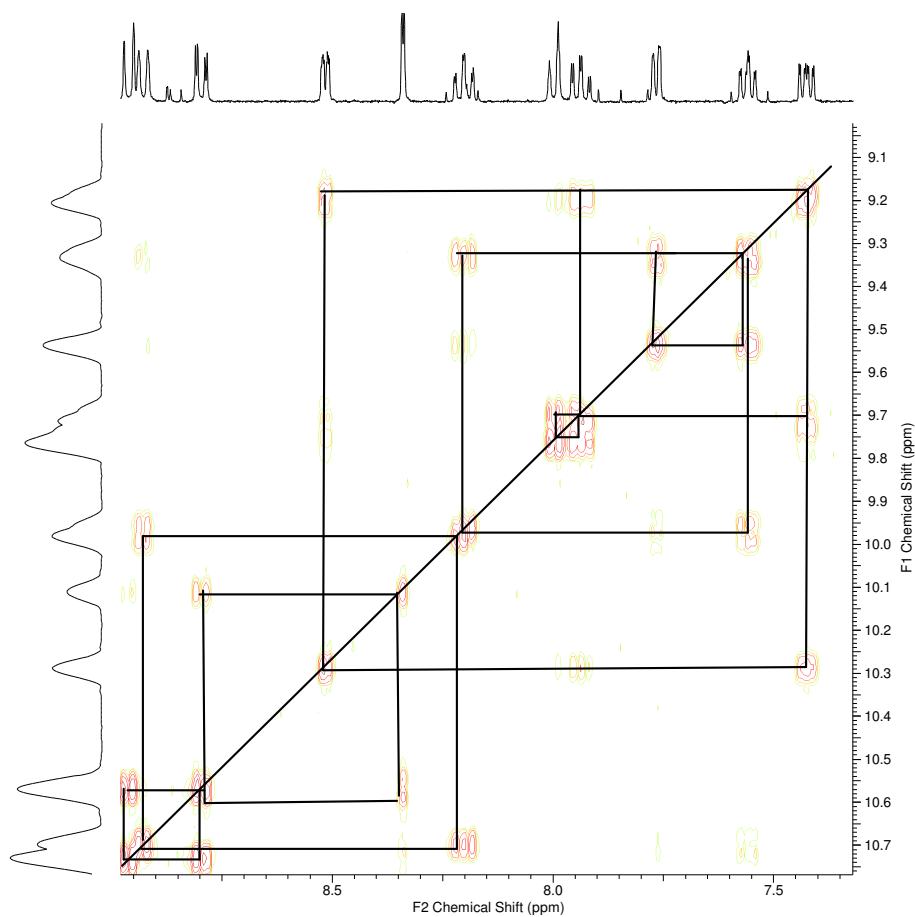


Figure 2.23: *H-H COSY NMR (400 MHz, DMSO- d_6) of $[Ru(d_8\text{-bpy})_2(bpp)](PF_6)_2$*

Table2.5: Difference in the chemical shift between the free bpp and bpp bound to the metal centre.

Assignment of proton signals with respect to chemical shift (ppm)			
		Free ligand	Complexed ligand
(a)	H5''	7.46	7.43
	H5	7.50	7.56
	H4	7.98	8.20
	H4''		7.93
	H3''	8.16	8.01
(b)	H3	8.47	8.93
	H3'	8.52	8.96
	H4'	8.63	8.80
	H6	8.74	7.77
	H6''		8.51
	H6'	9.40	8.34
	H5''	7.46	8.93
	H5	7.50	8.20

NMR interpretation for $[Ru(bpy)_2(2,5-dpp)](PF_6)_2$ using $[Ru(d_8-bpy)_2(2,5-dpp)](PF_6)_2$

Figure 2.24 shows the molecular structures of (E) $[Ru(bpy)_2(2,5-dpp)](PF_6)_2$ and (F) $[Ru(d_8-bpy)_2(2,5-bpp)](PF_6)_2$. Here H5 and H6 are the two distinct protons in the complex which can be easily identified from 1H NMR. H6 is the proton of the ortho carbon to that nitrogen which is bound to metal centre and is hence shifted to upfield region. The protons belonging to ring “a” are more upfield shifted than the protons belong to the ring “b”. The 1H NMR spectra is shown in **Figure 2.25** and all data are tabulated in **Table2.6**.

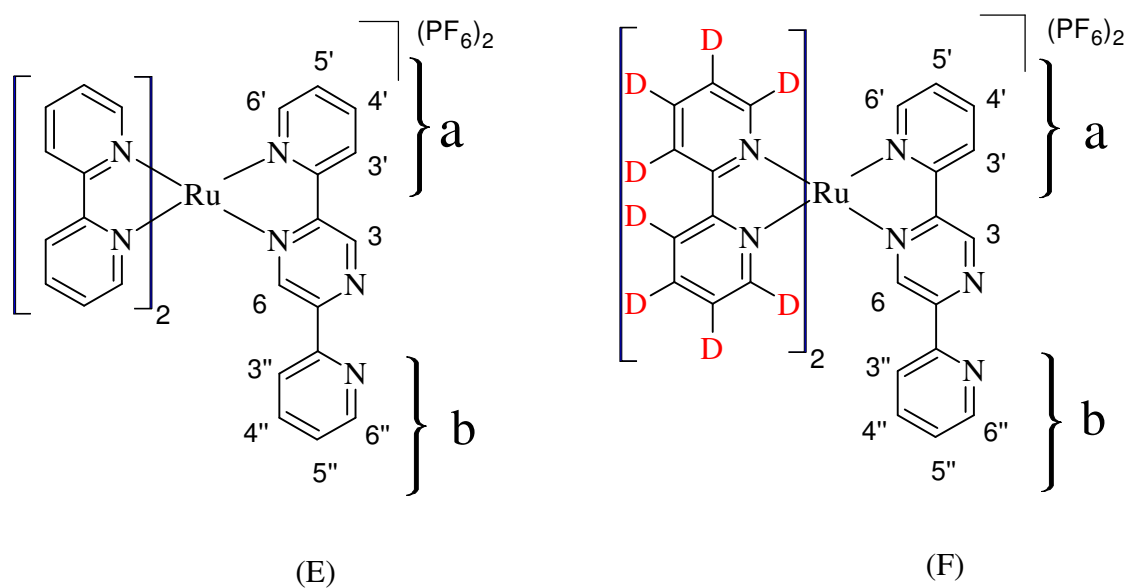


Figure 2.24: Molecular structure of (E) $[Ru(bpy)_2(2,5-dpp)](PF_6)_2$ and (F) $[Ru(d_8-bpy)_2(2,5-bpp)](PF_6)_2$

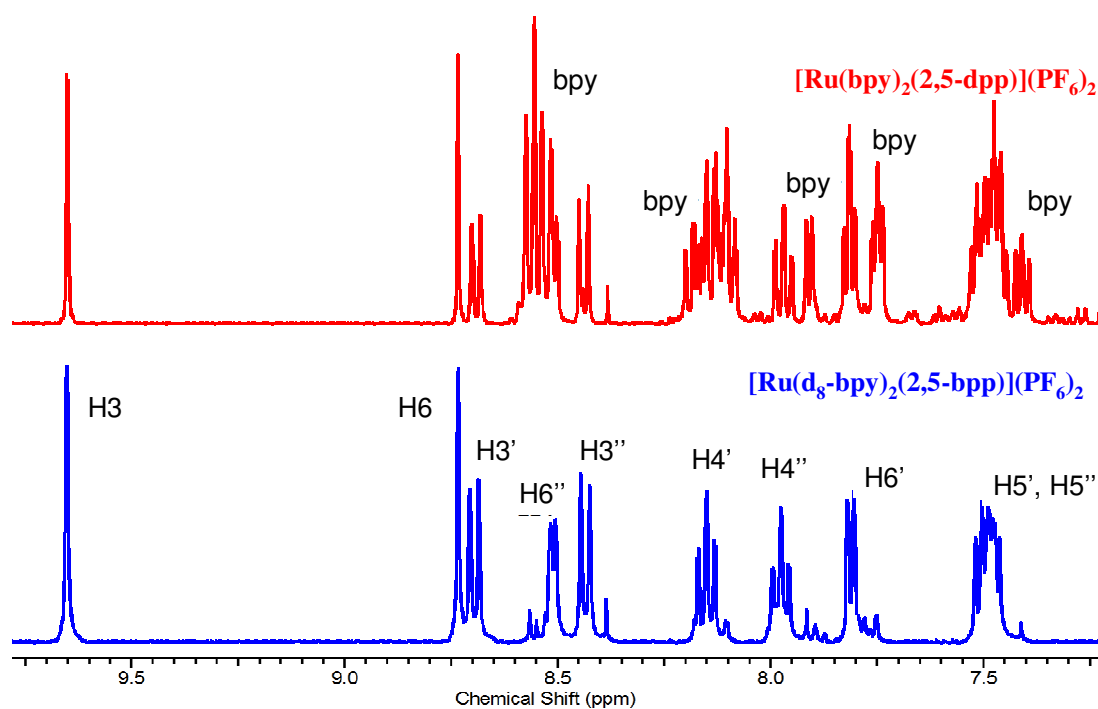


Figure 2.25: 1H NMR (400 MHz, Acetonitrile- d_3) of (E) $[Ru(bpy)_2(2,5-dpp)](PF_6)_2$ and (F) $[Ru(d_8-bpy)_2(2,5-bpp)](PF_6)_2$

Table 2.6: Difference in the chemical shift between the free 2,5-dpp and 2,5-dpp bound to metal centre.

Assignment of proton signals with respect to chemical shift (ppm)			
		Free ligand	Complexed ligand
(a)	H5'	7.88	7.44-7.53
	H4'	8.36	8.15
	H3'	7.39	8.70
	H6'	8.66	7.80
(b)	H3	9.56	9.69
	H6	9.56	8.75
	H6''	8.36	8.51
	H3''	8.66	8.43
	H4''	7.88	7.98
	H5''	7.39	7.44-7.53

NMR interpretation of $[Ru(dceb)_2(L_2)]^{2+}$ types complexes

The carboxy derivatised bipyridine could not be deuteriated due to synthetic problems. These complexes have four ethyl ester groups which will appear in the aliphatic region. The ruthenium complexes containing four ester groups will show 8 protons as multiplets at 4.5 ppm, along with 12 protons at 1.5 ppm as a multiplet. Integration of the ester group signals and subsequent comparison with the aromatic region can be used to investigate the number of ester groups present. Interpretation of the aromatic region is difficult due to complicated 1H NMR spectra. 2D H-H COSY NMR spectra were used to interpret part of the 1H NMR spectra of the metal complexes (see **Figures 2.26 to 2.34**).

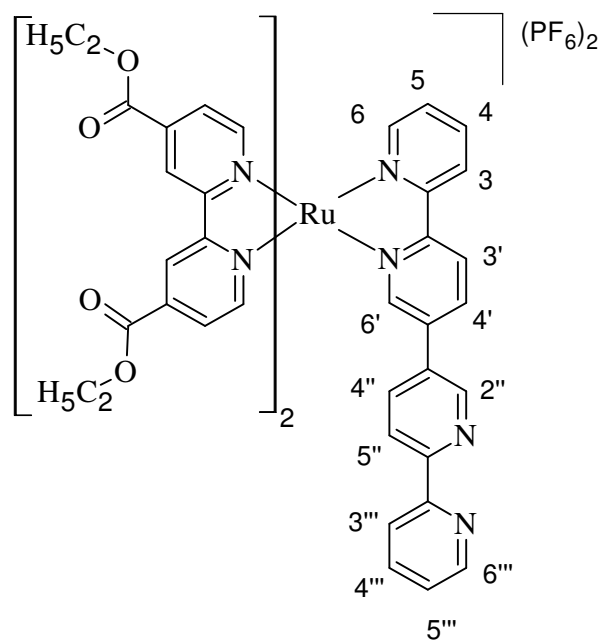
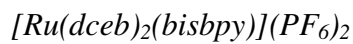


Figure 2.26: Molecular structure of $[\text{Ru}(\text{dceb})_2(\text{bisbpy})](\text{PF}_6)_2$

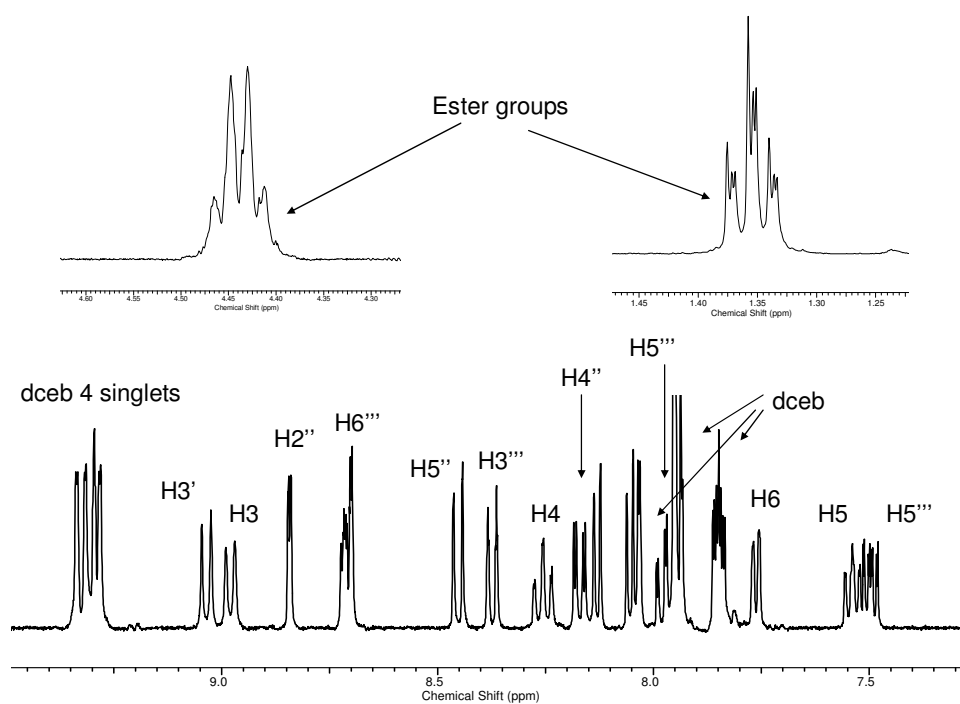


Figure 2.27: ^1H NMR(400 MHz, DMSO-d_6) of $[\text{Ru}(\text{dceb})_2(\text{bisbpy})](\text{PF}_6)_2$

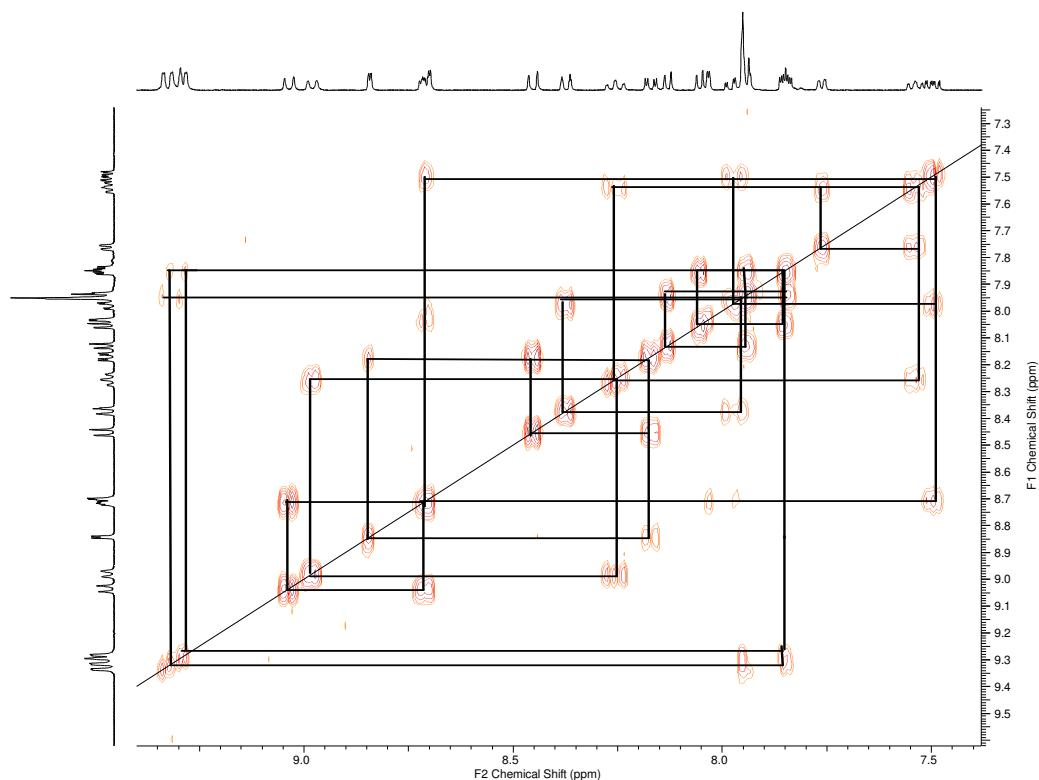


Figure 2.28: COSY NMR(400 MHz, DMSO- d_6) of $[Ru(dceb)_2(bisbpy)](PF_6)_2$

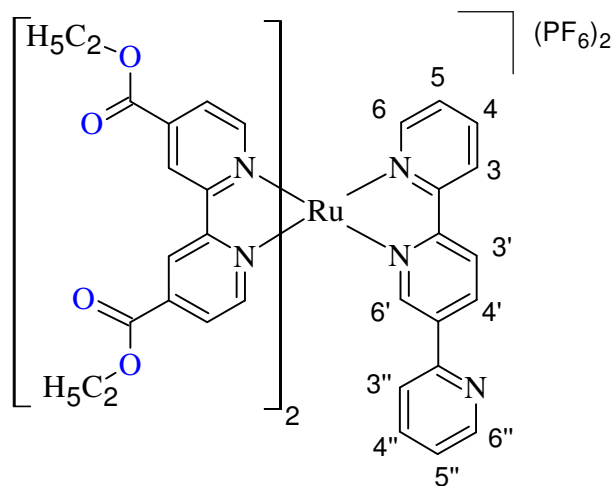
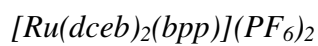


Figure 2.29: Molecular structure of $[Ru(dceb)_2(bpp)](PF_6)_2$

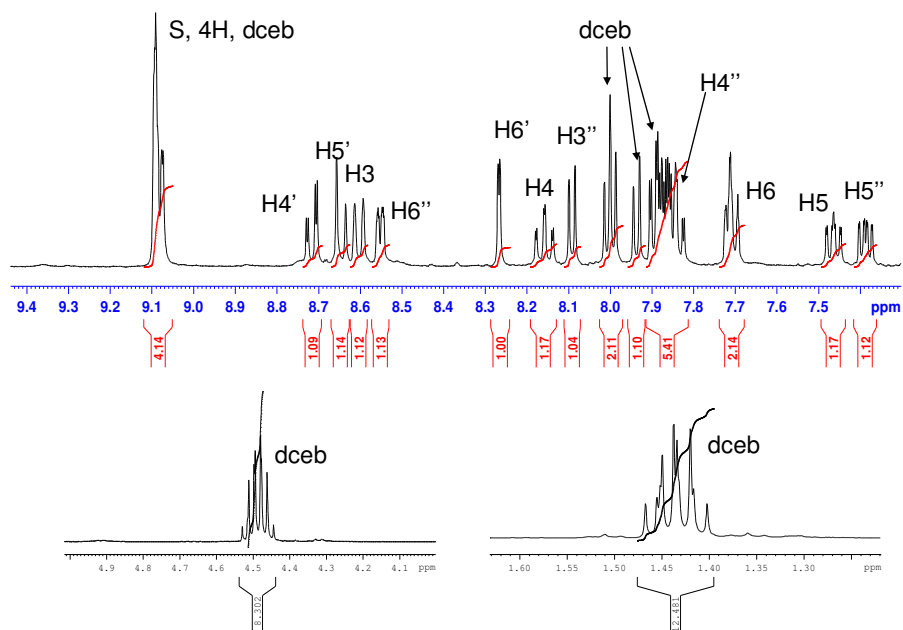


Figure 2.30: ^1H NMR(400 MHz, Acetonitrile- d_3) of $[\text{Ru}(\text{dceb})_2(\text{bpp})](\text{PF}_6)_2$

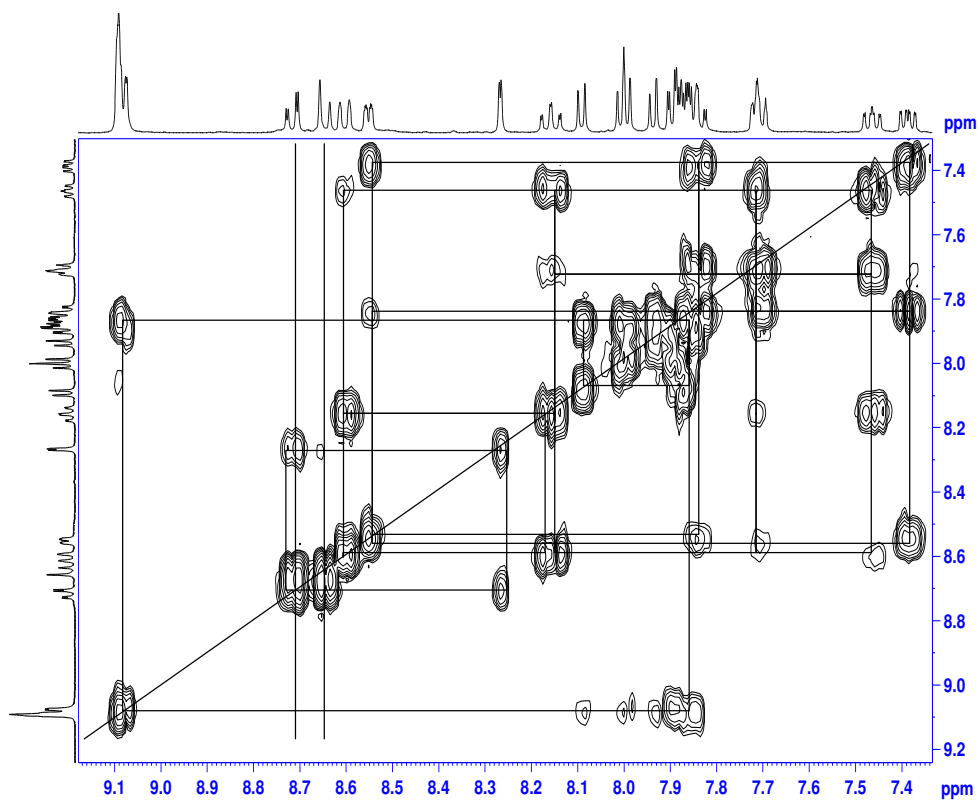


Figure 2.31: COSY NMR(400 MHz, Acetonitrile- d_3) of $[\text{Ru}(\text{dceb})_2(\text{bpp})](\text{PF}_6)_2$

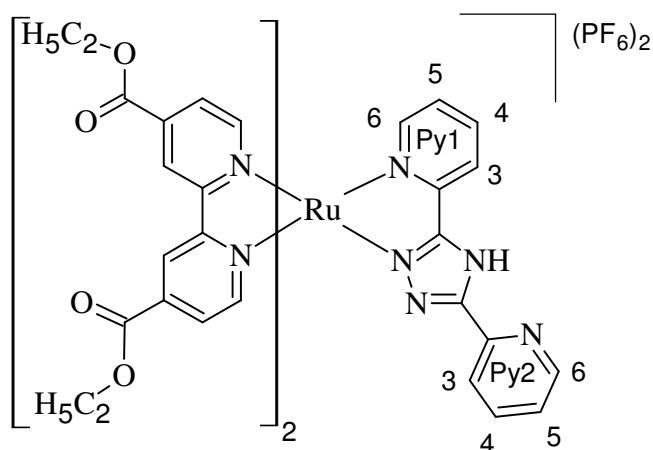
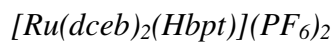


Figure 2.32: Molecular structure of $[Ru(dceb)_2(Hbpt)](PF_6)_2$

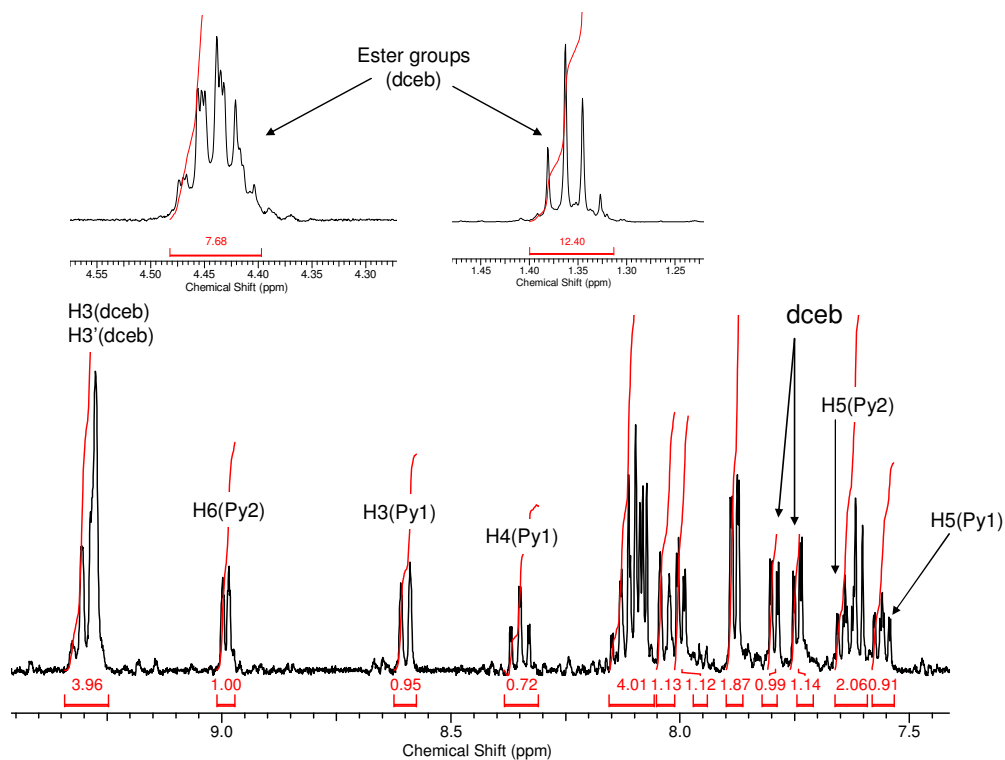


Figure 2.33: 1H NMR(400 MHz, $DMSO-d_6$) of $[Ru(dceb)_2(Hbpt)](PF_6)_2$

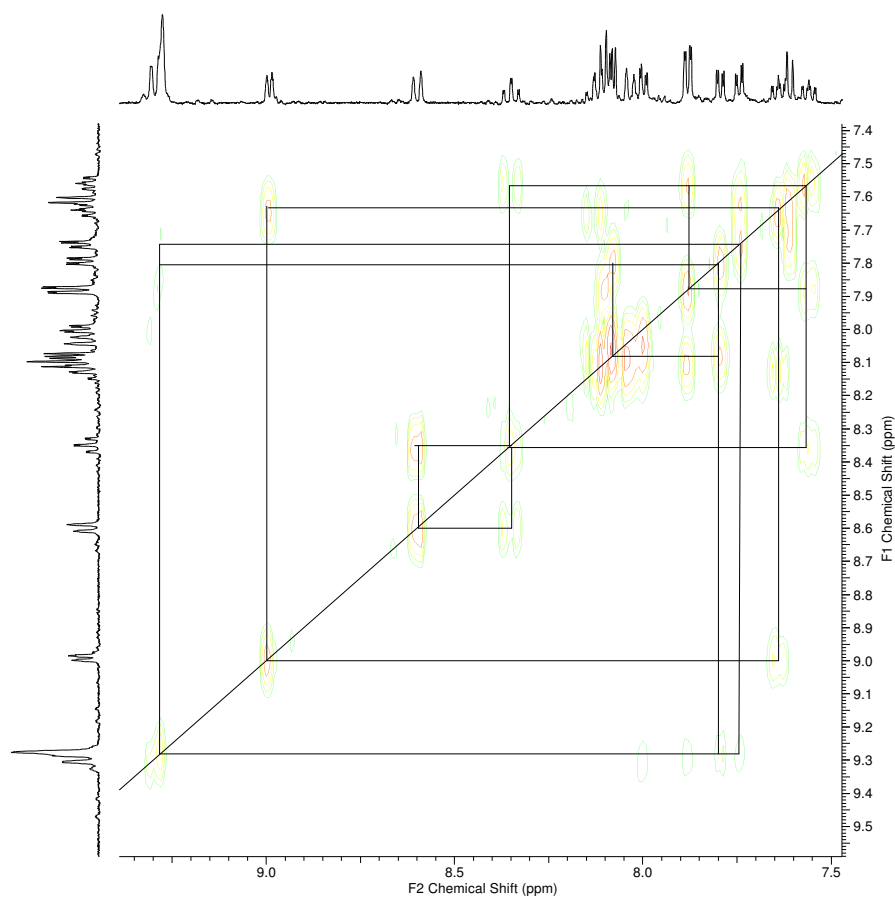


Figure 2.34: COSY NMR(400 MHz, DMSO- d_6) of $[Ru(dceb)_2(Hbpt)](PF_6)_2$

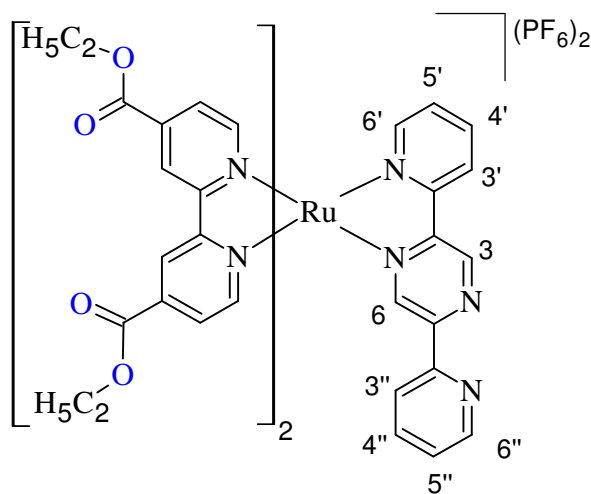
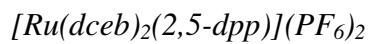


Figure 2.35: Molecular structure of $[Ru(dceb)_2(2,5-dpp)](PF_6)_2$

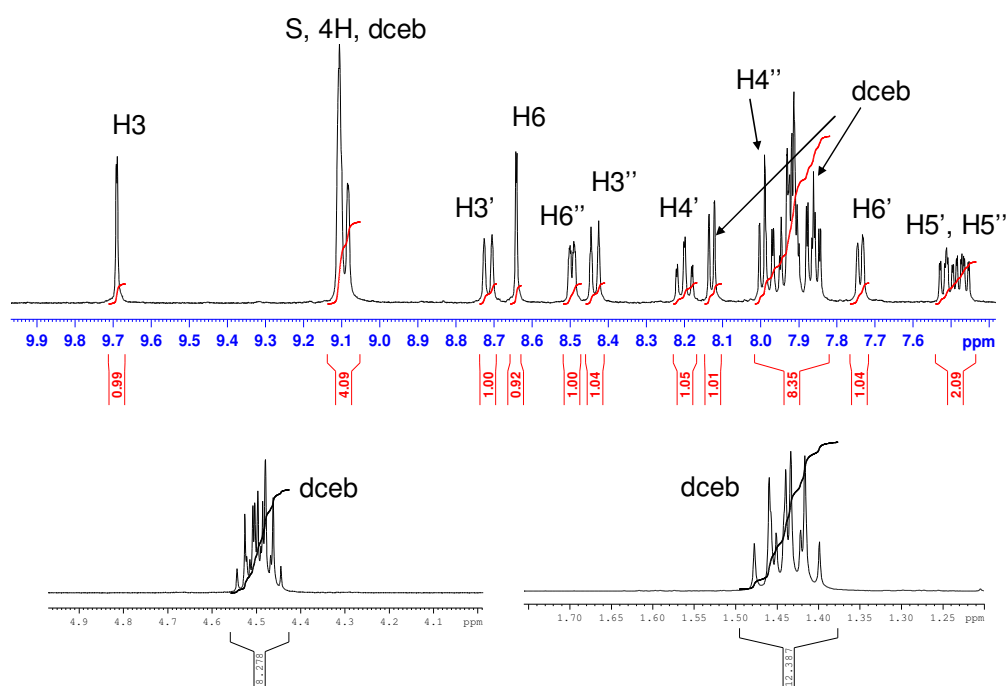


Figure 2.36: 1H NMR(400 MHz, Acetonitrile- d_3) of $[Ru(dceb)_2(2,5-dpp)](PF_6)_2$

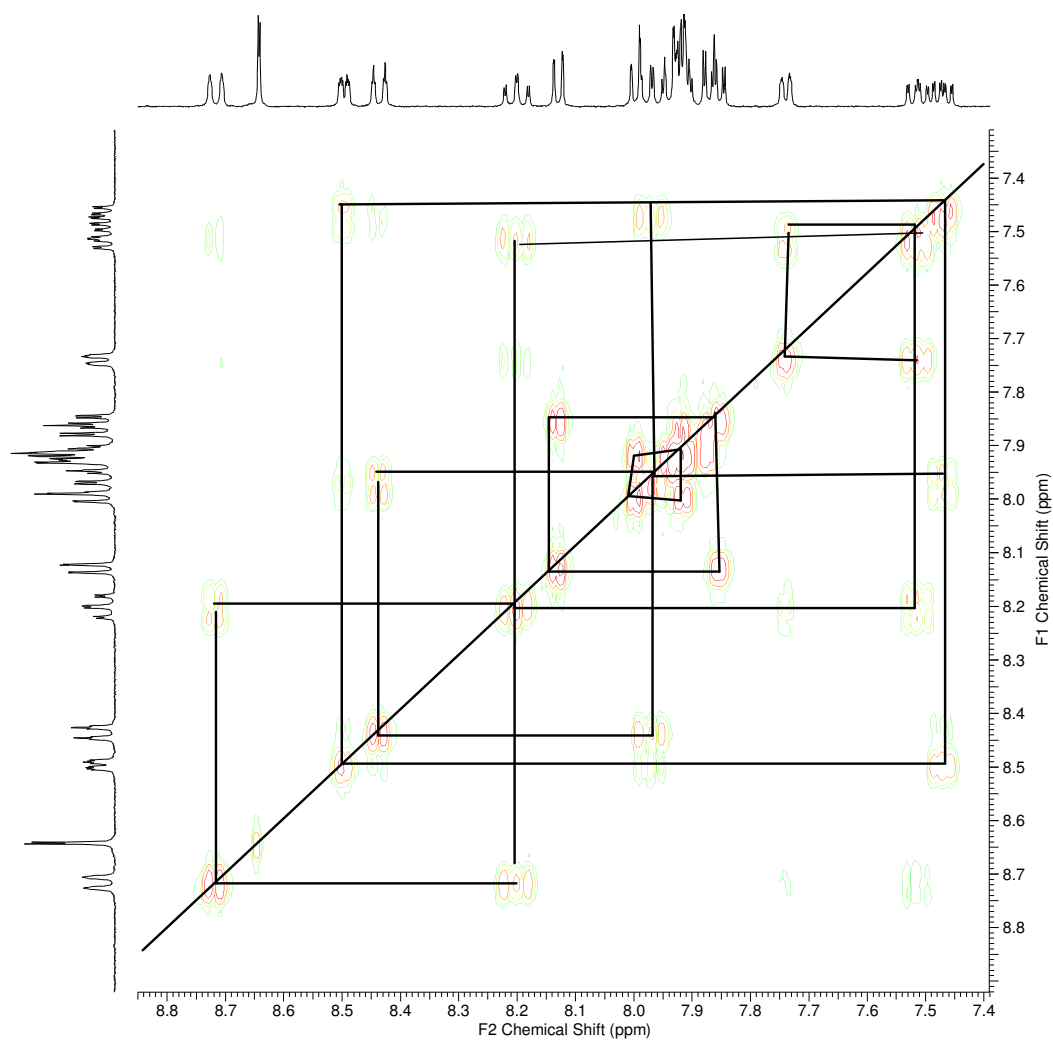


Figure 2.37: COSY NMR(400 MHz, Acetonitrile- d_3) of $[Ru(dceb)_2(2,5-dpp)](PF_6)_2$

2.5. Absorption and emission spectra of mononuclear complexes

The absorption and the emission spectra for the mononuclear complexes were carried out in acetonitrile. The absorption and emission data of all the complexes are presented in **Table 2.7**. The photophysical studies of $[\text{Ru}(\text{dceb})_2\text{Cl}_2]$ have previously been reported.^{42,46} $[\text{Ru}(\text{bpy})_2\text{Cl}_2]$ shows an intense band at 550 nm and at 377 nm in the UV region. $[\text{Ru}(\text{dceb})_2\text{Cl}_2]$ displays bands at 580 nm and 427 nm. The lower energy bands in the visible region are due to a metal \rightarrow ligand charge transfer (MLCT) corresponding to the metal t_{2g} orbital to the ligand π^* orbital and the bands in the UV region are due to ligand $\pi\text{-}\pi^*$ transitions. In the case of the $[\text{Ru}(\text{dceb})_2\text{Cl}_2]$ complex the bands are shifted more towards the red region due to the presence of two $-\text{COOC}_2\text{H}_5$ groups, which are electron-withdrawing in nature. Due to this reason the energy of the π^* orbital of the bpy ligand is lowered, and a lower energy metal to ligand CT transition result.

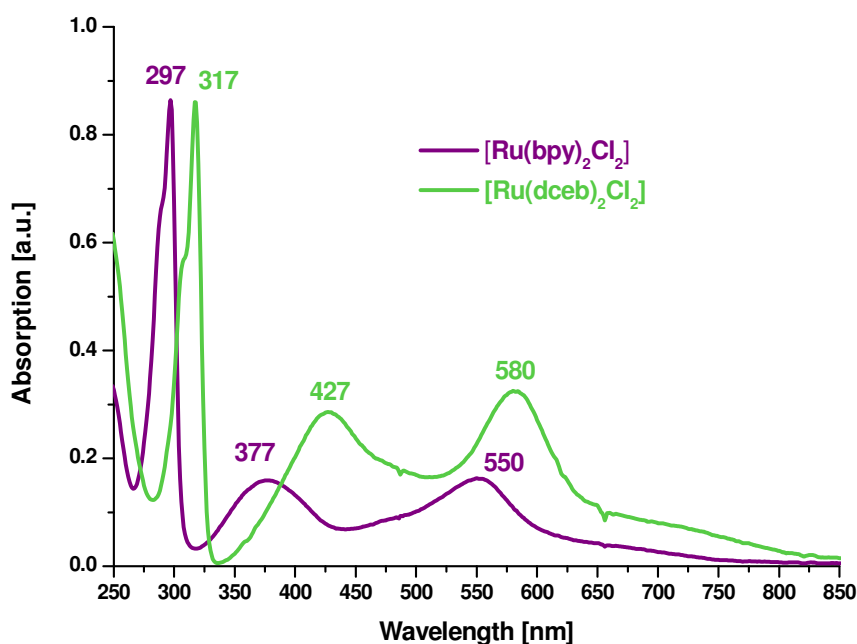


Figure 2.38: Absorption spectra of $[\text{Ru}(\text{bpy})_2\text{Cl}_2]$ and $[\text{Ru}(\text{dceb})_2\text{Cl}_2]$ in acetonitrile. Absorption intensities are normalised.

$[\text{Ru}(\text{bpy})_2(\text{L})]^{2+}$ type compounds typically have MLCT bands at ~ 450 nm.³¹ Due to the electron withdrawing effect of $-\text{COOC}_2\text{H}_5$ groups on the bpy ligands the

MLCT is also red shifted (>20 nm) in the mononuclear complexes $[\text{Ru}(\text{dceb})_2(\text{L})]^{2+}$; $\text{L} = \text{Hbpt}$, bpp , bisbpy and $2,5\text{-dpp}$).

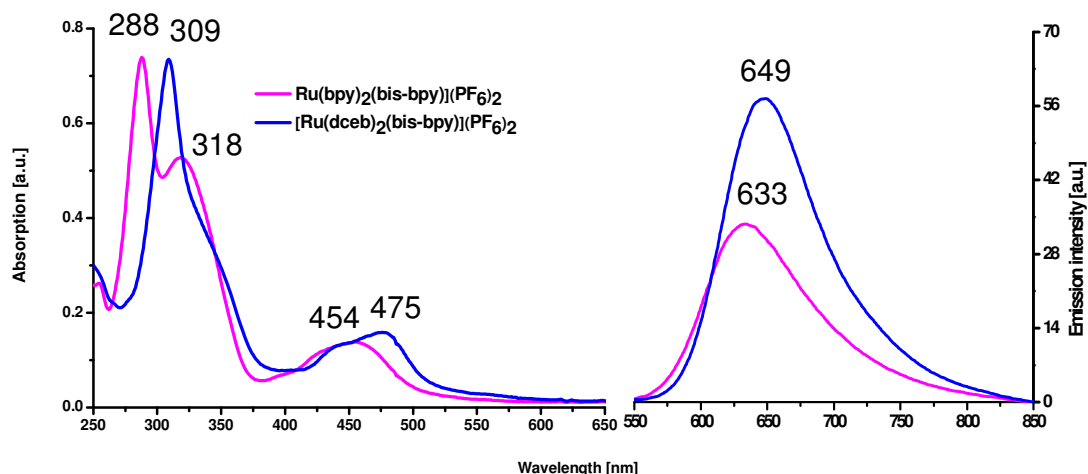


Figure 2.39: Absorption and emission spectra of $[\text{Ru}(\text{bpy})_2(\text{bisbpy})](\text{PF}_6)_2$ and $[\text{Ru}(\text{dceb})_2(\text{bisbpy})](\text{PF}_6)_2$ in MeCN (RT). Absorption intensities are normalised and emission spectra were recorded using sample OD as ~ 0.15 A.U. at 450 nm.

The band observed in the visible region at 454 nm for $[\text{Ru}(\text{bpy})_2(\text{bisbpy})](\text{PF}_6)_2$ (**Figure 2.39**) is assigned to a MLCT transition. The corresponding transition in $[\text{Ru}(\text{dceb})_2(\text{bisbpy})](\text{PF}_6)_2$ occurs at 475 nm. Both the complexes absorbed at approximately 300 nm and this is attributed to $\pi\text{-}\pi^*$ transitions. $[\text{Ru}(\text{bpy})_2(\text{bisbpy})](\text{PF}_6)_2$ has a lower energy $\pi\text{-}\pi^*$ transition than $[\text{Ru}(\text{dceb})_2(\text{bisbpy})](\text{PF}_6)_2$ which is due the carboxy substituted bpy.

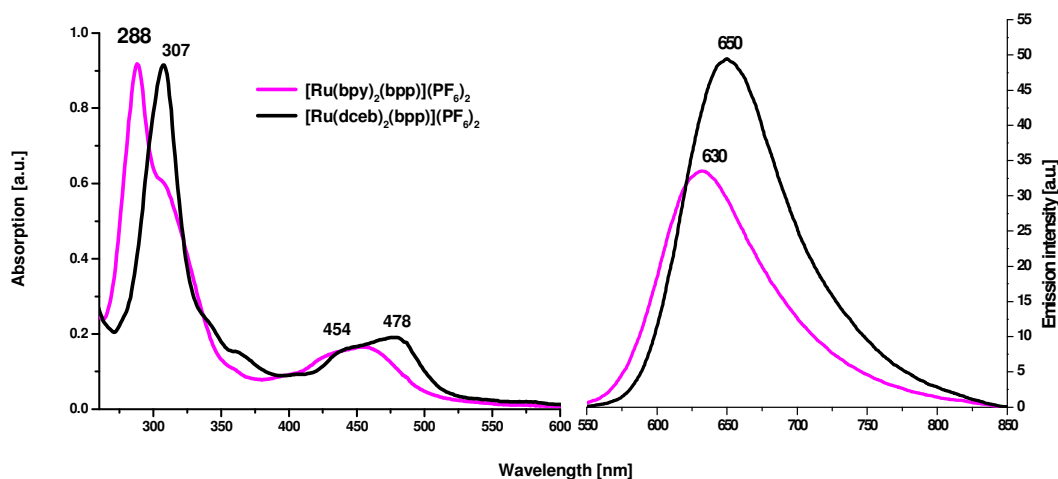


Figure 2.40: Absorption and emission spectra of $[\text{Ru}(\text{bpy})_2(\text{bpp})](\text{PF}_6)_2$ and $[\text{Ru}(\text{dceb})_2(\text{bpp})](\text{PF}_6)_2$ in MeCN (RT). Absorption intensities are normalised and emission spectra were recorded using sample OD as ~ 0.15 A.U. at 450 nm.

$[\text{Ru}(\text{bpy})_2(\text{bpp})](\text{PF}_6)_2$ displays a λ_{max} at 454 nm (**Figure 2.40**) in the visible region and a strong transition band at 288 nm. The lower energy band is the MLCT band and the higher energy band is due to a $\pi\text{-}\pi^*$ transition in the peripheral bpy ligand. For $[\text{Ru}(\text{dceb})_2(\text{bpp})](\text{PF}_6)_2$, the MLCT transition occurs at 478 nm which is lower in energy than the corresponding MLCT transition in $[\text{Ru}(\text{bpy})_2(\text{bpp})](\text{PF}_6)_2$. The higher energy $\pi\text{-}\pi^*$ transition for $[\text{Ru}(\text{dceb})_2(\text{bpp})](\text{PF}_6)_2$ is at 300 nm but this is lower in energy than the $\pi\text{-}\pi^*$ transition of $[\text{Ru}(\text{bpy})_2(\text{bpp})](\text{PF}_6)_2$. The lower energy MLCT and $\pi\text{-}\pi^*$ is due to low π^* energy level of dceb as mentioned.

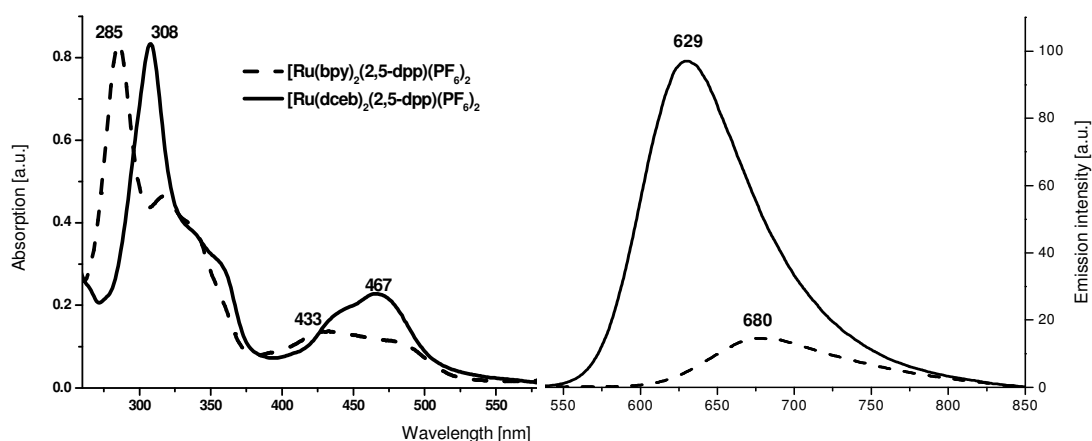


Figure 2.41: Absorption and emission spectra of $[\text{Ru}(\text{bpy})_2(2,5\text{-dpp})](\text{PF}_6)_2$ and $[\text{Ru}(\text{dceb})_2(2,5\text{-dpp})](\text{PF}_6)_2$ in MeCN (RT). Absorption intensities are normalised and emission spectra were recorded using sample OD as ~ 0.15 A.U. at 450 nm.

Absorption and emission data for $[\text{Ru}(\text{bpy})_2(2,5\text{-dpp})](\text{PF}_6)_2$ were previously reported.¹⁵ This complex has a band at 433 nm in the visible region with a shoulder at 480 nm (**Figure 2.41**). This is due to the low π^* energy level of the 2,5-dpp bridging ligand which has σ -donating ability as well as a strong π -accepting ability. It also absorbs in the region of 300-350 nm which may be due to π - π^* transitions in 2,5-dpp ligand (low π^* energy level). There is another π - π^* transition below 300 nm which is possibly due to the π - π^* transition of the bpy ligand. π - π^* transition for 2,5-dpp can not be assigned as it appears as overlapped transition band. An intense band for the π - π^* transition between 300-350 nm may be predicted for 2,5-dpp and for dceb (π - π^* transition) at 308 nm. $[\text{Ru}(\text{dceb})_2(2,5\text{-dpp})](\text{PF}_6)_2$ absorbs at 467 nm in the visible region which is the main MLCT transition. It is worth pointing out that the 450 nm bands for the two complexes are quite different in shape.

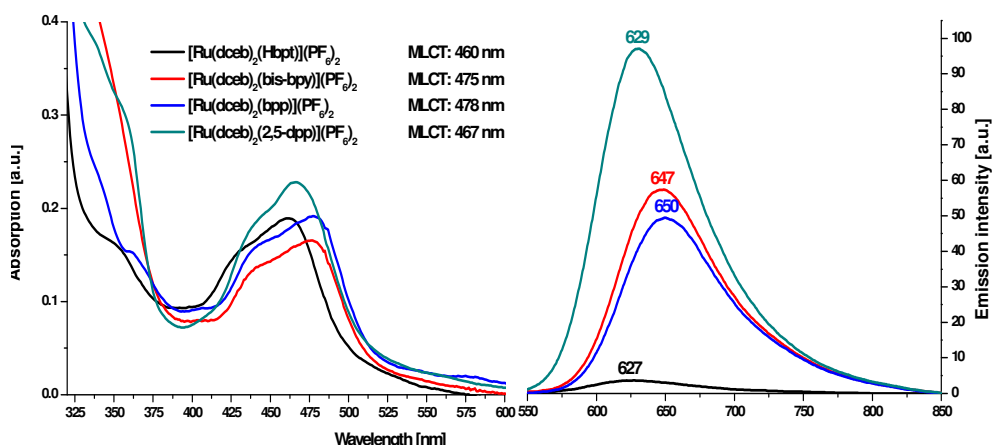


Figure 2.42: Absorption and emission spectra of $[\text{Ru}(\text{dceb})_2(\text{L})]^{2+}$ types complex; $\text{L} = \text{Hbpt}$, bisbpy , bpp , $2,5\text{-dpp}$. (The absorption and emission spectra were recorded in acetonitrile at room temperature. The excitation wavelength was set at 450 nm and optical density for each solution was 0.15 A.U. at the excitation wavelength.)

Displayed in **Figure 2.42** are the absorption and emission spectra for $[\text{Ru}(\text{dceb})_2(\text{L}_2)]^{2+}$ type complexes, where the bridging ligands differ. From the absorption spectra it is clear that the complexes absorb in a similar region in the absorption spectrum. However, their emission spectra differ from each other. $[\text{Ru}(\text{dceb})_2(\text{bpp})]^{2+}$ (650 nm) and $[\text{Ru}(\text{dceb})_2(\text{bisbpy})]^{2+}$ (647 nm) emit at a similar wavelengths and are lower in energy than $[\text{Ru}(\text{dceb})_2(\text{Hbpt})]^{2+}$ (627 nm) and $[\text{Ru}(\text{dceb})_2(2,5\text{-dpp})]^{2+}$ (629 nm). Here all four bridging ligands are neutral in nature but their σ -donation properties are different. Hbpt^{47-49} and $2,5\text{-dpp}^{50,51}$ have lower π - π^* energy and stronger σ -donation properties than the other two bridging ligands, bpp and bisbpy .

The emission properties of $[\text{Ru}(\text{L}_1)_2(\text{L}_2)]^{2+}$ type complexes are quite interesting because the above emission spectra shows significant differences. When the $[\text{Ru}(\text{L}_1)_2(\text{L}_2)]^{2+}$ complex contains the bridging ligands (2,5-dpp and Hbpt) with a strong π -acceptor as well as an σ -donor properties then the emission appears at higher energy (627 nm for $[\text{Ru}(\text{dceb})_2(\text{Hbpt})]^{2+}$ and 629 nm for $[\text{Ru}(\text{dceb})_2(2,5\text{-dpp})]^{2+}$),⁴⁷⁻⁵¹ whereas the bridging ligands (bpp and bisbpy) have only σ -donation properties, and the emission is observed at a lower energy (650 nm for $[\text{Ru}(\text{dceb})_2(\text{bpp})]^{2+}$ and 647 nm for $[\text{Ru}(\text{dceb})_2(\text{bisbpy})]^{2+}$). Introduction of ethyl ester groups to the peripheral bpy ligands also affects the emission properties. The introduction of ethyl ester groups

leads not only to an increase in the intensity of emission band but also increase in the emission wavelength (i.e., lower in energy). The exception was observed for $[\text{Ru}(\text{L}_1)_2(2,5\text{-dpp})]^{2+}$ complexes where the bridging ligand is 2,5-dpp. For the latter type complexes, the emission spectra show that with the introduction of ethyl ester groups the emission band moves to higher energy (i.e., lower wavelength) with an increase in intensity.

Table 2.7: List of absorption maxima and emission maxima of $[\text{Ru}(\text{L}_1)_2(\text{L}_2)]^{2+}$ type complexes.

Complex	Absorption ^a	Emission ^b
	(nm)/($\epsilon \times 10^4 \text{ M}^{-1} \text{ cm}^{-1}$)	298K(nm)
$[\text{Ru}(\text{dceb})_2(\text{Hbpt})](\text{PF}_6)_2$	460/(1.56)	627
$[\text{Ru}(\text{bpy})_2(\text{bisbpy})](\text{PF}_6)_2$	454/(1.16)	633
$[\text{Ru}(\text{d}_8\text{-bpy})_2(\text{bisbpy})](\text{PF}_6)_2$	454/(1.16)	633
$[\text{Ru}(\text{dceb})_2(\text{bisbpy})](\text{PF}_6)_2$	475/(1.13)	647
$[\text{Ru}(\text{bpy})_2(\text{bpp})](\text{PF}_6)_2$	454/(1.18)	630
$[\text{Ru}(\text{d}_8\text{-bpy})_2(\text{bpp})](\text{PF}_6)_2$	454/(1.18)	630
$[\text{Ru}(\text{dceb})_2(\text{bpp})](\text{PF}_6)_2$	478/(1.51)	650
$[\text{Ru}(\text{bpy})_2(2,5\text{-dpp})](\text{PF}_6)_2$	433/(0.95)	680
$[\text{Ru}(\text{d}_8\text{-bpy})_2(2,5\text{-dpp})](\text{PF}_6)_2$	433/(0.95)	680
$[\text{Ru}(\text{dceb})_2(2,5\text{-dpp})](\text{PF}_6)_2$	467/(1.79)	629

(a) The absorption and emission spectra were recorded in *acetonitrile* in *RT*. (b) Excitation wavelength used for emission spectra was 450 nm. Optical density of highest MLCT transition band was 0.15 A.U.

From the above discussion it can be concluded that the absorption and emission properties of $[\text{Ru}(\text{L}_1)_2(\text{L}_2)]^{2+}$ (L_1 = Peripheral ligand; L_2 = bridging ligand) type complexes are dependent on both the peripheral and bridging ligands. For $[\text{Ru}(\text{L}_1)_2(\text{L}_2)]^{2+}$ type complexes with the same peripheral ligands the MLCT bands and emission wavelength are dependent on the nature of the bridging ligands. If $[\text{Ru}(\text{L}_1)_2(\text{L}_2)]^{2+}$ have the same bridging ligands then the photophysical properties are dependent on the peripheral ligand, for example the MLCT band of $[\text{Ru}(\text{dceb})_2(\text{bpp})]^{2+}$ is 20 nm red shifted compared to the mononuclear complex $[\text{Ru}(\text{dceb})_2(\text{bpp})]^{2+}$. The absorption and emission data obtained for $[\text{Ru}(\text{d}_8\text{-$

$\text{bpy})_2(\text{L}_2)]^{2+}$ and $[\text{Ru}(\text{bpy})_2(\text{L}_2)]^{2+}$ (see **Table 2.7**) are similar in nature and suggests that deuteration has no effect on the absorption and emission properties of the complexes at room temperature.

2.6. Conclusion

Synthetic procedures for a number of novel polypyridyl-based ligands were discussed in the beginning of this chapter. 2,2-bipyridine (bpy) was successfully functionalised with ethyl ester groups at the 4 and 4' positions. Two novel bridging ligands (bpp and bisbpy) were synthesised and their reaction conditions were also optimised. A mechanistic study suggested two catalytic cycles are involved in the one step Negishi coupling reaction for the synthesis of bpp ligand. A Ni(0) homo coupling reaction was observed for bisbpy providing maximum yield (~80%) at room temperature.

Several synthetic reaction conditions were applied to optimise the yield of $[\text{Ru}(\text{dceb})_2\text{Cl}_2]$. These studies carried out suggested that DMF as a solvent is not favourable for the synthesis of $[\text{Ru}(\text{dceb})_2\text{Cl}_2]$ due to its complicated work up procedure and low yield of the product obtained. Therefore, a new route for the synthesis of $[\text{Ru}(\text{dceb})_2\text{Cl}_2]$ was found by modifying the reaction conditions of the reported literature procedure such as carrying out the reaction under nitrogen atmosphere and increasing the amount of solvent used in the reaction. This alteration led to the increase in the percentage of the yield of the product to 90% and reduction of the reaction time from 3 days⁴² to 24 hours. Stability of these carboxy ester groups were also studied in acidic and basic conditions. The experiment was first carried out in both room temperature and in high temperature. The study revealed that the carboxy ester groups are stable at room temperature with acidic and basic conditions but not at high temperature. This study also provided a different synthetic route for synthesising N719 which can also be used as a photosensitiser.

A number of novel $[\text{Ru}(\text{L}_1)_2(\text{L}_2)]^{2+}$ analogous mononuclear complexes were synthesised where $\text{L}_1 = \text{bpy}$, $\text{d}_8\text{-bpy}$ and dceb and $\text{L}_2 = \text{Hbpt}$, bpp , bisbpy and $2,5\text{-dpp}$. NMR interpretation of these mononuclear complexes was difficult in terms of identifying the proton signals as the polypyridyl complexes contain identical pyridyl

ring protons. These pyridyl ring protons have identical environment therefore appeared with identical chemical shifts and coupling constants. The proton signals were difficult to identify even with the help of 2D COSY NMR. Hence, the interpretation of these complexes was resolved with the help of partial deuteration of peripheral bpy ligands. Using this approach, only resonances for bridging ligand appeared in the ^1H NMR spectra which helped to identify the proton signals for bridging ligand first, and peripheral bpy ligand protons were then identified comparing both the deuterated and non deuterated ruthenium complexes. It has also been investigated that highest MLCT transition band for $[\text{Ru}(\text{dceb})_2(\text{L}_2)]^{2+}$ homologous complexes are 20-30 nm red shifted than $[\text{Ru}(\text{bpy})_2(\text{L}_2)]^{2+}$ homologous complexes. The emission property also differed in case of $[\text{Ru}(\text{dceb})_2(\text{L}_2)]^{2+}$ type complexes. Increase in the emission intensity and emission wavelength of $[\text{Ru}(\text{dceb})_2(\text{L}_2)]^{2+}$ type complexes were observed when compared to $[\text{Ru}(\text{bpy})_2(\text{L}_2)]^{2+}$ type complexes.

2.7. Experimental

2.7.1. Materials and instrumental techniques

All the solvents used for spectroscopy were of spectroscopic grade. $\text{RuCl}_3 \cdot 3\text{H}_2\text{O}$, 2,2'-bipyridine, 4,4'-dimethyl-2,2'-bipyridine, anhydrous DMF, $[\text{Pd}(\text{PPh}_3)_4]$, $[\text{Ni}(\text{PPh}_3)_2\text{Cl}_2]$ and 2-Pyridylzincbromide in THF used for the reactions below were obtained from Sigma-Aldrich and used without further purification. All other solvents and reagents used were reagent grade. $[\text{Ru}(\text{bpy})_2\text{Cl}_2] \cdot 2\text{H}_2\text{O}$, $^2,4\text{-}^8\text{H}_2$ -2,2'-bipyridine ($\text{d}_8\text{-bpy}$),⁵² 4,4'-dicarboxy-2,2'-bipyridine(dcb),^{25,29} 5-bromo-2,2'-bipyridine(5Brbpy)²³ and 2,5-bis(2-pyridyl)pyridine (2,5-dpp)^{53,54} were synthesised as reported in the literature. Completely inert atmosphere and standard Schlenk technique were used for the synthesis of $[\text{Ru}(\text{bpy})_2\text{Cl}_2]$ and $[\text{Ru}(\text{dceb})_2\text{Cl}_2]$ in anhydrous DMF. Schlenk technique was also applied for Pd(0) catalysed Negishi coupling reaction and Ni(0) catalysed Ullman type homo coupling reaction in anhydrous solvents. ^1H NMR (400 MHz) spectra were recorded in deuterated solvents ($\text{d}_6\text{-DMSO}$, $\text{d}_3\text{-acetonitrile}$) on a Bruker AC400 NMR and AC600 NMR Spectrometer with TMS or residual solvent peaks as reference. XWIN-NMR processor and ACDLABS 12.0 NMR processor software were employed to process the free induction decay (FID) profiles. The H-H 2-D COSY NMR involved the

accumulation of 128 FIDs of 16 scans. Elemental analyses (CHN) were carried out using Exador Analytical CE440 by the Microanalytical Department, University College Dublin, Ireland. UV-vis absorption spectra were recorded on a Shimadzu 3100 UV-Vis/NIR spectrophotometer with interfaced to an Elonex PC575 desktop computer using 1-cm path length quartz cells. The detection wavelength was 190-900 nm. The ASCII data for every UV-Vis spectra were further processed using Microcal Origin 8 pro software. Emission spectra were recorded on a Perkin-Elmer LS0B luminescence spectrophotometer. The solvent used for the room temperature emission spectroscopy was spectroscopic grade acetonitrile. All the spectra were initially generated by Perkin-Elmer FL Winlab custom built software and further the ASCII data were processed by Microcal Origin 8 pro software. The optical densities of all the sample solution were approximately 0.15 A.U.. The excitation wavelength employed for ruthenium mononuclear complexes was 450 nm.

2.7.2. Organic ligands

*3,5-bis(2-pyridyl)-4-hydro-1,2,4-triazole(Hbpt)*⁵⁵

1g (9.60 mmol) of 2-cyano pyridine and 5g (156 mmol) of hydrazine was heated at 100 °C for three hours. The solution yielded the intermediate orange product 3,6-bis(pyridine-2-yl)-1,2,4,5-tetrazine. The product was then heated at reflux with 120 cm³ of 2(M) HCl and allowed to cool at room temperature and neutralised with 2(M) NH₃-solution yielding the yellow precipitate 3,5-bis(2-pyridyl)-4-amino-1,2,4-triazole. The product was added to 150 cm³ of 50% H₃PO₂ and heated to reflux for 10 minutes and subsequently cooled to 0°C. Then 15 g of NaNO₂ was added carefully to the reaction mixture. The reaction mixture was stirred at room temperature for 6 hours yielding 3,5-bis(2-pyridyl)-4-hydro-1,2,4-triazole(Hbpt) as a white precipitate, which was washed with water and collected by filtration. Yield: 750 mg (3.36 mmol, 35%). ¹H NMR (DMSO-d₆, 400 MHz) δ (ppm) 8.83(d, 2 H), 8.28(d, 2 H), 8.10(dd, 2 H), 7.69(td, 2H).

5-bromo-2,2'-bipyridine (5Brbpy)

0.299 gm (0.258 mmol) of Pd(PPh₃)₄ and 2 g (8.44 mmol) of 2,5-dibromobipyridine were added to a dried two neck round bottom flask under nitrogen atmosphere. The temperature was kept low using ice bath during the addition of 19.35 ml (8.4 mmol)

of 2-pyridylzinc bromide to the reaction mixture. The reaction mixture was then stirred for 12 hours at room temperature under nitrogen atmosphere. The reaction mixture was then poured into a saturated aqueous solution of EDTA/ Na_2CO_3 until some yellow flakes appear. The aqueous mixture was extracted with dichloromethane and dried over MgSO_4 . Dichloromethane was evaporated in air and the crude product was purified by alumina column using hexane/ethyl acetate (9:1) as eluent. Yield: 1.57 g (6.67 mmol, 79.5%). ^1H NMR (400 MHz, DMSO-d_6) δ ppm 7.49 (dd, $J = 7.45$, 4.80 Hz, 1 H), 7.97 (td, $J = 7.71$, 7.71 Hz, 1 H), 8.20 (dd, $J = 8.46$, 2.40 Hz, 1 H), 8.30 - 8.39 (m, 2 H), 8.67 - 8.73 (m, 1 H), 8.82 (d $J = 2.40$, 1 H)

2,2':5',3'':6'',2'''-quaterpyridine (bisbpy)

557 mg (0.85 mmol) of $[\text{Ni}(\text{PPh}_3)_2\text{Cl}_2]$ were dissolved in 10 cm^3 of anhydrous DMF. The reaction mixture became blue. The solution was then purged with nitrogen for 15 minutes at 20°C . 55.63 mg (0.85 mmol) of zinc-powder was added and the solution was stirred for another 30 minutes under a nitrogen atmosphere. The solution turned green and finally deep brown. Then 200 mg (0.85 mmol) of 5-bromo bipyridine was added to the deep brown solution and stirred for a further 18 hours at 20°C under a nitrogen atmosphere. Completion of reaction was monitored by TLC. The reaction mixture was then poured into 150 cm^3 of 3 molar aqueous NH_3 . The product was extracted with ethyl acetate. Ethyl acetate was evaporated by rotary evaporator and the crude product was thoroughly washed with hexane. Yield: 109 mg (0.35 mmol, 83%). ^1H NMR (400 MHz, DMSO-d_6) δ ppm 7.50 (dd, $J = 7.52$, 4.74 Hz, 2 H), 8.00 (td, $J = 7.83$, 7.77 Hz, 2 H), 8.43 (dd, $J = 8.34$, 2.53 Hz, 2 H), 8.47 (d, $J = 7.83$ Hz, 2 H), 8.54 (d, $J = 8.08$ Hz, 2 H), 8.74 (d, $J = 4.11$ Hz, 2 H), 9.19 (d, $J = 1.77$ Hz, 2 H). Elemental analysis for $\text{C}_{20}\text{H}_{14}\text{N}_4 \cdot 0.2\text{H}_2\text{O}$: M.W. = 313.96; Calc. C 76.51, H 4.62, N 17.85, Found. C 76.84, H 4.63 and N 17.24%.

2,2':5',2''-terpyridine (bpp)

0.299 g (0.258 mmol) of $[\text{Pd}(\text{PPh}_3)_4]$ and 2 g (8.44 mmol) of 2,5-dibromobipyridine were added to a two necked round bottom flask under a nitrogen atmosphere. 38.7 cm^3 (16.8 mmol) of 2-pyridylzincbromide (in THF) was then added to the flask under a nitrogen atmosphere. The reaction mixture was then stirred for 15 hours in the dark at 20°C under nitrogen atmosphere. Subsequently the reaction mixture was poured into a saturated aqueous solution of EDTA/ Na_2CO_3 . The aqueous solution was

extracted with dichloromethane and the organic layer was dried over MgSO_4 . The solvent was evaporated in air and the crude product was purified on a neutral alumina column using hexane/ethyl acetate (9:1) as mobile phase. Yield: 1.57 g (6.75 mmol, 80%). ^1H NMR (400 MHz, DMSO-d_6) δ ppm 7.46 (dd, $J = 7.58, 4.80$ Hz, 1 H), 7.50 (dd, $J = 6.69, 5.43, 1.01$ Hz, 1 H), 7.98 (d, $J = 7.58$ Hz, 2H), 8.16 (d, $J = 8.08$ Hz, 1 H), 8.47 (d, $J = 8.08$ Hz, 1 H), 8.52 (d, $J = 8.34$ Hz, 1 H), 8.63 (d, $J = 8.34$ Hz, 1 H), 8.70 - 8.78 (m, 2 H), 9.40 (d, $J = 2.27$ Hz, 1 H). Elemental analysis for $\text{C}_{20}\text{H}_{14}\text{N}_4$: M.W. = 233.26; Calc. C 77.23, H 4.75, N 18.01, Found. C 77.07, H 4.77 and N 18.25%.

2,5-di(pyridin-2-yl)pyrazine (2,5-dpp)^{53,54}

The toluenesulphonyl-2-acetylpyridine oxime (26.91 mmol, 7.80 g) was dissolved in 100 ml of ethanol and reacted with 1.5 equivalents of freshly prepared potassium ethanolate in 150 ml of ethanol. Potassiumtosylate was filtered off, and diethylether was added to the filtrate to precipitate more tosylate, which was filtered off again. The filtrate was extracted three times with 2M aqueous HCl. The aqueous phase was separated, mixed with an excess of NH_4OH and stirred vigorously for 36 hours at room temperature. The orange precipitate was filtered off and recrystallised from an ethanol water mixture (3:1 volume ratio). Yield: 540 mg (1.92 mmol, 7%). ^1H NMR (400 MHz, CDCl_3) δ ppm 7.42 (dd, $J = 7.52, 4.86, 1.26$ Hz, 2 H), 7.92 (td, $J = 7.83, 7.71$ Hz, 2 H), 8.48 (d, $J = 7.89$ 2 H), 8.77 (d, $J = 4.80$ Hz, 2 H), 9.72 (s, 2 H).

2.7.3. Metal complexes

[Ru(dceb) $_2$ Cl $_2$]

Method-A: (DMF as reaction solvent)

60 mg (0.23 mmol) of $\text{RuCl}_3 \cdot 3\text{H}_2\text{O}$ were refluxed in 10 cm^3 anhydrous DMF for 20 minutes under nitrogen atmosphere and then 138 mg (0.46 mmol) of dceb (4,4'-diethoxycarbonyl-2,2'-bipyridine) was added slowly over 30 minutes. The solution became dark green. The reaction mixture was refluxed for another 30 minutes. Then the reaction mixture was cooled down to room temperature under nitrogen atmosphere. The volume of the reaction mixture was reduced by rotary evaporation and 25 cm^3 of acetone was added. The reaction mixture was again refluxed for 30 minutes and filtered immediately. The dark green filtrate was kept at low temperature

(0-4 °C) for 4 hours and dark green crystals were washed with diethyl ether and collected by filtration. Yield: 124 mg (0.16 mmol, 70%). ^1H NMR (400 MHz, $\text{DMSO-}d_6$) δ ppm 1.31 (t, $J = 7.07$ Hz, 6 H), 1.45 (t, $J = 7.07$ Hz, 6 H), 4.36 (q, $J = 7.07$ Hz, 4 H), 4.53 (q, $J = 6.99$ Hz, 4 H), 7.50 (dd, $J = 6.06, 1.77$ Hz, 2 H), 7.77 (d, $J = 6.06$ Hz, 2 H), 8.27 (dd, $J = 5.81, 1.77$ Hz, 2 H), 8.96 (s, 2 H), 9.14 (s, 2 H), 10.11 (d, $J = 6.06$ Hz, 2 H).

Method-B: (EtOH as reaction solvent)

260 mg (1 mmol) $\text{RuCl}_3 \cdot 3\text{H}_2\text{O}$ were heated at reflux in 30 cm^3 ethanol for 20 minutes under a nitrogen atmosphere. Then, 600 mg (2 mmol) of 4,4'-diethoxycarbonyl-2,2'-bipyridine(dceb) was added slowly over 30 minutes. The reaction mixture was refluxed for further 24 hours under nitrogen atmosphere. The ethanol was removed by rotary evaporation. The product was washed with diethyl ether and was collected by filtration. Yield : 694 mg (0.9 mmol, 90%). ^1H NMR (400 MHz, $\text{DMSO-}d_6$) δ ppm 1.31 (t, $J = 7.07$ Hz, 6 H), 1.45 (t, $J = 7.07$ Hz, 6 H), 4.36 (q, $J = 7.07$ Hz, 4 H), 4.53 (q, $J = 6.99$ Hz, 4 H), 7.50 (dd, $J = 6.06, 1.77$ Hz, 2 H), 7.77 (d, $J = 6.06$ Hz, 2 H), 8.27 (dd, $J = 5.81, 1.77$ Hz, 2 H), 8.95 (s, 2 H), 9.13 (s, 2 H), 10.12 (d, $J = 5.81$ Hz, 2 H). Elemental analysis for $\text{C}_{32}\text{H}_{32}\text{Cl}_2\text{N}_4\text{O}_8\text{Ru}$: M.W. = 772.59. Calc. C 49.75, H 4.17, N 7.25, Found: C 49.35, H 4.17 and N 7.00%.

$[\text{Ru}(\text{dceb})_2(\text{NCS})_2] \cdot 2\text{H}_2\text{O}$

500 mg (0.65 mmol) of $[\text{Ru}(\text{dceb})_2\text{Cl}_2] \cdot 2\text{H}_2\text{O}$ and 123 mg (1.62 mmol) of NH_4NCS were refluxed in ethanol under a N_2 atmosphere for 12 hours. The reaction solution was cooled down at room temperature and ethanol was removed by rotary evaporation. Then excess NH_4NCS was washed with water. The product was collected by filtration and was air dried. Yield: 532 mg (0.62 mmol, 96%). ^1H NMR (400 MHz, $\text{DMSO-}d_6$) δ ppm 9.46(d, 2H), 9.25(s, 2H), 9.01(s, 2H), 8.42(d, 2H), 7.81(d, 2H), 7.61(d, 2H).

$[\text{Ru}(\text{dceb})_2(\text{Hbpt})](\text{PF}_6)_2$

42 mg (1.879 mmol) of Hbpt were dissolved in 30 cm^3 ethanol/water (3:1) and heated for 15 minutes. 100 mg (0.129 mmol) of $[\text{Ru}(\text{dceb})_2\text{Cl}_2]$ in ethanol was added slowly over 30 minutes. The total volume of the reaction mixture was kept to 50 cm^3 and the

reaction mixture was refluxed for further 6 hours. The reaction mixture turned dark red. The ethanol was completely removed by rotary evaporation and another 20 cm³ of water was added to the reaction mixture. The red aqueous reaction mixture was filtered and an aqueous solution of NH₄PF₆ was added in excess to the filtrate to yield a brick red precipitate. The precipitate was washed with diethyl ether and collected by filtration. The crude product was further purified by recrystallisation using toluene/acetone solution. Yield: 98.7 mg (0.092 mmol, 75%). ¹H NMR (400 MHz, DMSO-*d*₆) δ ppm 1.30 - 1.40 (m, 12 H) 4.39 - 4.49 (m, 8 H) 7.56 (dd, *J* = 7.58, 5.94 Hz, 1 H) 7.59 - 7.67 (m, 2 H) 7.74 (dd, *J* = 5.94, 1.64 Hz, 1 H) 7.79 (dd, *J* = 5.81, 1.77 Hz, 1 H) 7.88 (dd, *J* = 5.94, 1.64 Hz, 2 H) 8.00 (dd, *J* = 6.06, 1.77 Hz, 1 H) 8.03 (d, *J* = 7.83 Hz, 1 H) 8.05 - 8.19 (m, 4 H) 8.31 - 8.40 (m, 1 H) 8.60 (d, *J* = 8.08 Hz, 1 H) 8.99 (d, *J* = 5.56 Hz, 1 H) 9.25 - 9.32 (m, 4 H). Elemental analysis for C₄₄H₄₁F₁₂N₉O₈P₂Ru. M.W. = 1216.86; Calc: C 43.43, H 3.56, N 10.36. Found: C 43.27, H 3.35 and N 10.26%.

[Ru(bpy)₂(bisbpy)](PF₆)₂.2H₂O

This complex was synthesised following the procedure of the synthesis of complex [Ru(dceb)₂(Hbpt)](PF₆)₂. 179 mg (0.577 mmol) of bisbpy and 200 mg (0.384 mmol) of [Ru(bpy)₂Cl₂].2H₂O were reacted. Recrystallisation was carried out using toluene/acetone solution. Yield: 303 mg (0.299 mmol, 78%). ¹H NMR (600 MHz, DMSO-*d*₆) δ ppm 7.51 (dd, *J* = 7.53, 4.89 Hz, 1 H), 7.53 - 7.61 (m, 6 H), 7.72 (d, *J* = 4.89 Hz, 1 H), 7.76 (d, *J* = 5.65 Hz, 2 H), 7.85 - 7.89 (m, 1 H), 7.94 (d, *J* = 5.27 Hz, 1 H), 7.96 (d, *J* = 1.88 Hz, 1 H), 7.99 (td, *J* = 7.81, 7.69 Hz, 1 H), 8.14 (dd, *J* = 8.28, 2.26 Hz, 1 H), 8.16 - 8.24 (m, 6 H), 8.37 - 8.41 (m, 1 H), 8.47 (d, *J* = 7.91 Hz, 1 H), 8.66 (dd, *J* = 8.47, 2.07 Hz, 1 H), 8.71 - 8.74 (m, 1 H), 8.80 (d, *J* = 2.26 Hz, 1 H), 8.81 - 8.88 (m, 5 H), 8.94 (d, *J* = 7.91 Hz, 1 H), 8.99 (d, *J* = 8.66 Hz, 1 H). Elemental analysis for C₄₀H₃₀F₁₂N₈P₂Ru. 2H₂O. M.W. = 1049.75; Calc: C 45.77, H 3.26, N 10.67. Found: C 46.15, H 2.86 and N 10.09%.

[Ru(d₈-bpy)₂(bisbpy)](PF₆)₂.3H₂O

This complex was synthesised following the procedure of the synthesis of complex [Ru(dceb)₂(Hbpt)](PF₆)₂. 86.67 mg (0.2796 mmol) bpp and 100 mg (0.1864 mmol) of [Ru(d₈-bpy)₂Cl₂] were taken. [Ru(d₈-bpy)₂Cl₂] was slowly added to the reaction over

1 hour of duration. Recrystallisation was carried out in ethanol/water. Yield: 137 mg (0.133 mmol, 71.37%). ^1H NMR (600 MHz, $\text{DMSO-}d_6$) δ ppm 7.49 (dd, $J = 7.34$, 4.71, Hz, 1 H), 7.55 (td, $J = 7.15$, 7.71 Hz, 1 H), 7.74 (d, $J = 5.65$ Hz, 1 H), 7.94 (s, 1 H), 7.97 (d, $J = 7.72$, 1.51 Hz, 1 H), 8.12 (dd, $J = 8.47$, 2.45 Hz, 1 H), 8.17 - 8.21 (m, 1 H), 8.37 (d, $J = 7.91$ Hz, 1 H), 8.44 (d, $J = 8.28$ Hz, 1 H), 8.63 (dd, $J = 8.47$, 2.07 Hz, 1 H), 8.70 (d, $J = 4.14$ Hz, 1 H), 8.78 (s, 1 H), 8.92 (d, $J = 8.28$ Hz, 1 H), 8.97 (d, $J = 8.28$ Hz, 1 H). Elemental analysis for $\text{C}_{40}\text{H}_{14}\text{D}_{16}\text{F}_{12}\text{N}_8\text{P}_2\text{Ru} \cdot 3\text{H}_2\text{O}$. M.W. = 1083.86; Calc: C 44.33, H 2.98, N 10.34. Found: C 46.15, H 2.72 and N 10.00%.

[Ru(dceb)₂(bisbpy)](PF₆)₂·2H₂O

This complex was synthesised following the procedure of the synthesis of complex $[\text{Ru}(\text{dceb})_2(\text{Hbpt})](\text{PF}_6)_2$. 114 mg (0.369) bisbpy and 200 mg (0.259 mmol) of $[\text{Ru}(\text{dceb})_2\text{Cl}_2]$ were reacted. $[\text{Ru}(\text{dceb})_2\text{Cl}_2]$ were added over 1 hour of duration. Recrystallisation was carried out using toluene/ethanol solution. Yield: 243 mg (0.187 mmol, 76%). ^1H NMR (400 MHz, $\text{DMSO-}d_6$) δ ppm 1.33 - 1.39 (m, 12 H), 4.39 - 4.48 (m, 8 H), 7.50 (dd, $J = 7.52$, 4.74 Hz, 1 H), 7.54 (td, $J = 7.20$, 7.71 Hz, 1 H), 7.76 (d, $J = 5.56$ Hz, 1 H), 7.85 (d, $J = 5.75$, 3.73 Hz, 2 H), 7.92 - 8.00 (m, 4 H), 8.03 (d, $J = 2.02$ Hz, 1 H), 8.05 (d, $J = 6.06$ Hz, 1 H), 8.13 (d, $J = 6.06$ Hz, 1 H), 8.17 (dd, $J = 8.46$, 2.40 Hz, 1 H), 8.26 (td, $J = 7.89$, 7.71 Hz, 1 H), 8.37 (d, $J = 8.08$ Hz, 1 H), 8.45 (d, $J = 8.34$ Hz, 1 H), 8.69 - 8.73 (m, 2 H), 8.84 (d, $J = 2.27$ Hz, 1 H), 8.98 (d, $J = 8.34$ Hz, 1 H), 9.04 (d, $J = 8.59$ Hz, 1 H), 9.28 (s, 1 H), 9.30 (s, 1 H), 9.31 (s, 1 H), 9.34 (s, 1 H). Elemental analysis for $\text{C}_{52}\text{H}_{46}\text{F}_{12}\text{N}_8\text{O}_8\text{P}_2\text{Ru} \cdot 2\text{H}_2\text{O}$. M.W. 1338. Calc: C 46.68, H 3.77, N 8.37, Found. C 46.26, H 3.29 and N 8.10%.

[Ru(bpy)₂(bpp)](PF₆)₂

This complex was synthesised following the procedure of the synthesis of complex $[\text{Ru}(\text{dceb})_2(\text{Hbpt})](\text{PF}_6)_2$. 134.4 mg (0.577) bpp and 200 mg (0.384 mmol) of $[\text{Ru}(\text{bpy})_2\text{Cl}_2]$ were taken. Recrystallisation was carried out using acetone/water solution. Yield: 302 mg (0.322 mmol, 84%). ^1H NMR (400 MHz, $\text{DMSO-}d_6$) δ ppm 7.43 (dd, $J = 7.33$, 4.80, Hz, 1 H, bpy), 7.52 (dd, $J = 7.52$, 5.87, Hz, 1 H, bpy), 7.54 - 7.58 (m, 3 H, bpy, bpp), 7.60 (dd, $J = 7.45$, 5.81 Hz, 1 H, bpy), 7.73 - 7.81 (m, 3 H, bpy, bpp), 7.85 (d, $J = 5.56$ Hz, 1 H, bpy), 7.90 (d, $J = 5.56$ Hz, 1 H, bpy), 7.91 - 8.01 (m, 2 H, bpp), 8.12 - 8.28 (m, 5 H, bpy, bpp), 8.34 (s, 1 H, bpp), 8.52 (d, $J = 4.80$ Hz,

1 H, bpp), 8.79 (d, $J = 8.59$ Hz, 1 H, bpp), 8.81 - 8.89 (m, 4 H, bpy), 8.92 (d, $J = 7.83$ Hz, 1 H, bpp), 8.95 (d, $J = 8.34$ Hz, 1 H, bpp). Elemental analysis for $C_{35}H_{27}F_{12}N_7O_8P_2Ru$. M.W. = 948.64; Calc: C 44.88, H 2.91, N 10.47. Found: C 45.06, H 2.95 and N 9.88%.

[Ru(d₈-bpy)₂(bpp)](PF₆)₂.H₂O

This complex was synthesised following the procedure of the synthesis of complex [Ru(dceb)₂(Hbpt)](PF₆)₂. 65.15 mg (0.2796 mmol) bpp and 100 mg (0.1864 mmol) of [Ru(d₈-bpy)₂Cl₂] were taken. [Ru(d₈-bpy)₂Cl₂] was slowly added to the reaction over 1 hour. Recrystallisation was carried out in ethanol/water. Yield: 134 mg (0.141 mmol, 75%). ¹H NMR (400 MHz, DMSO-*d*₆) δ ppm 7.43 (dd, $J = 7.45, 4.80$ Hz, 1 H), 7.56 (dd, $J = 7.33, 5.81$ Hz, 1 H), 7.77 (d, $J = 4.80$ Hz, 1 H), 7.91 - 7.97 (m, 1 H), 7.97 - 8.03 (m, 1 H), 8.20 (td, $J = 7.96, 7.72$ Hz, 1 H), 8.34 (d, $J = 1.77$ Hz, 1 H), 8.51 (d, $J = 4.42$ Hz, 1 H), 8.80 (d, $J = 8.59$ Hz, 1 H), 8.93 (d, $J = 8.08$ Hz, 1 H), 8.96 (d, $J = 8.34$ Hz, 1 H). Elemental analysis of $C_{35}H_{11}D_{16}F_{12}N_7P_2Ru.H_2O$. M.W. = 970.74; Calc: C 43.30, (H+D) 3.01, N 10.10. Found: C 43.27, H 2.73 and N 9.87%.

[Ru(dceb)₂(bpp)](PF₆)₂.H₂O

This complex was synthesised following the procedure for the synthesis of [Ru(dceb)₂(Hbpt)](PF₆)₂. 86 mg (0.369 mmol) bpp and 200 mg (0.259 mmol) of [Ru(dceb)₂Cl₂] were taken. Recrystallisation was carried out in acetone/water. Yield: 256 mg (0.209 mmol, 85%). ¹H NMR (400 MHz, Acetonitrile-*d*₃) δ ppm 1.39 - 1.48 (m, 12 H), 4.42 - 4.54 (m, 8 H), 7.39 (dd, $J = 7.52, 4.74$ Hz, 1 H), 7.46 (dd, $J = 7.45, 5.81$ Hz, 1 H), 7.67 - 7.74 (m, 2 H), 7.79 - 7.91 (m, 5 H), 7.94 (d, $J = 5.81$ Hz, 1 H), 7.97 - 8.03 (m, 2 H), 8.09 (d, $J = 6.06$ Hz, 1 H), 8.16 (td, $J = 7.89, 7.71$ Hz, 1 H), 8.27 (s, 1 H), 8.55 (d, $J = 4.80$ Hz, 1 H), 8.60 (d, $J = 8.08$ Hz, 1 H), 8.65 (d, $J = 8.34$ Hz, 1 H), 8.72 (d, $J = 8.59$ Hz, 1 H), 9.04 - 9.12 (m, 4 H). Elemental analysis for $C_{47}H_{43}F_{12}N_7O_8P_2Ru.H_2O$ M.W. = 1242.89. Calc: C 45.42, H 3.65, N 7.89. Found: C 45.78, H 3.70 and N 7.94%.

[Ru(bpy)₂(2,5-dpp)](PF₆)₂⁶

This complex was synthesised following the general procedure of the synthesis of complex [Ru(dceb)₂(Hbpt)](PF₆)₂. 135 mg (0.577 mmol) 2,5-dpp and 200 mg (0.384 mmol) of [Ru(bpy)₂Cl₂] were taken. [Ru(bpy)₂Cl₂] was slowly added to the reaction

mixture over 1 hour of duration. Recrystallisation was performed in acetone/water. Yield: 310 mg (0.33 mmol, 86%). ^1H NMR (400 MHz, Acetonitrile- d_3) δ ppm 7.41 (dd, $J = 7.45, 5.81$ Hz, 1 H, bpy), 7.43 - 7.54 (m, 5 H, dpp), 7.71 - 7.77 (m, 2 H, bpy), 7.79 - 7.84 (m, 2 H, dpp), 7.91 (d, $J = 6.32$ Hz, 1 H, bpy), 7.97 (td, $J = 7.71, 7.71$ Hz, 1 H, dpp), 8.06 - 8.22 (m, 5 H, bpy, dpp), 8.44 (td, $J = 8.08, 7.71$ Hz, 1 H, dpp), 8.47 - 8.59 (m, 5 H, bpy, dpp), 8.69 (d, $J = 8.08$ Hz, 1 H, dpp), 8.73 (d, para coupling $J = 1.26$ Hz, 1 H, dpp), 9.65 (d, para coupling $J = 1.26$ Hz, 1 H, dpp). Elemental analysis for $\text{C}_{34}\text{H}_{26}\text{F}_{12}\text{N}_8\text{P}_2\text{Ru}$: M.W. = 937.62. Calc. C 43.55, H 2.79, N 11.95, found C 43.11, H 2.94 and N 11.46%.

[Ru(d₈-bpy)₂(2,5-dpp)](PF₆)₂·H₂O

This complex was synthesised following the procedure of the synthesis of complex $[\text{Ru}(\text{dceb})_2(\text{Hbpt})](\text{PF}_6)_2$. 65.42 mg (0.2796 mmol) 2,5-dpp and 100 mg (0.1864 mmol) of $[\text{Ru}(\text{d}_8\text{-bpy})_2\text{Cl}_2]$ were taken. $[\text{Ru}(\text{d}_8\text{-bpy})_2\text{Cl}_2]$ was slowly added to the reaction over 1 hour of duration. Recrystallisation was performed in acetone/water. Yield: 131 mg (0.137 mmol, 73%). ^1H NMR (400 MHz, Acetonitrile- d_3) δ ppm 7.44 - 7.53 (m, 2 H), 7.79 - 7.83 (m, 1 H), 7.98 (td, $J = 7.77, 7.71$ Hz, 1 H), 8.15 (td, $J = 7.96, 7.52$ Hz, 1 H), 8.43 (d, $J = 7.83$ Hz, 1 H), 8.51 (d, $J = 4.29$ Hz, 1 H), 8.70 (d, $J = 8.08$ Hz, 1 H), 8.72 - 8.77 (m, 1 H), 9.61 - 9.69 (m, 1 H). Elemental analysis for $\text{C}_{34}\text{H}_{10}\text{D}_{16}\text{F}_{12}\text{N}_8\text{P}_2\text{Ru} \cdot \text{H}_2\text{O}$: M.W. = 971.73. Calc. C 42.02, (H+D) 2.80, N 11.53, found C 42.14, H 2.94 and N 11.63%.

[Ru(dceb)₂(2,5-dpp)](PF₆)₂·2H₂O

This complex was synthesised following general procedure of the synthesis of complex $[\text{Ru}(\text{dceb})_2(\text{Hbpt})](\text{PF}_6)_2$. 86.34 mg (0.369 mmol) 2,5-dpp and 200 mg (0.259 mmol) of $[\text{Ru}(\text{dceb})_2\text{Cl}_2]$ were taken. $[\text{Ru}(\text{dceb})_2\text{Cl}_2]$ was added over one hour of duration. Recrystallisation was performed in acetone/water. Yield: 256 mg (0.209 mmol, 85%). ^1H NMR (400 MHz, Acetonitrile- d_3) δ ppm 1.37 - 1.50 (m, 12 H), 4.43 - 4.55 (m, 8 H), 7.47 (dd, $J = 7.64, 4.74$ Hz, 1 H), 7.51 (dd, $J = 7.58, 5.56$ Hz, 1 H), 7.74 (t, $J = 4.99$ Hz, 1 H), 7.83 - 7.89 (m, 2 H), 7.89 - 8.02 (m, 6 H), 8.13 (d, $J = 5.81$ Hz, 1 H), 8.20 (t, $J = 7.96$ Hz, 1 H), 8.44 (t, $J = 7.83$ Hz, 1 H), 8.50 (d, $J = 4.67$ Hz, 1 H), 8.64 (d, $J = 1.26$ Hz, 1 H), 8.72 (d, $J = 8.08$ Hz, 1 H), 9.06 - 9.14 (m, 4 H), 9.69 (d, $J = 1.26$ Hz, 1 H). Elemental analysis for $\text{C}_{46}\text{H}_{46}\text{F}_{12}\text{N}_8\text{O}_{10}\text{P}_2\text{Ru} \cdot 2\text{H}_2\text{O}$. M.W. = 1289.95 Calc: C 43.78, H 3.67, N 8.88. Found: C 43.53, H 3.31 and N 8.49%.

2.8. References

-
- (1) Lancaster, K. M.; Gerken, J. B.; Durrell, A. C.; Palmer, J. H.; Gray, H. B. *Coord. Chem. Rev.* **2010**, *254*, 1803-1811.
 - (2) Mongey, K. F.; Vos, J. G.; MacCraith, B. D.; McDonagh, C. M. *Coord. Chem. Rev.* **1999**, *185-186*, 417-429.
 - (3) Shan, B. Z.; Zhao, Q.; Goswami, N.; Eichhorn, D. M.; Rillema, D. P. *Coord. Chem. Rev.* **2001**, *211*, 117-144.
 - (4) Ward, M. D. *Coord. Chem. Rev.* **2006**, *250*, 3128-3141.
 - (5) Au, Y.-K.; Wong, W.-T. *Coord. Chem. Rev.* **1997**, *162*, 417-475.
 - (6) Chan, S.; Wong, W.-T. *Coord. Chem. Rev.* **1995**, *138*, 219-296.
 - (7) Garcia, C. G.; de Lima, J. F.; Murakami Iha, N. Y. *Coord. Chem. Rev.* **2000**, *196*, 219-247.
 - (8) Ford, W. E.; Wessels, J. M.; Rodgers, M. A. J. *J. Phy. Chem. B* **1997**, *101*, 7435-7442.
 - (9) Galoppini, E.; Guo, W.; Zhang, W.; Hoertz, P. G.; Qu, P.; Meyer, G. J. *J. Am. Chem. Soc.* **2002**, *124*, 7801-7811.
 - (10) Ning, Z.; Zhang, Q.; Wu, W.; Tian, H. *J. Organomet. Chem.* **2009**, *694*, 2705-2711.
 - (11) Vougioukalakis, G. C.; Philippopoulos, A. I.; Stergiopoulos, T.; Falaras, P. *Coord. Chem. Rev.* **2011**, *255*, 2602-2621.
 - (12) Walter, M. G.; Warren, E. L.; McKone, J. R.; Boettcher, S. W.; Mi, Q.; Santori, E. A.; Lewis, N. S. *Chem. Rev.* **2010**, *110*, 6446-6473.
 - (13) Concepcion, J. J.; Jurss, J. W.; Norris, M. R.; Chen, Z.; Templeton, J. L.; Meyer, T. J. *Inorg. Chem.* **2010**, *49*, 1277-1279.
 - (14) Tinker, L. L.; McDaniel, N. D.; Curtin, P. N.; Smith, C. K.; Ireland, M. J.; Bernhard, S. *Chem. Eur. J.* **2007**, *13*, 8726-8732.
 - (15) Elvington, M.; Brown, J.; Arachchige, S. M.; Brewer, K. J. *J. Am. Chem. Soc.* **2007**, *129*, 10644-10645.
 - (16) Rau, S.; Schäfer, B.; Gleich, D.; Anders, E.; Rudolph, M.; Friedrich, M.; Görls, H.; Henry, W.; Vos, J. G. *Angew. Chem. Int. Ed.* **2006**, *45*, 6215-6218.
 - (17) Rau, S.; Walther, D.; Vos, J. G. *Dalton Trans.* **2007**, 915-919.
 - (18) Coleman, A.; Brennan, C.; Vos, J. G.; Pryce, M. T. *Coord. Chem. Rev.* **2008**, *252*, 2585-2595.

- (19) Doherty, M. D.; Grills, D. C.; Fujita, E. *Inorg. Chem.* **2009**, *48*, 1796-1798.
- (20) O'Regan, B.; Gratzel, M. *Nature* **1991**, *353*, 737-740.
- (21) Pechy, P.; Rotzinger, F. P.; Nazeeruddin, M. K.; Kohle, O.; Zakeeruddin, S. M.; Humphry-Baker, R.; Gratzel, M. *Chem. Comm.* **1995**, 65-66.
- (22) Donnici, C. L.; Maximo Filho, D. H.; Moreira, L. L. c. C.; Reis, G. T. d.; Cordeiro, E. S.; Oliveira, I. M. F. d.; Carvalho, S.; Paniago, E. B. *J. Braz. Chem. Soc.* **1998**, *9*, 455-460.
- (23) Fang, Y.-Q.; Hanan, G. S. *Synlett* **2003**, *2003*, 0852,0854.
- (24) Liska, P.; Vlachopoulos, N.; Nazeeruddin, M. K.; Comte, P.; Graetzel, M. *J. Am. Chem. Soc.* **1988**, *110*, 3686-3687.
- (25) Nazeeruddin, M. K.; Kay, A.; Rodicio, I.; Humphry-Baker, R.; Mueller, E.; Liska, P.; Vlachopoulos, N.; Graetzel, M. *J. Am. Chem. Soc.* **1993**, *115*, 6382-6390.
- (26) Singh, N.; Lee, D. G. *Organic Process Research & Development* **2001**, *5*, 599-603.
- (27) Oki, A. R.; Morgan, R. J. *Synth. Commun.* **1995**, *25*, 4093-4097.
- (28) Sprintschnik, G.; Sprintschnik, H. W.; Kirsch, P. P.; Whitten, D. G. *J. Am. Chem. Soc.* **1977**, *99*, 4947-4954.
- (29) Greenway, G. M.; Greenwood, A.; Watts, P.; Wiles, C. *Chem. Comm.* **2006**, 85-87.
- (30) Wiederholt, K.; McLaughlin, L. W. *Nucleic Acids Res.* **1999**, *27*, 2487-2493.
- (31) Barigelletti, F.; De Cola, L.; Balzani, V.; Hage, R.; Haasnoot, J. G.; Reedijk, J.; Vos, J. G. *Inorg. Chem.* **1989**, *28*, 4344-4350.
- (32) Hage, R.; Dijkhuis, A. H. J.; Haasnoot, J. G.; Prins, R.; Reedijk, J.; Buchanan, B. E.; Vos, J. G. *Inorg. Chem.* **1988**, *27*, 2185-2189.
- (33) Bentiss, F.; Lagrennee, M.; Vezin, H.; Bouanis, M.; Mernari, B. *J. Heterocyclic Chem.* **2002**, *39*, 93-96.
- (34) Liu, Q.; Duan, H.; Luo, X.; Tang, Y.; Li, G.; Huang, R.; Lei, A. *Adv. Syn. Cat.* **2008**, *350*, 1349-1354.
- (35) Lützen, A.; Hapke, M. *Eur. J. Org. Chem.* **2002**, *2002*, 2292-2297.
- (36) Milne, J. E.; Buchwald, S. L. *J. Am. Chem. Soc.* **2004**, *126*, 13028-13032.
- (37) Kiehne, U.; Bunzen, J.; Staats, H.; Lutzen, A. *Synthesis* **2007**, 1061-1069.
- (38) Inagaki, A.; Nakagawa, H.; Akita, M.; Inoue, K.; Sakai, M.; Fujii, M. *Dalton Trans.* **2008**, 6709-6723.

- (39) Cassidy, L.; Horn, S.; Cleary, L.; Halpin, Y.; Browne, W. R.; Vos, J. G. *Dalton Trans.* **2009**, 3923-3928.
- (40) Leadbeater, N. E.; Resouly, S. M. *Tetrahedron Lett.* **1999**, 40, 4243-4246.
- (41) Schwalbe, M.; Schäfer, B.; Görls, H.; Rau, S.; Tschierlei, S.; Schmitt, M.; Popp, J.; Vaughan, G.; Henry, W.; Vos, J. G. *Eur. J. Inorg. Chem.* **2008**, 2008, 3310-3319.
- (42) Hou, Y.-J.; Xie, P.-H.; Zhang, B.-W.; Cao, Y.; Xiao, X.-R.; Wang, W.-B. *Inorg. Chem.* **1999**, 38, 6320-6322.
- (43) Herber, R. H.; Nan, G.; Potenza, J. A.; Schugar, H. J.; Bino, A. *Inorg. Chem.* **1989**, 28, 938-942.
- (44) Park, Y.; Mee Jung, Y.; Sarker, S.; Lee, J.-J.; Lee, Y.; Lee, K.; Jin Oh, J.; Joo, S.-W. *Sol. Energy Mater. Sol. Cells* **2010**, 94, 857-864.
- (45) Finnie, K. S.; Bartlett, J. R.; Woolfrey, J. L. *Langmuir* **1998**, 14, 2744-2749.
- (46) Shklover, V.; Nazeeruddin, M. K.; Zakeeruddin, S. M.; Barba, C.; Kay, A.; Haibach, T.; Steurer, W.; Hermann, R.; Nissen, H. U.; Gratzel, M. *Chem. Mat.* **1997**, 9, 430-439.
- (47) Mulhern, D.; Brooker, S.; Görls, H.; Rau, S.; Vos, J. G. *Dalton Trans.* **2006**, 51-57.
- (48) Burke, H. M.; Gallagher, J. F.; Indelli, M. T.; Vos, J. G. *Inorg. Chim. Acta* **2004**, 357, 2989-3000.
- (49) MacQueen, D. B.; Petersen, J. D. *Coord. Chem. Rev.* **1990**, 97, 249-260.
- (50) Marcaccio, M.; Paolucci, F.; Paradisi, C.; Roffia, S.; Fontanesi, C.; Yellowlees, L. J.; Serroni, S.; Campagna, S.; Denti, G.; Balzani, V. *J. Am. Chem. Soc.* **1999**, 121, 10081-10091.
- (51) Ferrari, M. B.; Fava, G. G.; Pelosi, G.; Predieri, G.; Vignali, C.; Denti, G.; Serroni, S. *Inorg. Chim. Acta* **1998**, 275-276, 320-326.
- (52) Browne, W. R.; Vos, J. G. *Coord. Chem. Rev.* **2001**, 219-221, 761-787.
- (53) Yuste, C.; Bentama, A.; Marino, N.; Armentano, D.; Setifi, F.; Triki, S.; Lloret, F.; Julve, M. *Polyhedron* **2009**, 28, 1287-1294.
- (54) Escuer, A.; Comas, T.; Vicente, R.; Ribas, J. *Trans. Met. Chem.* **1993**, 18, 42-44.
- (55) Geldard, J. F.; Lions, F. *J. Org. Chem.* **1965**, 30, 318-319.

Chapter 3

Synthesis and characterisation of Ru(II)/Re(I) complexes

Chapter 3 covers the synthesis and characterisation of Ru(II)-Re(I) heterodinuclear complexes which contain carboxy functionalised peripheral ligands and different bridging ligands. Various reaction conditions for the synthesis of the carboxy functionalised ruthenium-rhenium heterodinuclear complexes are discussed. This chapter tries to understand the different isomerism pattern for Ru(II)-Re(I) heterodinuclear complexes with the help of NMR and IR spectroscopy. The absorption and emission spectra of these complexes were recorded and described. This chapter also introduces a preliminary surface immobilisation study for Ru(II)/Re(I) heterodinuclear and mononuclear Re(I) complexes containing carboxy and phosphonate ester groups.

3.1. Introduction

Photo-catalysis is being widely investigated to convert solar energy to chemical energy, using d^6 transition metal complexes in recent years.¹⁻⁶ These metal complexes are used to reduce small molecules like water and CO_2 to produce hydrogen or CO.⁷⁻¹⁰ Transferring electrons from the light absorbing unit to the catalytic centre is required for artificial photosynthesis.^{6,11-22} Recently, Ru(II)-Re(I) heterodinuclear complexes have been used for visible light driven conversion of CO_2 to products including CO, formate or oxalate.^{23,24} Reduction of CO_2 to chemical energy can create a new green, and pollution free world as an alternative solution for the recent energy crisis and the global warming. Ruthenium(II) carbonyl complexes^{7,25} and cobalt(III) trisbipyridine complexes²⁶ were extensively used as photocatalysts for the reduction of CO_2 . The Ru and Co polypyridyl metal complexes absorb light in the visible region; therefore can act as a photosensitiser as well as an active catalytic centre for the reduction of CO_2 . CO was found as the principle reduced product of CO_2 in all the reported catalytic processes. Rhenium(I) carbonyl complexes have been studied by many research groups to understand and investigate the catalytic process involved in the photo-reduction of CO_2 . Rhenium(I) carbonyl complexes absorb light in the UV region (~ 365 nm) whereas Ru(II)-Re(I) heterodinuclear complexes absorb light at longer wavelengths, greater than 430 nm.^{7,27-33} Therefore, Ru-Re heterodinuclear photocatalysts are more advantageous over the rhenium mononuclear carbonyl complexes in terms of visible light driven photocatalysis.

Currently, artificial photosynthesis is a vibrant research topic. The list of photocatalysts reported by different groups are as follows. Vogler *et al.*,³⁴ Sahai *et al.*,³⁵ Kalyanasundaram *et al.*^{36,37}, Bardwell *et al.*,³⁸ Van *et al.*³⁹, Encinas *et al.*⁴⁰ and Ishitani *et al.*^{23,41-51} reported several mononuclear rhenium(I) and ruthenium(II)-rhenium(I) heterodinuclear complexes. Most recently, a rhenium complex, typically named as rhenium(I) phenanthroline-polyoxometalate hybrid reported by Ettedgui *et al.*⁵² were used as active photocatalysts for the reduction CO_2 . In all the cases, the ruthenium(II) moiety acted as a photosensitiser where the peripheral ligands at the ruthenium(II) centre were 2,2-bipyridine and 4,4'-dimethyl-2,2'-bipyridine. Rhenium(I) tricarbonylchloride acted as an active catalytic centre.

Bridging ligands play an important role in binding photosensitisers and photocatalytic metal centre together to form a heterodinuclear photocatalyst. The bridging ligand is the mediator, which transfers the excited state electrons to the catalytic centre. This chapter will focus on the synthesis of novel Ru(II)-Re(I) heterodinuclear complexes and their characterisation with the help of partial deuteration. A number of ruthenium mononuclear complexes were synthesised in **Chapter 2**, and were selected for preparing Ru(II)-Re(I) heterodinuclear complexes. The bridging ligands utilised here are quite different from those previously reported by Ishitani and co-workers. Previously reported bridging ligands used by Ishitani's research group are made of two bipyridine units connected with an aliphatic chain. Structurally, the reported bridging ligands are not conjugated. The Ru-Re heterodinuclear complexes containing non-conjugated bridging ligands were also successful in reducing CO₂ with high turnover numbers of more than 240. The main reason behind such high turn-over numbers is the correct energy level overlap between bridging ligand and the catalytic Re centre. The bridging ligands used here are conjugated in nature. Therefore, it is anticipated that conjugation in the ligand will facilitate electron transfer from the ruthenium photosensitiser to the rhenium catalytic centre. Moreover, the conjugated bridging ligands should also meet the criteria of energy level overlapping for the effective electron transfer. The Ru-Re heterodinuclear complexes synthesised and characterised in this chapter are examples of a number of Ru-Re heterodinuclear complexes containing carboxy ester groups. Carboxy groups are known as good anchors for the semiconductors, therefore Ru-Re heterodinuclear complexes can be bound to the surface of semiconductors. A list of the bridging ligands used for synthesising Ru-Re heterodinuclear complexes are shown in **Figure 3.1**.

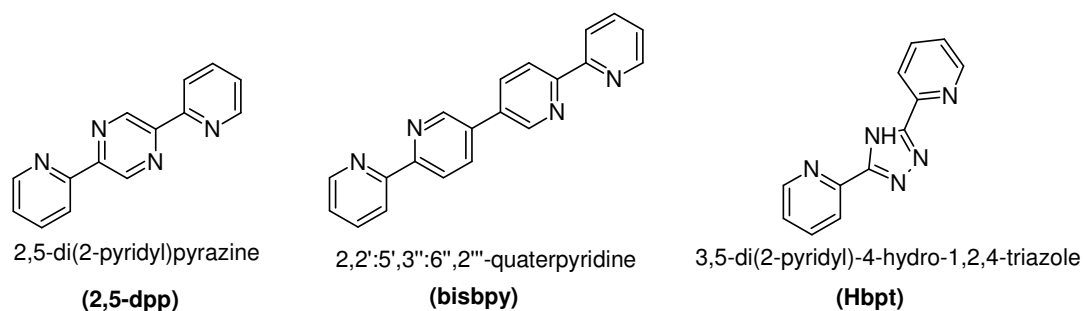


Figure 3.1: List of bridging ligands and their structures

The aim of this chapter is to report the synthesis, characterisation and isomerisation of carboxy derivatised Ru(II)/Re(I) complexes. NMR interpretation and the isomerisation pattern observed are discussed with the help of partial deuteration of the complexes. Photocatalysis using a Ru-Re heterodinuclear system was first introduced by Ishitani *et al.*^{50,53,54} who synthesised a series of Ru-Re heterodinuclear catalysts for CO₂ reduction. Here the ultimate aim is to carry out heterogeneous catalysis on the surface of semiconductors using Ru-Re photocatalysts. In **Chapter 2**, a number of photocatalysts were designed for the production of hydrogen on semiconductor surfaces. Similarly, in this chapter carboxy derivatised Ru-Re catalysts are designed based on different bridging ligands. The designed photocatalysts are shown in **Figure 3.2**. This chapter will also address the synthetic modifications of Ru(II)/Re(I) heterodinuclear complexes which contain carboxy ester groups and the effect of carboxy ester groups on the electronic absorption and emission spectra.

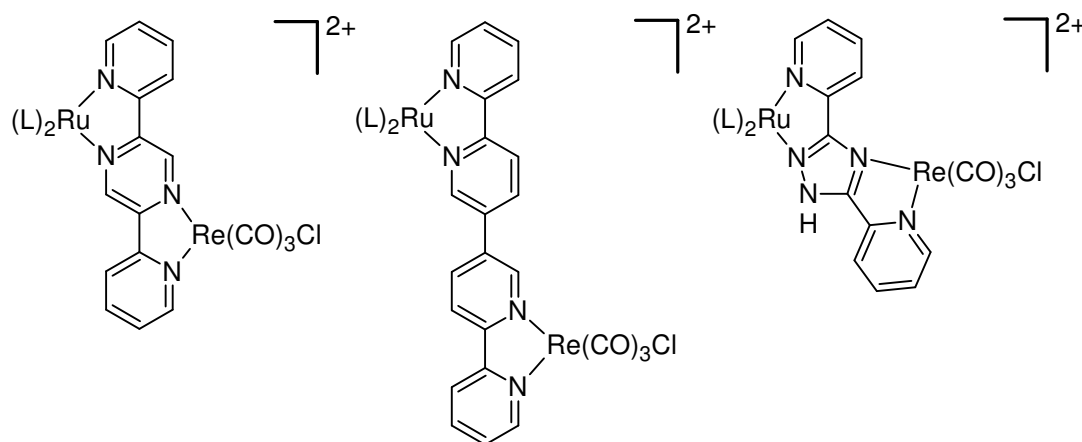


Figure 3.2: List of ruthenium(II)-rhenium(I) heterodinuclear complexes synthesised ($L = 2,2'$ -bipyridine, d_8 - $2,2'$ -bipyridine, $4,4'$ -diethylcarboxy- $2,2'$ -bipyridine).

Photocatalytic CO₂ reduction can then be carried out without sacrificial agents and organic solvent, when the complexes are bound to a semiconductor surface. The proposed idea depends on the efficiency of the photocatalysts, and therefore it is necessary to first measure their catalytic efficiency in homogeneous system. The main

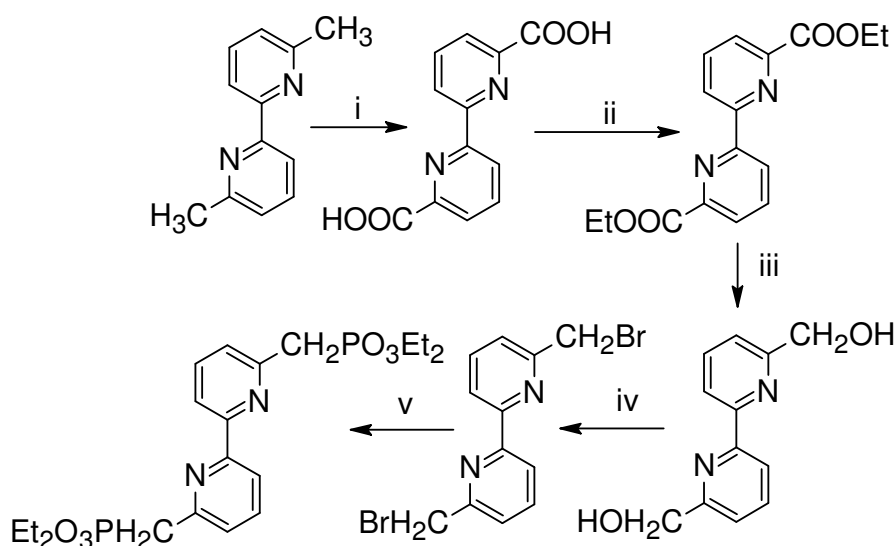
problem with the homogeneous system is sacrificial agents and organic solvents. Depending on the surface binding properties, a number of rhenium(I) carbonyl mononuclear complexes were also synthesised with carboxy and phosphonate functionalised bipyridine ligands. This chapter introduces the first example of a phosphonate derivatised rhenium carbonyl complex. The procedure for anchoring photocatalysts on the surface of semiconductor will also be discussed (see **Section 3.7**).

3.2. Synthetic procedures for organic ligands

The synthesis and characterisation of the bridging ligands were discussed in **Chapter 2**. A new organic ligand is introduced in this chapter which is 4,4'-diphosphonato-2,2'-bipyridine (dpb).

3.2.1. 4,4'-diphosphonato-2,2'-bipyridine (dpb)

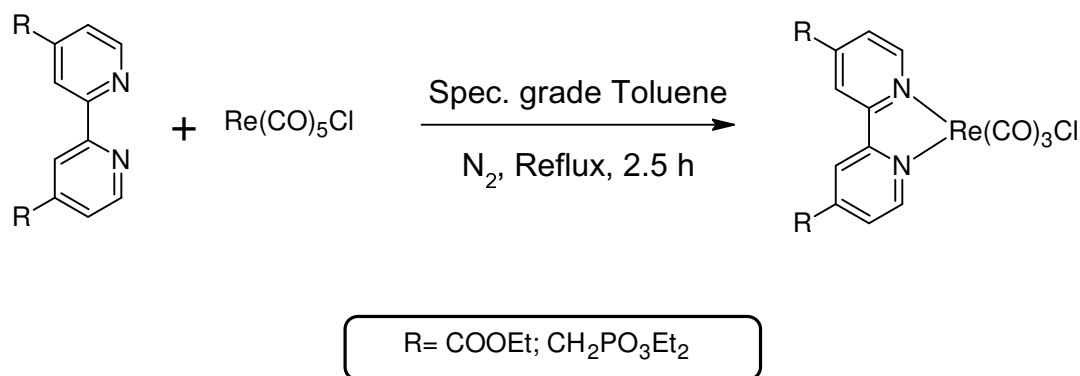
The synthetic procedure for the phosphonate derivatised bpy ligand was reported.^{55,56} Different synthetic procedures can be followed to derivatise the 4 and 4' position of the bpy ligand with phosphonate ester groups but there are various drawbacks and synthetic difficulties involved with them. Therefore, a simpler synthetic procedure which was used for the derivatisation of the bpy ligand is shown in **Scheme 3.1**. The route outlined in **Scheme 3.1** was also chosen because of high yields.⁵⁷ Although this route is a multi-step synthesis, there is no need to purify the intermediate products because high yield (~ 90%) of product was obtained in each step. The reagents used in this synthetic procedure are not costly and are commercially available. Step-v of this route was modified to simplify the synthetic procedure rather than following the reported procedure where 4,4'-bis(diethylmethylphosphonato)-2,2'-bipyridine (dpb) was purified using column chromatography. It was observed that the crude product of step-v was an oily liquid following the removal of the solvent (chloroform) and excess triethylphosphite. This oily crude product was washed with pentane and the solid was isolated. The product was used for the synthesis of a rhenium carbonyl complex. The final product was characterised by ¹H NMR and ³¹P NMR spectroscopy.



Scheme 3.1: Synthetic route for 4,4'-Bis(diethylmethylphosphonato)-2,2'-bipyridine (dpb), where i) $K_2Cr_2O_7/H_2SO_4$, ii) $EtOH/H_2SO_4$, iii) $NaBH_4/EtOH$, iv) HBr/H_2SO_4 , v) $P(OEt)_3/CHCl_3$.

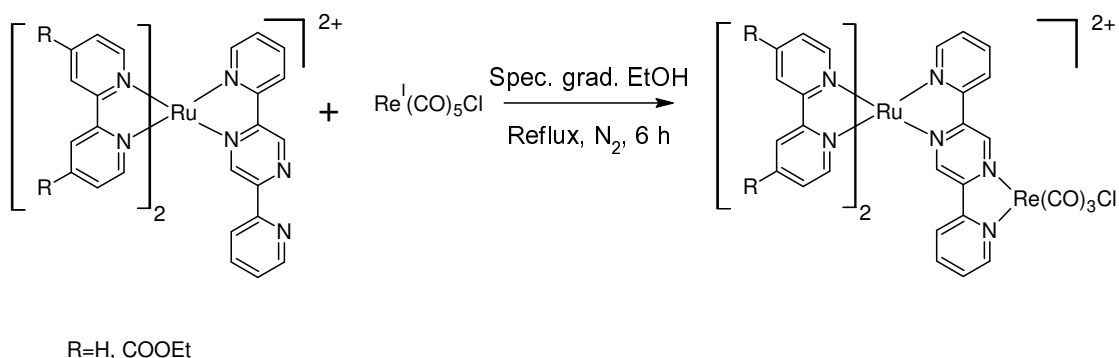
3.3. Synthetic procedures for Ru(II)/Re(I) metal complexes

A number of rhenium(I) tricarbonyl mononuclear complexes were synthesised using toluene. Two new rhenium(I) tricarbonyl complexes were reported in this chapter which are based on carboxy and phosphonate functionalised bpy ligands. These complexes can also be bound to the semiconductor surface in order to carry out heterogeneous catalysis. The reaction for synthesising such rhenium mononuclear complexes is shown in **Reaction 3.1**.



Reaction 3.1: Reaction for synthesising $[(L)Re(CO)_3Cl]$ complexes, $L = dceb$ and dpb

The synthetic procedure involving methanol as a solvent⁵⁸ was modified and ethanol was employed as a solvent to synthesise Ru-Re heterodinuclear complexes containing carboxy ester (ethyl) groups. These carboxy ester groups are not stable at high temperature and can be hydrolysed. Due to this reason, modification of the synthetic procedure was essential. Spectroscopic grade ethanol was used as a reaction solvent instead of methanol so that there is no exchange of methyl and ethyl ester groups at high reflux temperature. Further more, the ruthenium complex dissolves better in ethanol. The work up procedure was also altered considering the carboxy ester groups. Column chromatography was not performed to purify these complexes since they stick to the column, and hence lowers the over all yield. Therefore, two work up procedures were applied to purify the products. The reaction for synthesising $[\text{Ru}(\text{R}_2\text{bpy})_2(2,5\text{-dpp})\text{Re}(\text{CO})_3\text{Cl}]^{2+}$ complexes ($\text{R} = \text{H}, \text{COOC}_2\text{H}_5$) is shown in **Reaction 3.2**.



Reaction 3.2: The reaction for synthesising $[\text{Ru}(\text{R}_2\text{bpy})_2(2,5\text{-dpp})\text{Re}(\text{CO})_3\text{Cl}]^{2+}$ ($\text{R} = \text{H}, \text{COOC}_2\text{H}_5$)

The same reaction procedure was further applied as a general reaction procedure for synthesising other ruthenium(II)-rhenium(I) heterodinuclear complexes. A list of the synthesised Ru-Re heterodinuclear complexes are provided in **Figure 3.2**. Any excess of rheniumpentacarbonylchloride ($[\text{Re}(\text{CO})_5\text{Cl}]$) in the crude product can be removed by washing with non-polar organic solvents, as the ruthenium-rhenium heterodinuclear complexes are not soluble in non-polar solvents like hexane and pentane. The non-polar solvent was usually faint green in colour following washing and this is thought to be due to a small portion of rhenium oxide (which is green in

colour) formed during the reaction which is a result of decomposition of the ruthenium-rhenium heterodinuclear complex. The reaction colour turned from red to greenish red if the reaction was carried out for more than 6 hours. It is recommended to carry out the reaction within 6 hours to prevent the possible decomposition of the heterodinuclear complexes, leading to lowering of the yield of the product.

Another way of removing rhenium oxide is by passing the reaction solution through a cellite layer. But, there is a drawback in applying this procedure for the carboxy derivatised complexes. Cellite contains 80-90% silica and also other metals like sodium and potassium, which may result in the ester compounds undergoing hydrolysis and further may then be absorbed on to the cellite particles. When Ru-Re heterodinuclear compounds were passed through a cellite layer, the compounds were absorbed on to the cellite which turned red in colour. It proved impossible to remove the complexes from the cellite layer, even washing with highly polar solvents like acetonitrile did not remove them.

Using the above optimised reactions and modified work up procedures, a number of novel Ru-Re heterodinuclear and Re(I) mononuclear complexes were synthesised. The compounds were characterised by NMR, IR, UV-Vis and emission spectroscopy.

3.4. Infrared spectroscopy

Infrared spectroscopy is an important tool for the characterisation of metal carbonyl compounds. According to the literature, mononuclear rheniumtricarbonyl complexes can exist in two types of structural isomers; i) *fac*-isomer ii) *mer*-isomer.^{49,59} Ishitani commented on different possible isomers for Ru-Re heterodimetallic complexes, however, no structural information was provided.⁵⁴ Wallendael *et al.* and Sahai *et al.* also mentioned the broadening of the IR bands as a result of possible isomers. However, IR study did not help to distinguish the possible isomeric forms.^{35,58} The ruthenium-rhenium heterodinuclear complexes synthesised in this chapter can exist in many isomeric forms considering both the ruthenium and rhenium moiety. The structural forms of these possible isomers are shown in **Figure**

3.3 and list of carbonyl stretching frequencies of Ru(II)/Re(I) complexes are listed in **Table 3.1**.

Table 3.1: Carbonyl stretching frequencies of Ru(II)/Re(I) complexes

Compounds	IR Stretching frequency (cm ⁻¹) ^a		
	A'(1)	A'(2)	A''
[(dceb)Re(CO) ₃ Cl]	2019	1916	1892
[(dpb)Re(CO) ₃ Cl]	2022	1922	1899
[Ru(bpy) ₂ (μ-2,5-dpp)Re(CO) ₃ Cl] ²⁺	2022	1914(broad)	-
[Ru(d ₈ -bpy) ₂ (μ-2,5-dpp)Re(CO) ₃ Cl] ²⁺	2022	1912(broad)	-
[Ru(dceb) ₂ (μ-2,5-dpp)Re(CO) ₃ Cl] ²⁺	2022	1930	1910
[Ru(bpy) ₂ (μ-bisbpy)Re(CO) ₃ Cl] ²⁺	2020	1914(broad)	1894
[Ru(dceb) ₂ (μ-bisbpy)Re(CO) ₃ Cl] ²⁺	2022	1918(broad)	-
[Ru(dceb) ₂ (μ-Hbpt)Re(CO) ₃ Cl] ²⁺	2019	1911	1890

a) THF was used as a solvent for IR spectroscopy.

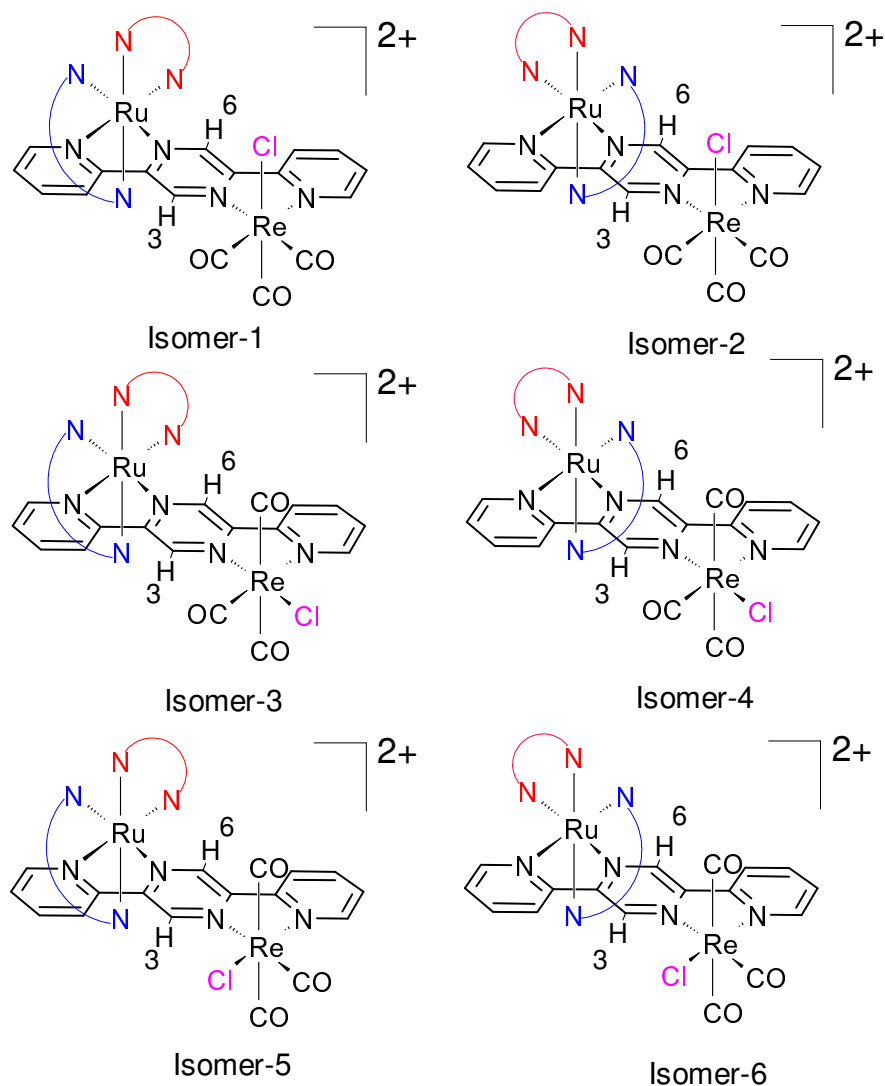


Figure 3.3: Different isomeric forms of $[Ru(L)_2(\mu\text{-}2,5\text{-dpp})Re(CO)_3Cl]^{2+}$, $L = \text{bpy}$, $d_8\text{-bpy}$ and $dceb$

Typically, facial (*fac*-) and meridional (*mer*-) isomers are characterised by IR spectroscopy and show different IR stretching bands. FTIR spectra of ruthenium-rhenium heterodinuclear complexes show three bands in the region of 1850-2050 cm^{-1} . These IR bands are assigned to rhenium carbonyl ($[Re(\text{bpy})(CO)_3Cl]$ has C_s symmetry) stretching vibrations $[A'(1), A'(2) \text{ and } A'']$.^{60,61} *fac*- $[(\text{dmb})Re(CO)_3Cl]$ shows three intense bands at 2018, 1909, and 1878 cm^{-1} , whereas the *mer*- isomer has two intense bands 1944 and 1894 cm^{-1} .^{62,63}

All the synthesised rhenium mononuclear complexes and ruthenium-rhenium heterodinuclear complexes are *fac*- isomers according to literature values because all the complexes has one IR band above 2000 cm^{-1} .^{42,63} The IR bands for different types of synthesised metal carbonyl complexes are shown in **Figure 3.4**.

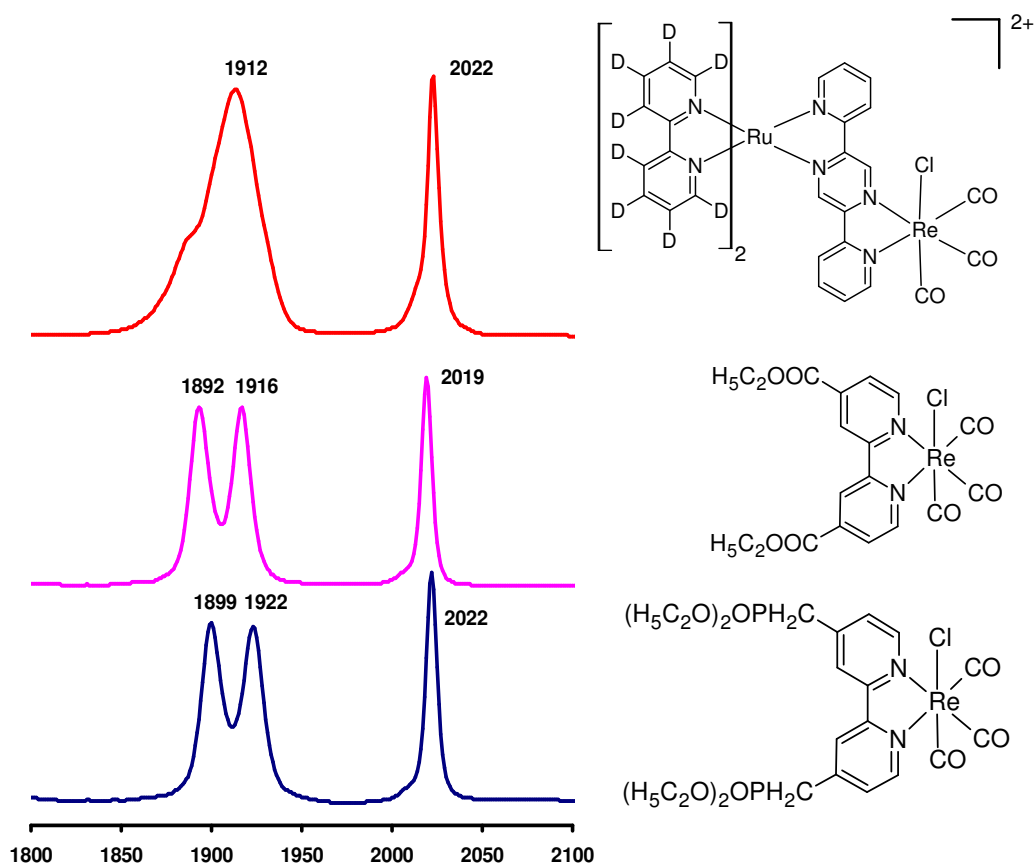


Figure 3.4: Comparison of FTIR (in THF) spectra of *fac*- $[(dceb)\text{Re}(\text{CO})_3\text{Cl}]$, *fac*- $[(dpb)\text{Re}(\text{CO})_3\text{Cl}]$ and $[Ru(d_8\text{-bpy})_2(2,5\text{-dpp})\text{Re}(\text{CO})_3\text{Cl}]^{2+}$

In **Figure 3.3** isomers 3 to 6 are *mer*- while 1 and 2 are *fac*- at the rhenium centre. Therefore, the existences of isomer 3 to 6 are ruled out by IR spectroscopy because experimental data suggests the existence of only *fac*- isomers. Isomers 1 and 2 have identical bonding properties (C_s symmetry, see **Figure 3.5**) therefore will have very similar stretching frequencies in the IR spectra. In case of the heterodinuclear complexes, the lower region IR band is not resolved due to the overlapping of the IR bands. This phenomenon may be explained by the possible electronic effect from charged ruthenium centre on the bridging ligand as well as on the rhenium metal

centre. This electronic effect may also be facilitating the π -back donation from rhenium metal centre to the carbonyl groups and further results in overlapping of the IR bands. The solvent polarity (THF was used as solvent to record the IR spectra) can also cause of broadening of the lower region IR band.

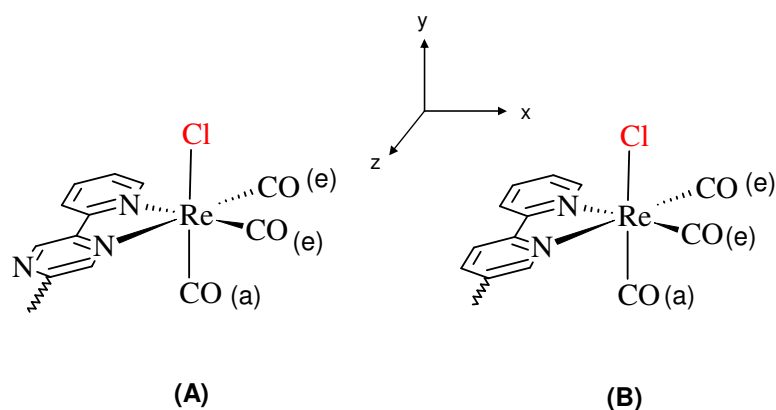


Figure 3.5: (A) Rhenium centre in $[Ru(L)_2(2,5-dpp)Re(CO)_3Cl]$ (B) Rhenium centre in $[Ru(L)_2(bisbpy)Re(CO)_3Cl]$. $L = bpy, d_8-bpy, dceb$, (a) and (e) represent axial and equatorial CO groups respectively.

Two different geometrical isomers for the Ru-(2,5-dpp)-Re heterodinuclear complex are shown in **Figure 3.6**. These two possible isomers have identical bonding properties towards the rhenium centre therefore keeping the same C_s symmetry (see **Figure 3.5**).

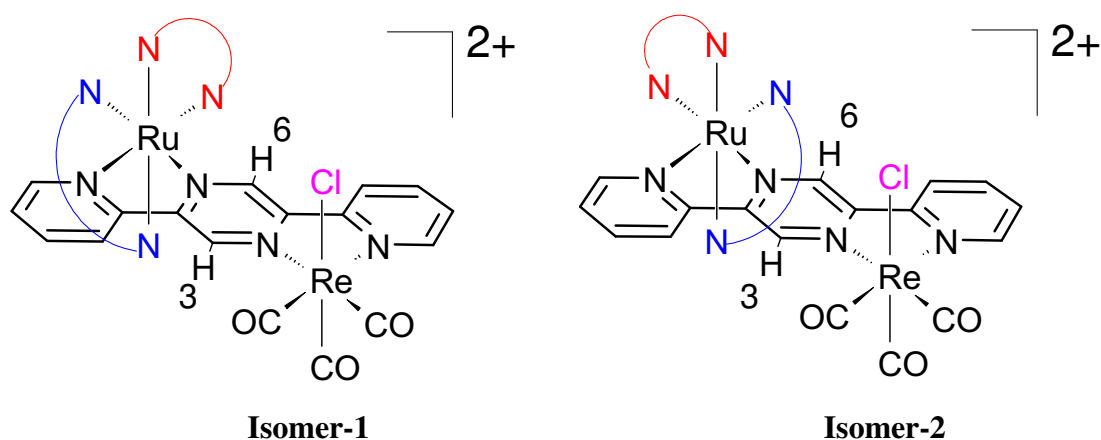


Figure 3.6: Two geometrical isomers of Ru-(2,5-dpp)-Re complex, isomer-1 and 2.

The IR stretching bands for other rhenium and Ru-Re heterodinuclear complexes are tabulated in **Table 3.1**. $[\text{Ru}(\text{dceb})_2(\mu\text{-Hbpt})\text{Re}(\text{CO})_3\text{Cl}]^{2+}$ has two separate equatorial metal carbonyl bands. Hbpt is a strong σ -donor ligand therefore it supplies the electron density to the $d\pi$ -orbital of the rhenium metal which may favour more π -back donation to the carbonyl groups which is trans to the nitrogen of the central triazole ring.^{58,64} As a result, the CO bond becomes longer and the metal carbonyl bands appear in the lower region of the IR spectra (see **Figure 3.7**).

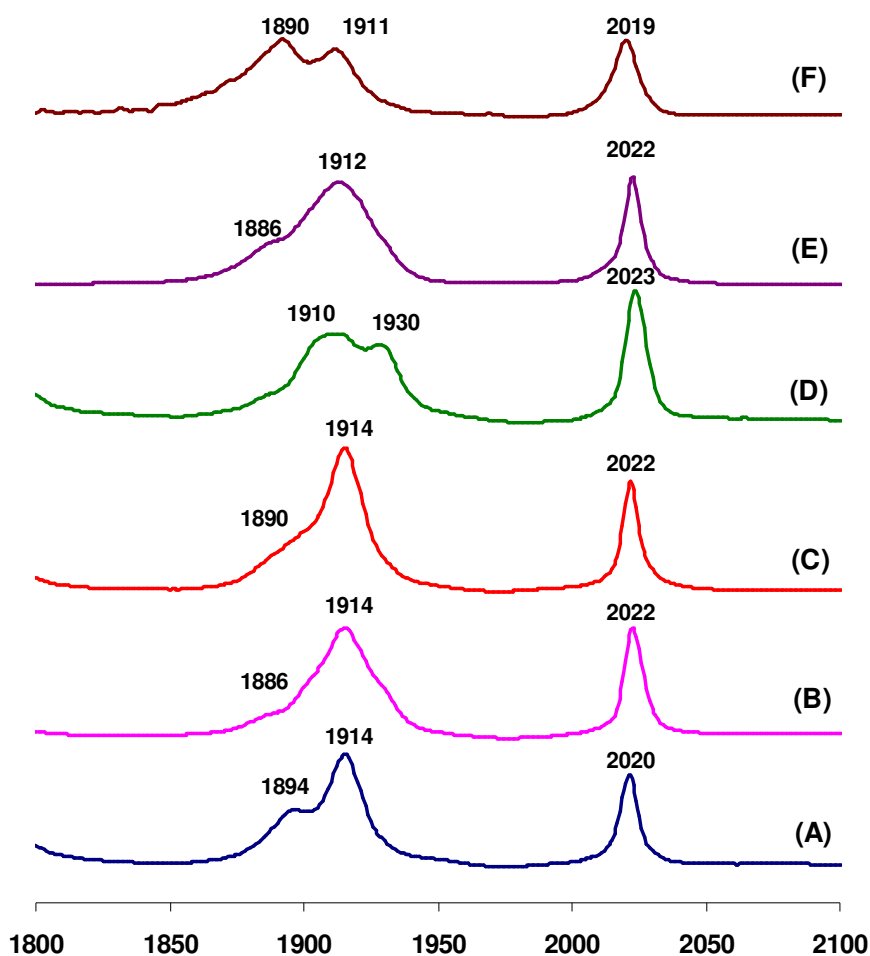


Figure 3.7: IR spectra (solution in THF) of Ru-Re heterodinuclear complexes (A) $[\text{Ru}(\text{bpy})_2(\text{bisbpy})\text{Re}(\text{CO})_3\text{Cl}]^{2+}$; (B) $[\text{Ru}(\text{bpy})_2(2,5\text{-dpp})\text{Re}(\text{CO})_3\text{Cl}]^{2+}$; (C) $[\text{Ru}(\text{dceb})_2(\text{bisbpy})\text{Re}(\text{CO})_3\text{Cl}]^{2+}$; (D) $[\text{Ru}(\text{dceb})_2(2,5\text{-dpp})\text{Re}(\text{CO})_3\text{Cl}]^{2+}$; (E) $[\text{Ru}(\text{d}_8\text{-bpy})_2(2,5\text{-dpp})\text{Re}(\text{CO})_3\text{Cl}]^{2+}$; (F) $[\text{Ru}(\text{dceb})_2(\text{Hbpt})\text{Re}(\text{CO})_3\text{Cl}]^{2+}$.

3.5. Characterisation of compounds using NMR spectroscopy

3.5.1. Organic ligands

4,4'-Bis(diethylmethylphosphonato)-2,2'-bipyridine (dpb) was synthesised using 4,4'-diethoxycarbonyl-2,2'-bipyridine (dceb) as starting material. Characterisation of dceb ligand was previously discussed in **Chapter 2**. The ^1H NMR spectra of dpb ligand and other intermediate products are provided in **Figures 3.8-3.10**.

4,4'-Bis(hydroxymethyl)-2,2'-bipyridine

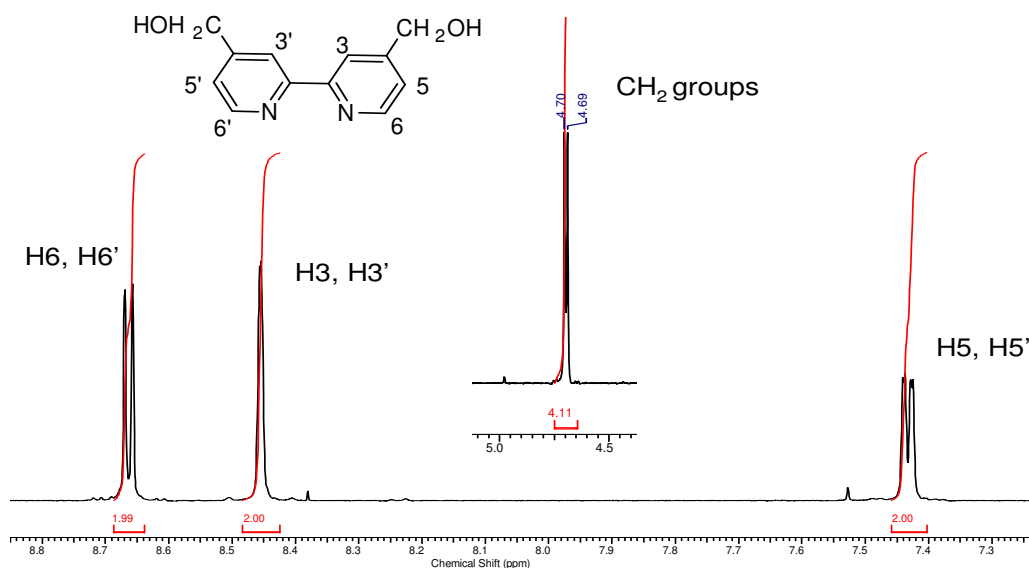


Figure 3.8: ^1H NMR(DMSO- d_6 , 400 MHz) of 4,4'-bis(hydroxymethyl)-2,2'-bipyridine

The above **Figure 3.8** represents the ^1H NMR spectra of 4,4'-bis(hydroxymethyl)-2,2'-bipyridine. H6 (H6') protons appear at 8.66 ppm because of the closeness of these protons to the electron withdrawing nitrogen. The singlet at 8.45 ppm is assigned to the H3 (H3') protons. Another doublet in the aromatic region at 7.43 ppm is defined as H5 (H5') proton. The singlet at 4.70 ppm is assigned to the methylene- CH_2 group which is shifted downfield, because of the neighbouring electronegative oxygen atom.

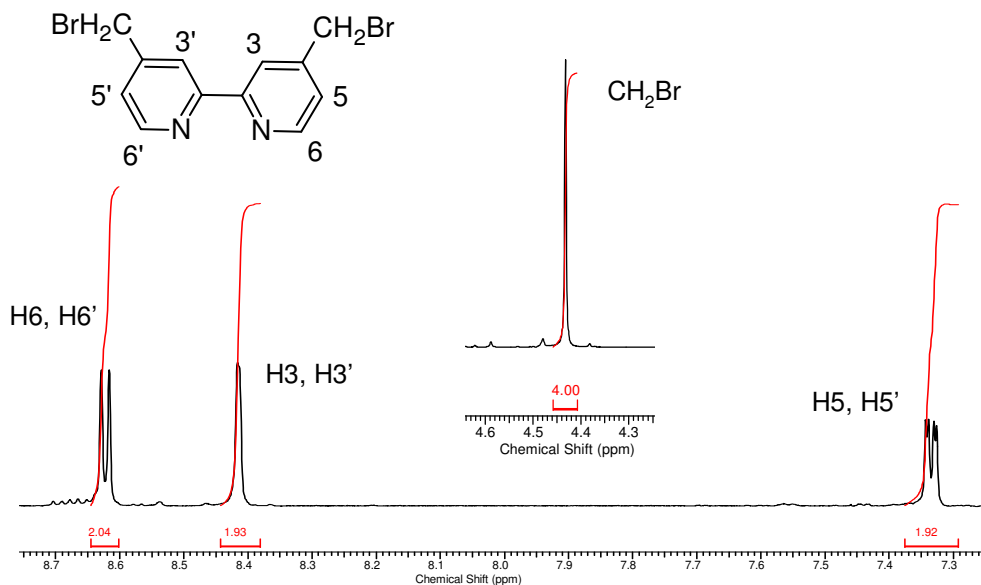
4,4'-Bis(bromomethyl)-2,2'-bipyridine

Figure 3.9: ^1H NMR(CDCl_3 , 400 MHz) of 4,4'-bis(bromomethyl)-2,2'-bipyridine

The above **Figure 3.9** represents the ^1H NMR spectra of 4,4'-bis(bromomethyl)-2,2'-bipyridine. H6 and H6' are equivalent and shifted downfield to 8.62 ppm due to the effect of the neighbouring electronegative nitrogen atom. Similarly, H3 and H3' have identical environments and therefore appear as a singlet at 8.42 ppm. The doublet at 7.33 ppm is assigned to the H5 (and H5') protons. The signal for the methylene- CH_2 groups is shifted downfield to 4.43 ppm because of the neighbouring electronegative bromine atom.

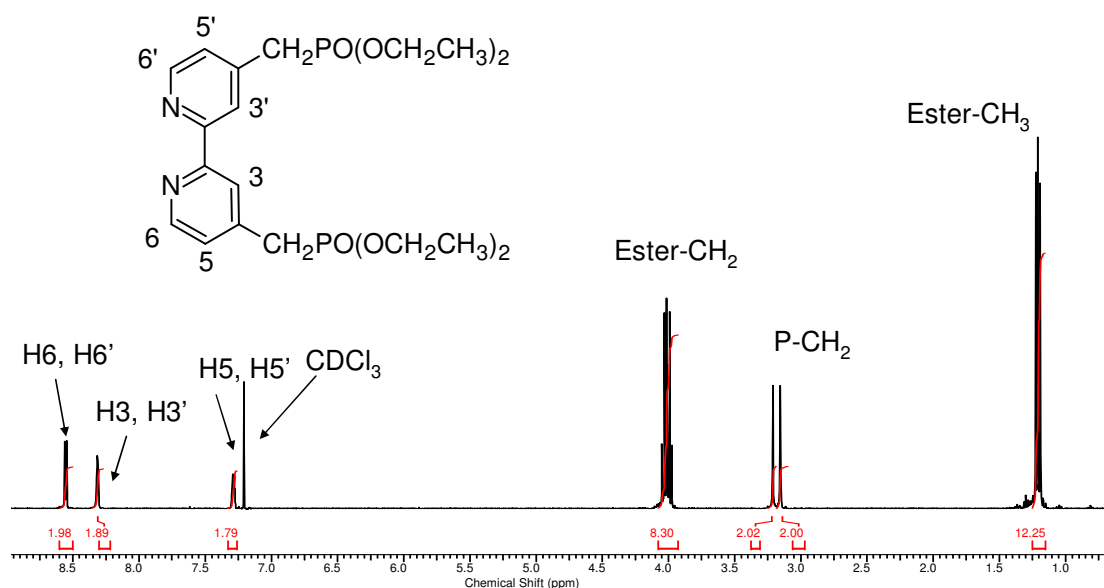
4,4'-Bis(diethylmethylphosphonato)-2,2'-bipyridine (dpb)

Figure 3.10: ^1H NMR(CDCl_3 , 400 MHz) of 4,4'-bis(diethylmethylphosphonato)-2,2'-bipyridine (dpb)

Figure 3.10 represents the ^1H NMR spectra of 4,4'-bis(diethylmethylphosphonato)-2,2'-bipyridine (dpb). H6 and H6' protons appear as a single doublet at 8.55 ppm. H5 and H5' are far from the nitrogen atoms and therefore appear at 7.29 ppm. The singlet at 8.31 ppm in the aromatic region is assigned to H3 and H3' protons as they have identical environments. The phosphonate ester groups appear at 4 ppm (ester $-\text{CH}_2$ groups, 8H) and 1.23 ppm (ester $-\text{CH}_3$ groups, 12H) in the ^1H NMR spectra. Integration in the aliphatic region suggests that four ester groups are present in the compound. The $\text{P}-\text{CH}_2$ group appears at 3.21 ppm with a coupling constant of 20 Hz in the ^1H NMR spectrum. The characteristic phosphorous peak at 34 ppm in the ^{31}P NMR also confirms the phosphonate group in the compound.

3.5.2. NMR spectra of $[(X_2bpy)Re(CO)_3Cl]$ complexes; $X = COOEt$ and $CH_2PO(OEt)_2$

1H NMR spectra of $[(dceb)Re(CO)_3Cl]$ and $[(dpb)Re(CO)_3Cl]$ are shown in **Figure 3.11** and **3.12** respectively. Here H3 and H3' have identical environments. Similarly H6 and H5 also have identical environments with H6' and H5' respectively. H3, (H3'), H6, (H6'), H5 (H5') protons in the mononuclear complex are shifted downfield compared to the free ligand due to the effect of the electronegative chlorine atom. According to the literature, the doublet at 9.34 ppm is assigned to H6 and H6' protons.^{58,65,66} The signals for the ester groups were found at the same position as that in the free ligand. The IR data for both rhenium mononuclear complexes suggest that they exist as *fac*- isomers. There was no evidence in the NMR spectra to suggest the presence of the *mer*- isomer.⁶⁷ From, the current NMR spectra it is evident that rhenium compounds exist only as *fac*- isomers.

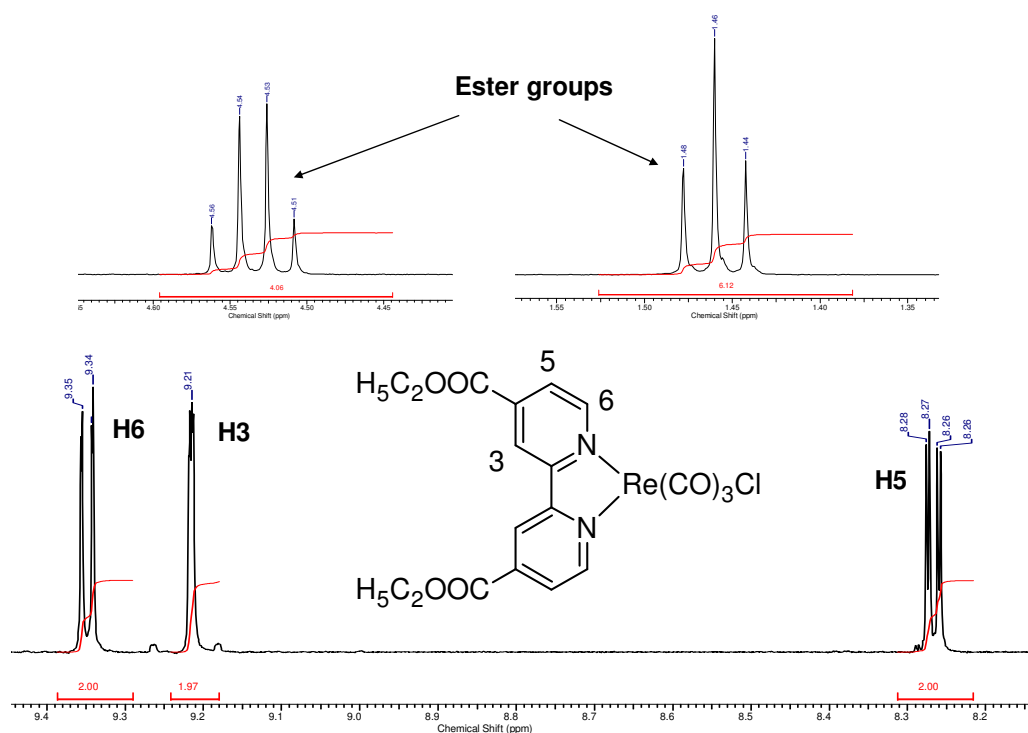


Figure 3.11: 1H NMR(Acetone- d_3 , 400 MHz) of $[(dceb)Re(CO)_3Cl]$

The above **Figure 3.11** represents the 1H NMR spectra of $[(dceb)Re(CO)_3Cl]$. According to literature (as discussed above),^{35,58,64,68} H6, H5 and H3 were identified at

9.35 ppm, 8.27 ppm and 9.22 ppm respectively. The ester CH₂ and CH₃ signals for the ethyl ester groups are assigned at 4.54 ppm and 1.46 ppm respectively.

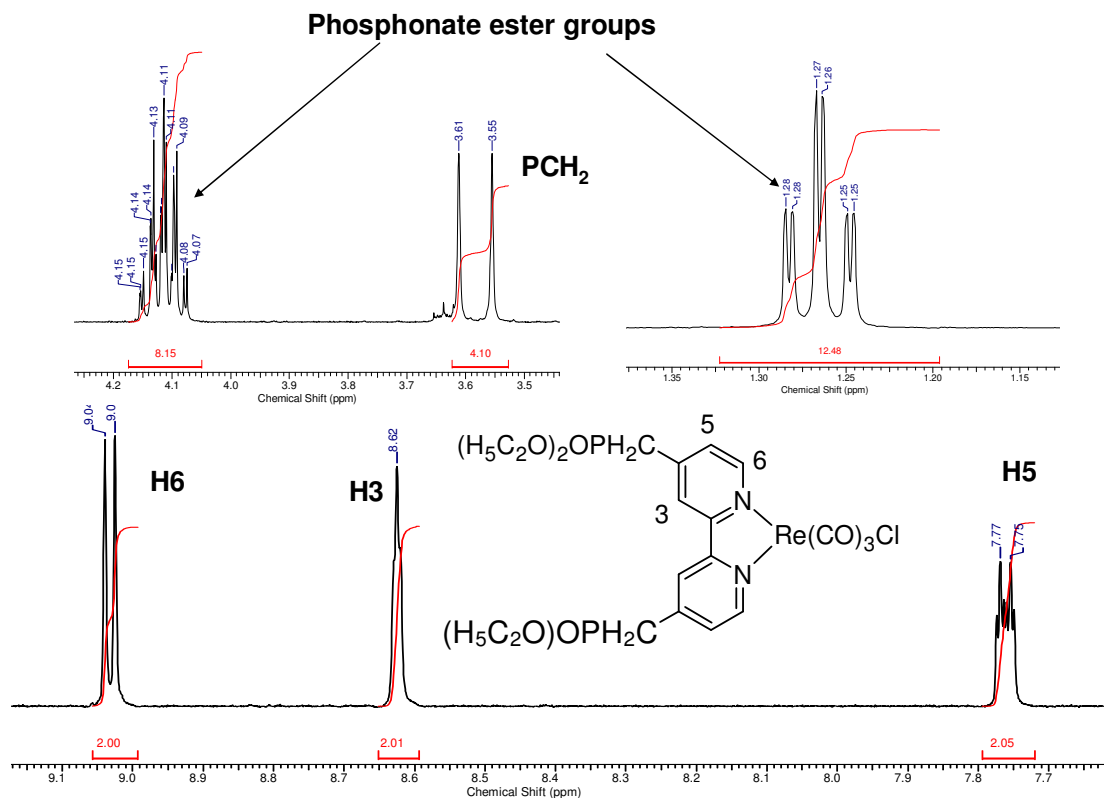


Figure 3.12: ^1H NMR(Acetone- d_6 , 400 MHz) of $[(\text{dpb})\text{Re}(\text{CO})_3\text{Cl}]$

The above **Figure 3.12** represents the ^1H NMR spectra for $[(\text{dpb})\text{Re}(\text{CO})_3\text{Cl}]$. According to the literature (as discussed above),^{35,58,64,68} H6, H5 and H3 were identified at 9.03 ppm, 7.76 ppm and 8.62 ppm respectively. The phosphonate ester CH₂ and CH₃ signals are assigned to multiplets at 4.05-4.17 ppm and 1.27-1.30 ppm. The P-CH₂ peak appears as a doublet with a coupling constant of 20 Hz at 3.55-3.61 ppm.

3.5.3. Ru-Re heterodinuclear metal complexes

Deuteration is a tool often used in polypyridyl transition metal complex chemistry to help interpret its complicated NMR spectra. The deuteration technique was also applied here to resolve NMR spectra. Two types of Ru(II)-Re(I) heterodinuclear complexes were synthesised, one with a deuteriated peripheral bpy ligand and another with a non deuteriated peripheral bpy ligand. In case of a deuteriated bpy ligand, the only resonances observed in the NMR spectra are those for the bridging ligand. The molecular structure of these heterodinuclear complexes are shown in **Figure 3.13**.

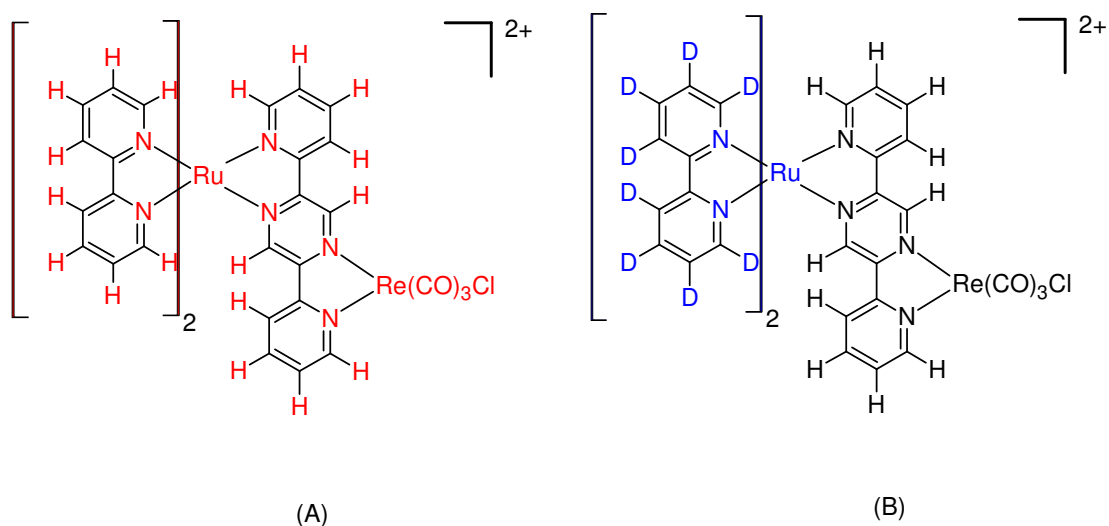


Figure 3.13: (A) $Ru(bpy)_2(\mu\text{-}2,5\text{-dpp})Re(CO)_3Cl]^{2+}$ (B) $Ru(d_8\text{-}bpy)_2(\mu\text{-}2,5\text{-dpp})Re(CO)_3Cl]^{2+}$

The NMR spectra of $Ru(bpy)_2(\mu\text{-}2,5\text{-dpp})Re(CO)_3Cl]^{2+}$ is complicated in nature because of the overlapping of several proton signals. Few NMR signals can be identified but the rest of the signals remained un-identified even with the help of COSY NMR experiments. $Ru(d_8\text{-}bpy)_2(\mu\text{-}2,5\text{-dpp})Re(CO)_3Cl]^{2+}$ was synthesised where the peripheral bpy ligands are deuteriated and therefore the resonances for bpy ligands were avoided. This approach helped to identify the proton signals from the bridging ligand 2,5-dpp with the help of 2D COSY NMR. 1H NMR spectra of

$\text{Ru}(\text{bpy})_2(\mu\text{-}2,5\text{-dpp})\text{Re}(\text{CO})_3\text{Cl}]^{2+}$ and $\text{Ru}(\text{d}_8\text{-bpy})_2(\mu\text{-}2,5\text{-dpp})\text{Re}(\text{CO})_3\text{Cl}]^{2+}$ were compared in **Figure 3.14**.

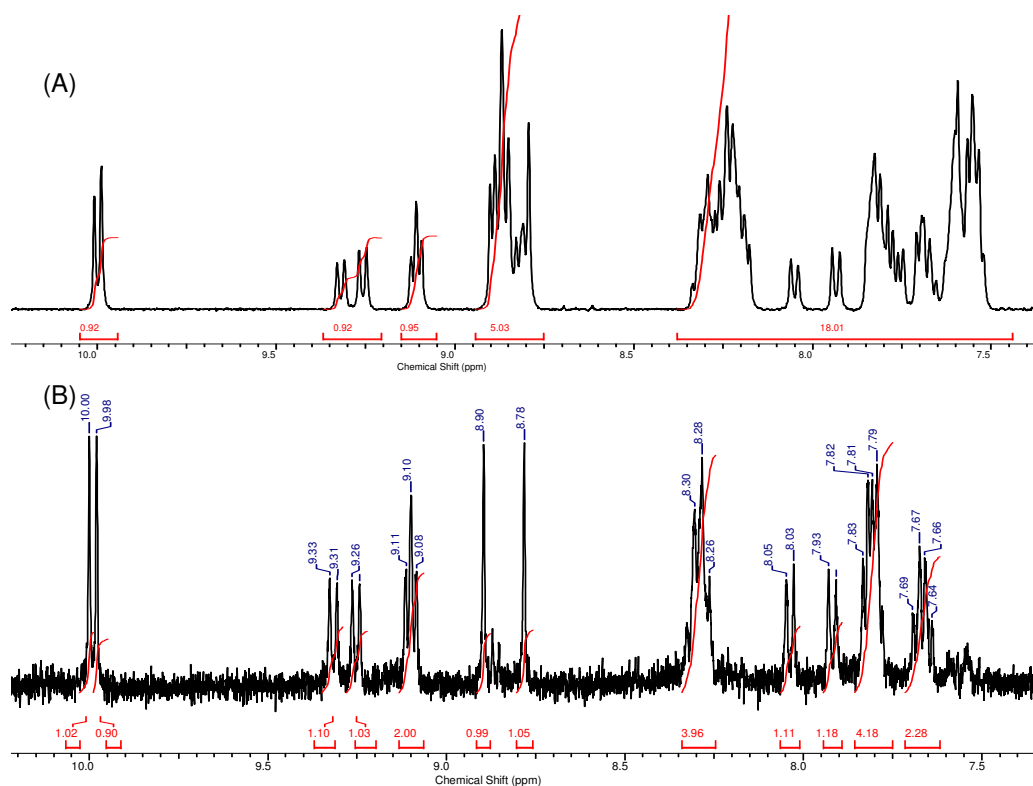


Figure 3.14: ^1H NMR($\text{DMSO-}d_6$, 400 MHz) spectra of (A) $[\text{Ru}(\text{bpy})_2(\mu\text{-}2,5\text{-dpp})\text{Re}(\text{CO})_3\text{Cl}]^{2+}$ and (B) $[\text{Ru}(\text{d}_8\text{-bpy})_2(\mu\text{-}2,5\text{-dpp})\text{Re}(\text{CO})_3\text{Cl}]^{2+}$

The total number of protons were found as 20 from the integration of the proton NMR for the compound $[\text{Ru}(\text{d}_8\text{-bpy})_2(\mu\text{-}2,5\text{-dpp})\text{Re}(\text{CO})_3\text{Cl}]^{2+}$. The expected number of protons for $[\text{Ru}(\text{d}_8\text{-bpy})_2(\mu\text{-}2,5\text{-dpp})\text{Re}(\text{CO})_3\text{Cl}]^{2+}$ is 10 (2,5-dpp, 10H) because the peripheral bpy ligands are deuteriated. The experimental result suggests that $[\text{Ru}(\text{d}_8\text{-bpy})_2(\mu\text{-}2,5\text{-dpp})\text{Re}(\text{CO})_3\text{Cl}]^{2+}$ may contain two different isomers in equal amount. The presence of two different isomers was also suggested by IR spectroscopy. Therefore both NMR and IR spectroscopy support the assumption of two different isomers existing in the compound $[\text{Ru}(\text{d}_8\text{-bpy})_2(\mu\text{-}2,5\text{-dpp})\text{Re}(\text{CO})_3\text{Cl}]^{2+}$ (**Figure 3.6**).

$[\text{Ru}(\text{d}_8\text{-bpy})_2(\mu\text{-}2,5\text{-dpp})\text{Re}(\text{CO})_3\text{Cl}]^{2+}$ will appear in the ^1H NMR spectra with two singlets, four doublets of doublet and four doublets and the neighbouring protons

should couple in the 2D COSY NMR (see **Figure 3.15**). According to ^1H NMR spectra of $[\text{Ru}(\text{d}_8\text{-bpy})_2(\mu\text{-2,5-dpp})\text{Re}(\text{CO})_3\text{Cl}]^{2+}$, two different isomers are present in the compound. It is difficult to predict which proton belongs to which isomeric form. 2D COSY NMR suggests that the two singlets at 10.2 ppm(0) do not couple with any other protons. These two singlets can be assigned to two H3 protons of the central pyrazine rings of two different isomers. This assignment for H3 proton was made by comparing the Ru-Re heterodinuclear complex and the homologous Ru-mononuclear complex (see **Figure 3.16**).

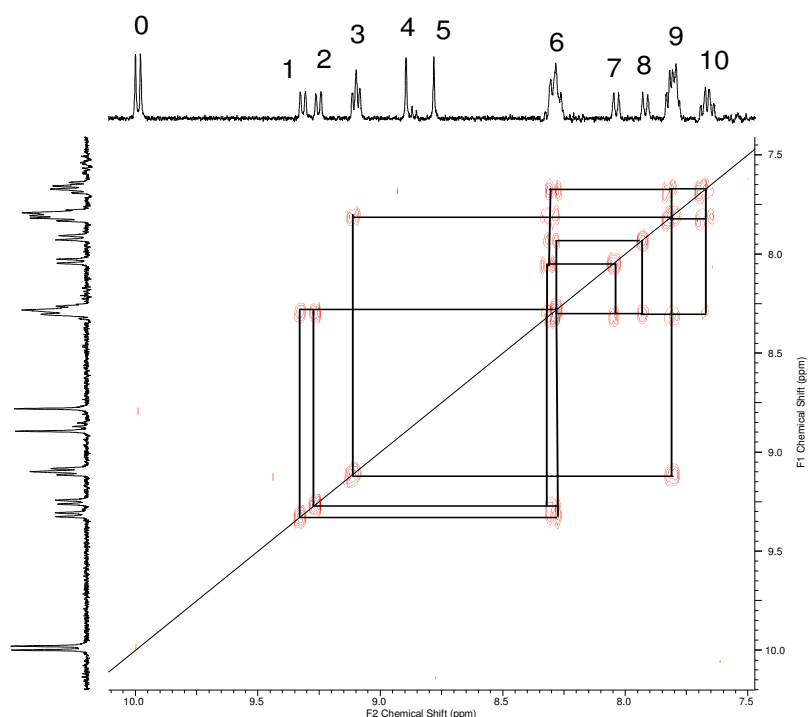


Figure 3.15: 2D COSY NMR($\text{DMSO-}d_6$, 400 MHz) of $[\text{Ru}(\text{d}_8\text{-bpy})_2(\mu\text{-2,5-dpp})\text{Re}(\text{CO})_3\text{Cl}]^{2+}$

Singlets 4 and 5 are assigned to two H6 protons from two different Ru-Re isomers. The H6 proton in the Ru-Re heterodimetallic complex is shifted downfield compared to the Ru-mononuclear complex. In the COSY NMR, the doublets 1 (8.34 Hz) and 2 (8.59 Hz) couple with the multiplet labelled 6. However, multiplet 6 integrates as four protons. This indicates multiplet 6 contains four proton signals and also indicates two more overlapping proton signals. Multiplet 6 couples with doublet 7 (7.84 Hz), 8 (8.34 Hz), multiplet 9 and long range couples with multiplet 10. Multiplet 9 and 10 integrates as 4 protons and two protons respectively. From the coupling interaction in

the 2D COSY NMR, it appears there are two isomers. All the NMR signals have similar environments except doublets 1, 2, 7 and 8. Signal 0, singlets 4 and 5 do not show any coupling interactions. Therefore, it is difficult to assign other proton signals for the two Ru-Re isomers.

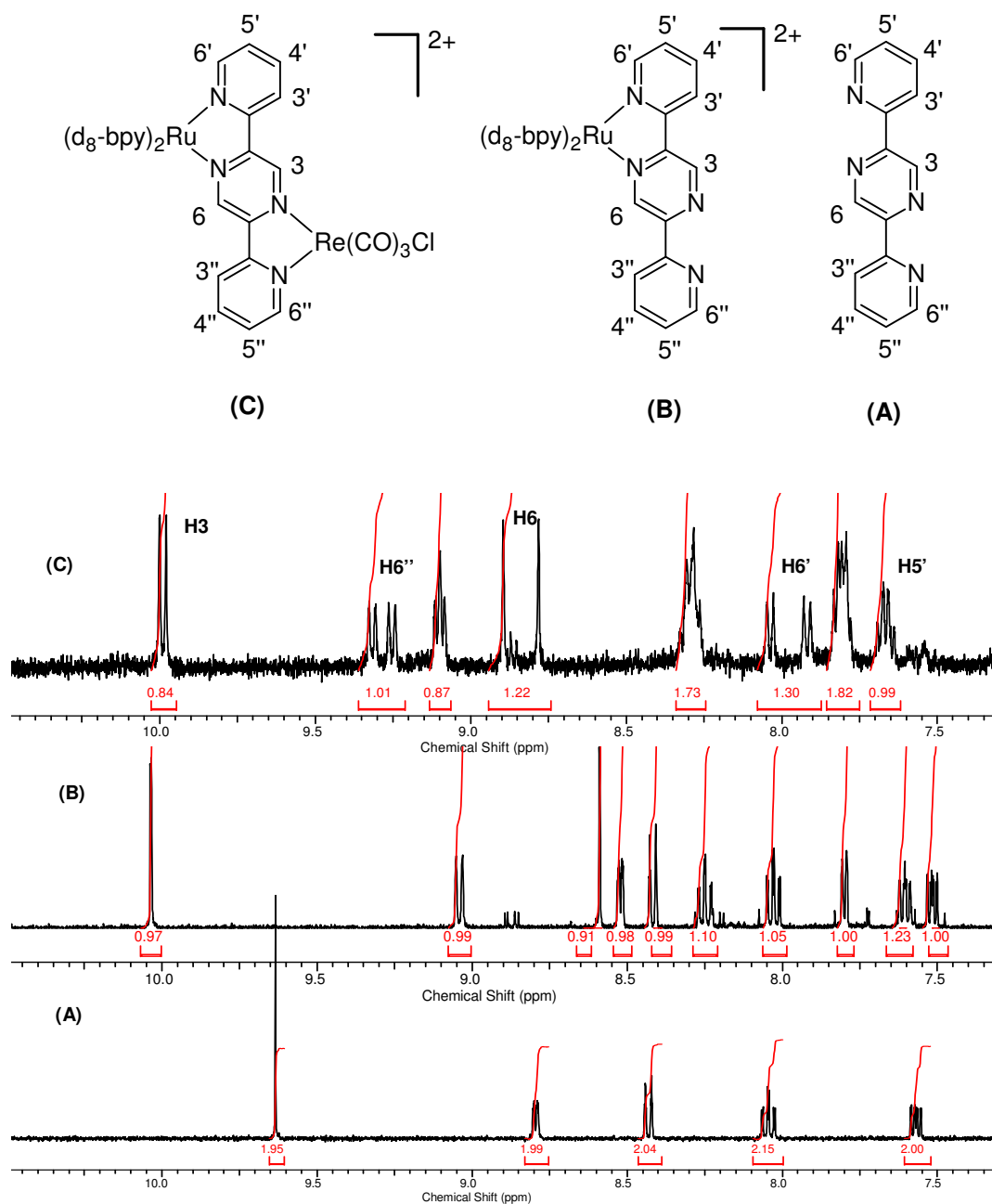


Figure 3.16: Comparison of ^1H NMR($\text{DMSO-}d_6$, 400 MHz) spectra of (A) 2,5-dpp, (B) $[\text{Ru}(\text{d}_8\text{-bpy})_2(2,5\text{-dpp})]^{2+}$ and (C) $[\text{Ru}(\text{d}_8\text{-bpy})_2(\mu\text{-}2,5\text{-dpp})\text{Re}(\text{CO})_3\text{Cl}]^{2+}$

However, on the basis of the chemical shifts of the H6 protons, it is possible that the isomers are based on the different orientations of the peripheral bpy ligands at the ruthenium centre. Comparison of ^1H NMR spectra of $[\text{Ru}(\text{d}_8\text{-bpy})_2(\mu\text{-2,5-dpp})\text{Re}(\text{CO})_3\text{Cl}]^{2+}$ and $[\text{Ru}(\text{d}_8\text{-bpy})_2(2,5\text{-dpp})]^{2+}$ also show more difference in the chemical shifts of the H6' protons (doublets 1 and 2, difference in chemical shifts: 0.12 ppm) in two isomers compared to the change in chemical shifts for H6'' protons (doublets 7 and 8, difference in chemical shifts: 0.07 ppm) which is near to the rhenium centre. Different orientations of peripheral bpy based ligands can create different chemical environments for H6' and H6 protons and as a result, H6 and H6' have different chemical shifts in the NMR spectra. This result is in agreement with the prediction of two isomers (IR data) which are based on two different orientations of two peripheral $\text{d}_8\text{-bpy}$ ligands at the ruthenium centre, and the predicted two isomers are shown below in **Figure 3.17**.

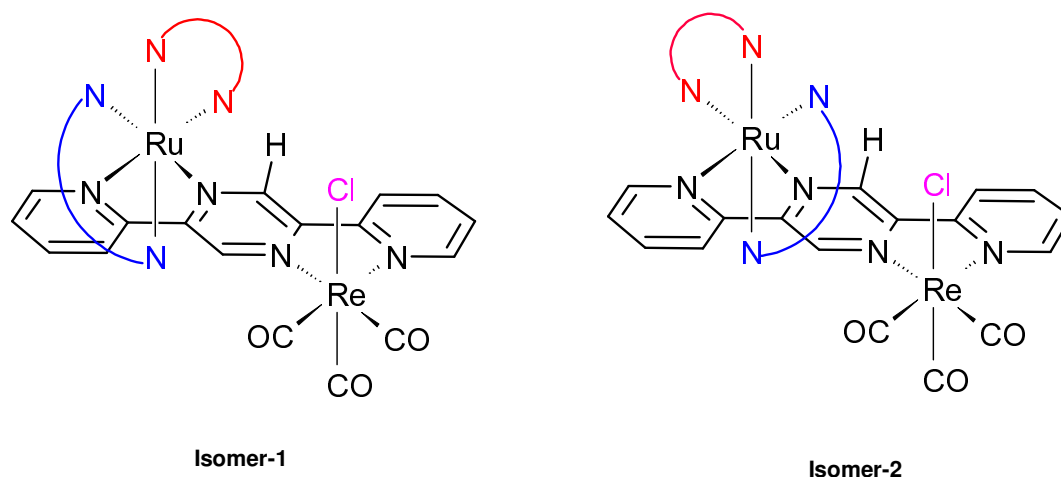


Figure 3.17: Isomer-1 and isomer-2.

The ^1H NMR for the two isomers are shown in **Figure 3.18** and **Figure 3.19** respectively on the basis of the NMR results obtained. The chemical shifts for a number of protons are listed in **Table 3.2** and other proton signals remained unresolved due to overlapping.

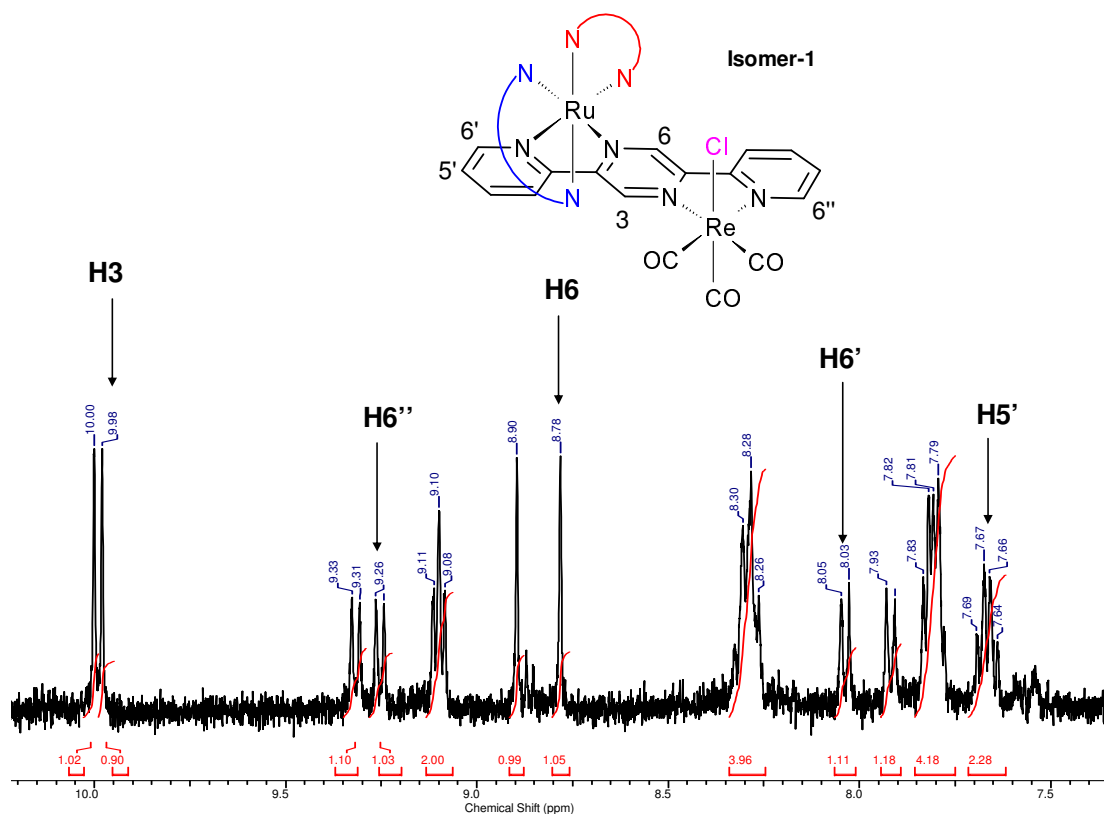


Figure 3.18: Assignment of NMR(DMSO-*d*₆, 400 MHz) signals for isomer-1.

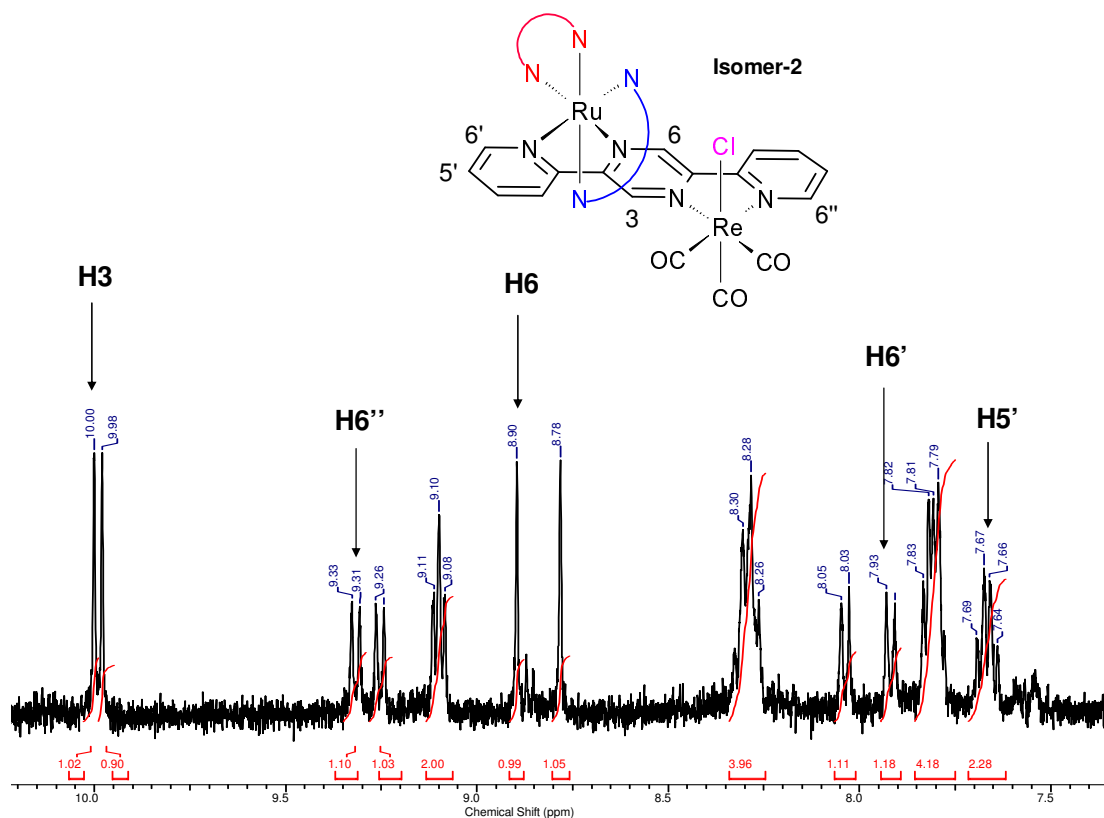


Figure 3.19: Assignment of NMR(DMSO-*d*₆, 400 MHz) signals for isomer-2.

Table 3.2: Chemical shifts of 2,5-dpp protons in isomer-1 and isomer-2 of $[Ru(bpy)_2(\mu-2,5-dpp)Re(CO)_3Cl]^{2+}$ and $[Ru(d_8-bpy)_2(\mu-2,5-dpp)Re(CO)_3Cl]^{2+}$.

Chemical shift of the protons (ppm)		
Protons	Isomer-1	Isomer-2
H3	9.98	10.00
H6	8.78	8.90
H6''	9.25	9.32
H6'	8.04	7.92
H5'	7.67	7.67

According to the NMR study on $[Ru(d_8-bpy)_2(\mu-2,5-dpp)Re(CO)_3Cl]^{2+}$, it can be further suggested that similar types of *fac*- isomers also exist for other ruthenium-rhenium heterodinuclear complexes. The structure of $[Ru(dceb)_2(\mu-2,5-dpp)Re(CO)_3Cl]^{2+}$ is shown below in **Figure 3.20**.

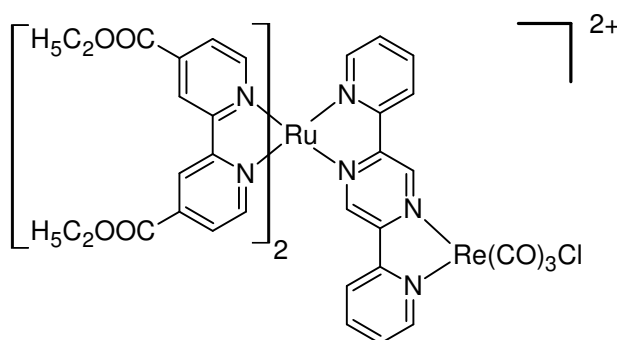


Figure 3.20: $[Ru(dceb)_2(\mu-2,5-dpp)Re(CO)_3Cl]^{2+}$

A fractional crystallisation study in ethanol/acetone solution was attempted to separate the two isomers, but the experiment was unsuccessful. Similar NMR experiments were obtained for the remaining Ru-Re heterodinuclear complexes synthesised in this study. 2D COSY NMR (see **Figure 3.22**) was not useful in fully assigning the NMR spectra in this case, as there are a number of signals that overlap with each other. The H3 and H6 protons in the pyrazine ring were assigned based on the orientation of peripheral dceb ligands on the ruthenium centre as discussed above. The assignment of H5', H3 and H6 protons for different isomers of $[Ru(dceb)_2(\mu-2,5-$

$\text{dpp})\text{Re}(\text{CO})_3\text{Cl}]^{2+}$ are shown in **Figure 3.21** and **Figure 3.18**. Other proton signals remained unresolved due to overlapping signals. The assessments were made by comparing the ^1H NMR spectra of $[\text{Ru}(\text{dceb})_2(\mu\text{-}2,5\text{-dpp})\text{Re}(\text{CO})_3\text{Cl}]^{2+}$ and $[\text{Ru}(\text{d}_8\text{-bpy})_2(\mu\text{-}2,5\text{-dpp})\text{Re}(\text{CO})_3\text{Cl}]^{2+}$ (see **Figure 3.21**). A number of proton signals are listed in **Table 3.3** (some proton signals were unresolved).

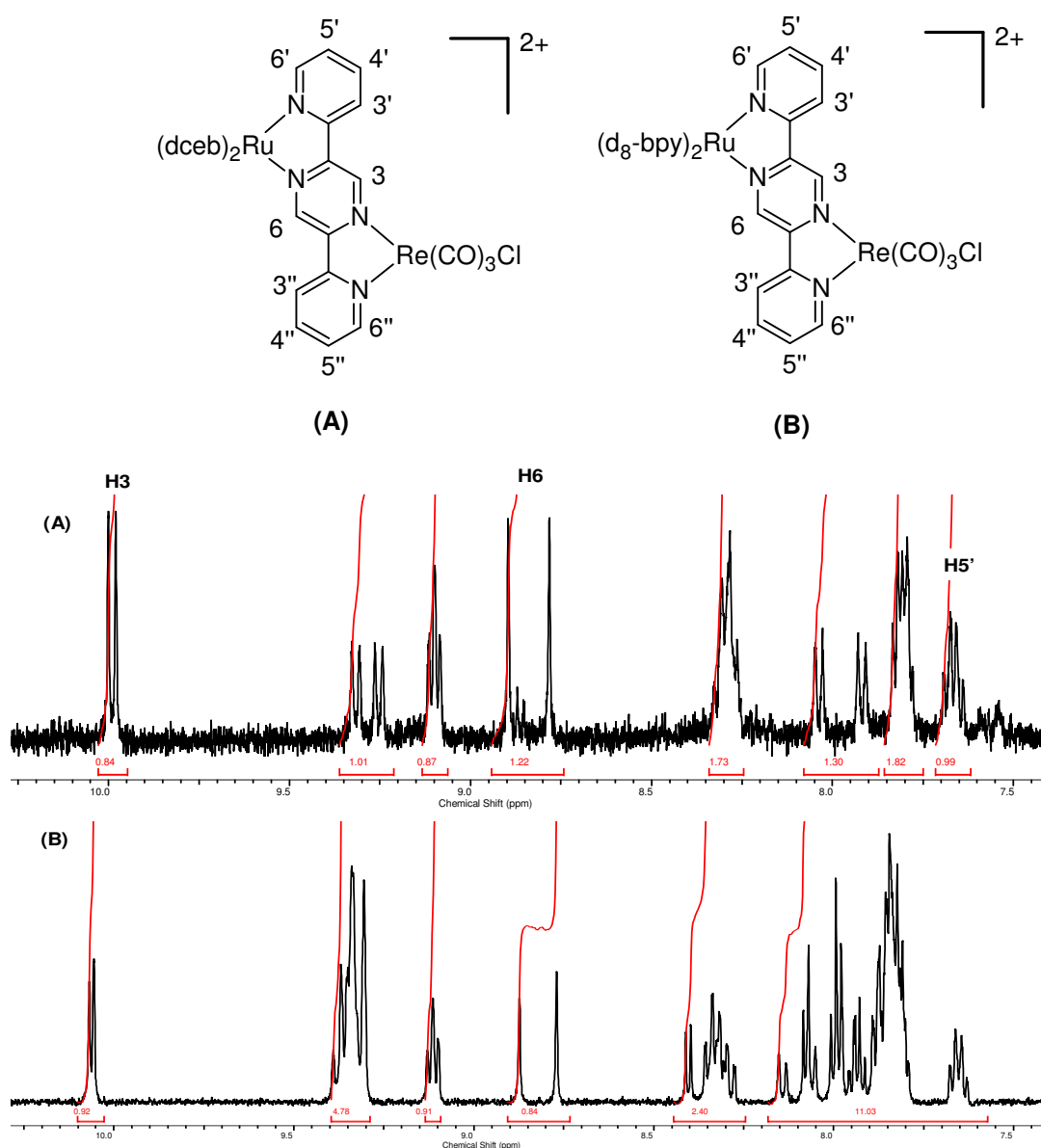


Figure 3.21: Comparison of ^1H NMR($\text{DMSO-}d_6$, 400 MHz) spectra of $[\text{Ru}(\text{d}_8\text{-bpy})_2(\mu\text{-}2,5\text{-dpp})\text{Re}(\text{CO})_3\text{Cl}]^{2+}$ (A) and $[\text{Ru}(\text{dceb})_2(\mu\text{-}2,5\text{-dpp})\text{Re}(\text{CO})_3\text{Cl}]^{2+}$ (B)

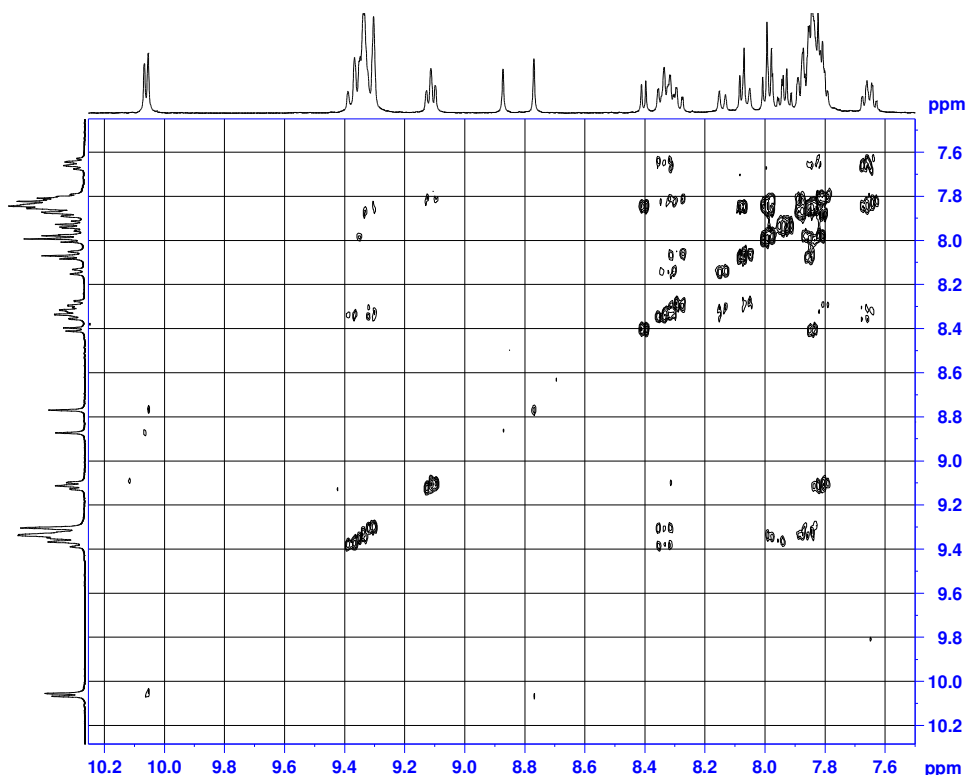


Figure 3.22: 2D COSY NMR(DMSO- d_6 , 400 MHz) of $[Ru(dceb)_2(\mu\text{-}2,5\text{-}dpp)Re(CO)_3Cl]^{2+}$.

Table 3.3: Chemical shifts of 2,5-dpp protons in isomer-1 and isomer-2 of $[Ru(dceb)_2(\mu\text{-}2,5\text{-}dpp)Re(CO)_3Cl]^{2+}$.

Chemical shift of the protons (ppm)		
Protons	Isomer-1	Isomer-2
H3	10.05	10.06
H6	8.78	9.11
H5'	7.60	7.60

Another bridging ligand bisbpy was introduced to prepare further ruthenium-rhenium heterodinuclear complexes. The 1H NMR spectra obtained for these complexes remained unresolved, because the corresponding 2D COSY NMR spectra were difficult to interpret. The NMR spectra for the Ru-bisbpy-Re heterodinuclear complexes are different from the analogous ruthenium mononuclear complexes.

Integration of all the protons in the Ru-bisbpy-Re complexes clearly demonstrates each compound contains two isomers. A comparison of ^1H NMR spectra of bisbpy, the Ru-bisbpy mononuclear complex and the Ru-bisbpy-Re heterodinuclear complex are provided in **Figures 3.23 to 3.26** (see 2D COSY in **Figure 3.24** and **3.26**). The ^1H NMR spectra for $[\text{Ru}(\text{dceb})_2(\mu\text{-Hbpt})\text{Re}(\text{CO})_3\text{Cl}]^{2+}$ also remained unresolved although a comparison of ^1H NMR spectra with the homologous Ru-mononuclear complex is also shown in **Figure 3.27**.

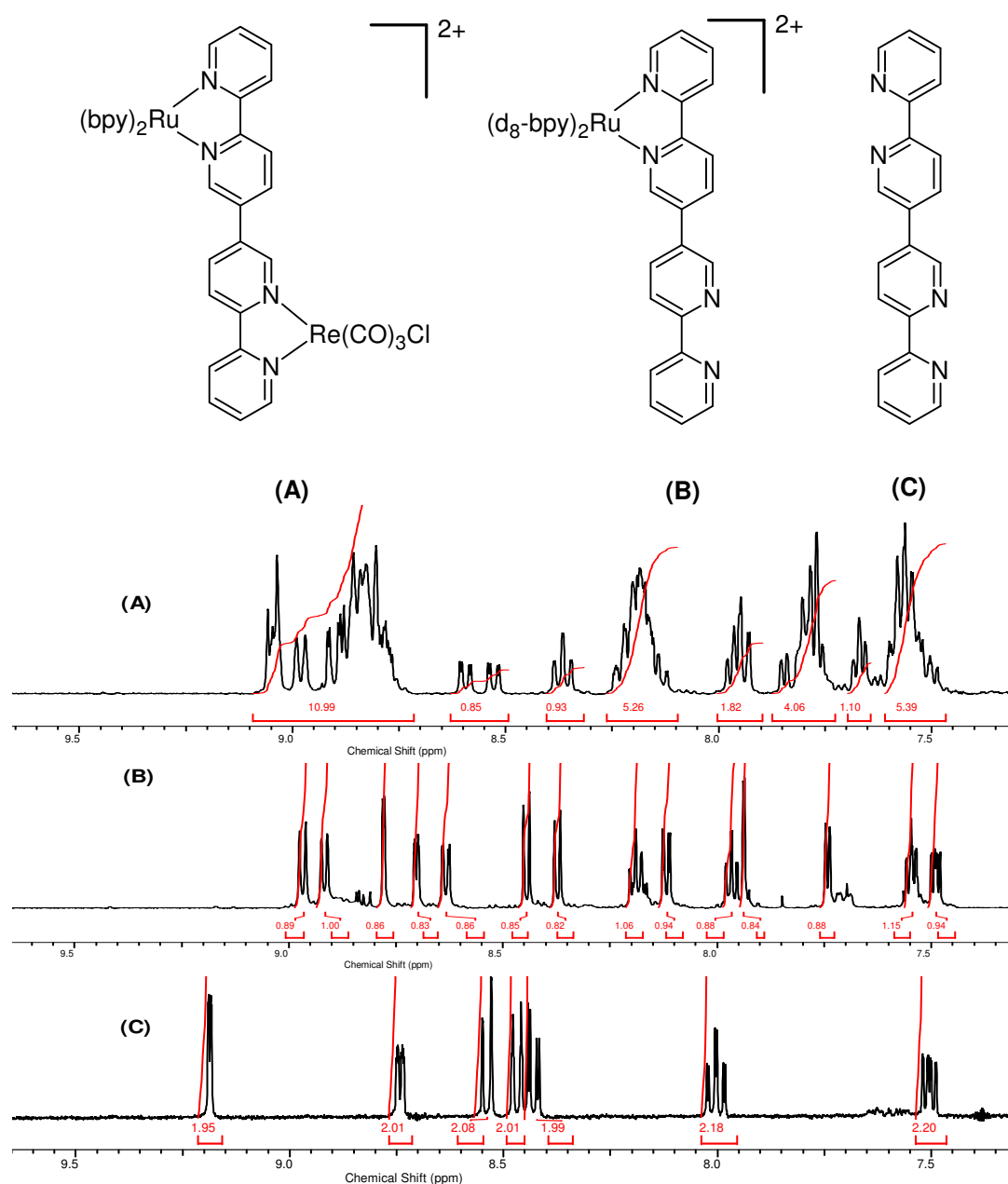


Figure 3.23: ^1H NMR(DMSO- d_6 , 400 MHz) of (A) $[\text{Ru}(\text{bpy})_2(\mu\text{-bisbpy})\text{Re}(\text{CO})_3\text{Cl}]^{2+}$, (B) $[\text{Ru}(\text{bpy})_2(\text{bisbpy})]^{2+}$ and (C) bisbpy

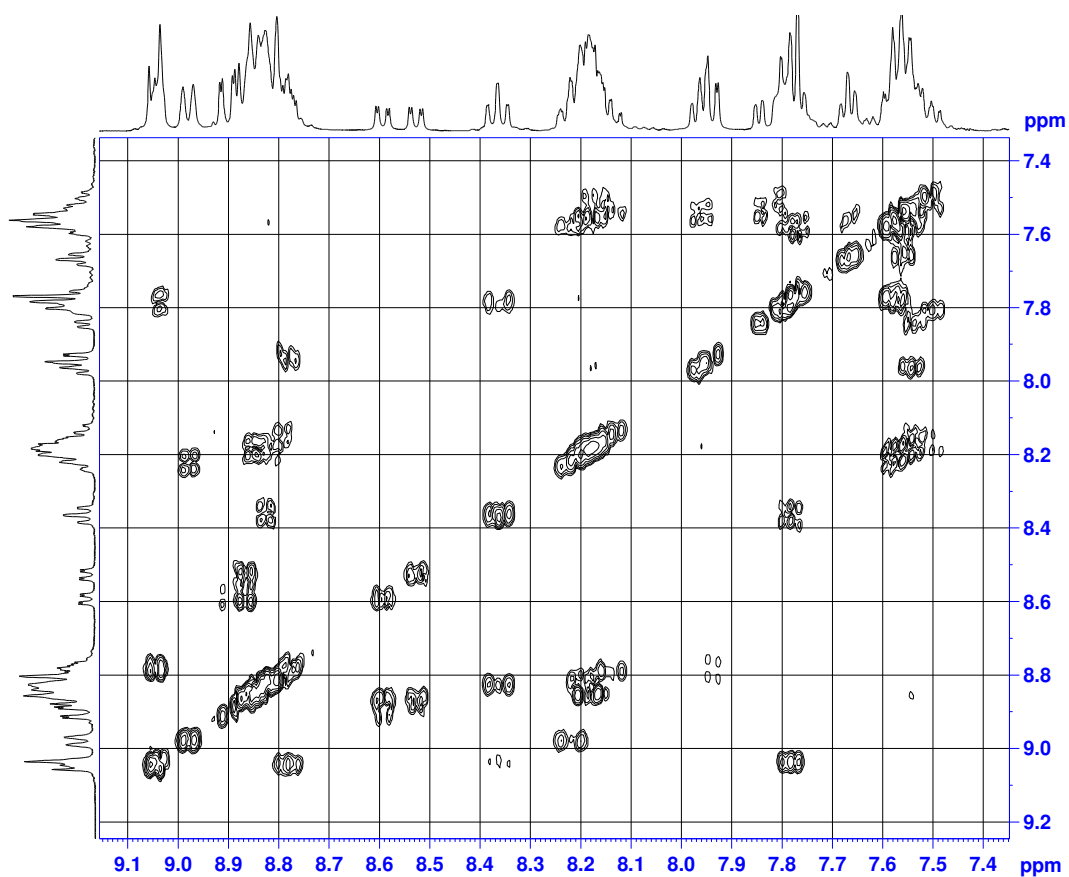


Figure 3.24: COSY NMR(DMSO- d_6 , 400 MHz) of $[Ru(bpy)_2(\mu\text{-bisbpy})Re(CO)_3Cl]^{2+}$.

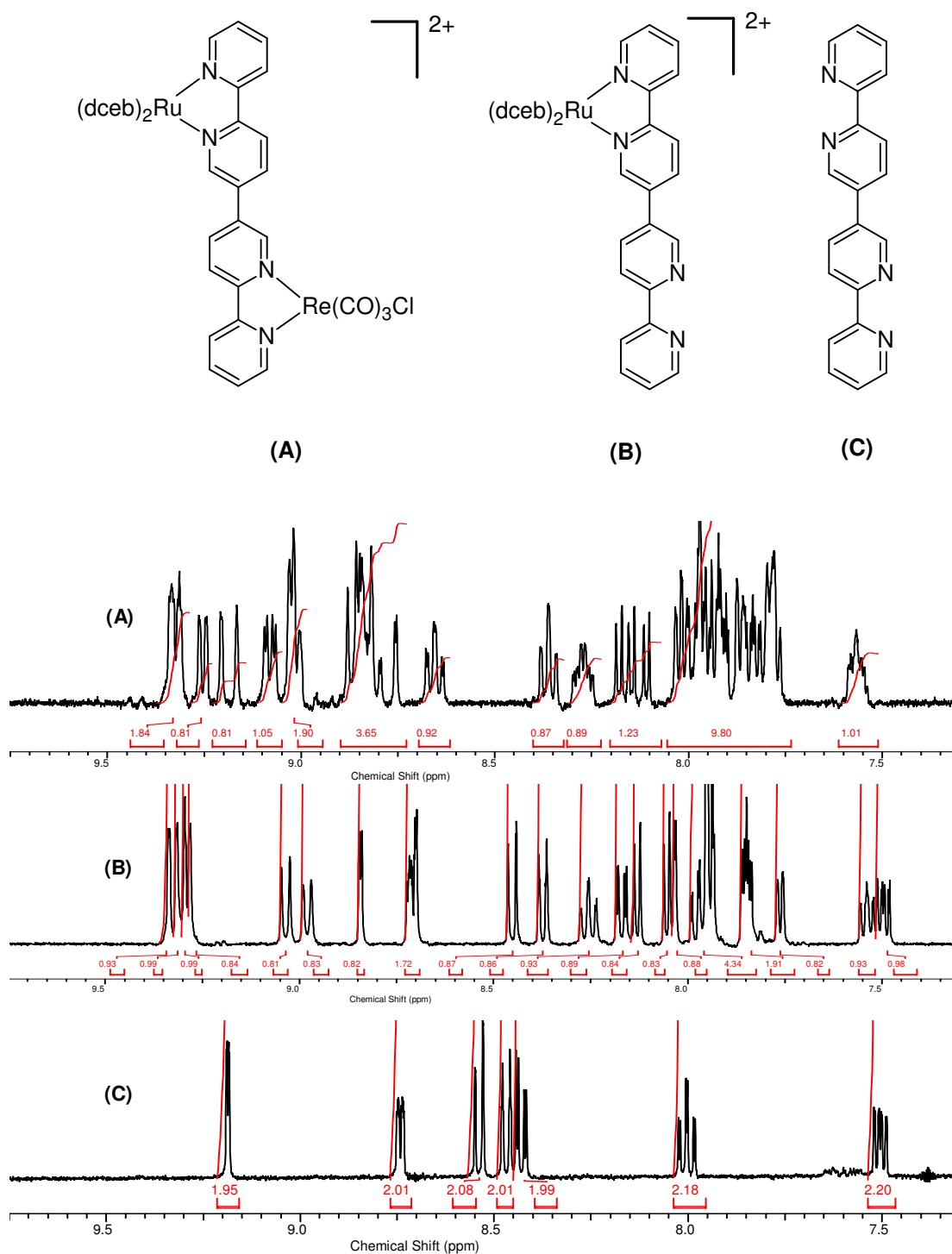


Figure 3.25: ^1H NMR(DMSO- d_6 , 400 MHz) of (A) $[\text{Ru}(\text{dceb})_2(\mu\text{-bisbpy})\text{Re}(\text{CO})_3\text{Cl}]^{2+}$, (B) $[\text{Ru}(\text{dceb})_2(\text{bisbpy})]^{2+}$ and (C) bisbpy .

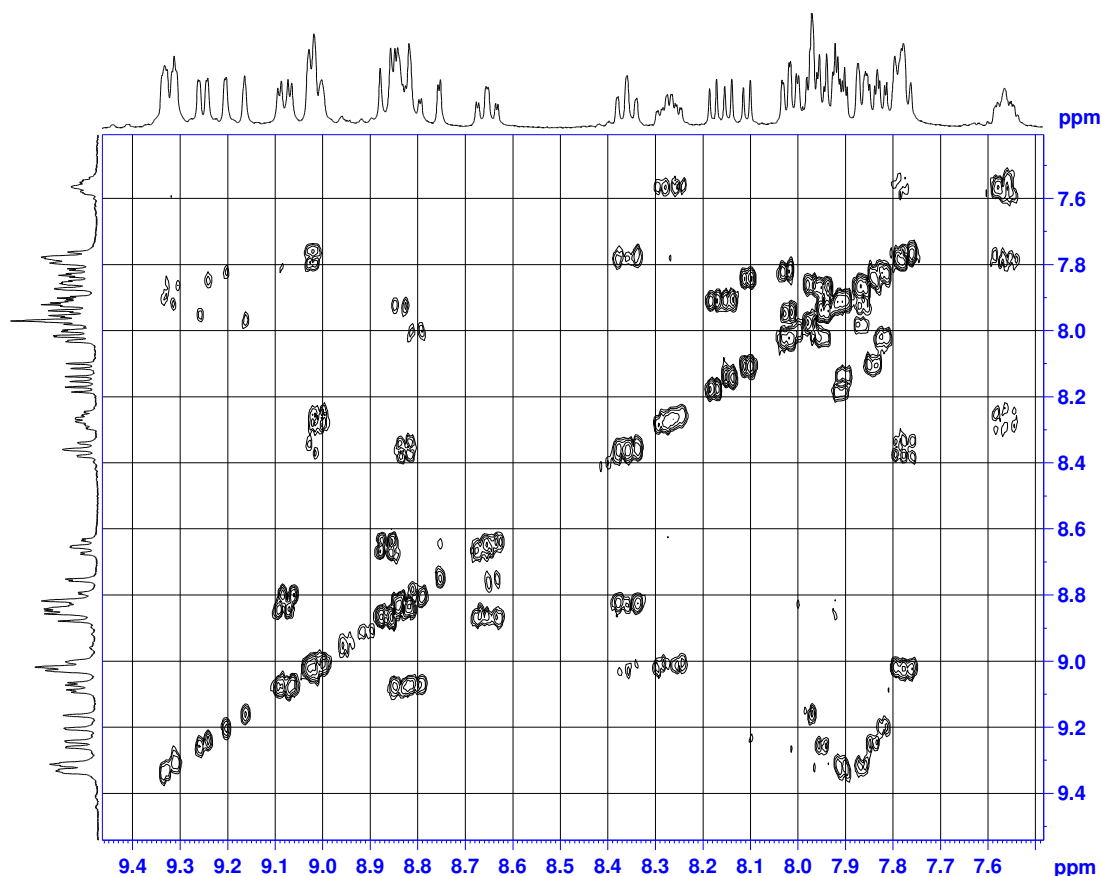


Figure 3.26: COSY NMR(DMSO- d_6 , 400 MHz) of $[Ru(dceb)_2(\mu\text{-bisbpy})Re(CO)_3Cl]^{2+}$

The NMR assignment for $[Ru(dceb)_2(\mu\text{-Hbpt})Re(CO)_3Cl]^{2+}$ was made considering the corresponding 2D COSY NMR spectra (**Appendix A**) and the 1H NMR spectra of its analogous mononuclear complex. The protons in the 2nd pyridyl ring (Py2) coordinated to the $Re(CO)_3Cl$ moiety are found slightly upfielded. Some of the protons are not assigned due to unresolved 2D COSY NMR spectra. A comparison of 1H NMR spectra of $[Ru(dceb)_2(\mu\text{-Hbpt})Re(CO)_3Cl]^{2+}$ and $[Ru(dceb)_2(Hbpt)]^{2+}$ is displayed in **Figure 3.27** and the detail chemical shifts of the Hbpt protons in both Ru-Hbpt-Re and Ru-Hbpt are summarised in **Table 3.4**.

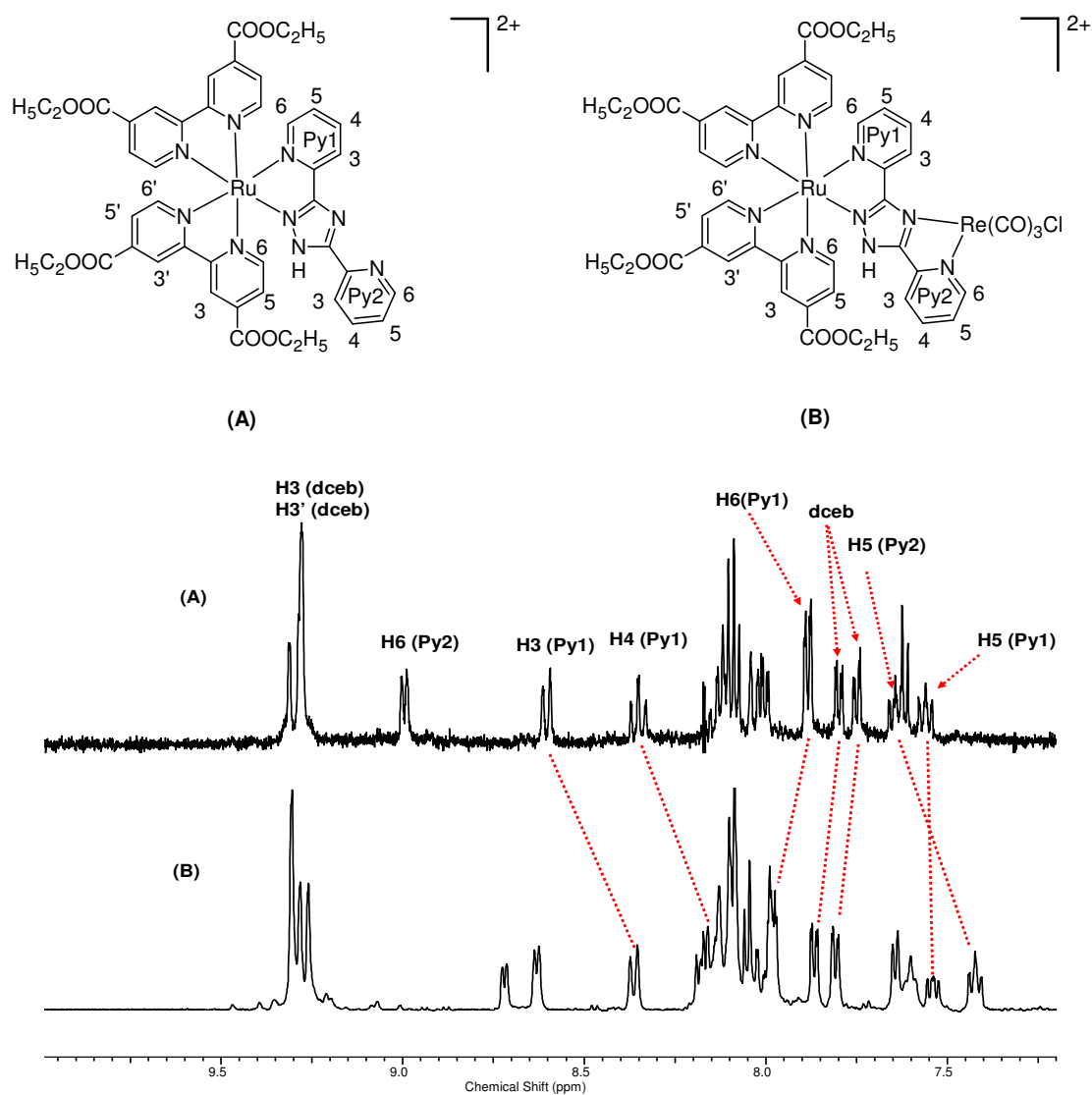


Figure 3.27: ^1H NMR ($\text{DMSO-}d_6$, 400 MHz) of (A) $[\text{Ru}(\text{dceb})_2(\text{Hbpt})]^{2+}$ and (B) $[\text{Ru}(\text{dceb})_2(\mu\text{-Hbpt})\text{Re}(\text{CO})_3\text{Cl}]^{2+}$

Table 3.4: Chemical shifts of the Hbpt protons in $[\text{Ru}(\text{dceb})_2(\mu\text{-Hbpt})\text{Re}(\text{CO})_3\text{Cl}]^{2+}$ and in $[\text{Ru}(\text{dceb})_2(\text{Hbpt})]^{2+}$

Protons (Hbpt)	Ru-Hbpt-Re (ppm)	Ru-Hbpt (ppm)
H5(Py1)	7.54	7.56
H5 (Py2)	7.42	7.64
H6 (Py1)	-	7.88
H6(Py2)	-	9.00
H4(Py1)	8.18	8.35
H3(Py1)	8.36	-

3.6. Absorption and emission spectroscopy of Ru(II)/Re(I) complexes

The absorption and emission spectra were recorded in spectroscopic grade acetonitrile. A list of absorption and emission data, recorded at room temperature (20 ± 2 °C) is provided in **Table 3.5**.

Table 3.5: Absorption and emission data of ruthenium(II)/rhenium(I) complexes

Complex	Absorption ^a	Emission ^{a, b}
	(nm)/($\epsilon \times 10^4 \text{ M}^{-1} \text{ cm}^{-1}$)	298K (nm)
[(bpy)Re(CO) ₃ Cl]	390/(0.37)	600
[(dceb)Re(CO) ₃ Cl]	410/(0.78)	-
[(dpb)Re(CO) ₃ Cl]	374/(0.36)	619
[Ru(bpy) ₃] ²⁺	452/(1.29)	615
[Ru(dceb) ₂ (Hbpt)](PF ₆) ₂	460/(1.56)	627
[Ru(dceb) ₂ (Hbpt)Re(CO) ₃ Cl](PF ₆) ₂	494/(1.10), 370(0.5)	688
[Ru(bpy) ₂ (bisbpy)](PF ₆) ₂	452/(1.16)	633
[Ru(bpy) ₂ (bisbpy)Re(CO) ₃ Cl](PF ₆) ₂	450/(1.29)	661
[Ru(dceb) ₂ (bisbpy)](PF ₆) ₂	475/(1.13)	647
[Ru(dceb) ₂ (bisbpy) Re(CO) ₃ Cl](PF ₆) ₂	475/(0.94)	647
[Ru(bpy) ₂ (2,5-dpp)](PF ₆) ₂	433/(0.95)	680
[Ru(bpy) ₂ (2,5-dpp) Re(CO) ₃ Cl](PF ₆) ₂	421 (0.8), 552/(0.9)	-
[Ru(dceb) ₂ (2,5-dpp)](PF ₆) ₂	467/(1.79)	629
[Ru(dceb) ₂ (2,5-dpp) Re(CO) ₃ Cl](PF ₆) ₂	449(1.9), 529/(1.8)	-

(a) Acetonitrile (RT) (b) Excitation wavelength was 450 nm. OD = 0.15 A.U. at 450 nm for Ru/Re dinuclear complex and at 400 nm for Re mononuclear complexes.

3.6.1. Absorption and emission spectra of mononuclear complexes

An understanding of the absorption and emission spectra of mononuclear ruthenium and rhenium-carbonyl complexes is essential before analysing the

absorption and emission spectra of Ru-Re heterodinuclear complexes. The absorption and emission properties of the ruthenium mononuclear complexes have been discussed in the previous chapter from where an increase in the MLCT band (> 452 nm) was observed with the introduction of the electron withdrawing carboxy ester groups compared to $[\text{Ru}(\text{bpy})_3]^{2+}$ (MLCT at 452 nm, **Table 3.5**). The absorption spectra of mononuclear rhenium complexes reported in this chapter are displayed in **Figure 3.28**. Past literature reports suggest that $[(\text{bpy})\text{Re}(\text{CO})_3\text{Cl}]$ has lowest energy absorption band at 390 nm which is assigned to a MLCT transition.^{27,35,69} The low energy absorption bands for the mononuclear rhenium complexes ($[(\text{dceb})\text{Re}(\text{CO})_3\text{Cl}]$ and $[(\text{dpb})\text{Re}(\text{CO})_3\text{Cl}]$) synthesised in this chapter are assigned to MLCT transitions on comparing to $[(\text{bpy})\text{Re}(\text{CO})_3\text{Cl}]$. The absorption maximum of $[(\text{dceb})\text{Re}(\text{CO})_3\text{Cl}]$ is found lower energy compared to that of $[(\text{bpy})\text{Re}(\text{CO})_3\text{Cl}]$ (**Table 3.5**). The dceb has a lower π^* level compared to the bpy ligand⁷⁰ and therefore results in lowering of the energy gap between HOMO and LUMO for $[(\text{dceb})\text{Re}(\text{CO})_3\text{Cl}]$ compared to $[(\text{bpy})\text{Re}(\text{CO})_3\text{Cl}]$.

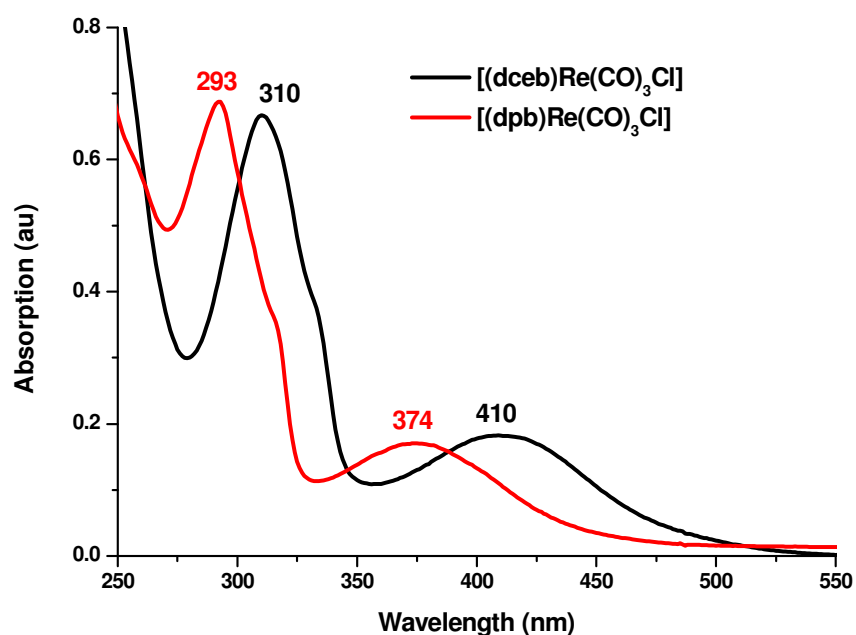


Figure 3.28: (black) absorption spectra of $[(\text{dceb})\text{Re}(\text{CO})_3\text{Cl}]$ and (red) absorption spectra of $[(\text{dpb})\text{Re}(\text{CO})_3\text{Cl}]$. Absorption spectra of both compounds were recorded in acetonitrile at room temperature (20 ± 2 °C)

Emission spectra of $[(dceb)Re(CO)_3Cl]$ and $[(dpb)Re(CO)_3Cl]$ were recorded in acetonitrile at room temperature. The emission maximum of $[(dpb)Re(CO)_3Cl]$ (617 nm) was red shifted relative to $[(bpy)Re(CO)_3Cl]$ (600 nm) and no emission was observed for $[(dceb)Re(CO)_3Cl]$ at room temperature (**Figure 3.29**). According to the literature, the emission states for the rhenium(I) complexes are defined as 3MLCT emitters.⁷¹⁻⁷⁸ Therefore, it can also be inferred that the 3MLCT state for the rhenium complex $[(dpb)Re(CO)_3Cl]$ is responsible for the emission wavelength observed at 617 nm. The $[(dceb)Re(CO)_3Cl]$ does not emit at room temperature and substantially quenched emission intensity was observed which indicates lowering the gap between HOMO and LUMO levels created by the electron withdrawing effect of the carboxy ester groups.⁵⁸

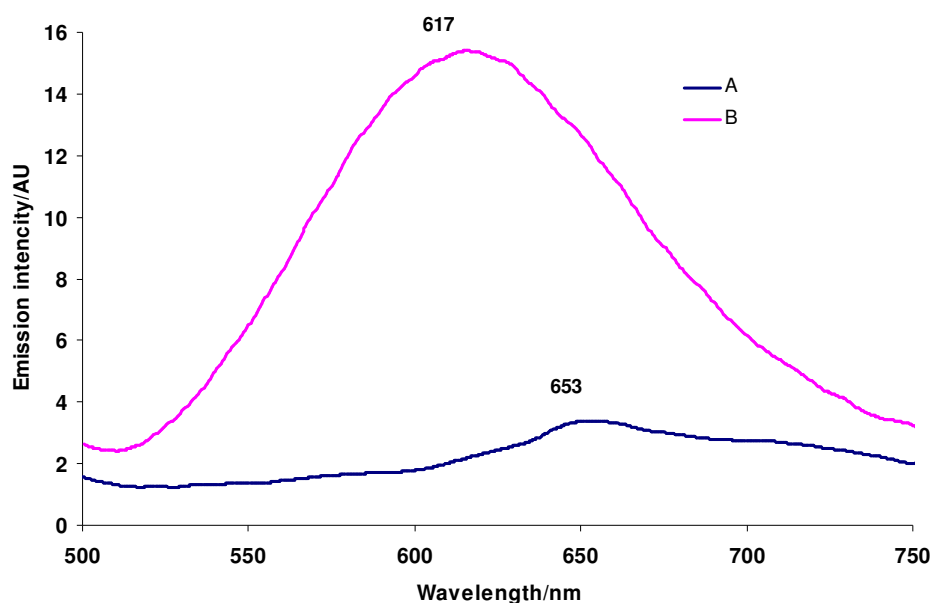


Figure 3.29: (A) emission spectrum of $[(dceb)Re(CO)_3Cl]$ (B) emission spectrum of $[(dpb)Re(CO)_3Cl]$. Emission spectra of both compounds were recorded in acetonitrile at room temperature ($20 \pm 2^\circ C$). OD at $\lambda_{ex} = 0.2$ A.U. $\lambda_{ex} = 400$ nm

3.6.2. Absorption and emission spectra of Ru(II)-Re(I) heterodinuclear complexes

A number of Ru-Re heterodimetallic complexes based on dpm and HAT bridging ligands were reported by Sahai *et al.*³⁵ The higher and the lower energy transitions for Ru-Re heterodimetallic complexes were assigned to the rhenium metal

to dpm or HAT based MLCT transitions and the ruthenium metal to dpm or HAT ligands MLCT transitions respectively.³⁵ For example, $[\text{Ru}(\text{bpy})_2(\text{dpm})\text{Re}(\text{CO})_3\text{Cl}]^{2+}$ has MLCT transitions at 558 nm and 414 nm with a shoulder at 377 nm. The absorption band at 558 nm was assigned to a $\text{d}\pi(\text{Re}) - \pi^*(\text{dpm})$ based transition and that at 414 nm was assigned to a $\text{d}\pi(\text{Re}) - \pi^*(\text{dpm})$ based transition.

A red shift in the lowest MLCT band was observed in heterodinuclear complexes containing the bridging ligands with low-lying π^* levels which indicates further lowering of the π^* levels of the bridge when attached to the $\text{Re}(\text{CO})_3\text{Cl}$ moiety.^{58,64,79,80} For example, mononuclear complex $[\text{Ru}(\text{bpy})_2(2,5\text{-dpp})]^{2+}$ has an absorption maximum at 433 nm while the heterodinuclear complex $[\text{Ru}(\text{bpy})_2(2,5\text{-dpp})\text{Re}(\text{CO})_3\text{Cl}]^{2+}$ has an absorption maximum at 552 nm. However, no shift in the MLCT bands was observed in case of Ru-bisbpy-Re heterodinuclear complexes compared to the corresponding mononuclear Ru-bisbpy complexes. For example, the mononuclear complex $[\text{Ru}(\text{bpy})_2(\text{bisbpy})]^{2+}$ and the heterodinuclear complex $[\text{Ru}(\text{bpy})_2(\text{bisbpy})\text{Re}(\text{CO})_3\text{Cl}]^{2+}$ have an absorption maximum at 452 nm and 450 nm respectively. Both the bpy units are twisted with respect to each other when the bisbpy ligand is bound to two metal centres (See **Diagram 3.1**). This hinders overlap between the π -orbitals on the two bpy units. As a result, the $\text{Ru}(\text{d}\pi) \rightarrow \text{bisbpy}(\pi^*)$ MLCT is unaffected following complexation with the rhenium metal centre on the other side of bisbpy ligand.

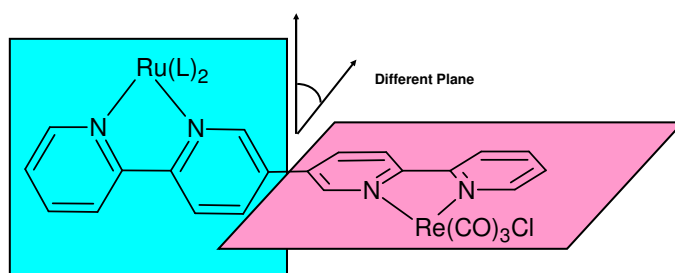


Diagram 3.1: Two bpy units of bisbpy are in two different planes, which restrict the interaction between two metal centres in Ru-bisbpy-Re complex.

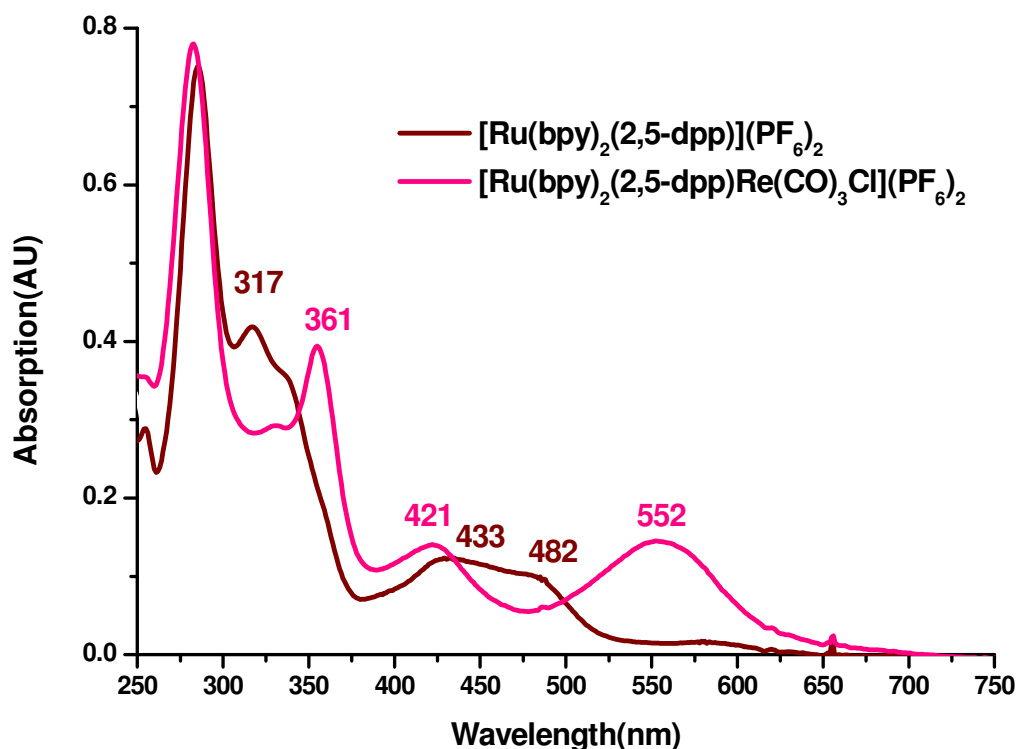


Figure 3.30: (Brown) absorption spectra of $[\text{Ru}(\text{bpy})_2(2,5\text{-dpp})]^{2+}$ and (purple-red) absorption spectra of $[\text{Ru}(\text{bpy})_2(\mu\text{-}2,5\text{-dpp})\text{Re}(\text{CO})_3\text{Cl}]^{2+}$. Absorption spectra of both compounds were recorded in acetonitrile at room temperature ($20 \pm 2^\circ\text{C}$).

Figure 3.30 displays the difference in absorption spectra for $[\text{Ru}(\text{bpy})_2(2,5\text{-dpp})]^{2+}$ and $[\text{Ru}(\text{bpy})_2(\mu\text{-}2,5\text{-dpp})\text{Re}(\text{CO})\text{Cl}]^{2+}$. It is important to mention that 2,5-dpp has a lower π^* level than the bpy ligands. According to the literature, the lower energy of the MLCT band is dominated by a $d\pi(\text{Ru})\text{-}\pi^*(2,5\text{-dpp})$ transition for the mononuclear ruthenium complex.⁸¹ $[\text{Ru}(\text{bpy})_2(2,5\text{-dpp})]^{2+}$ has two MLCT bands at 433 nm and at 482 nm. The MLCT transition at 433 nm was assigned to $d\pi(\text{Ru})\text{-}\pi^*(\text{bpy})$ and 482 nm to $d\pi(\text{Ru})\text{-}\pi^*(2,5\text{-dpp})$ transitions. It is also important to observe the intraligand $\pi\text{-}\pi^*$ transition for bpy and 2,5-dpp appears at ~ 290 nm and at 317 nm respectively. Similarly, $[\text{Ru}(\text{bpy})_2(2,5\text{-dpp})\text{Re}(\text{CO})_3\text{Cl}]^{2+}$ displays two $\pi\text{-}\pi^*$ transitions for bpy and 2,5-dpp ligands. Interestingly, in the case of the Ru-Re-heterodinuclear complex, a strong absorption band was observed at 361 nm. According to the literature, this is due to the introduction of a $\text{Re}(\text{CO})_3\text{Cl}$ moiety which lowers the π^* level of the 2,5-dpp ligand.^{58,64,79} This results in further lowering of the energy gap between HOMO and LUMO levels in the heterodinuclear complex. The smaller energy gap between the HOMO and the LUMO itself suggests a lower energy absorption maximum.

$[\text{Ru}(\text{bpy})_2(2,5\text{-dpp})\text{Re}(\text{CO})_3\text{Cl}]^{2+}$ has two MLCT bands at 552 nm and 421 nm. According to the literature,^{35,82} the absorption band at 552 nm is assigned to a $\text{d}\pi(\text{Ru}) - \pi^*(2,5\text{-dpp})$ MLCT transition and the absorption band at 421 nm is assigned to a $\text{d}\pi(\text{Re}) - \pi^*(2,5\text{-dpp})$ MLCT transition. The $\text{d}\pi(\text{Ru}) - \pi^*(2,5\text{-dpp})$ MLCT transition for $[\text{Ru}(\text{bpy})_2(2,5\text{-dpp})\text{Re}(\text{CO})_3\text{Cl}]^{2+}$ is red shifted from 482 nm to 552 nm compared to $[\text{Ru}(\text{bpy})_2(2,5\text{-dpp})]^{2+}$.

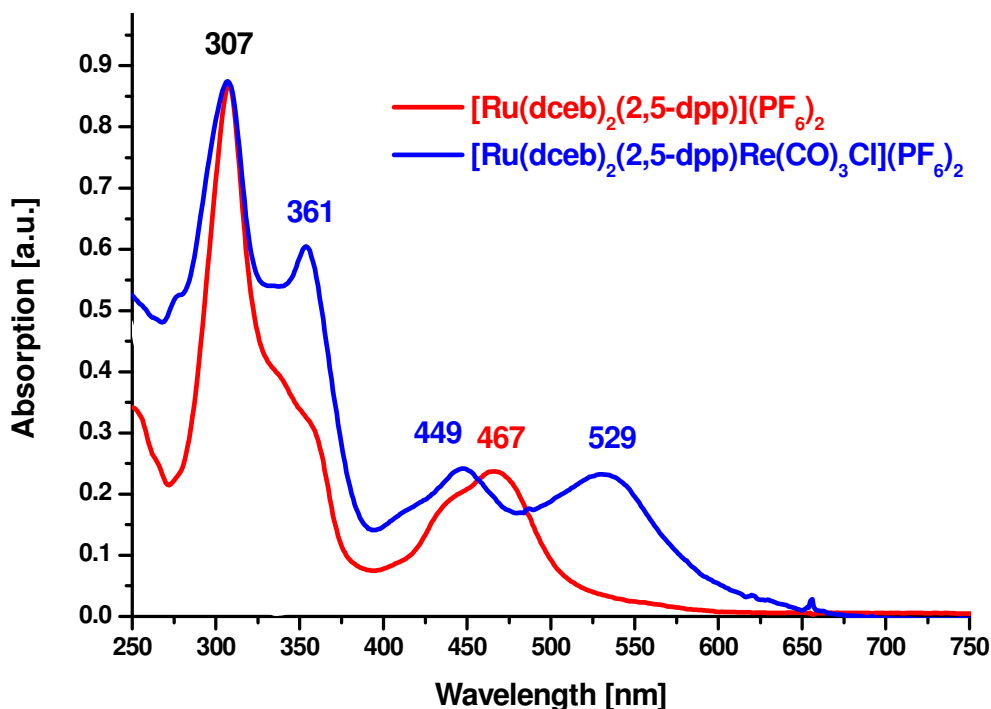


Figure 3.31: (Red) absorption spectra of $[\text{Ru}(\text{dceb})_2(2,5\text{-dpp})]^{2+}$ and (blue) absorption spectra of $[\text{Ru}(\text{dceb})_2(\mu\text{-}2,5\text{-dpp})\text{Re}(\text{CO})_3\text{Cl}]^{2+}$. Absorption spectra of both compounds were recorded in acetonitrile at room temperature ($20 \pm 2^\circ\text{C}$).

Shown in **Figure 3.31** are the absorption spectra of $[\text{Ru}(\text{dceb})_2(2,5\text{-dpp})]^{2+}$ and $[\text{Ru}(\text{dceb})_2(2,5\text{-dpp})\text{Re}(\text{CO})_3\text{Cl}]^{2+}$. $[\text{Ru}(\text{dceb})_2(2,5\text{-dpp})]^{2+}$ has a MLCT band at 467 nm which is due to a $\text{d}\pi(\text{Ru}) - \pi^*(2,5\text{-dpp})$ transition. Whereas $[\text{Ru}(\text{dceb})_2(2,5\text{-dpp})\text{Re}(\text{CO})_3\text{Cl}]^{2+}$ has two MLCT bands at 529 nm and at 449 nm. According to the literature, the 529 nm absorption band is due to a $\text{d}\pi(\text{Ru}) - \pi^*(2,5\text{-dpp})$ based transition while the absorption band at 449 nm is due to a $\text{d}\pi(\text{Re}) - \pi^*(2,5\text{-dpp})$ transition.^{35,82} The $\text{d}\pi(\text{Ru}) - \pi^*(\text{dceb})$ transition bands in $[\text{Ru}(\text{dceb})_2(2,5\text{-dpp})\text{Re}(\text{CO})_3\text{Cl}]^{2+}$ are difficult to identify and are overlapped by strong $\text{d}\pi(\text{M}) - \pi^*(2,5\text{-dpp})$ transitions ($\text{M} = \text{Ru}$ and Re). Interestingly, the $\text{d}\pi(\text{Ru}) - \pi^*(2,5\text{-dpp})$

transition in $[\text{Ru}(\text{dceb})_2(2,5\text{-dpp})\text{Re}(\text{CO})_3\text{Cl}]^{2+}$ is 62 nm red shifted compared to the $d\pi(\text{Ru}) - \pi^*(2,5\text{-dpp})$ transition in $[\text{Ru}(\text{dceb})_2(2,5\text{-dpp})]^{2+}$. $[\text{Ru}(\text{dceb})_2(2,5\text{-dpp})\text{Re}(\text{CO})_3\text{Cl}]^{2+}$ has another two intraligand transitions which can be identified as dceb and 2,5-dpp based $\pi - \pi^*$ transition at 307 nm and 361 nm respectively.

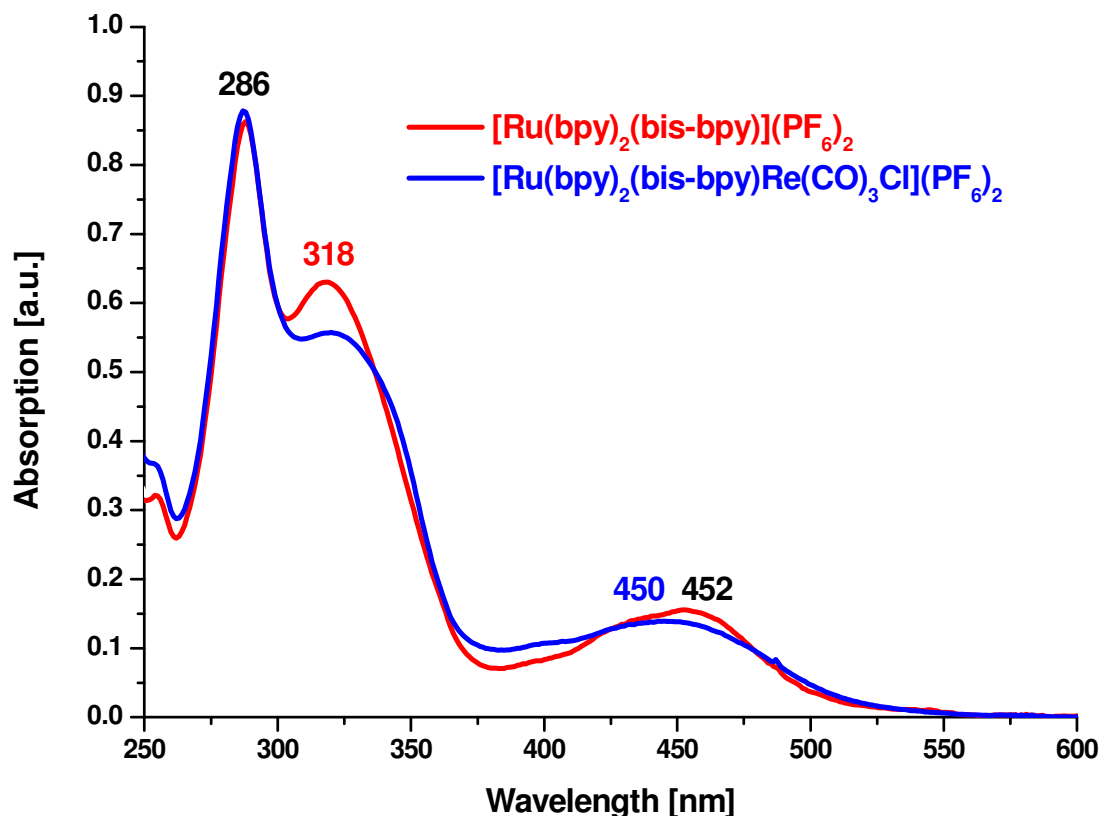


Figure 3.32: (Red) absorption spectra of $[\text{Ru}(\text{bpy})_2(\text{bisbpy})]^{2+}$ and (blue) absorption spectra of $[\text{Ru}(\text{bpy})_2(\mu\text{-bisbpy})\text{Re}(\text{CO})_3\text{Cl}]^{2+}$. Absorption spectra of both compounds were recorded in acetonitrile at room temperature ($20 \pm 2^\circ\text{C}$).

Shown in **Figure 3.32** are the absorption spectra for $[\text{Ru}(\text{bpy})_2(\text{bisbpy})]^{2+}$ and $[\text{Ru}(\text{bpy})_2(\text{bisbpy})\text{Re}(\text{CO})_3\text{Cl}]^{2+}$. $[\text{Ru}(\text{bpy})_2(\text{bisbpy})]^{2+}$ has a MLCT band at 452 nm which is a $d\pi(\text{Ru}) - \pi^*(\text{bisbpy})$ transition because bisbpy has a lower π^* level than bpy. $[\text{Ru}(\text{bpy})_2(\text{bisbpy})\text{Re}(\text{CO})_3\text{Cl}]^{2+}$ has one MLCT band at 450 nm which is identical with the analogous ruthenium monomer. The 450 nm absorption band is dominated by a $d\pi(\text{Ru}) - \pi^*(\text{bisbpy})$ MLCT transition as the $d\pi(\text{Re}) - \pi^*(\text{Mebpy-Mebpy})$ MLCT transition was observed at 361 nm for similar type of mononuclear rhenium complex $[(\text{Mebpy-Mebpy})\text{Re}(\text{CO})_3\text{Cl}]$.^{42,50,58} The bpy-based $\pi - \pi^*$ transitions are observed at 286 nm for both $[\text{Ru}(\text{bpy})_2(\text{bisbpy})]^{2+}$ and

$[\text{Ru}(\text{bpy})_2(\text{bisbpy})\text{Re}(\text{CO})_3\text{Cl}]^{2+}$. The absorption features of both the complexes remains identical in shape therefore it can be suggested that there is poor electronic interaction or no interaction between the two metal centres.

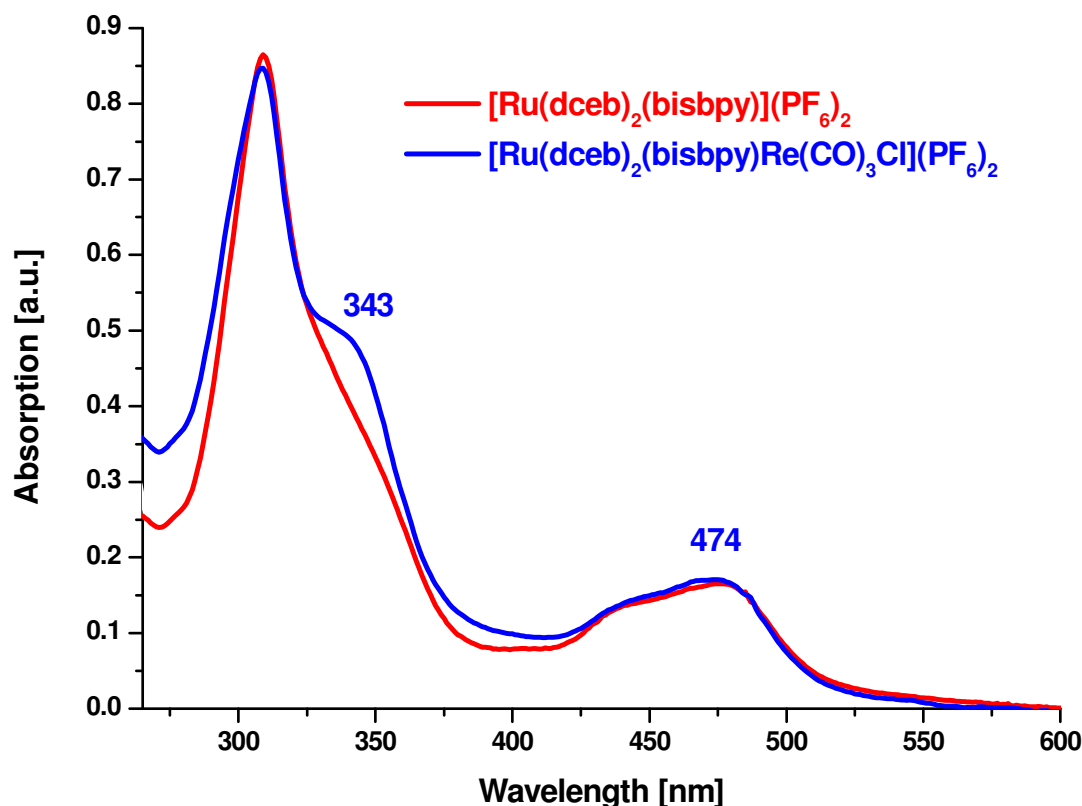


Figure 3.33: (Red) absorption spectra of $[\text{Ru}(\text{dceb})_2(\text{bisbpy})]^{2+}$ and (blue) absorption spectra of $[\text{Ru}(\text{dceb})_2(\mu\text{-bisbpy})\text{Re}(\text{CO})_3\text{Cl}]^{2+}$. Absorption spectra of both compounds were recorded in acetonitrile at room temperature ($20 \pm 2^\circ\text{C}$).

Shown in **Figure 3.33** are the absorption spectra for $[\text{Ru}(\text{dceb})_2(\text{bisbpy})]^{2+}$ and $[\text{Ru}(\text{dceb})_2(\text{bisbpy})\text{Re}(\text{CO})_3\text{Cl}]^{2+}$. A similar explanation is used to identify the bands in $[\text{Ru}(\text{dceb})_2(\text{bisbpy})\text{Re}(\text{CO})_3\text{Cl}]^{2+}$ as for $[\text{Ru}(\text{bpy})_2(\text{bisbpy})\text{Re}(\text{CO})_3\text{Cl}]^{2+}$. However, dceb has a lower π^* level than bpy because of the carboxy functionalisation. $[\text{Ru}(\text{dceb})_2(\text{bisbpy})]^{2+}$ and $[\text{Ru}(\text{dceb})_2(\text{bisbpy})\text{Re}(\text{CO})_3\text{Cl}]^{2+}$ have identical MLCT bands which may be $d\pi(\text{Ru}) - \pi^*(\text{bisbpy})$ transitions as bisbpy has a lower π^* energy level than dceb. Appearance of a shoulder around 343 nm and an increase in the absorption intensity in the region of 325 nm to 425 nm clearly suggests that there is an addition of electronic transition which is due to $d\pi(\text{Re}) - \pi^*(\text{bisbpy})$ transitions.⁴² The absorption features of both complexes suggest that there is poor electronic interaction between two metal centres through this bisbpy ligand.

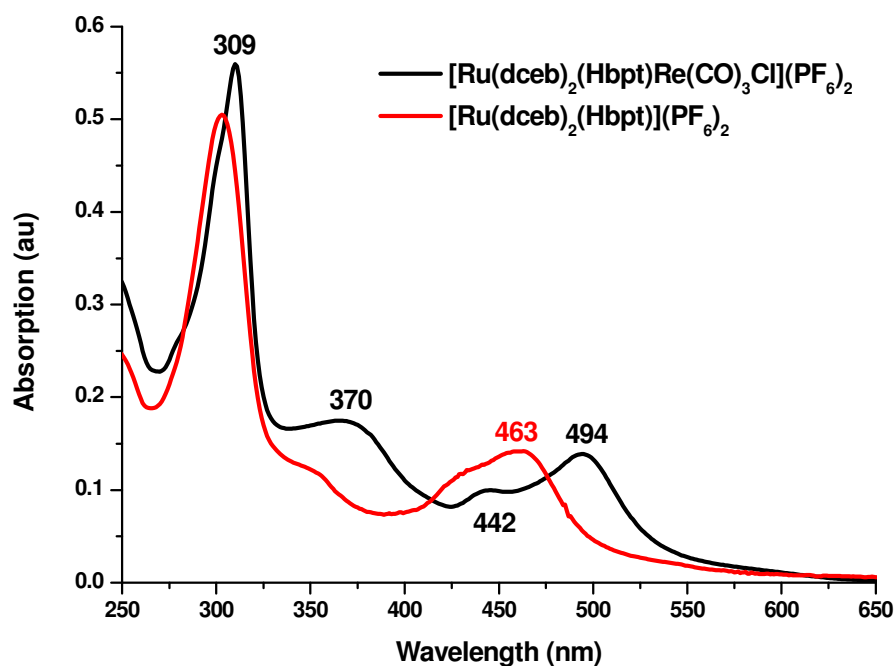


Figure 3.34: (Red) absorption spectra of $[\text{Ru}(\text{dceb})_2(\text{Hbpt})]^{2+}$ and (black) absorption spectra of $[\text{Ru}(\text{dceb})_2(\mu\text{-Hbpt})\text{Re}(\text{CO}_3)\text{Cl}]^{2+}$. Absorption spectra of both compounds were recorded in acetonitrile at room temperature ($20 \pm 2^\circ\text{C}$).

Figure 3.34 represents the absorption spectra of $[\text{Ru}(\text{dceb})_2(\text{Hbpt})]^{2+}$ and $[\text{Ru}(\text{dceb})_2(\mu\text{-Hbpt})\text{Re}(\text{CO}_3)\text{Cl}]^{2+}$. Three different MLCT transitions at 370 nm, 442 nm and 494 nm were observed for $[\text{Ru}(\text{dceb})_2(\mu\text{-Hbpt})\text{Re}(\text{CO}_3)\text{Cl}]^{2+}$. As previously discussed, the highest MLCT transition is assigned to a $d\pi(\text{Ru}) - \pi^*(\text{Hbpt})$ transition for mononuclear Ru-Hbpt complex. A red shift in the lowest MLCT band clearly indicates the lowering of π^* level of Hbpt ligand. A 31 nm red shift was observed for the $d\pi(\text{Ru}) - \pi^*(\text{Hbpt})$ MLCT transition in Ru-Hbpt-Re heterodinuclear complex (494 nm) in comparison to the homologous Ru-mononuclear complex (463 nm).

The emission spectra of heterodinuclear Ru-Re complexes are displayed in **Figure 3.35** to **3.39**. $[\text{Ru}(\text{bpy})_2(\text{bisbpy})\text{Re}(\text{CO})_3\text{Cl}](\text{PF}_6)_2$ shows an emission band at 661 nm whereas the corresponding ruthenium mononuclear complex $[\text{Ru}(\text{bpy})_2(\text{bisbpy})](\text{PF}_6)_2$ shows at 633 nm (see **Figure 3.35**). The red shift in emission wavelength from 633 nm to 661 nm is due to the coordination of the $\text{Re}(\text{CO})_3\text{Cl}$ moiety which stabilises the π^* level of bisbpy.^{35,36,82} On the other hand,

the emission wavelength did not change for $[\text{Ru}(\text{dceb})_2(\text{bisbpy})\text{Re}(\text{CO})_3\text{Cl}](\text{PF}_6)_2$ with the introduction of the $\text{Re}(\text{CO})_3\text{Cl}$ moiety (see **Figure 3.36**).

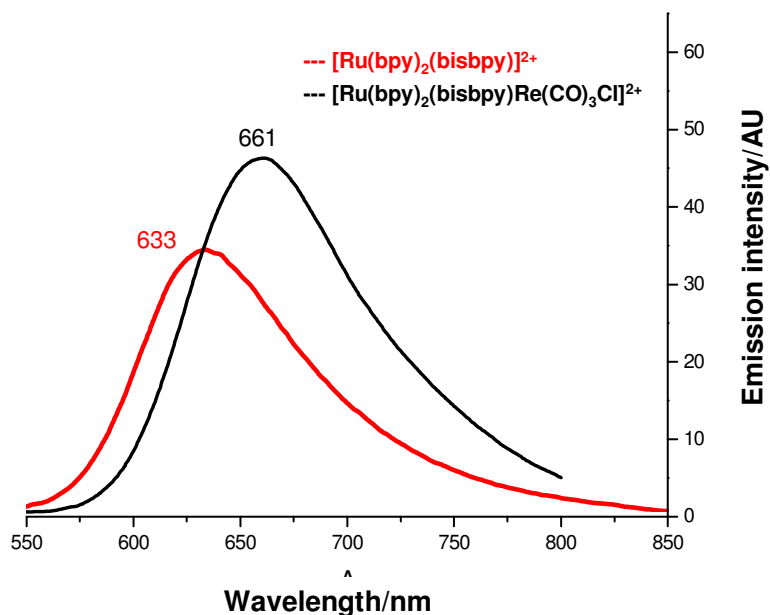


Figure 3.35: Emission spectra of $[\text{Ru}(\text{bpy})_2(\text{bisbpy})]^{2+}$ and $[\text{Ru}(\text{bpy})_2(\text{bisbpy})\text{Re}(\text{CO})_3\text{Cl}]^{2+}$. Emission spectra of both compounds were recorded in acetonitrile at room temperature ($20 \pm 2^\circ\text{C}$). OD at $\lambda_{\text{ex}} = 0.15$ A.U. $\lambda_{\text{ex}} = 450$ nm

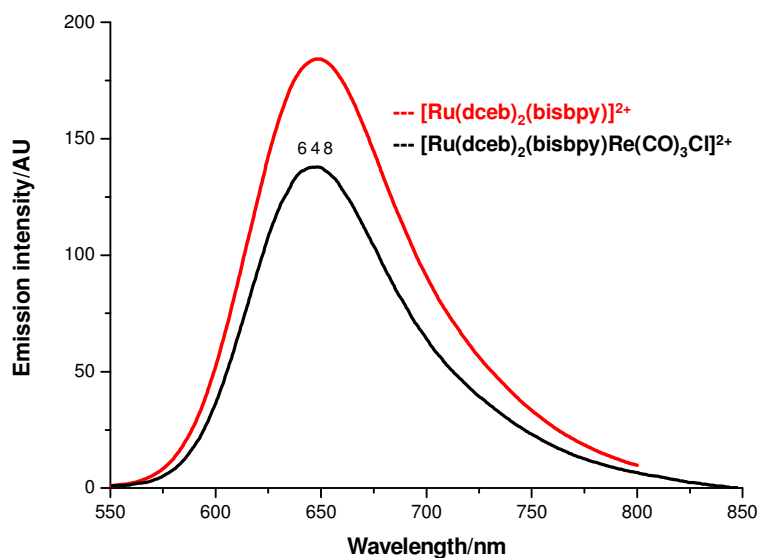


Figure 3.36: Emission spectra of $[\text{Ru}(\text{dceb})_2(\text{bisbpy})]^{2+}$ and $[\text{Ru}(\text{dceb})_2(\text{bisbpy})\text{Re}(\text{CO})_3\text{Cl}]^{2+}$. Emission spectra of both compounds were recorded in acetonitrile at room temperature ($20 \pm 2^\circ\text{C}$). OD at $\lambda_{\text{ex}} = 0.15$ A.U. $\lambda_{\text{ex}} = 450$ nm

$[\text{Ru}(\text{L})_2(\mu\text{-}2,5\text{-dpp})\text{Re}(\text{CO})\text{Cl}]^{2+}$ complexes ($\text{L} = \text{bpy}$ and dceb) also have very weak or no emission at room temperature compared to mononuclear $[\text{Ru}(\text{L})_2(2,5\text{-}$

dpp)]²⁺ which indicates a interaction between two metal centres. Also, the 2,5-dpp is a strong π - acceptor ligand and hence its π^* levels are stabilised by the coordination of the Re(CO)₃Cl moiety resulting in red shift in the emission maxima and substantial quenching in the emission intensity (see **Figure 3.37** and **3.38**). A red shift in the emission wavelength was also observed for [Ru(dceb)₂(Hbpt)Re(CO)₃Cl](PF₆)₂ (at 688 nm) compared to [Ru(dceb)₂(Hbpt)](PF₆)₂ (at 627 nm) (see **Figure 3.39**).

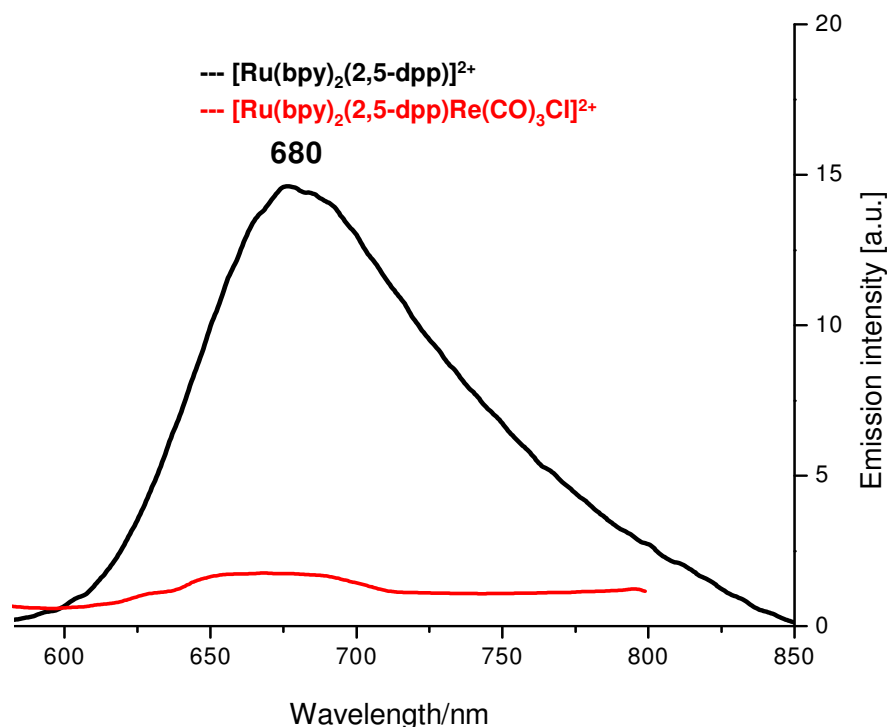


Figure 3.37: Emission spectra of [Ru(bpy)₂(2,5-dpp)]²⁺ and [Ru(bpy)₂(2,5-dpp)Re(CO)₃Cl]²⁺. Emission spectra of both compounds were recorded in acetonitrile at room temperature (20 ± 2 °C). OD at λ_{ex} = 0.15 A.U. λ_{ex} = 450 nm

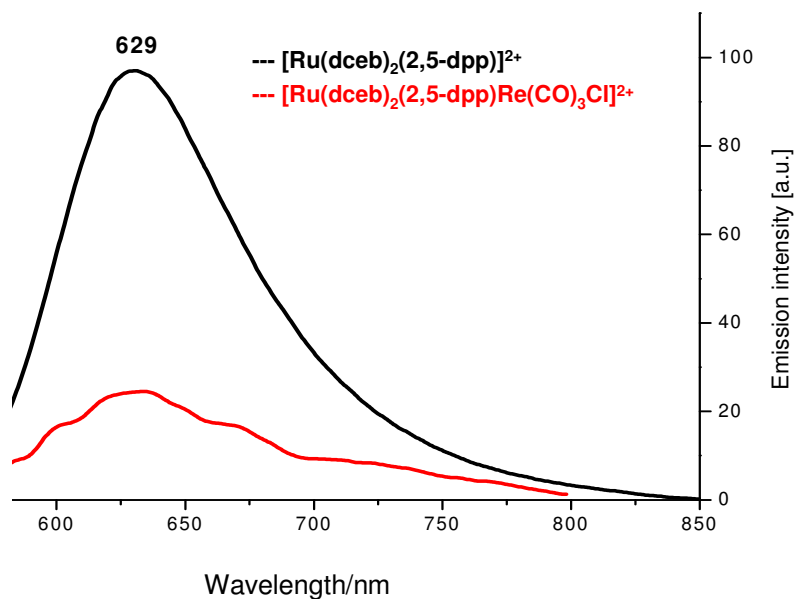


Figure 3.38: Emission spectra of $[\text{Ru}(\text{dceb})_2(2,5\text{-dpp})]^{2+}$ and $[\text{Ru}(\text{dceb})_2(2,5\text{-dpp})\text{Re}(\text{CO})_3\text{Cl}]^{2+}$. Emission spectra of both compounds were recorded in acetonitrile at room temperature ($20 \pm 2^\circ\text{C}$). OD at $\lambda_{\text{ex}} = 0.15 \text{ A.U.}$ $\lambda_{\text{ex}} = 450 \text{ nm}$

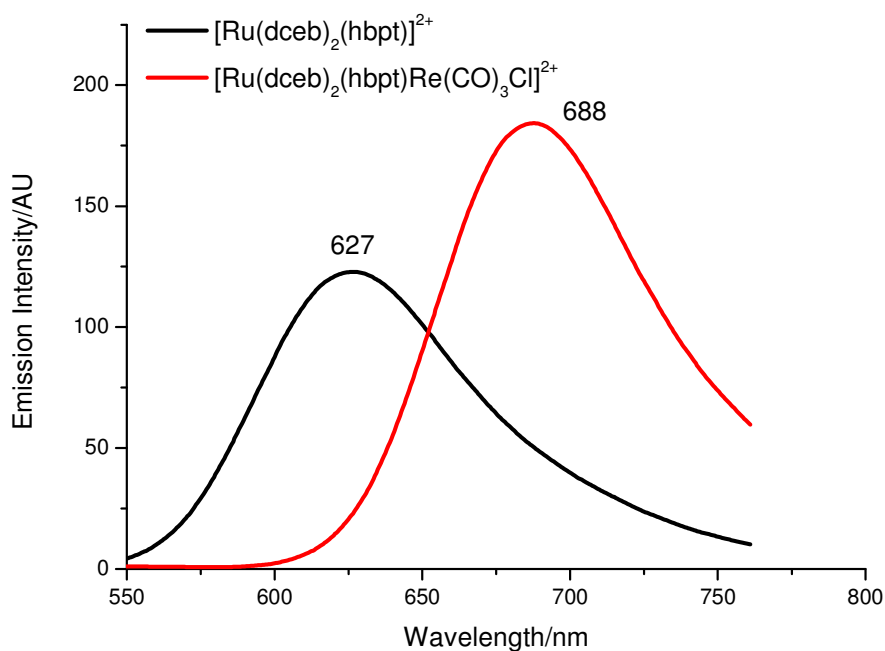


Figure 3.39: Emission spectra of $[\text{Ru}(\text{dceb})_2(\text{Hbpt})]^{2+}$ and $[\text{Ru}(\text{dceb})_2(\text{Hbpt})\text{Re}(\text{CO})_3\text{Cl}]^{2+}$. Emission spectra of both compounds were recorded in acetonitrile at room temperature ($20 \pm 2^\circ\text{C}$). OD at $\lambda_{\text{ex}} = 0.15 \text{ A.U.}$ $\lambda_{\text{ex}} = 450 \text{ nm}$

3.7. Immobilisation of carboxy ester containing Ru(II)/Re(I) complexes on nickel oxide surface

The aim of this aspect of the project was to immobilise the photocatalysts containing carboxy groups to the surface of semiconductors. This preliminary experiment was performed using a nickel oxide surface as the semiconductor. The immobilisation of the complexes was performed in two steps. The first step was to activate the nickel oxide surface using aqueous NaOH solution as it was thought that a neutral nickel oxide surface is not effective towards hydrolysing the carboxy ester groups and hence no binding takes place. Secondly, binding of the carboxy ester functionalised Ru-Re heterodinuclear complexes to the semiconductor surface. Activation of nickel oxide using NaOH results a layer of $\text{Ni(OH)}_2/\text{NiOH}$ on the electrode surface which may possibly result in basic conditions for hydrolysing the carboxy ester groups present in Ru-Re heterodinuclear complexes. This novel approach was applied for $[(\text{dceb})\text{Re}(\text{CO})_3\text{Cl}]$, $[\text{dpb})\text{Re}(\text{CO})_3\text{Cl}]$, $[\text{Ru}(\text{dceb})_2(\text{bisbpy})\text{Re}(\text{CO})_3\text{Cl}]^{2+}$, $[\text{Ru}(\text{dceb})_2(2,5\text{-dpp})\text{Re}(\text{CO})_3\text{Cl}]^{2+}$ and $[\text{Ru}(\text{dceb})_2(\mu\text{-Hbpt})\text{Re}(\text{CO})_3\text{Cl}]^{2+}$. The only characterisation carried out to date is UV-Vis spectroscopy (see **Figure 3.41**).

The visual appearances of the nickel oxide surfaces, activated nickel oxide surface and complex immobilised nickel oxide surface is displayed in **Figure 3.40**, and a detailed immobilisation procedure is shown by a schematic diagram in **Scheme 3.2**. Further spectroscopic data is required to confirm that the complexes are immobilised onto the nickel oxide surface.

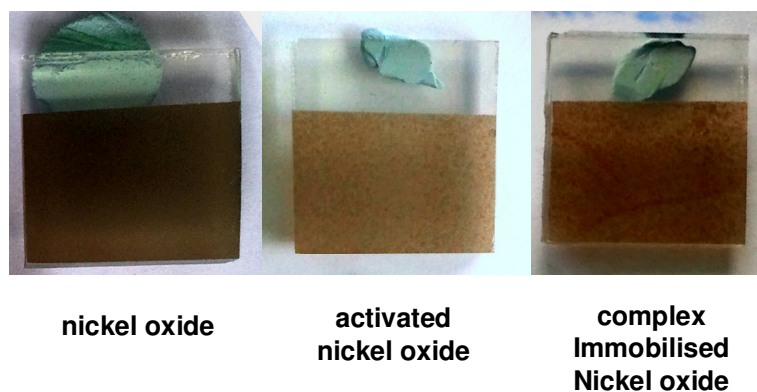
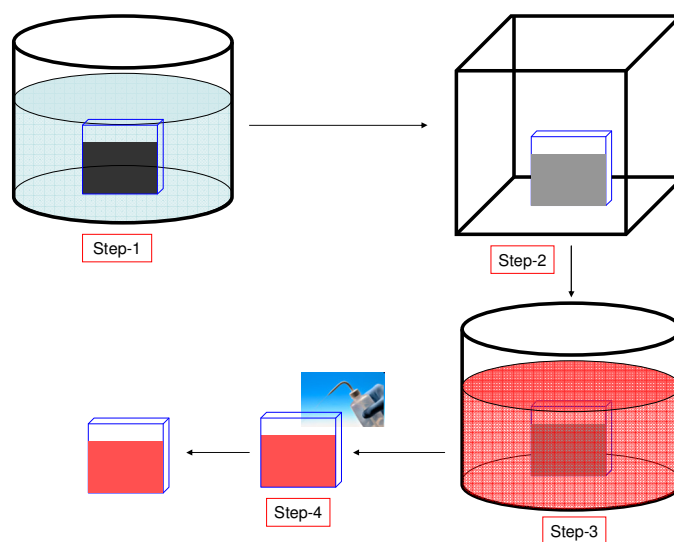


Figure 3.40: Visual appearance of nickel oxide surface, activated nickel oxide surface and a $[Ru(dceb)_2(Hbpt)Re(CO)_3Cl]^{2+}$ complex immobilised nickel oxide surface.



Scheme 3.2: Compound immobilisation procedure on the nickel oxide surface.

Step-1: The nickel oxide surface was activated using a aqueous solution of NaOH. The nickel oxide coated sample was placed into a concentrated NaOH solution for 6 hours.

Step-2: The activated nickel oxide surface was then removed from the concentrated NaOH-solution and was kept at 70 °C for 3 hours to dry.

Step-3: The dried activated nickel oxide surface was then placed into a concentrated solution of the complex in acetone for 12 hours.

Step-4: The compound immobilised on the nickel oxide surface was removed from the solution and air dried for 1 min.

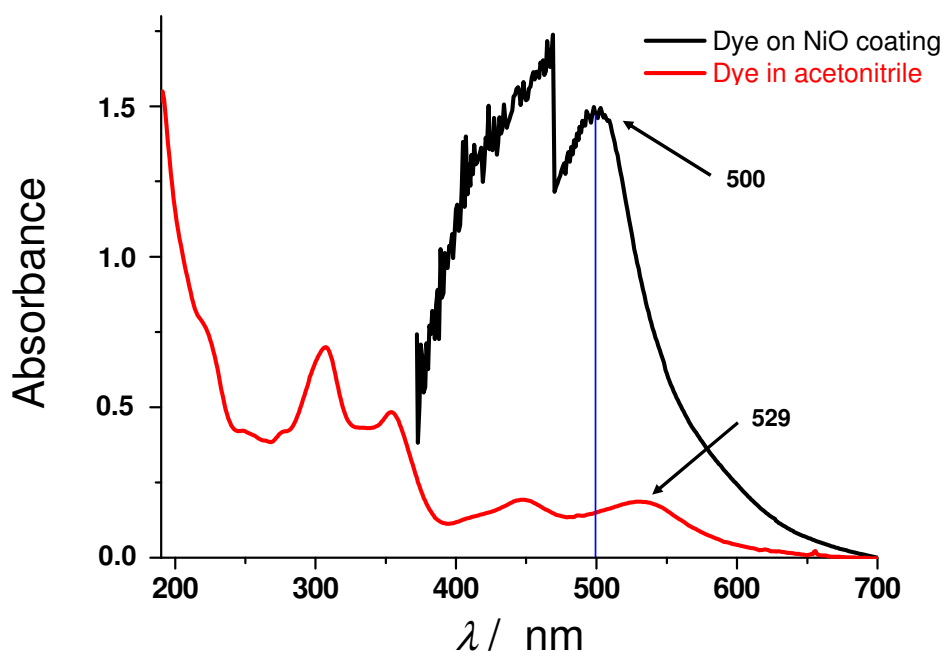


Figure 3.41: (Red) UV-Vis spectrum of $[Ru(dceb)_2(2,5-dpp)Re(CO)_3Cl]^{2+}$ in acetonitrile at room temperature and (black) UV-Vis spectrum of nickel oxide bound $[Ru(dceb)_2(2,5-dpp)Re(CO)_3Cl]^{2+}$

A comparison of the UV-Vis spectra of $[Ru(dceb)_2(2,5-dpp)Re(CO)_3Cl]^{2+}$ in solution (in ACN) and on the surface of nickel oxide surface is shown in **Figure 3.41**. The visible band at 500 nm for the nickel oxide bound Ru-Re sample is tentatively assigned to the ruthenium metal to 2,5-dpp ligand transition.

3.8. Conclusion

A synthetic modification was carried out to obtain a better yield of 4,4'-bis(diethylphosphonato)-2,2'-bipyridine. Washing with pentane, the crude product in step "v" (**Scheme 3.1**) simplified the work up procedure compared to the literature procedure which involved column chromatography for the purification. The synthetic conditions for Ru(II)-Re(I) heterodinuclear complexes were altered considering the ethyl carboxy ester groups. Ethanol was used as solvent to prevent the possible exchange of ethyl ester groups with another group. Time dependent study suggested

that refluxing the reaction mixture for longer than 6 hours could lead to a lower yield because of the decomposition of rhenium compounds. The careful observation of the reaction conditions yielded improved methods for synthesising Ru(II)-Re(I) heterodinuclear complexes containing carboxy ester groups.

Infrared spectroscopy data suggested only the formation of *fac*- isomers in the Ru(II)-Re(I) heterodinuclear complexes. The lower region overlapped IR bands (broad) were not properly understood and may be due to the presence of possible different geometrical isomers based on the ruthenium moiety. The presence of different isomers in the heterodinuclear complexes was evident in the ^1H NMR for some of the heterodinuclear complexes.

Absorption spectra of $[\text{Ru}(\text{L}_1)_2(2,5\text{-dpp})\text{Re}(\text{CO})_3\text{Cl}]^{2+}$ complexes showed a red shift of the $d\pi(\text{Ru}) - \pi^*(2,5\text{-dpp})$ transition compared to the homologous ruthenium mononuclear complex. This phenomenon clearly suggested lowering of the π^* energy level of 2,5-dpp with the introduction of a rhenium metal centre. The ligand centred transition ($\pi-\pi^*$) for 2,5-dpp was also red shifted in the absorption spectra from 317 nm to 361 nm. Ru-(2,5-dpp)-Re heterodinuclear complexes have negligible emission compared to the homologous Ru-(2,5-dpp) mononuclear complex. This result suggested quenching of the emission due to the introduction of the $\text{Re}(\text{CO})_3\text{Cl}$ moiety. On the other hand, the maximum MLCT transition wavelengths for Ru-(bisbpy)-Re type heterodinuclear complexes remained identical compared to homologous Ru-(bisbpy) mononuclear complex, which indicates there is less or no interaction between two metal centres. It was also observed that there is no difference in the emission wavelengths (room temperature) between Ru-(bisbpy)-Re heterodinuclear and homologous Ru-(bisbpy) mononuclear complexes. Highest MLCT transition wavelengths were red shifted for Ru-(Hbpt)-Re heterodinuclear complex (494 nm) compared to Ru-(Hbpt) mononuclear complex (463 nm).

A nickel oxide surface was activated with NaOH solution to bind ester containing Ru-Re heterodinuclear complexes and rhenium carbonyl complexes. Treating the activated nickel oxide surface with the concentrated solution of metal complexes resulted in a coloured semiconductor (nickel oxide). The absorption band around 500 nm for the coloured surface partially supports the surface mobilisation.

However, the immobilisation study needs further data to fully characterise the metal complex immobilised surface.

3.9. Experimental

3.9.1. Material and instrumental

All the solvents used for spectroscopy were of spectroscopic grade. 4,4'-dicarboxy theyl-2,2'-bipyridine (dceb), ruthenium mononuclear complexes used were synthesised in previous chapter 2. $\text{Re}(\text{CO})_5\text{Cl}$, NaBH_4 , HBr , $\text{P}(\text{OEt})_3$, spectroscopic grade ethanol, CHCl_3 and spectroscopic grade toluene used for the reactions below were obtained from Sigma-Aldrich and used without further purification. All other solvents and reagents used were reagent grade. Schlenk technique was exerted for the synthesis of Ru(II)-Re(I) hetero-bimetallic complexes. ^1H NMR (400 MHz) was recorded in deuteriated solvents (d_6 -DMSO, d_3 -acetonitrile, CDCl_3) on a Bruker AC400 NMR and AC600 NMR Spectrometer with TMS or residual solvent peaks as reference. XWIN-NMR processor and ACDLABS 12.0 NMR processor software were employed to process the free induction decay (FID) profiles. The H-H 2-D COSY NMR involved the accumulation of 128 FIDs of 16 scans. Elemental analyses (CHN) were carried out using Exador Analytical CE440 by the Microanalytical Department, University College Dublin, Ireland. Infrared spectra of metal carbonyl complexes were recorded on a Perkin Elmer 2000 FTIR spectrometer in 0.1 mm sodium chloride liquid solution cells. The solvent used for solution based IR spectroscopy was spectroscopic grade THF. Fourier transform infrared (FT-IR) spectra were obtained on Perkin Elmer Spectrum 100 FT-ATR. UV-Vis absorption spectra were recorded on a Shimadzu 3100 UV-Vis/NIR spectrophotometer with interfaced to an Elonex PC575 desktop computer using 1-cm path length quartz cells. The detection wavelength was 190-900 nm. The ASCII data for every UV-Vis spectra were further processed using Microcal Origin 8 pro software. Emission spectra were recorded on a Perkin-Elmer LS0B luminescence spectrophotometer. The solvent used for the room temperature emission spectroscopy was spectroscopic grade acetonitrile. All the spectra were initially generated by Perkin-Elmer FL Winlab custom built software and further the ASCII data were processed by Microcal Origin 8 pro

software. The optical densities of all the sample solution were 0.15 A.U. at the excitation wavelength.

3.9.2. Organic ligands

*4,4'-Bis(hydroxymethyl)-2,2'-bipyridine*⁵⁷

1 g of sodium borohydride was added in one portion to a suspension of 300 mg (1 mmol) 4,4'-diethylcarboxy-2,2'-bipyridine in 50 cm³ of ethanol. The mixture was heated at reflux for 3 hours and cooled to room temperature and then 40 cm³ of ammonium chloride saturated water solution was added. The ethanol was removed by rotary evaporation and the white solid obtained was dissolved in water. The resulting solution was extracted with ethyl acetate (5 × 50 cm³) and dried over magnesium sulphate. After washing, the solvent was removed by rotary evaporation. The desired product was used without further purification. Yield: 80% (172 mg, 0.8 mmol). ¹H NMR (400 MHz, DMSO-*d*₆) δ ppm 4.70 (s, 4 H), 7.43 (dd, *J* = 5.05, 1.52 Hz, 2 H), 8.45 (s, 2 H), 8.66 (d, *J* = 4.80 Hz, 2 H)

*4,4'-Bis(bromomethyl)-2,2'-bipyridine*⁵⁷

The 4,4'-Bis(hydroxymethyl)-2,2'-bipyridine (0.90 g, 0.42 mmol) was dissolved in a mixture of 48% HBr (5 cm³) and concentrated sulphuric acid (2 cm³). The resulting solution was refluxed for 6 hours and then cooled to room temperature. 10 cm³ of water was added to it. The pH was adjusted 7-8 with NaOH solution and the resulting precipitate was filtered, washed with water and air-dried. The product was dissolved in chloroform (10 cm³) and filtered. The solution was dried over magnesium sulfate and evaporated to dryness. The product was used without further purification. Yield: 85% (1.2 g, 0.35 mmol). ¹H NMR (400 MHz, CDCl₃) δ ppm 4.43 (s, 4 H), 7.33 (dd, *J* = 5.05, 1.77 Hz, 2 H), 8.42 (s, 2 H), 8.62 (d, *J* = 5.05 Hz, 2 H)

4,4'-Bis(diethylmethylphosphonato)-2,2'-bipyridine (dpb)

1.7 g (4.97 mmol) of 4,4'-dimethylbromo-2,2'-bipyridine in 11.3 cm³ chloroform was refluxed with 24.17 cm³ of triethylphosphite under a nitrogen atmosphere for 3 hours. Excess triethylphosphite and chloroform were removed under high vacuum. After the removal of solvent and excess triethylphosphite, an oily crude product was obtained

which was further washed with pentane and collected as a solid. Yield: 92% (2.08 g, 4.57 mmol). ^1H NMR (400 MHz, CDCl_3) δ ppm 1.21 (m, 12 H), 3.20 (d, 20 Hz, 4H), 3.96 - 4.06 (m, 8 H), 7.29 (d, $J = 5.05$, 2 H), 8.31 (s, 2 H), 8.55 (d, $J = 5.05$ Hz, 2 H). ^{31}P NMR (400 MHz, CDCl_3) δ ppm 34.17 ppm.

3.9.3. Metal complexes

$[\text{Re}(\text{dceb})(\text{CO})_3\text{Cl}]$

400 mg (1.10 mmol) of $\text{Re}(\text{CO})_5\text{Cl}$ and 331.75g (1.10 mmol) of dceb were added together in 50 cm^3 toluene which was purged with nitrogen for 20 minutes. Schlenk technique was employed in the synthesis. The reaction mixture was then refluxed for 2.5 hours under nitrogen atmosphere. The reaction mixture was cooled to room temperature and was kept at 0-4 $^\circ\text{C}$ for 12 hours. The orange yellow precipitate was collected by filtration followed by washing with toluene, pentane and diethyl ether. Yield: 82% (546.6 mg, 0.90 mmol). ^1H NMR (400 MHz, Acetone) δ ppm 1.46 (m, 6 H), 4.53 (m, 4 H), 8.27 (d, 2 H), 9.22 (s, 2 H), 9.35 (d 2 H). ν_{CO} (cm^{-1}) in THF: 2019, 1916, 1892 cm^{-1} . Elemental analysis for $\text{C}_{19}\text{H}_{16}\text{ClN}_2\text{O}_7\text{Re} \cdot 1.5\text{H}_2\text{O}$. M.W. = 633.02; Calc. C 36.05, H 3.03, N 4.43, Found. C 35.74, H 2.34 and N 4.04%.

$[\text{Re}(\text{dpb})(\text{CO})_3\text{Cl}]$

$[\text{Re}(\text{dpb})(\text{CO})_3\text{Cl}]$ was synthesised following the same reaction procedure of $[\text{Re}(\text{dceb})(\text{CO})_3\text{Cl}]$. 80.86 mg (0.22 mmol) of $\text{Re}(\text{CO})_5\text{Cl}$ and 102 mg (0.22 mmol) of dpb were reacted 50 cm^3 . Yield: 80% (134 mg, 0.17 mmol). ^1H NMR (400 MHz, Acetone- d_6) δ ppm 1.27 (m, 12 H), 3.55 - 3.61 (d, $J = 20$ Hz, 2 H), 4.05 - 4.17 (m, 8 H), 7.76 (d, $J = 5.81$ Hz, 2 H), 8.62 (s, 2 H), 9.03 (d, $J = 5.81$ Hz, 2 H). ν_{CO} (cm^{-1}) in THF: 2022, 1922, 1899 cm^{-1} . Elemental analysis for $\text{C}_{23}\text{H}_{30}\text{ClN}_2\text{O}_9\text{PRe}$. M.W. = 761.1 ; Calc. C 36.25, H 3.97, N 3.68, Found. C 36.40, H 3.86 and N 3.46%.

$[\text{Ru}(\text{dceb})_2(\mu\text{-bisbpy})\text{Re}(\text{CO})_3\text{Cl}](\text{PF}_6)_2$

30 cm^3 of spectroscopic grade ethanol was purged with nitrogen for 30 minutes. 50 mg (0.042 mmol) of $[\text{Ru}(\text{dceb})_2(\text{bisbpy})](\text{PF}_6)_2$ and 23.16 mg (.064 mmol) of $\text{Re}(\text{CO})_5\text{Cl}$ were added into the purged ethanol. The solution was subjected to vacuum prior to reflux. The reaction mixture was then refluxed in the dark for a further 6

hours under a nitrogen atmosphere. The reaction was monitored by TLC and IR. All the solvent was removed immediately by rotary evaporator after 6 hours of reaction. The crude product was washed with n-pentane and diethyl ether. The product was further purified by careful recrystallisation from acetone/toluene solution. Yield: 87% (57 mg, 0.0357 mmol). ^1H NMR (400 MHz, DMSO- d_6) δ ppm 1.32 - 1.39 (m, 12 H), 4.41 - 4.48 (m, 8 H), 7.51 - 7.61 (m, 1 H), 7.75 - 8.05 (m, 10 H), 8.07 - 8.20 (m, 1 H), 8.23 - 8.31 (m, 1 H), 8.36 (t, $J = 8.34$ Hz, 1 H), 8.62 - 8.70 (m, 1 H), 8.73 - 8.90 (m, 4 H), 8.98 - 9.05 (m, 2 H), 9.08 (dd, $J = 8.59, 3.03$ Hz, 1 H), 9.19 (d, $J = 16.93$ Hz, 1 H), 9.25 (d, $J = 8.08$ Hz, 1 H), 9.32 (d, $J = 8.34$ Hz, 2 H). ν_{CO} (cm^{-1}) in THF: 2022, 1918 (broad peak).

[Ru(bpy) $_2$ (μ -bisbpy)Re(CO) $_3$ Cl](PF $_6$) $_2$

50 mg (0.049 mmol) of [Ru(bpy) $_2$ (bisbpy)](PF $_6$) $_2$ and 26.58 mg (0.074 mmol) of Re(CO) $_5$ Cl were reacted in 30 cm^3 ethanol. Reaction condition and purification process were followed as for the synthesis of [Ru(dceb) $_2$ (μ -bisbpy)Re(CO) $_3$ Cl](PF $_6$) $_2$. No colour change was observed. Yield: 68 mg (0.042 mmol) (86%). ^1H NMR (400 MHz, DMSO- d_6) δ ppm 7.47 - 7.61 (m, 5 H), 7.65 - 7.69 (m, 1 H), 7.73 - 7.82 (m, 4 H), 7.85 (d, $J = 4.80$ Hz, 1 H), 7.92 - 7.99 (m, 2 H), 8.10 - 8.27 (m, 5 H), 8.34 - 8.40 (m, 1 H), 8.53 (dd, $J = 8.59, 2.02$ Hz, 1 H), 8.59 (dd, $J = 8.59, 2.02$ Hz, 1 H), 8.74 - 8.94 (m, 8 H), 8.98 (d, $J = 8.08$ Hz, 1 H), 9.01 - 9.07 (m, 2 H). ν_{CO} (cm^{-1}) in THF: 2020, 1914, 1894. Elemental analysis for C $_{43}$ H $_{30}$ ClF $_{12}$ N $_8$ O $_3$ P $_2$ ReRu. 4H $_2$ O. 0.2(toluene) M.W. = 1409.9; Calc. C 37.82, H 2.83, N 7.94, Found. C 37.48, H 2.44 and N 7.45%.

[Ru(dceb) $_2$ (μ -Hbpt)Re(CO) $_3$ (Cl)](PF $_6$) $_2$

300 mg (0.25 mmol) of [Ru(bpy) $_2$ (Hbpt)](PF $_6$) $_2$ and 134 mg (0.37 mmol) of Re(CO) $_5$ Cl were reacted in 30 cm^3 ethanol. Reaction condition and purification process were followed as for the synthesis of [Ru(dceb) $_2$ (μ -bisbpy)Re(CO) $_3$ Cl](PF $_6$) $_2$. No colour change was observed. Yield: 316 mg (0.23 mmol) (92%). ^1H NMR (400 MHz, DMSO- d_6) δ ppm 1.32 - 1.40 (m, 12 H), 4.40 - 4.49 (m, 8 H), 7.37 - 7.46 (m, 1 H), 7.48 - 7.68 (m, 2 H), 7.77 - 7.91 (m, 2 H), 7.92 - 8.22 (m, 10 H), 8.36 (d, $J = 7.83$ Hz, 1 H), 8.63-8.72 (m, 1 H), 9.21 - 9.34 (m, 4 H). ν_{CO} (cm^{-1}) in THF: 2019, 1911,

1890. Elemental analysis for $C_{47}H_{41}ClF_{12}N_9O_{11}P_2ReRu$. M.W. = 1520.53; Calc. C 37.13, H 2.72, N 8.29, Found. C 37.99, H 2.47 and N 8.05%.

[Ru(bpy)₂(μ-2,5-dpp)Re(CO)₃Cl](PF₆)₂

50 mg (0.054 mmol) of [Ru(bpy)₂(2,5-dpp)](PF₆)₂ and 29.29 mg (0.081 mmol) of Re(CO)₅Cl were reacted in 30 cm³ ethanol. Reaction condition and purification process were followed as for the synthesis of [Ru(dceb)₂(μ-bisbpy)Re(CO)₃Cl](PF₆)₂. The colour change of the reaction mixture was observed from yellowish-brown to purple. Yield: 87% (58.4 mg, 0.046 mmol). ¹H NMR (400 MHz, DMSO-*d*₆) δ ppm 7.44 - 7.63 (m, 6 H), 7.63 - 7.88 (m, 5 H), 8.12 - 8.38 (m, 7 H), 8.75 - 8.94 (m, 5 H), 9.05 - 9.15 (m, 1 H), 9.21 - 9.37 (m, 1 H), 10.00 (m, 1 H). ν_{CO} (cm⁻¹) in THF: 2022, 1914(broad peak). Elemental analysis for $C_{37}H_{26}ClF_{12}N_8O_3P_2ReRu \cdot 5H_2O \cdot 0.9(toluene)$. M.W. = 1416; Calc. C 36.72, H 3.07, N 7.91, Found. C 36.24, H 2.24 and N 7.43%.

[Ru(d₈-bpy)₂(μ-2,5-dpp)Re(CO)₃Cl](PF₆)₂

50 mg (0.052 mmol) of [Ru(d₈-bpy)₂(2,5-dpp)](PF₆)₂ and 29.29 mg (0.081 mmol) of Re(CO)₅Cl were reacted in 30 cm³ ethanol. Reaction condition and purification process were followed as for the synthesis of [Ru(dceb)₂(μ-bisbpy)Re(CO)₃Cl](PF₆)₂. The colour change of the reaction mixture was observed from yellowish-brown to purple. Yield: 91% (59.6 mg, 0.047 mmol). ¹H NMR (400 MHz, DMSO-*d*₆) δ ppm 7.62 - 7.71 (m, 1 H), 7.75 - 7.86 (m, 2 H), 7.92-8.04 (m, 1 H), 8.25 - 8.34 (m, 2 H), 8.78 (s, 1 H), 8.90 (s, 1 H), 9.10 (t, *J* = 5.68 Hz, 1 H), 9.21 - 9.36 (m, 1 H), 9.99 (d, *J* = 8.08 Hz, 1 H). ν_{CO} (cm⁻¹) in THF: 2022, 1912 (Broad)

[Ru(dceb)₂(μ-2,5-dpp)Re(CO)₃Cl](PF₆)₂

50 mg (0.041 mmol) of [Ru(dceb)₂(2,5-dpp)](PF₆)₂ and 22.24 mg (0.061 mmol) of Re(CO)₅Cl were reacted in 30 cm³ ethanol. The colour change of the reaction mixture was observed from red to reddish purple. Yield: 61 mg (0.40 mmol) (97%). ¹H NMR (400 MHz, DMSO-*d*₆) δ ppm 1.32 - 1.40 (m, 12 H), 4.36 - 4.54 (m, 8 H), 7.57 - 7.73 (m, 1 H), 7.79 - 8.02 (m, 9 H), 8.04 - 8.10 (m, 1 H), 8.25 - 8.45 (m, 3 H), 8.75-8.90

(m, 1H), 9.11 (m, 1 H), 9.29 - 9.40 (m, 5 H), 10.06 (d, $J = 5.30$ Hz, 1 H). ν_{CO} (cm^{-1}) in THF: 2022, 1930, 1910.

3.10. References

- (1) Talebinasab-Sarvari, M.; Ford, P. C. *Inorg. Chem.* **1980**, *19*, 2640-2646.
- (2) Browne, W. R.; O'Boyle, N. M.; McGarvey, J. J.; Vos, J. G. *Chem. Soc. Rev.* **2005**, *34*, 641-663.
- (3) Ye, S.; Kaim, W.; Albrecht, M.; Lissner, F.; Schleid, T. *Inorg. Chim. Acta* **2004**, *357*, 3325-3330.
- (4) Arias, M.; Concepción, J.; Crivelli, I.; Delgadillo, A.; Díaz, R.; Francois, A.; Gajardo, F.; López, R.; Leiva, A. M.; Loeb, B. *Chem. Phys.* **2006**, *326*, 54-70.
- (5) Vlcek Jr, A.; Zális, S. *Coord. Chem. Rev.* **2007**, *251*, 258-287.
- (6) Wenger, O. S. *Coord. Chem. Rev.* **2009**, *253*, 1439-1457.
- (7) Doherty, M. D.; Grills, D. C.; Muckerman, J. T.; Polyansky, D. E.; Fujita, E. *Coord. Chem. Rev.* **2009**, *254*, 2472-2482.
- (8) Inagaki, A.; Akita, M. *Coord. Chem. Rev.* **2009**, *254*, 1220-1239.
- (9) Morris, A. J.; Meyer, G. J.; Fujita, E. *Acc. Chem. Res.* **1982**, *42*, 1983-1994.
- (10) Morris, A. J.; Meyer, G. J.; Fujita, E. *Acc. Chem. Res.* **2009**, *42*, 1983-1994.
- (11) Ding, J.; Feng, K.; Tung, C.-H.; Wu, L.-Z. *J. Phys. Chem. C* **1982**, *115*, 833-839.
- (12) Yamazaki, H.; Shouji, A.; Kajita, M.; Yagi, M. *Coord. Chem. Rev.* **2010**, *254*, 2483-2491.
- (13) McConnell, I.; Li, G.; Brudvig, G. W. *Chem. Biol.* **2010**, *17*, 434-447.
- (14) Hammes-Schiffer, S. *Acc. Chem. Res.* **1982**, *42*, 1881-1889.
- (15) Worthy, W. *Chemical & Engineering News* **1989**, *67*, 37.
- (16) Bard, A. J.; Fox, M. A. *Acc. Chem. Res.* **1995**, *28*, 141-145.
- (17) Falkenström, M.; Johansson, O.; Hammarström, L. *Inorg. Chim. Acta* **2007**, *360*, 741-750.
- (18) Borg, O. A.; Godinho, S. S. M. C.; Lundqvist, M. J.; Lunell, S.; Persson, P. J. *Phys. Chem. A* **2008**, *112*, 4470-4476.

- (19) Abrahamsson, M.; Jaiger, M.; Kumar, R. J.; Ol'sterman, T.; Persson, P.; Becker, H.-C.; Johansson, O.; Hammarström, L. *J. Am. Chem. Soc.* **2008**, *130*, 15533-15542.
- (20) Lagref, J. J.; Nazeeruddin, M. K.; Grätzel, M. *Inorg. Chim. Acta* **2008**, *361*, 735-745.
- (21) Hammes-Schiffer, S. *Acc. Chem. Res.* **2009**, *42*, 1881-1889.
- (22) Dempsey, J. L.; Brunschwig, B. S.; Winkler, J. R.; Gray, H. B. *Acc. Chem. Res.* **2009**, *42*, 1995-2004.
- (23) Gholamkhass, B.; Mametsuka, H.; Koike, K.; Tanabe, T.; Furue, M.; Ishitani, O. *Inorg. Chem.* **2005**, *44*, 2326-2336.
- (24) Coe, B. J.; Curati, N. R. M.; Fitzgerald, E. C.; Coles, S. J.; Horton, P. N.; Light, M. E.; Hursthouse, M. B. *Organometallics* **2007**, *26*, 2318-2329.
- (25) Ooyama, D.; Kobayashi, T.; Shiren, K.; Tanaka, K. *J. Organomet. Chem.* **2003**, *665*, 107-113.
- (26) Grodkowski, J.; Neta, P. *J. Phys. Chem. A* **1992**, *104*, 1848-1853.
- (27) Stufkens, D. J.; Vlcek, A. *Coord. Chem. Rev.* **1998**, *177*, 127-179.
- (28) Riklin, M.; Tran, D.; Bu, X.; Laverman, L. E.; Ford, P. C. *J. Chem. Soc., Dalton Trans.* **2001**, 1813-1819.
- (29) Possamai, G.; Menna, E.; Maggini, M.; Carano, M.; Marcaccio, M.; Paolucci, F.; Guldi, D. M.; Swartz, A. *Photochem. Photobiol. Sci.* **2006**, *5*, 1154-1164.
- (30) Lazarides, T.; Barbieri, A.; Sabatini, C.; Barigelletti, F.; Adams, H.; Ward, M. D. *Inorg. Chim. Acta* **2007**, *360*, 814-824.
- (31) Coleman, A.; Brennan, C.; Vos, J. G.; Pryce, M. T. *Coord. Chem. Rev.* **2008**, *252*, 2585-2595.
- (32) Velayudham, M.; Rajagopal, S. *Inorg. Chim. Acta* **2009**, *362*, 5073-5079.
- (33) Velayudham, M.; Singaravadivel, S.; Rajagopal, S.; Ramamurthy, P. *J. Organomet. Chem.* **2009**, *694*, 4076-4083.
- (34) Vogler, A.; Kisslinger, J. *Inorg. Chim. Acta* **1986**, *115*, 193-196.
- (35) Sahai, R.; Rillema, D. P.; Shaver, R.; Van Wallendael, S.; Jackman, D. C.; Boldaji, M. *Inorg. Chem.* **1989**, *28*, 1022-1028.
- (36) Kalyanasundaram, K.; Nazeeruddin, M. K. *J. Chem. Soc., Dalton Trans.* **1990**, 1657-1662.
- (37) Kalyanasundaram, K.; Graetzel, M.; Nazeeruddin, M. K. *Inorg. Chem.* **1992**, *31*, 5243-5253.

- (38) Bardwell, D. A.; Barigelletti, F.; Cleary, R. L.; Flamigni, L.; Guardigli, M.; Jeffery, J. C.; Ward, M. D. *Inorg. Chem.* **1995**, *34*, 2438-2446.
- (39) Fraser, M. G.; Clark, C. A.; Horvath, R.; Lind, S. J.; Blackman, A. G.; Sun, X.-Z.; George, M. W.; Gordon, K. C. *Inorg. Chem.* **2011**, *50*, 6093-6106.
- (40) Encinas, S.; Barthram, A. M.; Ward, M. D.; Barigelletti, F.; Campagna, S. *Chem. Commun.* **2001**, 277-278.
- (41) Yamamoto, Y.; Tamaki, Y.; Yui, T.; Koike, K.; Ishitani, O. *J. Am. Chem. Soc.* **2010**, *132*, 11743-11752.
- (42) Takeda, H.; Ishitani, O. *Coord. Chem. Rev.* **2009**, *254*, 346-354.
- (43) Takeda, H.; Ohashi, M.; Tani, T.; Ishitani, O.; Inagaki, S. *Inorg. Chem.* **2010**, *49*, 4554-4559.
- (44) Ishitani, O.; George, M. W.; Ibusuki, T.; Johnson, F. P. A.; Koike, K.; Nozaki, K.; Pac, C.; Turner, J. J.; Westwell, J. R. *Inorg. Chem.* **1994**, *33*, 4712-4717.
- (45) Konno, H.; Kobayashi, A.; Sakamoto, K.; Fagalde, F.; Katz, N. E.; Saitoh, H.; Ishitani, O. *Inorg. Chim. Acta* **2000**, *299*, 155-163.
- (46) Ishitani, O.; Kanai, K.; Yamada, Y.; Sakamoto, K. *Chem. Commun.* **2001**, 1514-1515.
- (47) Konno, H.; Ishii, Y.; Sakamoto, K.; Ishitani, O. *Polyhedron* **2002**, *21*, 61-68.
- (48) Kobayashi, A.; Sakamoto, K.; Ishitani, O. *Inorg. Chem. Commun.* **2005**, *8*, 365-367.
- (49) Sato, S.; Morimoto, T.; Ishitani, O. *Inorg. Chem.* **2007**, *46*, 9051-9053.
- (50) Bian, Z.-Y.; Sumi, K.; Furue, M.; Sato, S.; Koike, K.; Ishitani, O. *Inorg. Chem.* **2008**, *47*, 10801-10803.
- (51) Yamamoto, Y.; Sawa, S.; Funada, Y.; Morimoto, T.; Falkenstroß, M.; Miyasaka, H.; Shishido, S.; Ozeki, T.; Koike, K.; Ishitani, O. *J. Am. Chem. Soc.* **2008**, *130*, 14659-14674.
- (52) Ettedgui, J.; Diskin-Posner, Y.; Weiner, L.; Neumann, R. *J. Am. Chem. Soc.* **1992**, *113*, 188-190.
- (53) Takeda, H.; Koike, K.; Inoue, H.; Ishitani, O. *J. Am. Chem. Soc.* **2008**, *130*, 2023-2031.
- (54) Bian, Z.-Y.; Sumi, K.; Furue, M.; Sato, S.; Koike, K.; Ishitani, O. *Dalton Trans.* **2009**, 983-993.

- (55) Trammell, S. A.; Moss, J. A.; Yang, J. C.; Nakhle, B. M.; Slate, C. A.; Odobel, F.; Sykora, M.; Erickson, B. W.; Meyer, T. J. *Inorg. Chem.* **1999**, *38*, 3665-3669.
- (56) Gallagher, L. A.; Serron, S. A.; Wen, X.; Hornstein, B. J.; Dattelbaum, D. M.; Schoonover, J. R.; Meyer, T. J. *Inorg. Chem.* **2005**, *44*, 2089-2097.
- (57) Gillaizeau-Gauthier, I.; Odobel, F.; Alebbi, M.; Argazzi, R.; Costa, E.; Bignozzi, C. A.; Qu, P.; Meyer, G. J. *Inorg. Chem.* **2001**, *40*, 6073-6079.
- (58) Van Wallendael, S.; Shaver, R. J.; Rillema, D. P.; Yoblinski, B. J.; Stathis, M.; Guarr, T. F. *Inorg. Chem.* **1990**, *29*, 1761-1767.
- (59) Polo, A. S.; Itokazu, M. K.; Frin, K. M.; de Toledo Patrocínio, A. O.; Murakami Iha, N. Y. *Coord. Chem. Rev.* **2006**, *250*, 1669-1680.
- (60) Houk, L. W.; Dobson, G. R. *Inorg. Chem.* **1966**, *5*, 2119-2123.
- (61) Gamelin, D. R.; George, M. W.; Glyn, P.; Grevels, F.-W.; Johnson, F. P. A.; Klotzbuecher, W.; Morrison, S. L.; Russell, G.; Schaffner, K.; Turner, J. J. *Inorg. Chem.* **1994**, *33*, 3246-3250.
- (62) Moldes, I.; Mathieu, R. *J. Organomet. Chem.* **1994**, *480*, 185-189.
- (63) Stor, G. J.; Morrison, S. L.; Stufkens, D. J.; Oskam, A. *Organometallics* **1994**, *13*, 2641-2650.
- (64) Yoblinski, B. J.; Stathis, M.; Guarr, T. F. *Inorg. Chem.* **1992**, *31*, 5-10.
- (65) Constable, E. C.; Seddon, K. R. *J. Chem. Soc., Chem. Commun.* **1982**, 34-36.
- (66) Llobet, A.; Doppelt, P.; Meyer, T. J. *Inorg. Chem.* **1988**, *27*, 514-520.
- (67) Patrocínio, A. O. v. T.; Murakami Iha, N. Y. *Inorg. Chem.* **1982**, *47*, 10851-10857.
- (68) Van Wallendael, S.; Perkovic, M. W.; Paul Rillema, D. *Inorg. Chim. Acta* **1993**, *213*, 253-260.
- (69) Ioachim, E.; Medlycott, E. A.; Hanan, G. S. *Inorg. Chim. Acta* **2006**, *359*, 2599-2607.
- (70) Hou, Y.-J.; Xie, P.-H.; Zhang, B.-W.; Cao, Y.; Xiao, X.-R.; Wang, W.-B. *Inorg. Chem.* **1999**, *38*, 6320-6322.
- (71) Wrighton, M. S.; Morse, D. L. *J. Am. Chem. Soc.* **1974**, *96*, 998-1004.
- (72) Worl, L. A.; Duesing, R.; Chen, P.; Ciana, L. D.; Meyer, T. J. *J. Chem. Soc., Dalton Trans.* **1991**, 849-854.
- (73) Hawecker, J.; Lehn, J.-M.; Ziessel, R. *J. Chem. Soc., Chem. Commun.* **1983**, 536-538.

- (74) Hayashi, Y.; Kita, S.; Brunschwig, B. S.; Fujita, E. *J. Am. Chem. Soc.* **2003**, *125*, 11976-11982.
- (75) Chan, W. K.; Hui, C. S.; Man, K. Y. K.; Cheng, K. W.; Wong, H. L.; Zhu, N.; Djurisic, A. B. *Coord. Chem. Rev.* **2005**, *249*, 1351-1359.
- (76) Lam, L. S. M.; Chan, W. K.; Djurisic, A. B.; Herbert Li, E. *Chem. Phys. Lett.* **2002**, *362*, 130-134.
- (77) Ziessel, R.; Juris, A.; Venturi, M. *Inorg. Chem.* **1998**, *37*, 5061-5069.
- (78) Ziessel, R.; Juris, A.; Venturi, M. *Chem. Commun.* **1997**, 1593-1594.
- (79) Simpson, T. J.; Gordon, K. C. *Inorg. Chem.* **1995**, *34*, 6323-6329.
- (80) R. Waterland, M.; J. Simpson, T.; C. Gordon, K.; K. Burrell, A. *J. Chem. Soc., Dalton Trans.* **1998**, 185-192.
- (81) Monserrat, K.; Foreman, T. K.; Graetzel, M.; Whitten, D. G. *J. Am. Chem. Soc.* **1981**, *103*, 6667-6672.
- (82) Rillema, D. P.; Sahai, R.; Matthews, P.; Edwards, A. K.; Shaver, R. J.; Morgan, L. *Inorg. Chem.* **1990**, *29*, 167-175.

Chapter 4

Synthesis and characterisation of iridium(III) mononuclear complexes

Chapter 4 introduces a series of monomeric cyclometallated iridium(III) complexes. These monomeric Ir(III) complexes contain carboxy ester functionalised cyclometallated phenylpyridine ligands and different bpy based ancillary ligands. Synthetic modifications are discussed in detail. These iridium complexes were characterised using ^1H , 2D COSY NMR spectroscopy and CHN analysis. Photophysical data for these Ir(III) complexes are also reported.

4.1. Introduction

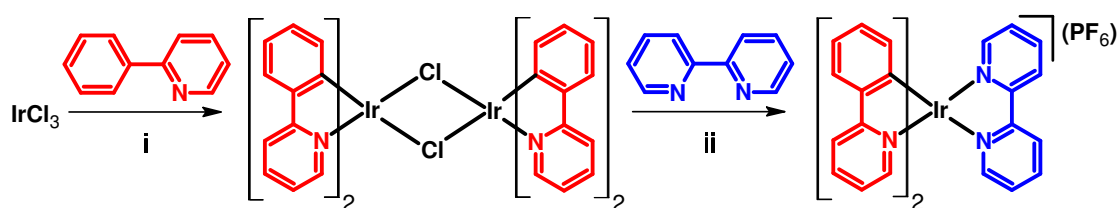
Conversion of solar radiation to suitable chemical energy remains a challenge and is a major concern with looming energy requirements.¹⁻⁵ In the race to find smart and renewable energy resources, DSSC solar cells have been developed.⁶⁻¹¹ However, these DSSC solar cells are not economically cost effective at present. Therefore, a substantial amount of research is currently focused on finding alternative catalytic systems which will be useful for the reduction of water to hydrogen and oxygen. Hydrogen is considered as one of the cleanest fuels at the moment and the conversion of solar energy into chemical fuels shows promise. At this stage, hydrogen production from water needs a breakthrough which will allow people to use hydrogen as a fuel in an environmentally friendly way.

Catalytic systems for hydrogen production from water need electron transfer from a light harvester (typically transition metal complexes) to a catalytic centre with the help of a sacrificial electron donor, which will further reduce the protons to molecular hydrogen.¹²⁻¹⁷ The development of catalytic systems has become an important concern in the production of hydrogen from water using visible light. The majority of the reported water reduction systems have used $[\text{Ru}(\text{bpy})_3]^{2+}$ as an active photosensitiser.¹⁸⁻²⁰ Recently, monomeric iridium complexes came under investigation when $[\text{Ir}(\text{ppy})_2(\text{bpy})]^+$ and analogous iridium complexes demonstrated improved catalytic efficiency over ruthenium complexes in solar driven hydrogen production.²¹⁻²⁷ Variation of the ligand architecture in such iridium complexes allows tuning of the energy gap between the highest occupied molecular orbital (HOMO) and the lowest unoccupied molecular orbital (LUMO), and therefore access to a library of iridium complexes with tuned photophysical and electrochemical properties. This diverse range of monomeric iridium complexes can be investigated as potential catalysts for the production of hydrogen.

Monomeric iridium complexes, not only are used as photosensitisers in hydrogen production from water but also have applications in other areas such as in solid phase synthesis,²⁸ oxygen production,²⁹⁻³³ drug discovery,^{34,35} material synthesis³⁶⁻³⁸ and more recently in organic light emitting devices (OLED).³⁹⁻⁴⁵ Their photophysical properties make iridium complexes diverse as luminophoric

materials.⁴⁶⁻⁵⁰ Transition metal complexes of ruthenium^{51,52} and osmium⁵³ and subsequently iridium metal complexes were explored in the field of OLEDs because these complexes are triplet state emitters.⁵⁴ An [Alq₃] chromophore (q denotes 8-hydroxyquinoline) (550 nm green light emission from a singlet excited state) was first introduced as an OLED by Tang and VanSlyke in 1987.⁵⁵ Bernhard and his group reported tuneable luminophoric cationic iridium complexes containing cyclometallated and bpy based ligands for the purpose of OLED and photosensitiser applications in the last decades.⁵⁶⁻⁵⁸ They have reported a series of cyclometallated iridium complexes by varying the ligand architecture which have yellow (560 nm),⁴³ green (531 nm)^{45,59} and blue-green (497 nm)⁴⁴ electroluminescence. Therefore, the development of monomeric iridium complexes based on ligand architecture is promising in the search of active photosensitisers for hydrogen production.

Bis-cyclometallated iridium complexes can be synthesised according to the two step procedure shown in **Scheme 4.1** in which the overall charge of the complex is determined by the nature of the ancillary ligand.^{27,60-63} Modification of cyclometallated and ancillary ligands allow the development of novel iridium complexes which can be further investigated as potential photosensitisers for hydrogen production. This reaction scheme was also applied for preparing cyclometallated iridium complexes containing carboxy ester groups. However, a modification was required in “step i” (see **Scheme 4.1**) to increase the yield of the desired chloro-bridge iridium complex containing a carboxy ester group.



Scheme 4.1: Reaction scheme for the synthesis of $[Ir(ppy)_2(bpy)](PF_6)$. A dichloro-bridged diiridium dimer involving a cyclometallating ligand (e.g., 2-phenylpyridine, ppy, red) is isolated and subsequently cleaved using an ancillary ligand (e.g., 2,2'-bipyridine, bpy, blue) to yield mononuclear iridium(III) complexes e.g., $[Ir(ppy)_2(bpy)](PF_6)$. i) ethoxy ethanol, reflux, 24 h, ii) DCM/EtOH, reflux 6 h.

The aim of this chapter is to synthesise and characterise a series of iridium mononuclear complexes, which are functionalised with a carboxy ester group. These monomeric iridium complexes can be used as potential photosensitisers for photo driven hydrogen production from water. Carboxy-functionalised iridium complexes can also be bound to the surface of semiconductors which allows heterogeneous photocatalysis. Functionalisation at the 4 position of the phenyl ring in phenylpyridine with an ethyl ester group was also carried out. A range of bpy-based ancillary ligands were chosen for synthesising monomeric iridium complexes. The molecular structure of bpy based ligands and the corresponding ligand abbreviations are shown in **Figure 4.1**.

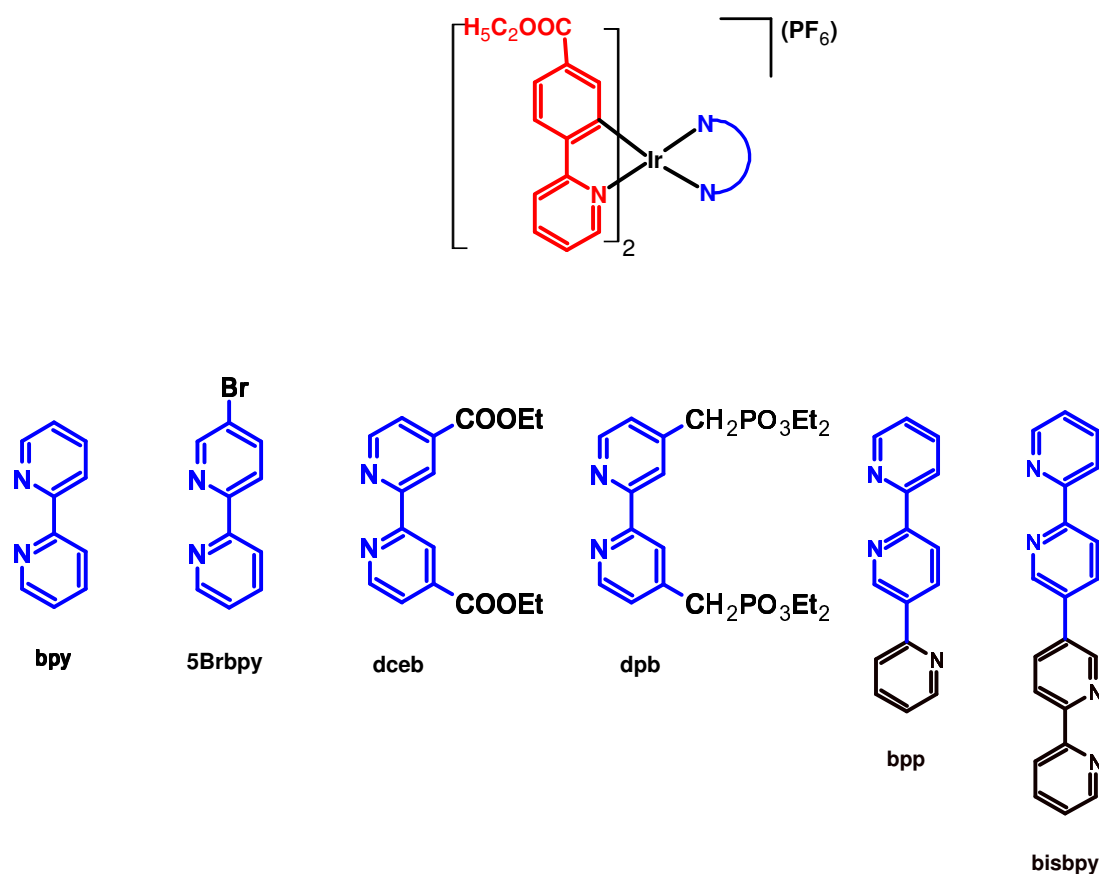


Figure 4.1: Molecular structures and abbreviations of bpy based ancillary ligands. (Red) phenyl pyridine with the carboxy ester group at 4 position of the phenyl ring. (Blue) bpy based ancillary ligands.

The ancillary ligands, dceb and dpb have carboxy esters and phosphonate groups respectively and therefore are expected to bind to the surface of

semiconductors.^{64,65} 5Brbpy has a bromo group that creates an electron withdrawing effect on the iridium metal centre. Bpp and bisbpy ligands can act as bridging ligands, therefore monomeric iridium complexes will be able to coordinate Pd and Pt catalytic metals to create Ir-Pd or Ir-Pt heterodimetallic complexes. The structures of Ir-Pt and Ir-Pd heterodimetallic complexes are shown in **Figure 4.2**.

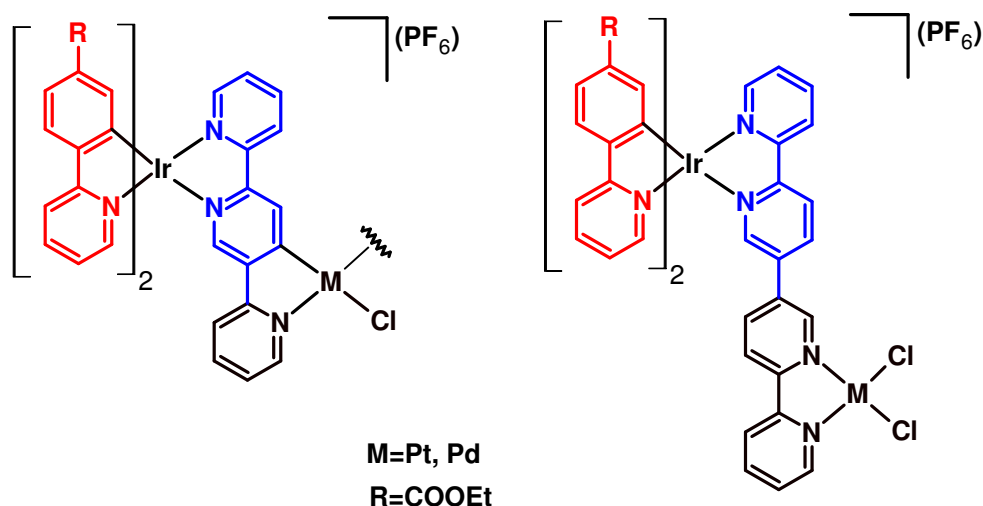


Figure 4.2: Novel carboxy ester derivatised Ir-Pd and Ir-Pt heterodinuclear photocatalysts

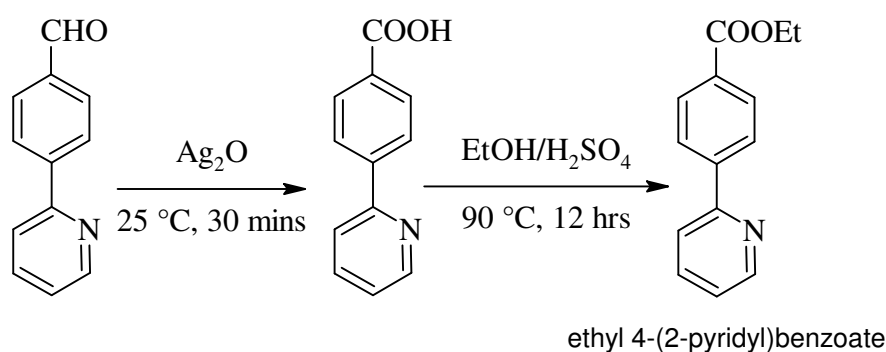
These heterodinuclear photocatalysts are expected to generate more hydrogen from water with the concept of *intramolecular* photocatalysis compared to inter molecular photocatalysis.⁶⁶⁻⁶⁸ The compounds prepared were characterised using ^1H NMR, 2D COSY NMR spectroscopy and CHN analysis. Electronic absorption, and emission spectra, and also lifetime data are included.

4.2. Synthetic procedures for organic ligands

The synthetic procedures of all the bpy based ligands (bpy, 5Brbpy, dceb, dpb, bpp, bisbpy) used in this chapter were discussed previously in **Chapter 2** and **Chapter 3**.

4.2.1. Synthesis of ethyl 4-(2-pyridyl)benzoate.

The 4 position of the phenyl ring in phenylpyridine was functionalised with an ethyl carboxy ester group. 4-(2-pyridyl)benzaldehyde was taken as the starting material. There are many reported procedures to synthesise the carboxy ester containing phenylpyridine, using catalysed reactions^{69,70} such as Negishi coupling,^{71,72} and other cross coupling reactions.⁷³ However, esterification was carried out using a two step procedure, which is inexpensive and less time consuming. The first step is the oxidation of the aldehyde group and the second step is an acid catalysed esterification (see **Scheme 4.2**). The oxidation of the aldehyde group can be carried out using various literature procedures.⁷⁴⁻⁷⁹ Here the oxidation was carried out using freshly prepared silver oxide by reacting AgNO_3 and aq. NaOH solution. The attempted reaction for the oxidation of aldehyde group takes less time and provides higher yield (~ 90%). The reaction was performed at room temperature and was complete in 30 minutes. The starting material 4-(2-pyridyl)benzaldehyde was found not to be completely soluble in the aqueous reaction mixture under the above conditions. 10 cm^3 of THF was added to the reaction mixture to fully dissolve the 4-(2-pyridyl)benzaldehyde. THF was removed from the filtrate by rotary evaporation after filtration of the reaction mixture. The presence of THF in the filtrate can cause the formation of a soluble acidified product which will not precipitate from the aqueous solution and further reduce the yield of 4-(2-pyridyl)benzoic acid. 4-(2-pyridyl)benzoic acid was further esterified using a well studied acid catalysed reaction.^{69,80} The detailed reaction procedure can be found in **Section 4.4** (also see **Scheme 4.2**).



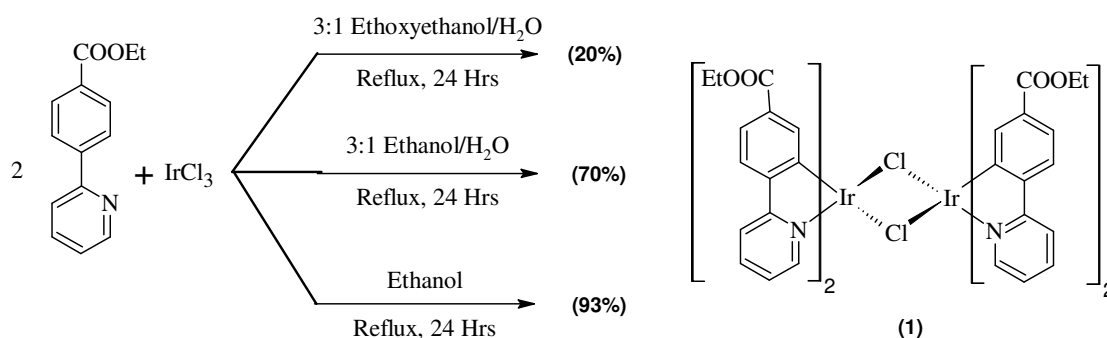
Scheme 4.2: Reaction scheme for synthesising ethyl 4-(2-pyridyl)benzoate

4.3. Synthetic procedures for metal complexes

4.3.1. Synthesis of $[Ir(ppy-COOEt)_2(\mu-Cl)]_2$

Several procedures have been reported to synthesise Ir(III) compounds, which consist of 2-phenylpyridine(ppy) or different functionalised ppy ligands.^{57,62,81} In most of the synthetic procedures, high boiling point solvents like ethoxy ethanol, methoxy ethanol and even glycerol were used as the reaction solvent along with 20-50% of water. In this case, the peripheral ligand ppy is functionalised with carboxy ester groups. A trial reaction was carried out with 3:1 ethoxy ethanol/water solvent system following a literature procedure, which reported the synthetic procedure of carboxy ester containing iridium complex.³⁹ The reported reaction conditions were applied, for the reactions shown in **Scheme 4.2**. A low yield was obtained which may be due to hydrolysis of the ester groups at high temperature. The crude reaction mixture contained a mixture of products, which were difficult to purify. It was observed that the reaction mixture turned greenish black in colour. Due to the synthetic and purification problems, the above reaction was modified as the high temperature and the aqueous reaction environment may have led to hydrolysis of the ester groups.

To improve the yield of the product, the solvent system for the reaction was altered from ethoxy ethanol/water to ethanol/water. The reaction mixture was heated at reflux for 24 hours in 3:1 ethanol/water. The presence of ethanol was expected to stabilise the ethyl ester groups on the ppy ligand. Also, ethanol has a lower boiling point (b.p. = 78 °C) by ~55 °C compared to ethoxy ethanol (b.p. = 135 °C). This reaction provided a better yield ~70% compared to the literature procedure with yield = 20%. Surprisingly, the product was soluble in a 3:1 ethanol/water mixture but not in water. Therefore, the product was precipitated from the reaction mixture with the addition of excess water. The various reactions carried out are shown in **Scheme 4.3**.



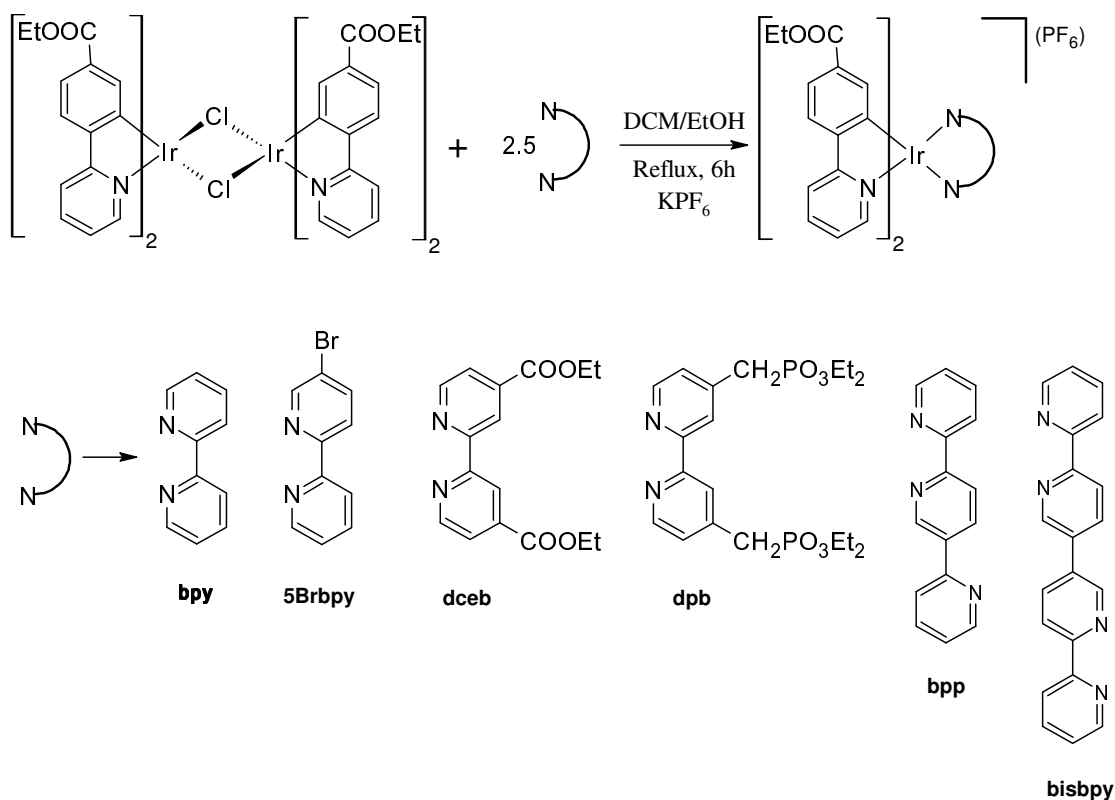
Scheme 4.3: Trial reaction conditions for synthesising $[\text{Ir}(\text{ppy-COOEt})_2(\mu\text{-Cl})]_2$ (**1**)

The solvent system was further modified from ethanol/water to ethanol to improve the yield of $[\text{Ir}(\text{ppy-COOEt})_2(\mu\text{-Cl})]_2$. Carrying out the reaction without water provided a 93% yield. The use of an inert (N_2) atmosphere did not increase the yield. In summary, absolute ethanol was found to be the best solvent for synthesising $[\text{Ir}(\text{ppy-COOEt})_2(\mu\text{-Cl})]_2$ and inert conditions were not required.

4.3.2. Synthesis of $[\text{Ir}(\text{ppy-COOEt})_2(\text{L})](\text{PF}_6)$ type complexes

The synthetic procedure for $[\text{Ir}(\text{ppy-COOEt})_2(\text{L})](\text{PF}_6)$ (L denotes N^N ligand) complexes using a DCM/ethanol solvent mixture has been well studied in the past (**Reaction 4.1**).^{2,81-84} A DCM/ethanol solvent mixture was also used and the reaction mixture was heated at reflux for 6 h to synthesise $[\text{Ir}(\text{ppy-COOEt})_2(\text{L})](\text{PF}_6)$ type complexes. The solvent was removed after cooling the reaction mixture. 30 cm^3 of water was then added to the reaction vessel and sonicated for 20 minutes to extract the product which tended to adhere to the wall of the round bottom flask. Therefore, the aqueous mixture was filtered to separate the unreacted reagents, $[\text{Ir}(\text{ppy-COOEt})_2(\mu\text{-Cl})]_2$ and the bpy based ligand which are not soluble in water. However, $[\text{Ir}(\text{ppy-COOEt})_2(\text{L})](\text{PF}_6)$ type complexes with one PF_6^- counter ion were also found soluble in water which created a problem. The increased solubility of $[\text{Ir}(\text{ppy-COOEt})_2(\text{L})](\text{PF}_6)$ type complexes may be due to the introduction of carboxy ester groups. The yield of the collected $[\text{Ir}(\text{ppy-COOEt})_2(\text{L})](\text{PF}_6)$ complexes from the aqueous layer was low and the aqueous filtrate was yellow in colour which indicates that a large amount of product was present in the filtrate. Therefore, the work up

procedure was modified slightly. The aqueous layer was extracted with DCM. A maximum yield of 60% was found for $[\text{Ir}(\text{ppy-COOEt})_2(\text{L})](\text{PF}_6)$ type complexes.



Reaction 4.1: Synthetic procedure for $[\text{Ir}(\text{ppy-COOEt})_2(\text{L})](\text{PF}_6)$ type complexes, where $\text{L} = \text{bpy}, 5\text{Brbpy}, \text{dceb}, \text{dpb}, \text{bpp}$ and bisbpy .

In the synthesis of $[\text{Ir}(\text{ppy-COOEt})_2(\text{bisbpy})](\text{PF}_6)$, a mixture of compounds (mononuclear and homo-dinuclear) were observed in the crude reaction mixture using the same reaction procedure as stated above (a solution of the chloro-bridged iridium complex was slowly added to a solution of excess bisbpy). Column chromatography was not the preferred method for purifying carboxy ester-containing Ir(III) complexes as the compound can be absorbed into the column. With this method, only a small amount of the product was obtained. The presence of $[\text{Ir}(\text{ppy-COOEt})_2(\text{bisbpy})](\text{PF}_6)$ was confirmed with ^1H NMR. However, there was not enough compound left to carry out further experiments. $[\text{Ir}(\text{ppy-COOEt})_2(\text{bpp})](\text{PF}_6)$ can be used as a precursor for synthesising Ir-Pt or Ir-Pd heterodinuclear complexes. Other monomeric iridium complexes $[\text{Ir}(\text{ppy-COOEt})_2(\text{bpy})](\text{PF}_6)$, $[\text{Ir}(\text{ppy-COOEt})_2(5\text{Brbpy})](\text{PF}_6)$ and $[\text{Ir}(\text{ppy-COOEt})_2(\text{dceb})](\text{PF}_6)$ were obtained in good yield. However, a significant lower yield

of 6% was obtained for $[\text{Ir}(\text{ppy-COOEt})_2(\text{dpb})](\text{PF}_6)$. This complex is an oil which may be due to the phosphonate groups. All the monomeric Ir(III) complexes were characterised by ^1H NMR, H-H 2D COSY NMR, and CHN analysis.

4.4. ^1H NMR spectroscopy of organic ligands

4.4.1. 4-(2-pyridyl)benzoic acid (ppy-COOH)

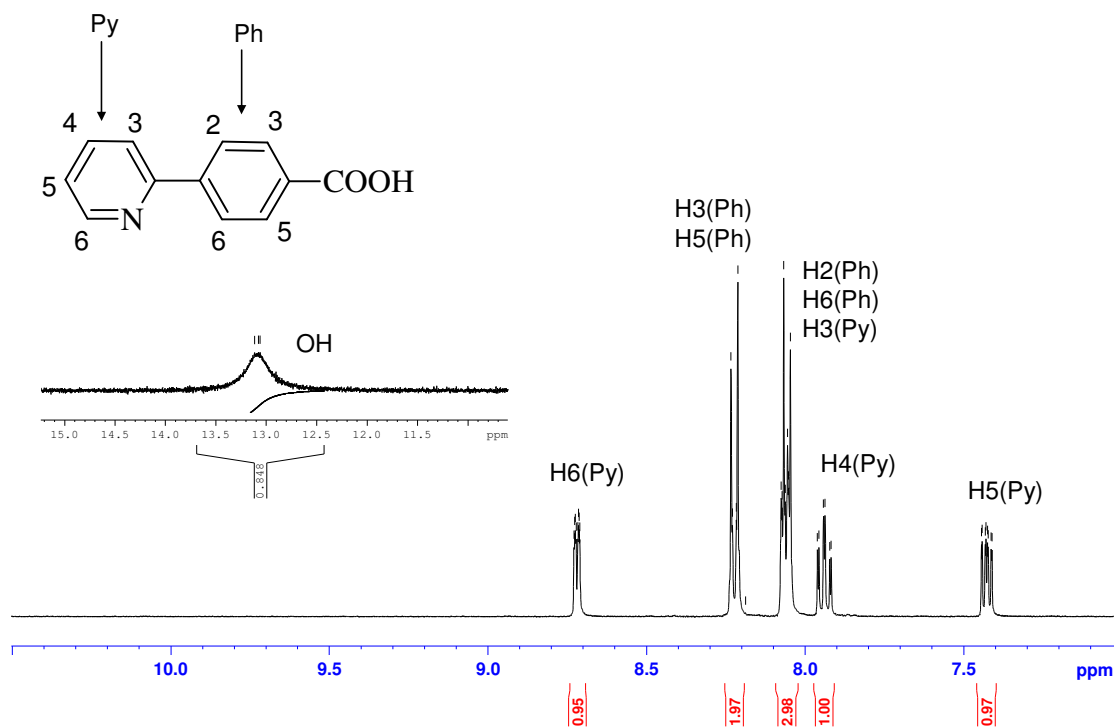


Figure 4.3: ^1H NMR ($\text{DMSO}-d_6$, 400 MHz) of ppy-COOH.

The above, **Figure 4.3** represents the ^1H NMR spectra of ppy-COOH. The ppy-COOH ligand was reported by Tang *et al.*, and the ^1H NMR spectra of ppy-COOH was assigned according to the literature.⁸⁵ The broad proton signal at a 13.2 ppm is assigned to the OH proton of the carboxylic acid group present in the compound. The doublet at 8.72 ppm is assigned to the H6 proton ($^3J = 4.84$ Hz) of the pyridine ring which is quite downfielded, due to the neighbouring electronegative nitrogen atom. The proton at 7.43 ppm is assigned to the H5 proton ($^3J = 7.52$ Hz) of the pyridine ring. The proton at 7.94 ppm is assigned to H4 proton ($^3J = 7.77$ Hz) of the pyridine ring. It is expected that the H3 proton of the pyridine ring is inside the multiplet at 8.01-8.10 ppm. The protons at both the 3 and 5 position of the phenyl ring have identical environments and therefore will appear in the same region. Similarly,

protons at both the 2 and 6 positions have identical environments. The protons at the 3 and 5 positions are shifted further downfield than the protons at the 2 and 6 positions because they are closer to the carboxy group. The multiplet at 8.17-8.27 ppm contains H2 and H6 (Ph ring) and the multiplet at 8.01-8.10 ppm contains H2 and H6 protons (Ph ring). The detailed chemical shifts of the protons are listed in **Table 4.1**.

Table 4.1: List of chemical shifts for the protons in ppy-COOH

	Protons	Hs	Protons	Chemical shift (ppm)	Type	J (Hz)
Py ring	H6	1	H6	8.72	d	4.84
	H5	1	H5	7.43	dd	7.52, 4.74
	H4	1	H4	7.98	dd	7.77, 7.77
	H3	1	H3	8.06	m	-
Ph ring	H2, H6	2	H2, H6	8.06	m	-
	H3, H5	2	H3, H5	8.22	m	-

4.4.2. Ethyl 4-(2-pyridyl)benzoate (ppy-COOEt)

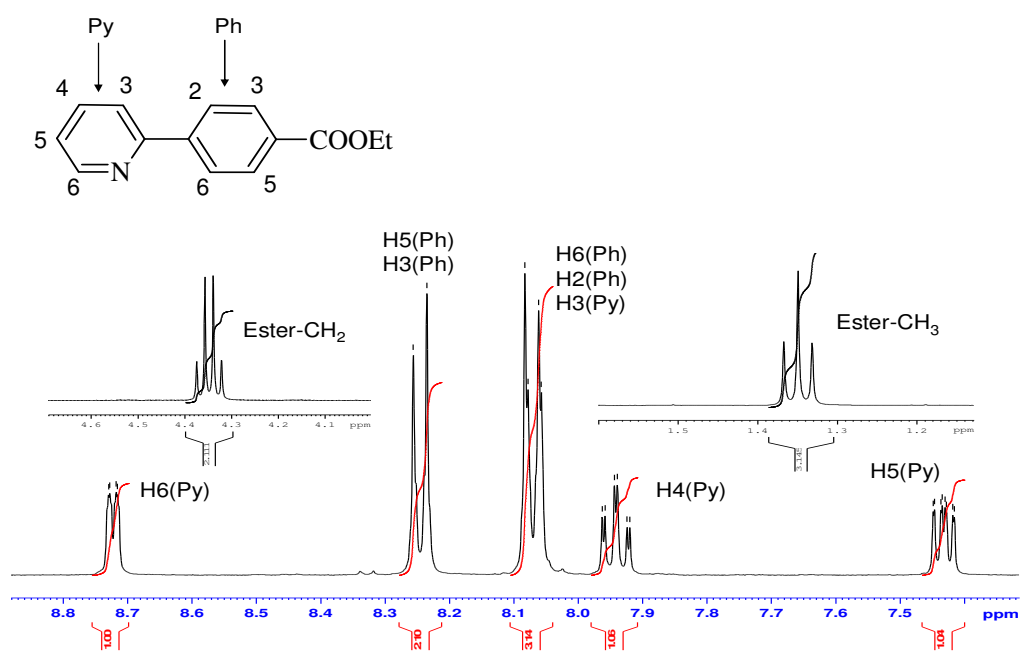


Figure 4.4: ^1H NMR (DMSO- d_6 , 400 MHz) of ppy-COOEt.

The above **Figure 4.4** represents the ^1H NMR spectrum of ethyl 4-(2-pyridyl)benzoate (ppy-COOEt). The synthesis and the ^1H NMR were previously reported by Gosmini *et al.*⁷⁰ The assignment of the protons in ppy-COOEt was made on the basis of the literature data. The carboxy group is esterified with an ethyl group, therefore the proton signals of the ester groups were found at 1.35 ppm (t, 6H, ester-CH₃) and at 4.35 ppm (q, 4H, ester-CH₂). A detailed list of proton signals is provided in **Table 4.2**.

Table 4.2: List of chemical shifts for the protons in ppy-COOH

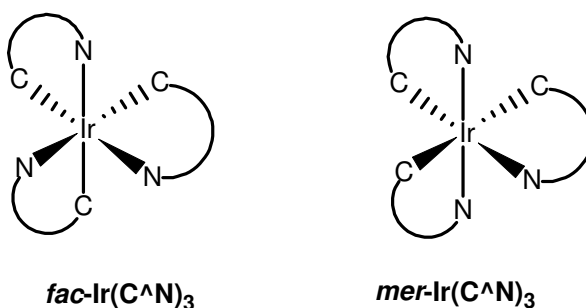
	Protons	Hs	Chemical shift (ppm)	Type	J (Hz)
Py ring	H6	1	8.72	d	4.80
	H5	1	7.43	dd	7.45, 4.80
	H4	1	7.94	dd	7.77, 7.77
	H3	1	8.07	m	-
Ph ring	H2, H6	2	8.07	m	-
	H3, H5	2	8.24	m	-
	ester CH ₃	3	1.35	t	7.07
	ester CH ₂	2	4.35	q	7.07

4.5. ^1H NMR spectroscopy of metal complexes

^1H NMR spectra of these iridium complexes are complex in nature. Although the signals in the aromatic region are not overlapping, the coupling constants and the chemical shifts for the protons in different pyridyl rings can be identical because of identical environments and therefore, difficult to interpret. The H5 protons in the phenyl rings of two peripheral ppy-COOEt ligands are assigned according to the reported cyclometallated iridium complexes,^{21,24,60,86} and rest of the protons in the ^1H NMR are assigned with the help of corresponding 2D COSY NMR spectra. Two types of arrangement (*fac*- and *mer*-) are possible for the phenylpyridyl-based Ir(III) tris-cyclometalates (see **Figure 4.5**). The arrangement of the ligands coordinated to the iridium metal centre shown in the **Figure 4.5** are kinetically-favoured products.⁸⁷

The ^1H NMR spectra and the corresponding 2D COSY NMR of $[\text{Ir}(\text{ppy-COOEt})_2(\text{L})](\text{PF}_6)$ type complexes are discussed in this chapter to fully interpret the NMR spectra. These heteroleptic iridium mononuclear complexes have two ppy-COOEt ligands and one bpy based ancillary ligand. Both the ppy-COOEt ligands are identical when there is a symmetrical bpy based ancillary ligand but these two ppy-COOEt ligands are not equivalent when there is an unsymmetrical ancillary bpy based ligand. For simplicity in the interpretation, Ph1 and Py1 denote the phenyl and pyridine rings for one ppy-COOEt ligand, and Ph2 and Py2 for another ppy-COOEt ligand. Iridium complexes with symmetrical and unsymmetrical bpy based ligands are shown in **Figure 4.5**.

(a)



(b)

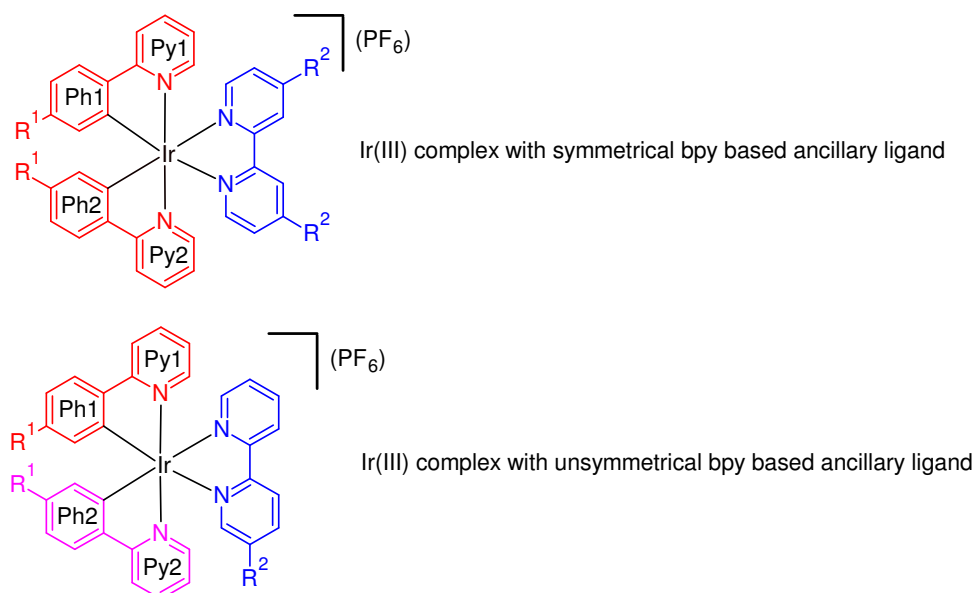


Figure 4.5: (a) The *fac*- and *mer*- isomers of tris heteroleptic Ir(III) complexes. (b) Iridium complexes with symmetrical and unsymmetrical bpy based ancillary ligand. R^1 and R^2 are different functional groups.

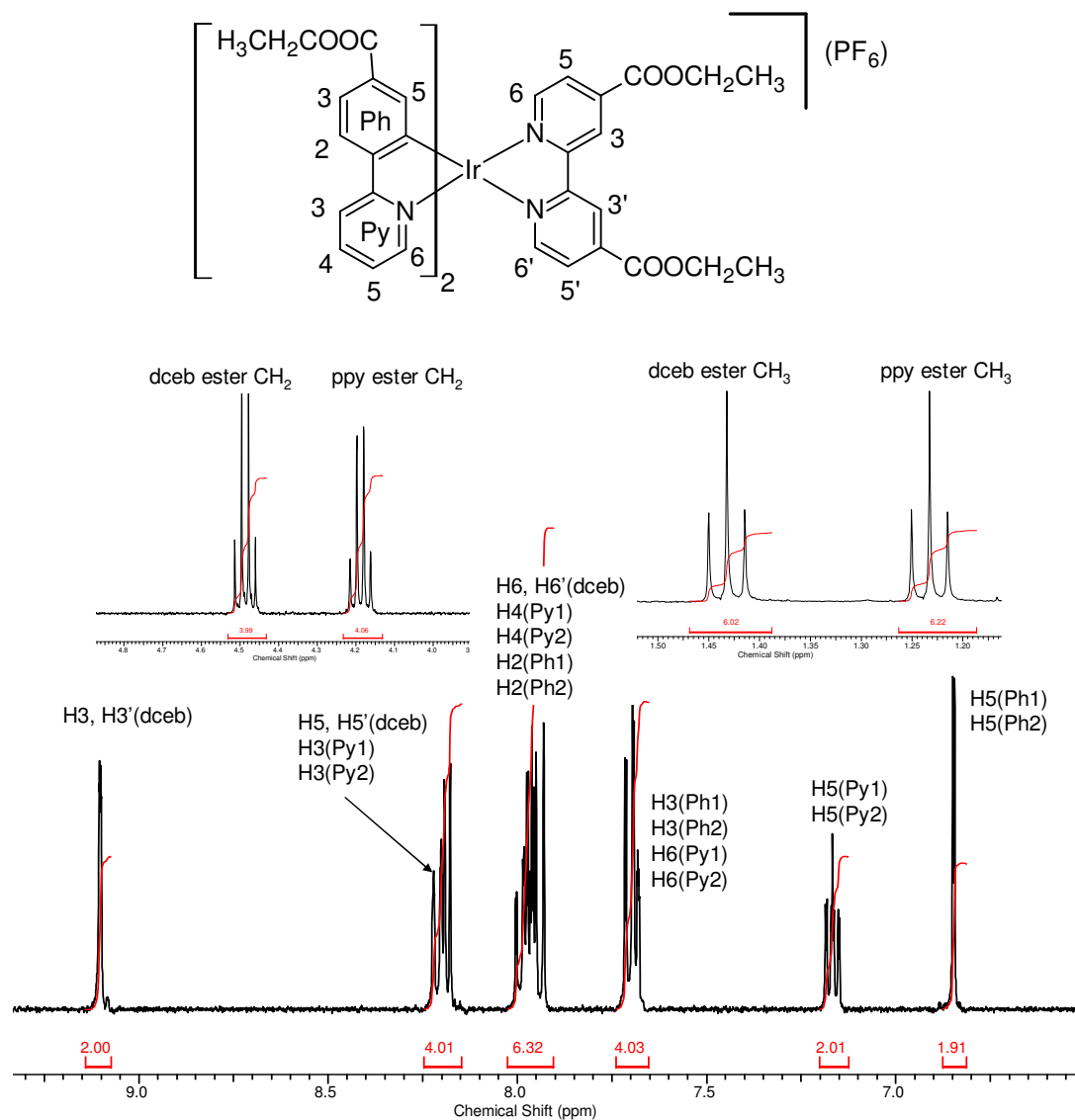
4.5.1. $[\text{Ir}(\text{ppy-COOEt})_2(\text{dceb})](\text{PF}_6)$ 

Figure 4.6: ^1H NMR($\text{Acetonitrile-}d_6$, 400 MHz) of $[\text{Ir}(\text{ppy-COOEt})_2(\text{dceb})](\text{PF}_6)$

Figure 4.6 represents the ^1H NMR spectra of $[\text{Ir}(\text{ppy-COOEt})_2(\text{dceb})](\text{PF}_6)$. The COSY NMR spectrum of $[\text{Ir}(\text{ppy-COOEt})_2(\text{dceb})](\text{PF}_6)$ is shown in **Figure 4.7** and the chemical shifts for all the protons are listed in **Table 4.3**. Dceb is considered as a symmetrical ligand as the 4 and 4' positions of bpy are functionalised with identical ethyl ester groups. Therefore, there are two types of ethyl ester groups in this complex, which are denoted as dceb and ppy-COOEt based ester groups. Both the ester groups have different environments, one is situated on the phenyl ring and one is on the pyridine ring.

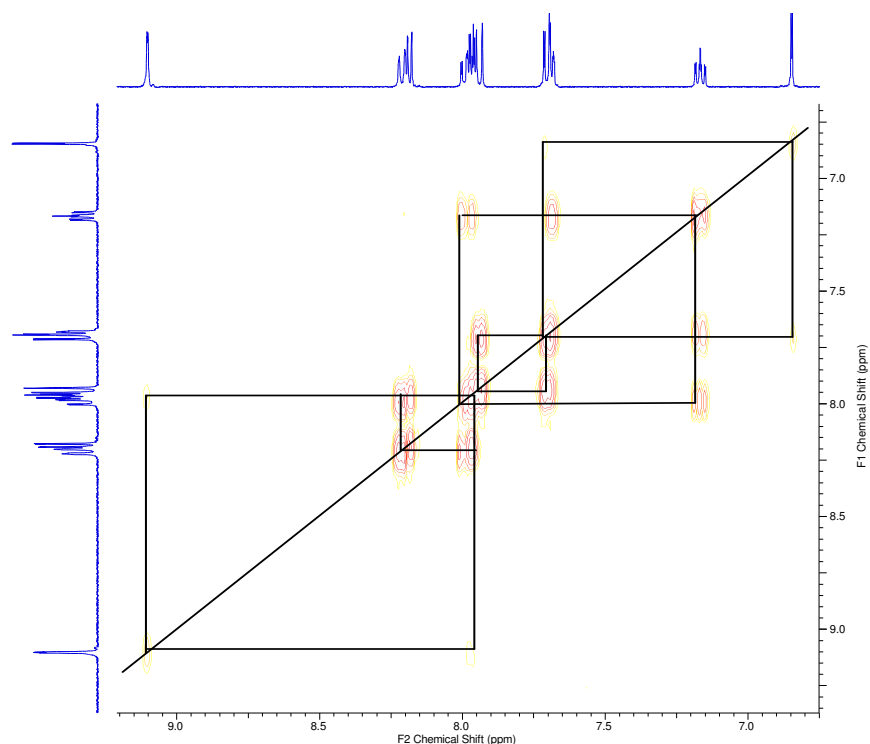


Figure 4.7: COSY NMR (Acetonitrile- d_3 , 400 MHz) of $[\text{Ir}(\text{ppy-COOEt})_2(\text{dceb})](\text{PF}_6)$

The quartet at 4.49 ppm is assigned to CH_2 protons of the ester groups in the dceb ligand and the quartet at 4.19 ppm is assigned to CH_2 protons of the ester groups in ppy-COOEt. The upfield shift of the CH_2 ester proton compared to that of the free ligand (CH_2 ester at 4.35 ppm) is due to the introduction of a negatively charged carbon atom in the phenyl ring after complexation. As both the ppy-COOEt ligands have identical environments therefore, the chemical shift of ester groups in ppy-COOEt show identical chemical shifts. The triplet at 1.43 ppm is assigned to CH_3 protons of the dceb ester groups (comparing the free dceb ester CH_3 proton signals) and the triplet at 1.23 ppm is assigned to the CH_3 protons of the ester groups in ppy-COOEt. The signal at 6.85 ppm is assigned to the H5 proton of the phenyl ring (Ph) in ppy-COOEt. H5 is shifted upfield due to the neighbouring negative carbon atom. H5 (Ph) ($^4J = 1.17$ Hz) couples with a proton which is a part of the multiplet at 7.63–7.76 ppm therefore assigned to H3 (Ph-ring). H3 (Ph-ring) further couples with the doublet at 7.94 ppm which is assigned to the H2 proton on the Ph-ring. The proton at 7.17 ppm ($^3J = 7.52$ Hz) is assigned to the H5 proton on the pyridine ring in ppy-COOEt.^{21,23,88} This H5 (Py) couples with two proton signals, one is a doublet at 7.63–7.67 ppm (assigned to H6, Py-ring) and the multiplet at 7.95–8.03 ppm (assigned to H4, Py ring). H4(Py) further couples with the doublet at 8.21 ppm which is assigned

to H3 proton on the Py-ring. The most downfield singlet at 9.10 ppm is assigned to the H3 (and H3') protons ($^4J = 1.64$ Hz) of the dceb ligand. The H3 proton further couples with the doublet at 8.19 ppm that is assigned to the H5 (and H5') proton (dceb). The H5 proton (dceb) further couples with the multiplet at 7.63-7.76 ppm and is assigned to the H6 (and H6') proton of the dceb ligand.

Table 4.3: List of chemical shifts for the protons in $[Ir(ppy-COOEt)_2(dceb)](PF_6)$

	Protons	Hs	Chemical shift(ppm)	Type	J(Hz)
dceb	H3, H3'	2	9.10	d	1.64
	H5, H5'	2	8.19	dd	5.56, 0.76
	H6, H6'	2	7.63-7.76	m	-
	Ester-CH ₂	4	4.49	q	7.07
	Ester-CH ₃	6	1.43	t	7.07
ppy-COOEt	H5(Ph1), H5(Ph2)	2	6.85	d	1.77
	H3(Ph1), H3(Ph2)	2	7.63-7.76	m	-
	H2(Ph1), H2(Ph2)	2	7.94	d	8.08
	H6(Py1), H6(Py2)	2	7.63-7.67	m	-
	H5(Py1), H5(Py2)	2	7.17	dd	7.52, 5.87
	H4(Py1), H4(Py2)	2	7.95-8.03	m	-
	H3(Py1), H3(Py2)	2	8.21	d	7.83
	Ester-CH ₂	4	4.19	q	7.07
	Ester-CH ₃	6	1.23	t	7.07

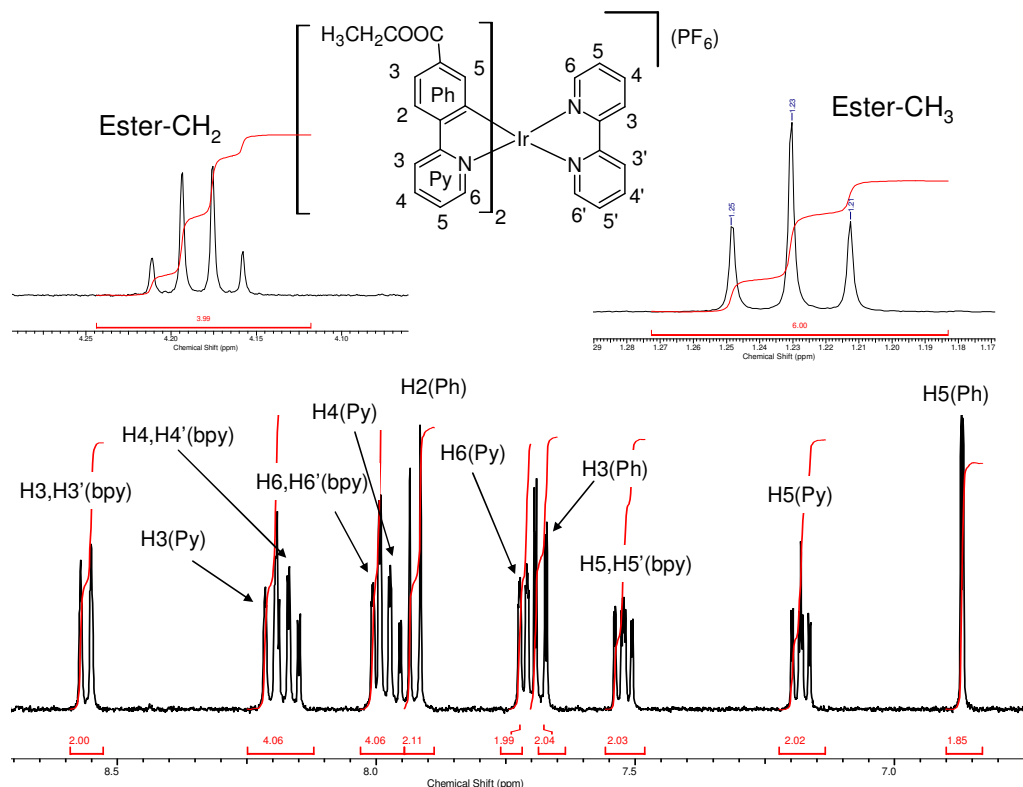
4.5.2. $[Ir(ppy-COOEt)_2(bpy)](PF_6)$ 

Figure 4.8: 1H NMR (Acetonitrile- d_6 , 400 MHz) of $[Ir(ppy-COOEt)_2(bpy)](PF_6)$

Figure 4.8 and **4.9** represent the 1H NMR spectra and 2D COSY NMR of the complex as $[Ir(ppy-COOEt)_2(bpy)](PF_6)$. Detailed chemical shifts and the coupling constants of the protons are listed in **Table 4.4**. The ancillary bipyridine (bpy) ligand has two identical pyridine rings therefore creates identical environments for both the ppy-COOEt ligands. Also, both the ppy-COOEt ligands attached to the iridium metal have similar chemical environments for both the pyridyl rings of the bpy ligand. Therefore, the protons in both pyridine rings of the bpy ligand show identical chemical shifts in the NMR spectra. For example, H6 and H6' appear as a single doublet. Similarly, H5 and H3 appear at the same ppm values where H5' and H3' protons (of bpy) appear respectively. The protons of both ppy-COOEt ligands show identical chemical shifts due to the symmetrical bpy ligand coordinated to the iridium metal centre. For example, H6 of one ppy-COOEt ligand shows an identical chemical shift to the H6 protons of another ppy-COOEt ligand.

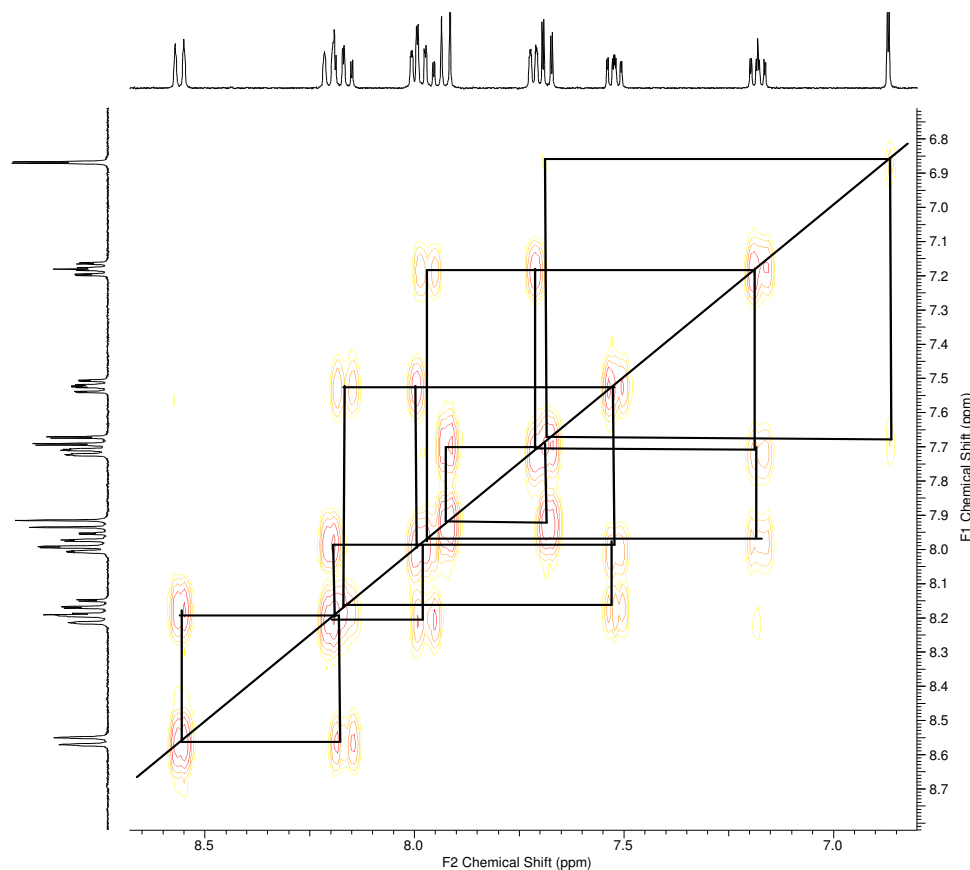


Figure 4.9: 2D COSY NMR(Acetonitrile- d_6 , 400 MHz) of $[Ir(ppy-COOEt)_2(bpy)](PF_6)$

The proton signal at 6.87 ppm is assigned to the H5 proton of the Ph-ring of the ppy-COOEt.^{26,89} This H6 proton is shifted upfield because of neighbouring negative carbon atom that is attached to the iridium metal. The H5 proton, further couples with the proton at 7.68 ppm that is assigned to H3 (Ph ring). The H3 proton couples with the signal at 7.72 ppm assigned to H2 and H6 protons (Ph ring). Interpretation of the pyridyl ring protons is the most difficult part as the proton signals have identical coupling constants. The doublet at 8.56 ppm is assigned to H3 (and H3') protons ($^3J = 8.08$ Hz) in the bpy ligand. H3 of the Py ring (in ppy-COOEt) is shielded by the phenyl ring. Therefore, H3 appears slightly upfield compared to H3 in the free bpy ring. The doublet at 8.22 ppm is assigned to the H3 proton of the Py ring (ppy-COOEt). H3 (bpy) couples with the proton at 8.14 ppm assigned to H4 (and H4') (bpy). H4 (bpy) couples with the proton at 7.18 ppm ($^3J = 7.45$ Hz) assigned to H5 and H5' (bpy). This H5 proton couples with a doublet at 8.01 ppm assigned to H6 and H6' proton (bpy). Therefore, all the bpy ring protons are assigned. Similarly, the H3

protons in the Py rings (ppy-COOEt) appear as multiplet in the region 8.13-8.22 ppm. H3 couples with H4 and H4 couples with H5 and H5 couples with H6. Protons in the Py ring (ppy-COOEt) are assigned to H4 at 7.98 ppm, H5 at 7.18 ppm ($^3J = 7.45$ Hz) and finally the H6 proton (Py1 and Py2) at 7.72 ppm ($^3J = 5.81$ Hz).

Table 4.4: List of chemical shifts for the protons in $[Ir(ppy-COOEt)_2(bpy)](PF_6)$

	Protons	Hs	Chemical shift (ppm)	Type	J(Hz)
bpy	H6,H6'	2	8.01	m	-
	H5,H5'	2	7.52	dd	7.71, 5.43
	H4, H4'	2	8.14	m	-
	H3, H3'	2	8.56	d	8.56
ppy-COOEt	H6(Py1), H6(Py2)	2	7.72	dd	5.81, 0.76
	H5(Py1), H5(Py2)	2	7.18	dd	7.45, 5.94
	H4(Py1), H4(Py2)	2	7.98	m	-
	H3(Py1), H3(Py2)	2	8.22	m	-
	H2(Ph1), H2(Ph2)	2	7.72	d	5.81
	H3(Ph1), H2(Ph2)	2	7.68	d	8.21
	H5(Ph1), H5(Ph2)	2	6.87	d	1.26
	Ester-CH ₂	4	4.18	q	7.07
	Ester-CH ₃	6	1.23	t	7.07

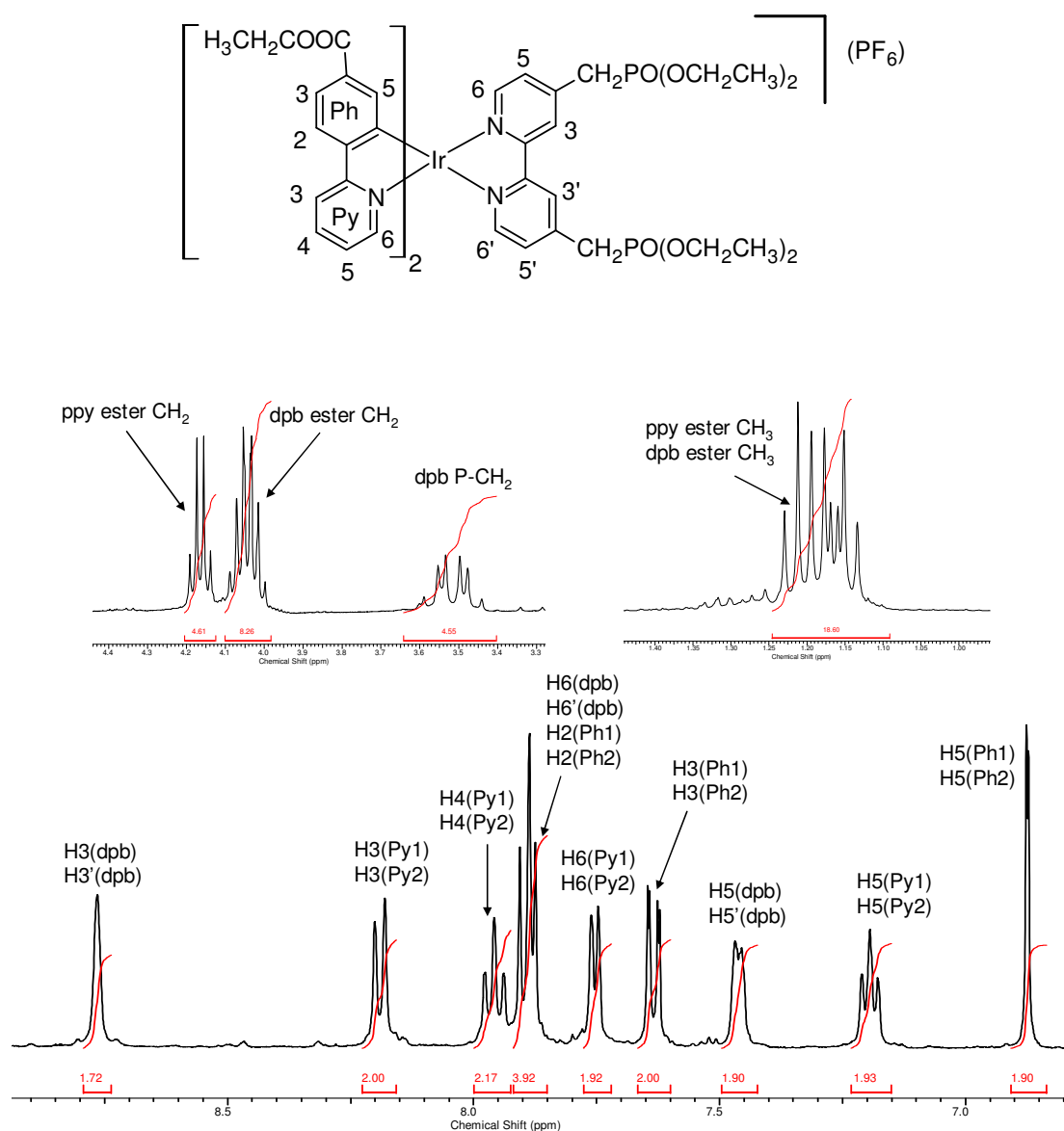
4.5.3. $[\text{Ir}(\text{ppy-COOEt})_2(\text{dpb})](\text{PF}_6)$ 

Figure 4.10: ^1H NMR ($\text{Acetonitrile-}d_6$, 400 MHz) of $[\text{Ir}(\text{ppy-COOEt})_2(\text{dpb})](\text{PF}_6)$

Figure 4.10 represents the ^1H NMR spectra of $[\text{Ir}(\text{ppy-COOEt})_2(\text{dpb})](\text{PF}_6)$. The COSY NMR for $[\text{Ir}(\text{ppy-COOEt})_2(\text{dpb})](\text{PF}_6)$ is provided in **Figure 4.11** and the list of chemical shifts for the protons are tabulated in **Table 4.5**. This complex is another example of an iridium complex where the ancillary bpy based ligand is symmetrical. The NMR spectrum of this complex is quite different from the two compounds shown in **Figures 4.8** and **4.9**. The proton at 7.19 ppm ($^3J = 6.32$ Hz) is assigned to the H5 proton of the Py ring (ppy-COOEt) and the proton at 7.96 ppm (3J

= 7.33 Hz) is assigned to the H4 proton of the Py ring (ppy-COOEt). The H4 proton further couples with a doublet at 8.19 ppm ($^3J = 8.08$ Hz) and is assigned to H3 (Py).

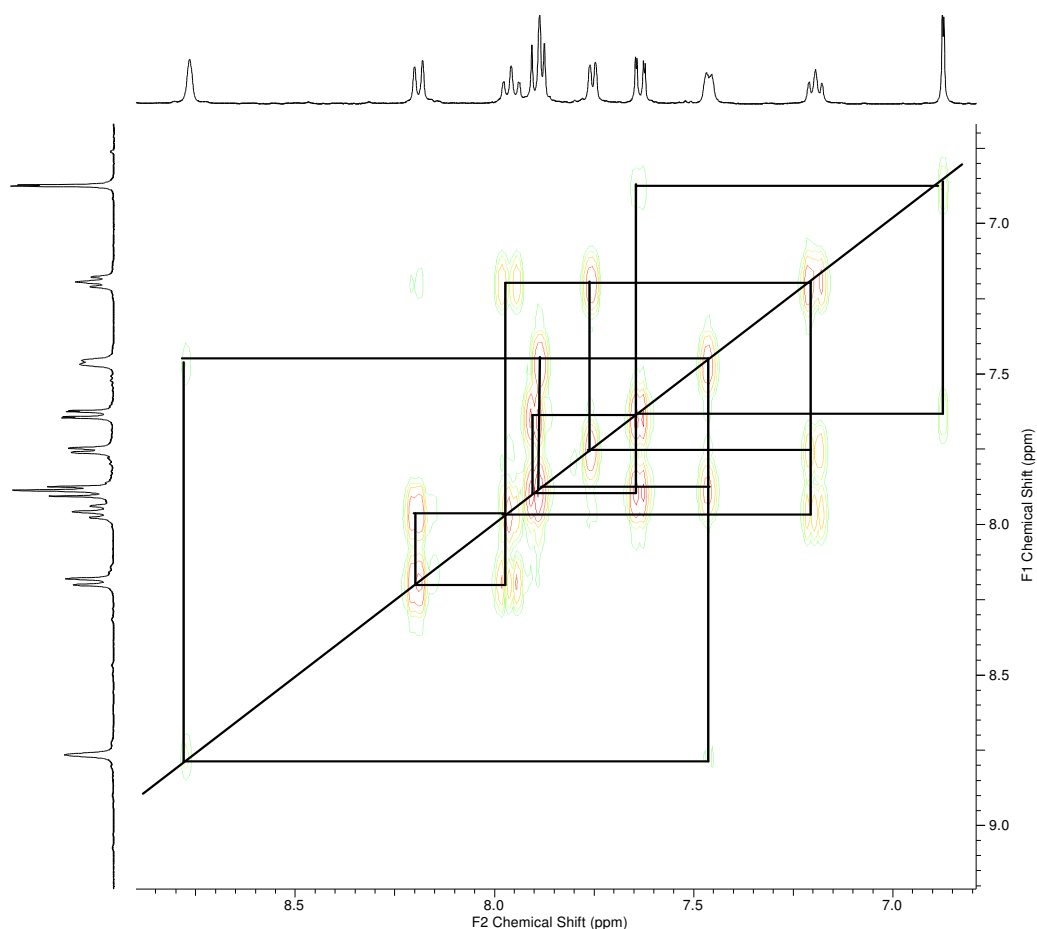


Figure 4.11: COSY NMR (Acetonitrile- d_6 , 400 MHz) of $[Ir(ppy-COOEt)_2(dpb)](PF_6)$

On the other hand, H5 at 6.87 ppm couples with a doublet at 7.46 ppm ($^3J = 5.31$ Hz) that is assigned to H6 (Py). The resonance (broad singlet) at 8.76 ppm is assigned to H3 (and H3') of dpb. The H3 proton further couples with a doublet at 7.46 ppm ($^3J = 5.31$ Hz) (H5, dpb). H5 couples with the multiplet at 7.86-7.92. Therefore, it can be concluded that H6 (dpb) is a part of this multiplet. The singlet at 6.87 ppm is assigned to the H5 protons from both Ph-rings of the ppy-COOEt ligands. H5 (Ph) couples with the doublet at 7.63 ppm ($^4J = 1.52$ Hz, long range coupling) that is assigned to H3 protons (Ph). The multiplet at 7.86-7.92 couples with H3 at 7.63 ppm. Therefore, the proton signal of H2 is expected to appear in the region 7.86-7.92 ppm. The ester groups in both the ppy-COOEt and the ancillary bpy based ligand dpb have similar

chemical shifts. The quartet at 4.16 ppm (4H) is assigned to the CH₂ protons of the ester groups in ppy-COOEt. The multiplet at 3.95-4.12 (8H) is assigned to the CH₂ protons of the phosphonate ester groups in the dpb ligand. CH₃ protons of both types of ester groups overlapped in the region 1.08-1.25 ppm. The P-CH₂ signals were observed in the region 3.43-3.62 ppm.

Table 4.5: List of chemical shifts for the protons in [Ir(ppy-COOEt)₂(dpb)](PF₆)

	Protons	Hs	Chemical shift (ppm)	Type	J(Hz)
dpb	H6, H6'	2	7.86-7.92	m	-
	H5, H5'	2	7.46	d	5.31
	H3, H3'	2	8.76	s	-
	Ester-CH ₂	8	3.95-4.12	m	-
	Ester-CH ₃	12	1.08-1.25	m	-
	P-CH ₂	4	3.42-3.62	m	-
ppy-COOEt	H5(Ph1), H5(Ph2)	2	6.87	d	1.52
	H3(Ph1), H3(Ph2)	2	7.63	dd	8.08, 1.77
	H2(Ph1), H2(Ph2)	2	7.86-7.92	m	-
	H6(Py1), H6(Py2)	2	7.46	d	5.31
	H5(Py1), H5(Py2)	2	7.19	dd	6.32,6.32
	H4(Py1), H4(Py2)	2	7.96	dd	7.33,7.33
	H3(Py1), H3(Py2)	2	8.19	d	8.08
	Ester-CH ₂	4	4.16	m	-
	Ester-CH ₃	6	1.08-1.25	m	-

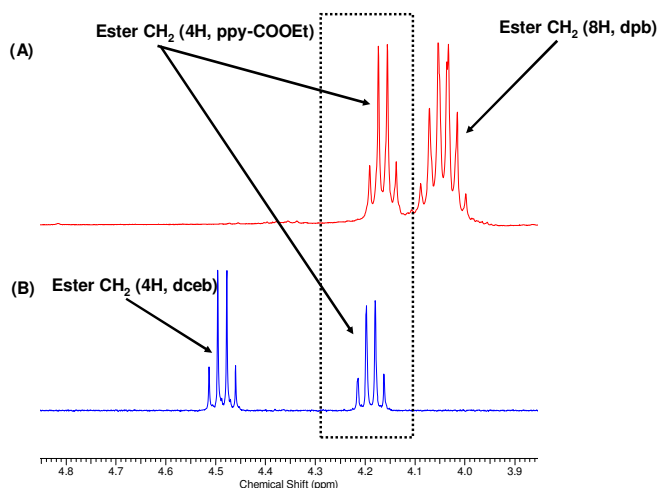


Figure 4.12: A comparison of the ester CH_2 groups signals (q) in (A) $[\text{Ir}(\text{ppy-COOEt})_2(\text{dpbb})](\text{PF}_6)$ and (B) $[\text{Ir}(\text{ppy-COOEt})_2(\text{dceb})](\text{PF}_6)$

There is a significant difference in the chemical shifts of the ester groups present in $[\text{Ir}(\text{ppy-COOEt})_2(\text{dpbb})](\text{PF}_6)$ and $[\text{Ir}(\text{ppy-COOEt})_2(\text{dceb})](\text{PF}_6)$. The ester CH_2 protons (q) for $[\text{Ir}(\text{ppy-COOEt})_2(\text{dceb})](\text{PF}_6)$ appear further downfield comparing to the ester CH_2 proton signal (q) in $[\text{Ir}(\text{ppy-COOEt})_2(\text{dpbb})](\text{PF}_6)$. The phosphonate ester groups are linked to the pyridine ring with a CH_2 group whereas, the ester groups on the dceb are directly attached to the pyridine ring. There are also differences in the chemical shifts for the $\text{H}_6(\text{H}_6')$, $\text{H}_5(\text{H}_5')$ and $\text{H}_3(\text{H}_3')$ proton signals. The difference in the aromatic region is illustrated in **figure 4.18** and **Table 4.6**. A comparison of the aliphatic regions between the complexes $[\text{Ir}(\text{ppy-COOEt})_2(\text{dpbb})](\text{PF}_6)$ and $[\text{Ir}(\text{ppy-COOEt})_2(\text{dceb})](\text{PF}_6)$ is shown below in **Figure 4.12**. NMR spectroscopic data also suggest identical chemical environments for the two-ester groups on the two different ppy-COOEt ligands, therefore it is possible to predict the possible geometry of the Ir(III) complex. Two possible geometries are (I) and (II) (**Diagram 4.1**), but crystallographic data is required to identify which is the correct geometry. NMR data categorically rules out geometry (III).

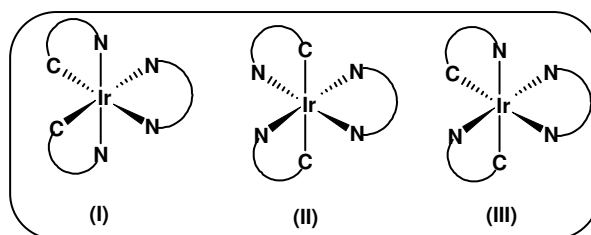


Diagram 4.1: Three possible geometries of $[\text{Ir}(\text{C}^{\text{N}})_2(\text{N}^{\text{N}})]^+$ type complexes

Table 4.6: Chemical shifts of dceb and dpb protons in $[Ir(ppy-COOEt)_2(L)](PF_6)$ type complexes

Protons	Type	Chemical shift (ppm)/ dceb ligand	Chemical shift (ppm)/ dpb ligand
H6, H6'	d	7.63-7.76	7.86-7.92
H5, H5'	d	8.19	7.46
H3, H3'	s	9.10	8.76
Ester-CH ₂	q	4.49	4.12
Ester-CH ₃	q	1.43	1.25

4.5.4. $[Ir(ppy-COOEt)_2(5Brbpy)](PF_6)$

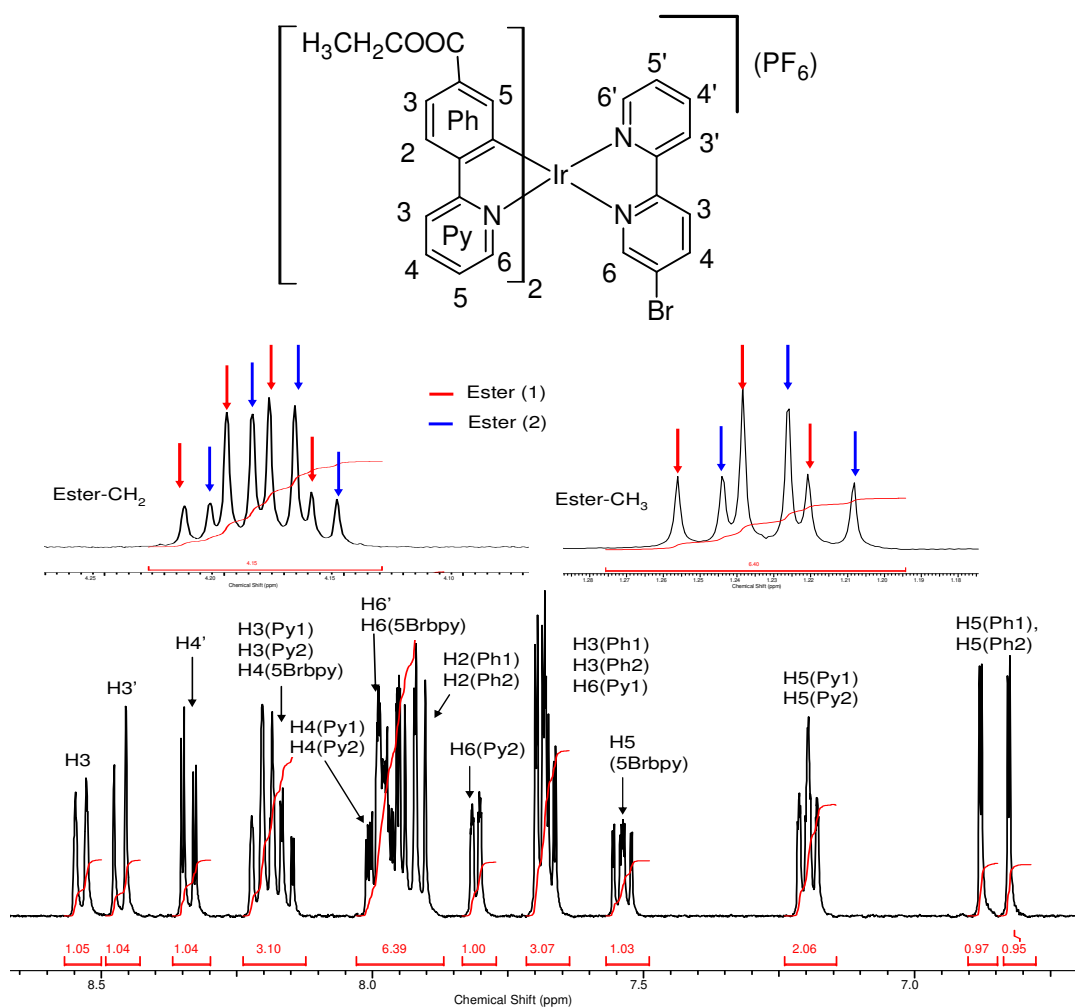


Figure 4.13: 1H NMR ($Acetonitrile-d_6$, 400 MHz) of $[Ir(ppy-COOEt)_2(5Brbpy)](PF_6)$

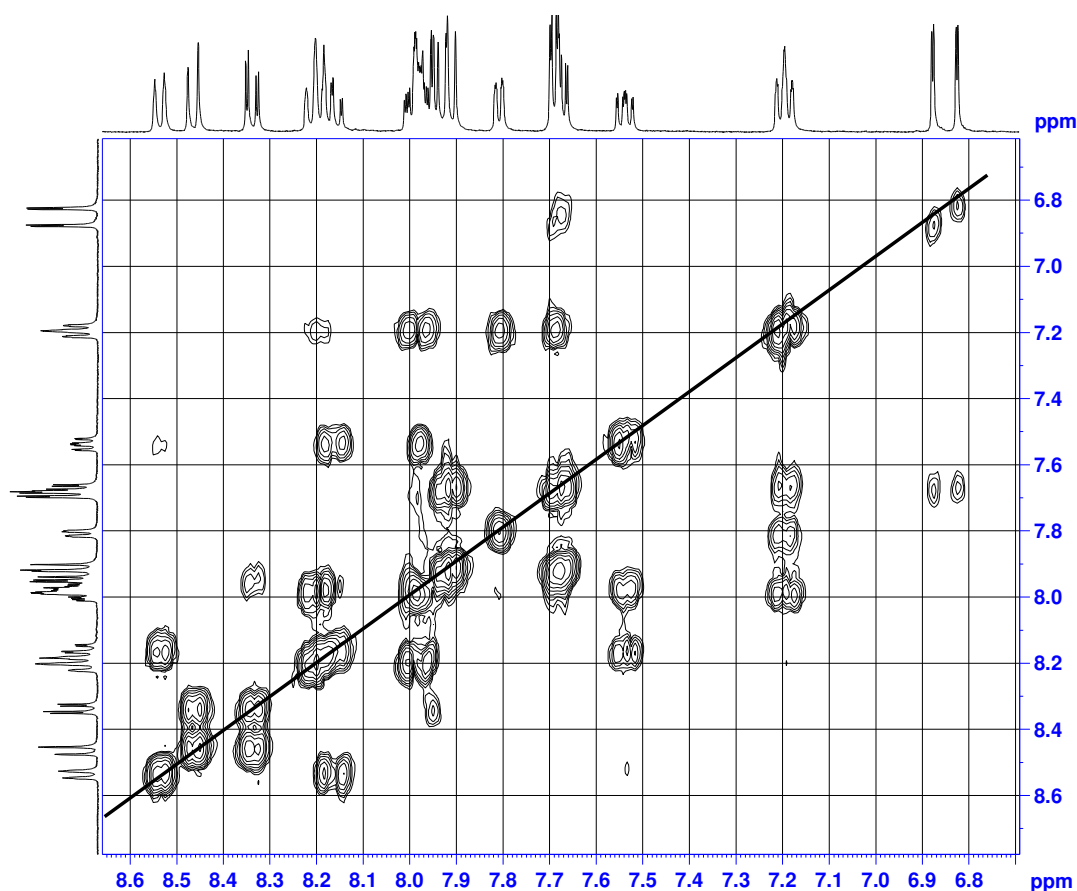


Figure 4.14: COSY NMR (Acetonitrile- d_6 , 400 MHz) of $[\text{Ir}(\text{ppy-COOEt})_2(5\text{Brbpy})](\text{PF}_6)$

Figure 4.13 represents the ^1H NMR spectra of $[\text{Ir}(\text{ppy-COOEt})_2(5\text{Brbpy})](\text{PF}_6)$. The COSY NMR spectrum of $[\text{Ir}(\text{ppy-COOEt})_2(5\text{Brbpy})](\text{PF}_6)$ is shown in **Figure 4.14** and the list of chemical shifts of all the protons is provided in **Table 4.7**. This compound is an example where the bpy ligand is unsymmetrical, i. e., the two pyridine rings of bpy are not chemically equivalent. The bpy ligand is functionalised with a bromine group at the 5 position in one of the pyridine rings. Two doublets (long range coupling) at 6.82 ppm and 6.88 ppm are assigned to the H5 protons of the two phenyl rings (of the two ppy-COOEt ligands). The multiplet at 7.64–7.71 ppm is assigned to the H3 protons (Ph1 and Ph2 of each ppy-COOEt) as both the H5 (Ph1 and Ph2 of each ppy-COOEt) couple with this multiplet. The multiplet further couples with the multiplet at 7.87–8.02 ppm which is assigned to two H2 protons (Ph1 and Ph2 of each ppy-COOEt) inside the multiplet. The multiplet at 7.16–7.23 ppm is assigned to the two H5 protons of the two pyridine rings (Py1 and Py2 of each ppy-COOEt) in two ppy-COOEt ligands.

Table 4.7: List of chemical shifts for the protons in $[Ir(ppy-COOEt)_2(5Brbpy)](PF_6)$

	Protons	Hs	Chemical shift (ppm)	Type	J(Hz)
5Brbpy	H6'	1	7.87-8.01	m	-
	H5'	1	7.54	dd	7.64, 5.49
	H4'	1	8.13-8.24	m	-
	H3'	1	8.54	d	8.08
	H6	1	7.87-8.02	m	-
	H4	1	8.34	dd	8.84, 2.27
	H3	1	8.47	d	8.34
ppy-COOEt	H5(Ph1)	1	6.82	s	-
	H5(Ph2)	1	6.88	s	-
	H3(Ph1), H3(Ph2)	2	7.64-7.71	m	-
	H2(Ph1), H2(Ph2)	2	7.87-8.02	m	-
	H6(Py1)	1	7.67-7.71	m	-
	H6(Py2)	1	7.81	d	6.57
	H5(Py1), H5(Py2)	2	7.16-7.23	m	-
	H4(Py1), H4(Py2)	2	7.87-8.02	m	-
	H3(Py1), H3(Py2)	2	8.13-8.24	m	-
	Ester-CH ₂	4	4.13-4.24	m	
	Ester-CH ₃	6	1.20-1.26	m	

H5 protons (Py1 and Py2 of each ppy-COOEt) further couple with two multiplets at 7.64-7.71 ppm, 7.87-8.02 ppm and with a doublet at 7.81 ppm ($^3J = 6.57$ Hz). These signals are assigned to H6 (Py1) at 7.67-7.71 ppm, H6 (Py2) at 7.81 ppm and two H4

protons (Py1 and Py2 of each ppy-COOEt) inside the multiplet at 7.87-8.02 ppm. It was observed that the multiplet (H4 protons in Py1 and Py2 of each ppy-COOEt) couple with another multiplet at 8.13-8.24 ppm assigned to two H3 protons in Py1 and Py2 rings. The doublet at 8.54 ppm is assigned to the H3' proton of 5Brbpy. H3' couples with one multiplet at 8.13-8.24 ppm. Therefore, H4' is assigned to a part of the multiplet at 8.13-8.24 ppm. H4' proton further couples with the proton at 7.54 ppm assigned to H5' of 5Brbpy. H5' shows a coupling with the multiplet at 7.87-8.01. Therefore, H6' (5Brbpy) can be expected inside the multiplet at 7.87-8.01 ppm. There is another doublet at 8.47 ppm assigned to the H3 proton which couples with a doublet at 8.34 ppm. Hence, H4 is defined as the doublet at 8.34 ppm. This H4 shows couples with a proton signal inside the multiplet at 7.87-8.02 ppm. H6 is therefore assigned to a proton signal inside the multiplet at 7.87-8.02 ppm.

4.5.5. $[Ir(ppy\text{-}COOEt)_2(bpp)](PF_6)$

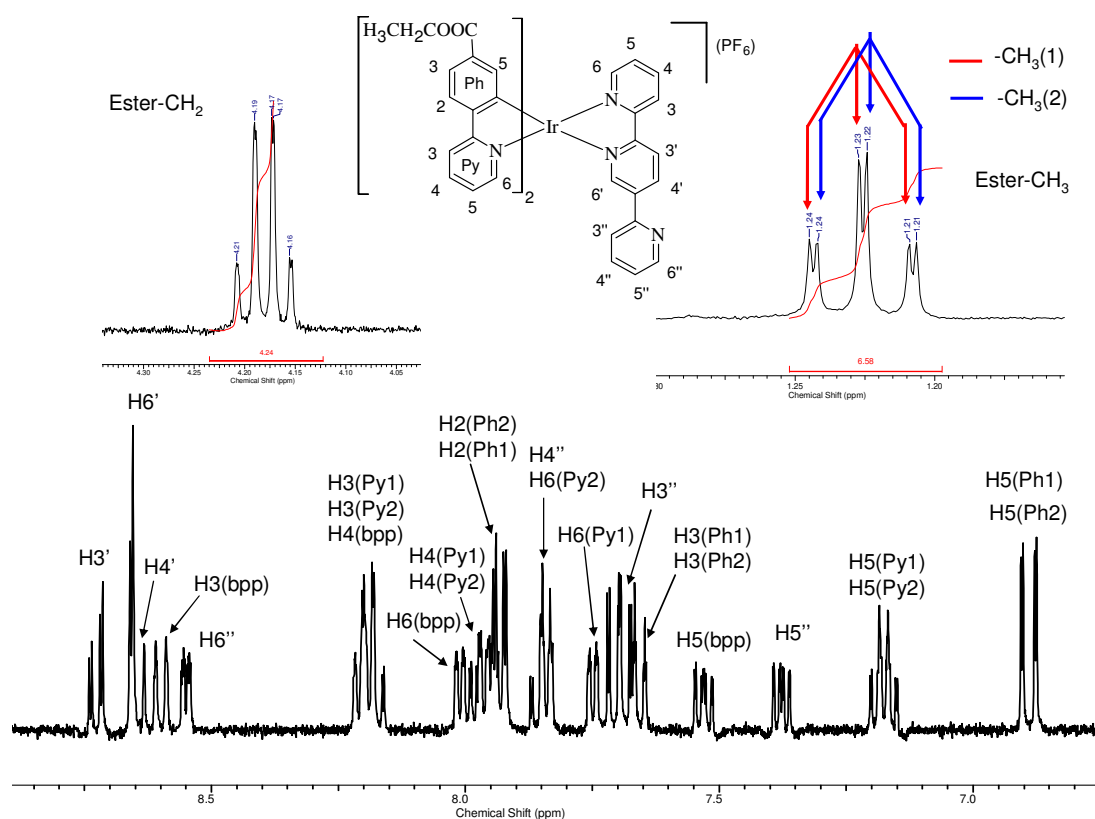


Figure 4.15: ^1H NMR (Acetonitrile- d_6 , 400 MHz) of $[\text{Ir}(\text{ppy-COOEt})_2(\text{bpp})](\text{PF}_6)$

Figure 4.15 represents the ^1H NMR spectrum of $[\text{Ir}(\text{ppy-COOEt})_2(\text{bpp})](\text{PF}_6)$. The COSY NMR spectrum of $[\text{Ir}(\text{ppy-COOEt})_2(\text{bpp})](\text{PF}_6)$ is shown in **Figure 4.16** and a list of chemical shifts for all the protons are tabulated in **Table 4.8**. The bpp ligand can be classified as an unsymmetrical bpy based ligand where the 5' position of central pyridine ring is functionalised with another pyridine group. The chemical shift slightly differs for the protons in two different ppy-COOEt ligands and also for two ester groups due to different chemical environments. One of the two outer pyridyl rings of the bpp ligand are denoted as occupied pyridine ring (coordinated to iridium metal centre) and the other as an unoccupied pyridine ring. The main difference in chemical shifts are expected for H6 and H3 with H6'' and H3'' respectively. H6'' and H3 protons are expected to experience a greater downfield shift than H6 and H3'' respectively based on metal coordination. The two singlet peaks at 6.88 ppm and 6.90 ppm are assigned to two H5 protons of the two-phenyl rings (Ph1 and Ph2).

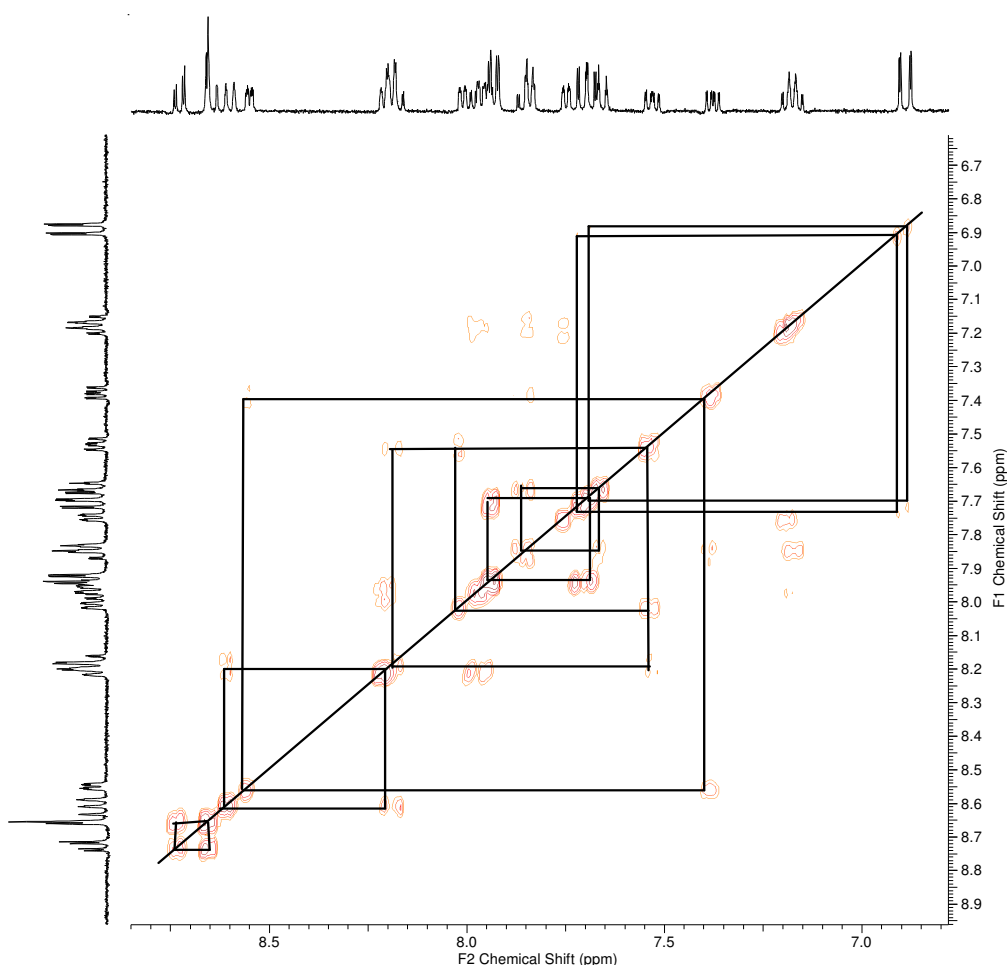


Figure 4.16: COSY NMR (Acetonitrile- d_6 , 400 MHz) of $[\text{Ir}(\text{ppy-COOEt})_2(\text{bpp})](\text{PF}_6)$

Table 4.8: List of chemical shifts for the protons in $[Ir(ppy-COOEt)_2(bpp)](PF_6)$

	Protons	Hs	Chemical shift (ppm)	Type	J(Hz)
bpp	H6'	1	8.62-8.67	m	-
	H4'	1	8.62-8.67	m	-
	H3'	1	8.72	d	8.08
	H6	1	7.90-8.03	m	-
	H5	1	7.53	dd	7.64, 5.49
	H4	1	8.15-8.23	m	-
	H3	1	8.60	d	8.34
	H6''	1	8.55	dd	5.68, 1.89
	H5''	1	7.38	d	7.58
	H4''	1	7.81-7.86	m	-
	H3''	1	7.70	d	8.59
ppy-COOEt	H5(Ph1)	1	6.88	d	1.26
	H5(Ph2)	1	6.90	d	1.26
	H3(Ph1)		7.66	d	8.08
	H3(Ph2)	1	7.75	dd	6.44, 1.39
	H2(Ph1), H2(Ph2)	2	7.90-8.03	m	-
	H6(Py1)	1	7.75	dd	6.44, 1.39
	H6(Py2)	1	7.81-7.86	m	-
	H5(Py1), H5(Py2)	2	7.18-7.20	m	-
	H4(Py1), H4(Py2)	2	7.90-8.03	m	-
	H3(Py1), H3(Py2)	2	8.15-8.23	m	-

The two H5 protons couple with the protons at 7.66 ppm and 7.75 ppm. Therefore, the doublet at 7.66 ppm ($^3J = 8.08$ Hz) and at 7.75 ppm are assigned to H3 (Ph1) and H3 (Ph2) respectively. H3 (Ph1) and H3 (Ph2) couple with a multiplet at 7.90-8.03 ppm and therefore can be suggested that H1 (Ph1) and H2 (Ph2) are inside the multiplet at 7.90-8.03. The multiplet at 7.18-7.20 ppm is an overlapped proton signal of H5 in Py1 and Py2 (ppy-COOEt). This multiplet further couples with three signals. These assigned protons are H6 (Py1) at 7.75 ppm, H6 (Py2) at 7.81-7.86 ppm and H4 (Py1 and Py2) at 7.90-8.03 ppm. The multiplet at 7.90-8.03 ppm couples with the multiplet at 8.15-8.23 ppm and therefore two H3 protons (Py1 and Py2) overlap at 8.15-8.23 ppm. The doublet at 8.72 ppm ($^3J = 8.08$ Hz) is assigned to the H3' proton that further couples with the multiplet at 8.62-8.67 ppm. This multiplet integrates as two protons. The H6' and H4' overlap at 8.62-8.67 ppm. Now there are two doublets at 8.60 ppm and 8.55 ppm. The doublet at 8.60 ppm has a coupling constant of 8.34 Hz and therefore is assigned to the H3 proton (bpp). The doublet at 8.55 ppm has a coupling constant of 5.68 Hz therefore assigned to H6''. H3 (bpp) couples with a proton signal at 8.15-8.23 ppm assigned to H4 (bpp). The proton H4 (bpp) couples with the H5 (bpp) proton at 7.53 ppm ($^3J = 7.64$ Hz). H5 (bpp) therefore couples with the proton signal inside the multiplet at 7.90-8.03 ppm that is assigned to H6 (bpp). H6'' couples with the proton signal at 7.38 ppm. This proton signal at 7.38 ppm ($^3J = 7.58$ Hz) is assigned to the H5'' proton. H5'' couples with the proton signal at 7.81-7.86 ppm that is assigned to H4''. H4'' couples with an overlapped proton signal H3'' at 7.70 ppm.

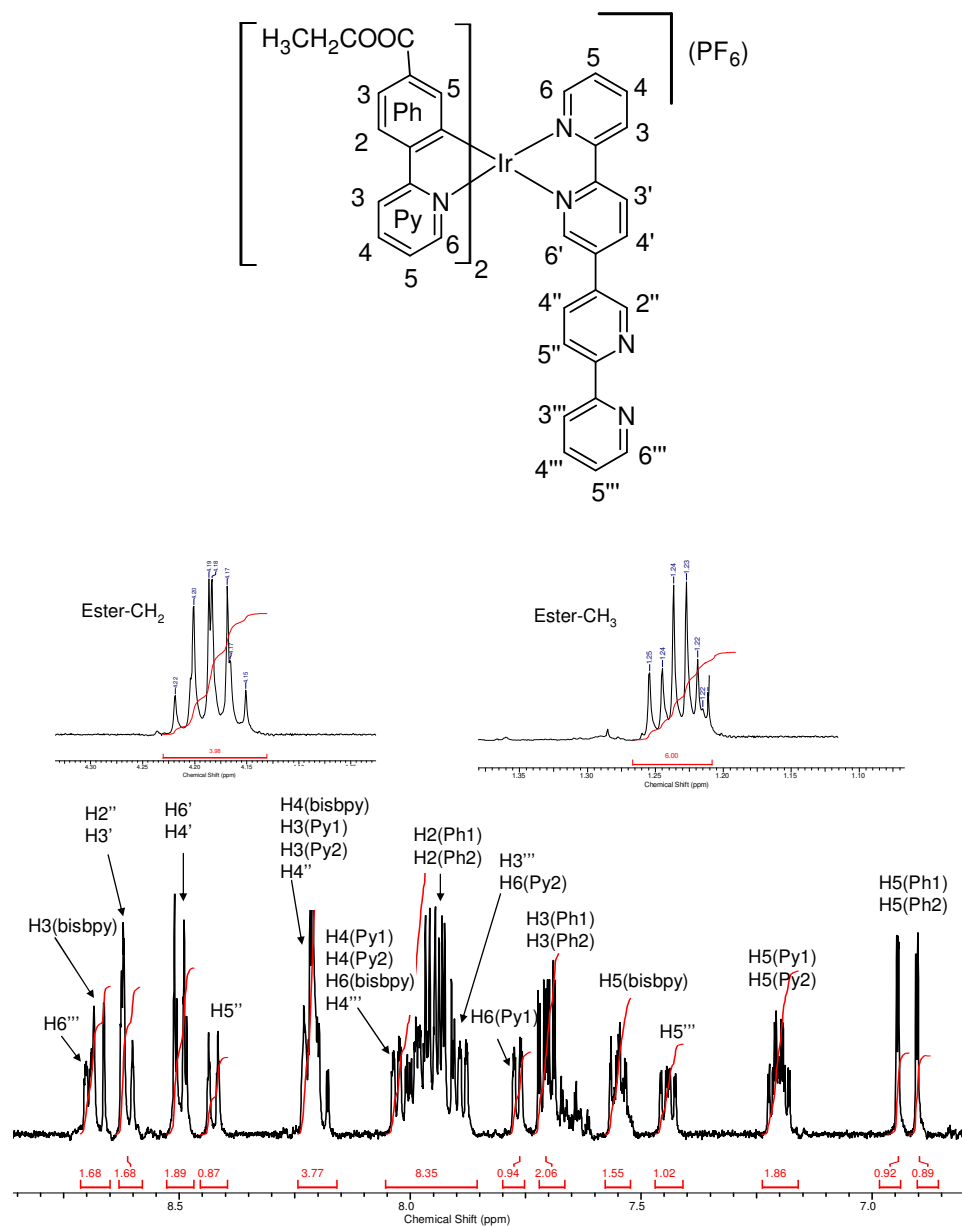
4.5.6. $[\text{Ir}(\text{ppy-COOEt})_2(\text{bisbpy})](\text{PF}_6)$ 

Figure 4.17: ^1H NMR ($\text{Acetonitrile-}d_6$, 400 MHz) of $[\text{Ir}(\text{ppy-COOEt})_2(\text{bisbpy})](\text{PF}_6)$

Figure 4.17 represents the ^1H NMR spectrum of $[\text{Ir}(\text{ppy-COOEt})_2(\text{bisbpy})](\text{PF}_6)$. The assignment of the protons in $[\text{Ir}(\text{ppy-COOEt})_2(\text{bisbpy})](\text{PF}_6)$ was made by a comparison of the ^1H NMR spectra of different iridium complexes shown in **Figure 4.18**. A list of the chemical shifts of all protons is tabulated in **Table 4.9**.

Table 4.9: List of chemical shifts for the protons in $[Ir(ppy-COOEt)_2(bisbpy)](PF_6)$

	Protons	Hs	Chemical shift (ppm)	Type	J(Hz)
bisbpy	H6	1	8.03	m	-
	H5	1	7.57	d	
	H4	1	8.17 - 8.24	m	-
	H3	1	8.65-8.71	m	-
	H6'	1	8.47 - 8.52	m	-
	H4'	1	8.47 - 8.52	m	-
	H3'	1	8.59 - 8.64	m	-
	H5''	1	8.43	d	8.08
	H4''	1	8.17 - 8.24	m	-
	H2''	1	8.59 - 8.64	m	-
	H6'''	1	8.65-8.71	m	-
	H5'''	1	7.44	dd	7.58,4.80
	H4'''	1	8.00	m	-
	H3'''	1	7.86 - 8.05	m	-
ppy-COOEt	H5(Ph1)	1	6.90	d	1.52
	H5(Ph2)	1	6.94	d	1.52
	H3(Ph1)	1	7.70	m	-
	H3(Ph2)	1	7.70	m	-
	H2(Ph1), H2(Ph2)	2	7.86-8.05	m	-
	H6(Py1)	1	7.77	d	5.81
	H6(Py2)	1	7.86-8.05	m	-
	H5(Py1), H5(Py2)	2	7.20-7.23	m	-
	H4(Py1), H4(Py2)	2	7.86-8.05	m	-
	H3(Py1), H3(Py2)	2	8.17-8.24	m	-

Bisbpy is also classified as an unsymmetrical bpy-based ligand. It can be assumed that the 5' position of bpy ligand is functionalised with another bipyridine unit. Therefore, the environments for both the ppy-COOEt ligands are different. As discussed above, the chemical shifts for ppy-COOEt ligands do not change significantly with the change of bpy based ancillary ligands. The protons in two ppy-COOEt ligands are assigned to H5 (Ph1) at 6.90 ppm, H5 (Ph2) at 6.94 ppm, H5 (Py1 and Py2) at 7.20-7.23 ppm, H3 (Ph1) at 7.70 ppm, H3 (Ph2) at 7.70 ppm ($^3J = 8.21$ Hz), H6 (Py1) at 7.77 ppm ($^3J = 5.81$ Hz), H6 (Py2) at 7.86-8.05 ppm, H2 (Ph1 and Ph2) at 7.86-8.05 ppm, H4 (Py1 and Py2) at 7.86-8.05 ppm and H3 (Py1 and Py2) at 8.17-8.24 ppm. The assignment of protons in bisbpy is difficult, especially the protons in the two central pyridine rings. The multiplet at 8.65-8.71 ppm is assigned to an overlapped proton signals of H6''' and H3 (bisbpy). H3 (bisbpy) shows coupling with the multiplet at 8.17 - 8.24 ppm therefore H4 (bisbpy) can be assigned to a part of this multiplet. The multiplet at 8.59 - 8.64 ppm is assigned to a combination of H3' and H2'' protons signals and the multiplet at 8.47 - 8.52 ppm is assigned to a combination of the proton signals of H4' and H6'. The doublet at 8.43 ppm ($^3J = 8.08$ Hz) is assigned to H5''. H4'' is assumed to be inside the multiplet at 8.17 - 8.24 ppm. The H5''' proton is assigned to the signal at 7.44 ppm ($^3J = 7.58$ Hz), H4''' at 8.00 ppm and H3''' at 7.86 - 8.05 ppm. The H5 proton is assumed to appear in the upfield region at 7.57 ppm. The signal at 8.03 ppm is assigned to H6. The ethyl ester CH₂ and CH₃ protons appeared as multiplets at 4.13-4.25 ppm and 1.2-1.26 ppm respectively.

The chemical shifts of the protons in the ppy-COOEt ligands do not change with the addition of a symmetrical bpy-based ancillary ligand within the coordination sphere of the iridium metal. The environment of the ppy-COOEt ligands does change slightly with the introduction of an unsymmetrical bpy ligand. However, this change in the chemical shift for the protons containing in two ppy-COOEt ligands are not significant (see **Figure 4.18**). This observation helped to interpret the proton signals of protons in ancillary bpy based ligands. **Figure 4.18** shows a comparison of the chemical shifts of the ppy-COOEt based protons in different iridium complexes.

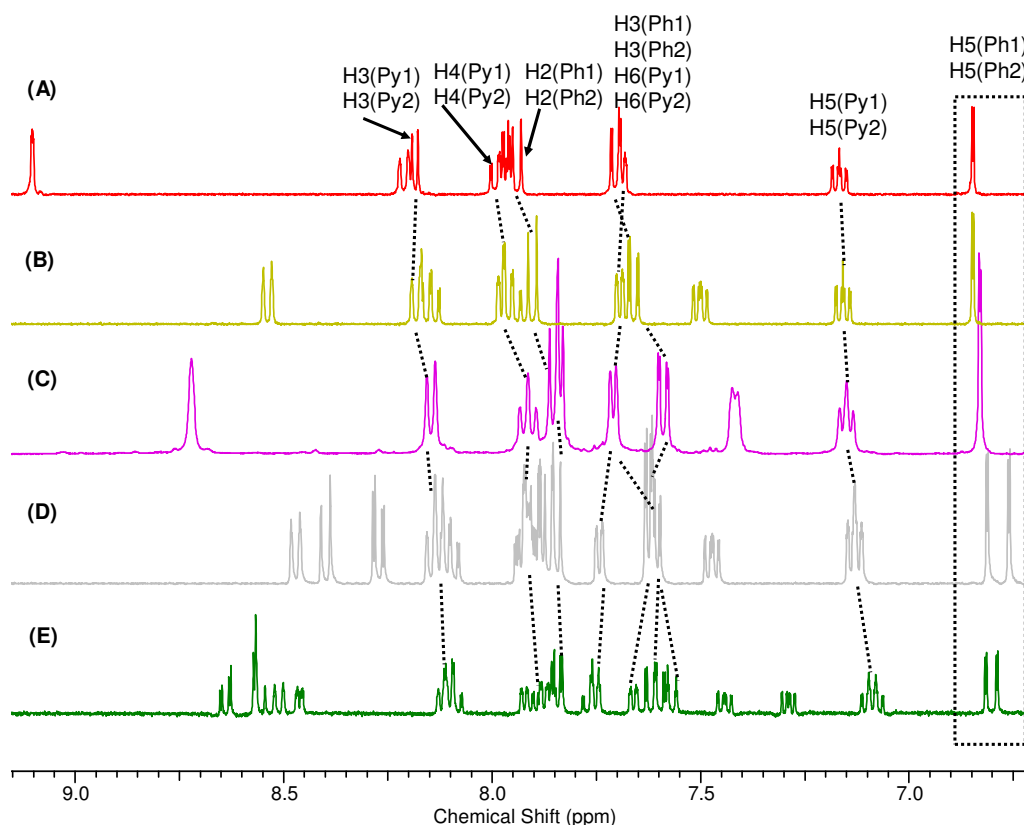


Figure 4.18: Chemical shifts of protons (ppy-COOEt) in different iridium complexes. ^1H NMR(Acetonitrile- d_3 , 400 MHz); (A) $[\text{Ir}(\text{ppy-COOEt})_2(\text{dceb})](\text{PF}_6)$; (B) $[\text{Ir}(\text{ppy-COOEt})_2(\text{bpy})](\text{PF}_6)$; (C) $[\text{Ir}(\text{ppy-COOEt})_2(\text{dpb})](\text{PF}_6)$; (D) $[\text{Ir}(\text{ppy-COOEt})_2(5\text{Brbpy})](\text{PF}_6)$; (E) $[\text{Ir}(\text{ppy-COOEt})_2(\text{bpp})](\text{PF}_6)$.

4.6. Electronic properties of monomeric iridium complexes

4.6.1 Absorption spectra

The absorption data for iridium complexes are summarised in **Table 4.10**. The absorption spectra were recorded in spectroscopic grade acetonitrile at room temperature. Absorption spectra of Ir(III) complexes are shown in **Figure 4.19**. For heteroleptic iridium complexes, there are ppy-COOEt and bpy based singlet excited states (S_1 and S_2) along with ppy-COOEt and bpy based MLCT states. It has been reported that the S_1 and S_2 states have mixed metal-to-ligand charge transfer (MLCT) and ligand(ppy)-to-ligand(phen) charge transfer (LLCT) character for the complex $[\text{Ir}(\text{ppy-F}_2)_2\text{Me}_4\text{phen}](\text{PF}_6)$.⁹⁰

Complex	Absorption (nm)/($\epsilon \times 10^3 \text{ M}^{-1} \text{ cm}^{-1}$)
$[\text{Ir}(\text{ppy-COOEt})_2(\mu\text{-Cl})]_2$	490/(0.96), 452/(4.74), 413/(5.91), 365/(7.94)
$[\text{Ir}(\text{ppy-COOEt})_2(\text{dpb})](\text{PF}_6)$	487/(0.72), 427/(4.29), 402/(4.94), 361/(7.67)
$[\text{Ir}(\text{ppy-COOEt})_2(\text{bpp})](\text{PF}_6)$	487/(0.98), 422/(4.38), 402/(4.99), 355/(9.56)
$[\text{Ir}(\text{ppy-COOEt})_2(\text{Br-bpy})](\text{PF}_6)$	485/(1.13), 422/(4.38), 402/(4.99), 348/(9.07)
$[\text{Ir}(\text{ppy-COOEt})_2(\text{bpy})](\text{PF}_6)$	495/(1.14), 428/(3.45), 404/(4.57), 356/(7.12)
$[\text{Ir}(\text{ppy-COOEt})_2(\text{dceb})](\text{PF}_6)$	489/(1.24), 420/(4.53), 382/(8.00), 353/(10.74)

Table 4.10: UV-Vis data of Ir(III) complexes. All spectra were obtained in acetonitrile at room temperature.

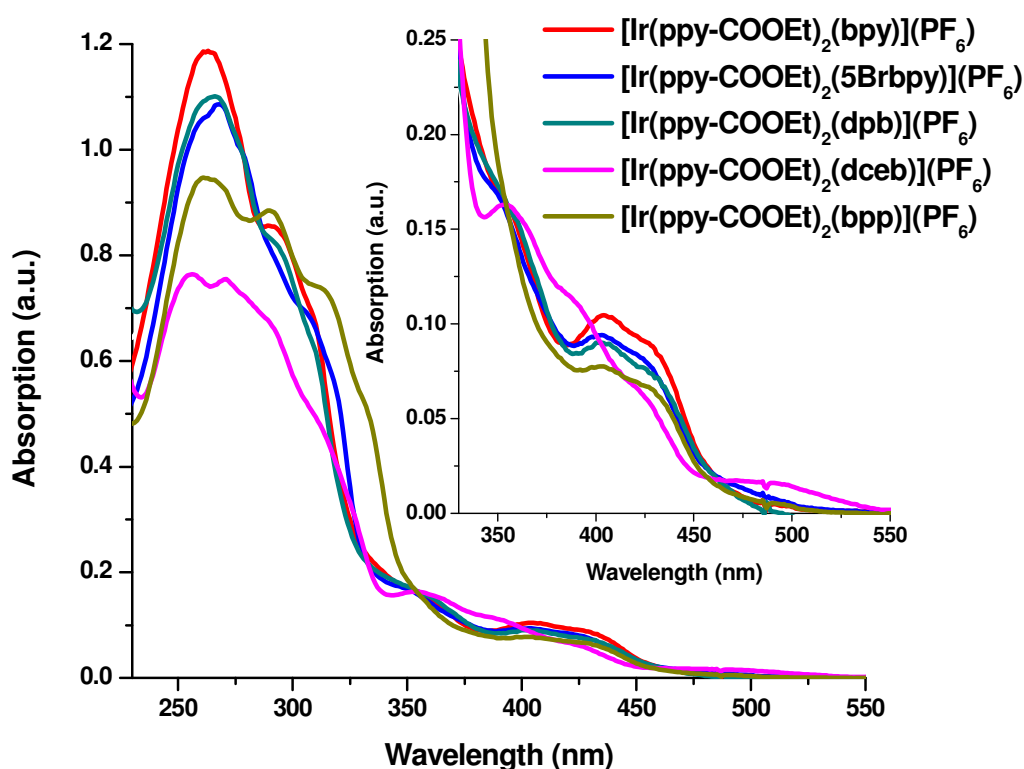


Figure 4.19: Absorption spectra of Ir(III) complexes. Acetonitrile was used as solvent to record the absorption spectra. Absorption spectra of all the compounds were recorded in acetonitrile at room temperature ($20 \pm 2^\circ \text{C}$).

The absorption bands for the iridium complexes in the UV region (< 300 nm) are attributed to the ligand-based transition ($\pi\text{-}\pi^*$) and the less intense absorption bands in the region greater than 300 nm are assigned to spin-allowed metal \rightarrow ligand charge transfer transitions ($^1\text{MLCT}$) and spin forbidden metal to ligand charge transfer ($^3\text{MLCT}$).^{39,40,91,92} A similar pattern of MLCT transition bands were observed in the absorption spectra for all $[\text{Ir}(\text{ppy-COOEt})_2(\text{L})](\text{PF}_6)$ type complexes, where L = bpy based ligands. It is worth noting that, $[\text{Ir}(\text{ppy-COOEt})_2(\text{dceb})](\text{PF}_6)$ has a different shape of absorption spectra in the region of 300-500 nm to that of the other Ir(III) complexes reported in this chapter. An absorption band for the complex $[\text{Ir}(\text{ppy-COOEt})_2(\text{dceb})](\text{PF}_6)$ was observed at 489 nm which is more intense compared to the corresponding absorption bands of other monomeric Ir(III) complexes. The dceb ligand has two carboxy ester groups which are electron withdrawing in nature and therefore, affects the MLCT transitions. For example, the analogous monomeric Ir(III) complex, $[\text{Ir}(\text{ppy})_2(\text{bpy})](\text{PF}_6)$ has a MLCT at 465 nm⁹³ whereas $[\text{Ir}(\text{ppy-COOEt})_2(\text{bpy})](\text{PF}_6)$ has the corresponding band at 495 nm. The Ir(III) complexes reported in this chapter contain carboxy ester functionalised phenyl pyridine peripheral ligands and bpy based ancillary ligand. The electron withdrawing effect of the carboxy ester groups results in a lowering of the π^* level of the phenyl pyridine and a red shift in the MLCT bands. For example, the $[\text{Ir}(\text{ppy})_2(\mu\text{-Cl})]_2$ complex has an absorption maximum at 434 nm with a shoulder at 484 nm⁸⁸ while the $[\text{Ir}(\text{ppy-COOEt})_2(\mu\text{-Cl})]_2$ complex has an absorption maximum at 452 nm with a shoulder at 490 nm. Therefore the absorption bands have been red shifted due to the introduction of the electron withdrawing carboxy ester groups.^{90,94,95} Further more, the bpy based ancillary ligands also contain electron withdrawing functional groups i.e., better π -accepting ligands such as 5Brbpy, dceb and dpb in the coordination sphere of the iridium metal centre. However, as it can be seen in the absorption spectra, there is no such variation in the MLCT transition bands for the iridium complexes containing different bpy based ancillary ligands.

4.6.2 Emission spectra and life time data

The emission and life time data for the iridium complexes are summarised in **Table 4.11**. Emission spectroscopy and lifetime were measured in nitrogen-purged dichloromethane solutions. Emission spectra of monomeric Ir(III) complexes are displayed in **Figure 4.20**.

Table 4.11: Emission and life time data of Ir(III) complexes

Complex	Emission ^a	Emission ^b	Life time ^{a, c}
	298K(nm)	298K(nm)	298K (ns)
[Ir(ppy-COOEt) ₂ Cl ₂]	540	541	122
[Ir(ppy-COOEt) ₂ (dpb)](PF ₆)	554	556	333
[Ir(ppy-COOEt) ₂ (bpy)](PF ₆)	568	572	333
[Ir(ppy-COOEt) ₂ (Br-bpy)](PF ₆)	564	571	333
[Ir(ppy-COOEt) ₂ (bpy)](PF ₆)	546	541	333
[Ir(ppy-COOEt) ₂ (dceb)](PF ₆)	619	622	250

a) Measured in nitrogen-purged dichloromethane, b) Acetonitrile, c) At room temperature. Emission spectra were recorded using a sample OD of ~ 0.15 A.U. and 350 nm as excitation wavelength.

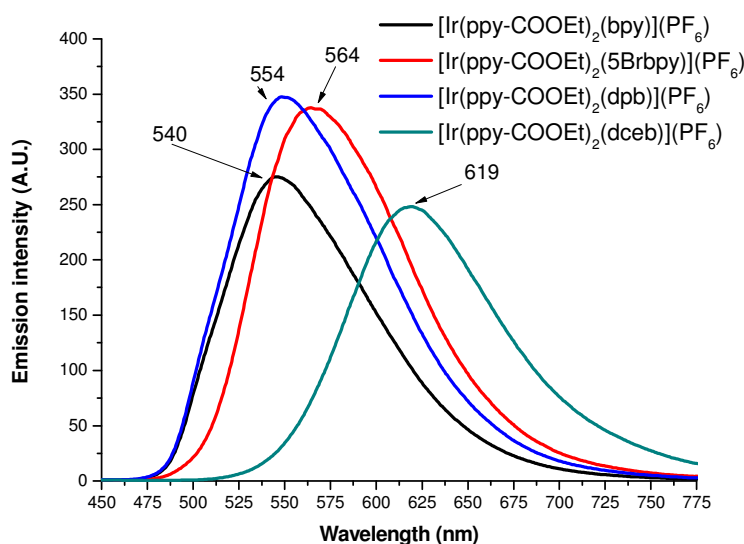


Figure 4.20: Emission spectra of monomeric Ir(III) complexes. Emission spectra were recorded in DCM using sample OD of ~ 0.15 A.U. and 350 nm as the excitation wavelength.

According to the literature, various electronic transitions are possible for the heteroleptic iridium complexes due to the mixing of different delocalised molecular orbitals ($^1\text{MLCT}$, $^3\text{MLCT}$, ^1LC , and ^3LC).^{92,96,97} Highly efficient phosphorescence was obtained for heteroleptic Ir(III) complexes from the low energy ancillary ligand due to inter ligand energy transfer (ILET) transition. It is suggested that the ILET is only possible when the triplet state of an ancillary ligand has a ^3LC state close in energy to the $^3\text{MLCT}$ state of the cyclometallated phenyl pyridine.^{50,92,98,99} Heteroleptic iridium complexes containing carboxy ester groups on the pyridine ring of the ppy ligand has been reported by Gratzel *et al.*. They observed a red shift in the emission wavelength.³⁹ They have suggested that introduction of a carboxy ester group strongly stabilises the LUMO level and slightly stabilises the HOMO level, ultimately reducing the gap between the HOMO and LUMO levels which is attributed to the red shift in the emission wavelength compared to the non-carboxy derivatised iridium complexes (see **Figure 4.21**).^{92,100} Lowry and Bernhard also commented on the lowest excited state of the heteroleptic iridium complexes. They suggested the possibility of intersystem crossing (ISC) to the energetically similar triplet states (^3LC and $^3\text{MLCT}$) and formation of an emissive, mixed (triplet) excited (T_1). Formation of the lowest T_1 emission state for heteroleptic iridium complexes suggested by Lowry and Bernhard is shown in **Figure 4.21**.

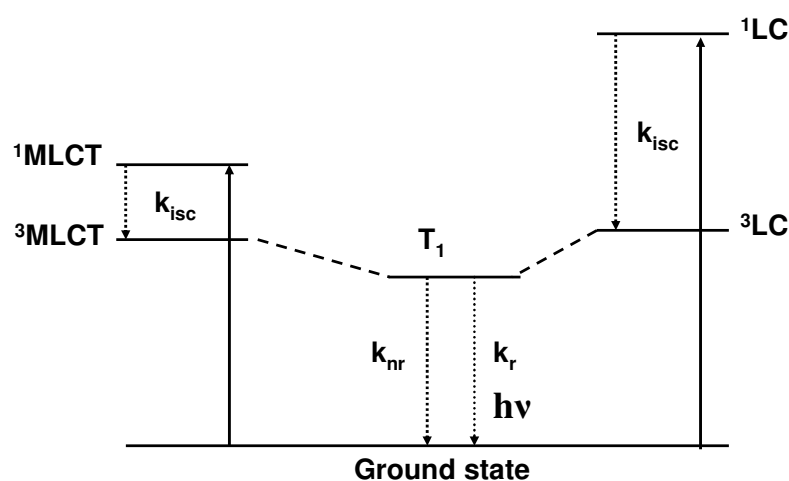


Figure 4.21: The energetic closeness and degree of overlap between $^3\text{MLCT}$ and ^3LC states results in the formation of a mixed lowest excited state (T_1). The excited molecule relaxes to the ground state through radiative (k_r) and nonradiative (k_{nr}) pathways.⁴⁰

As it can be seen in the emission spectra, different heteroleptic iridium complexes possess different emission wavelengths depending on the ancillary ligand attached, albeit it can not be inferred that the lowest emission state is potentially dominated by the ^3LC state of the ancillary bpy based ligand. For example, $[\text{Ir}(\text{COOEt})_2(\text{dceb})](\text{PF}_6)$ has a red shifted emission wavelength with a maximum at 619 nm whereas for $[\text{Ir}(\text{COOEt})_2(\text{bpy})](\text{PF}_6)$ emission maxima was at 540 nm. Excited-state properties of iridium(III) complexes can be tuned with deliberate functionalisation of the ligands through the use of different functional groups. The evolution of ^3LC (vibrationally structured, high-energy bands) and $^3\text{MLCT}$ character (structureless, low-energy bands) in the emission spectra are indicative of a mixed excited state.⁴⁰ In particular, the ancillary ligand structure with electronegative substituent such as carboxy ester (619 nm for dceb) and phosphonate group (564 nm for 5Brbpy) showed a negative inductive effect and profound influence on orbital energies. Electron-withdrawing groups stabilise the HOMO level by abstracting electron density from the metal $d\pi$ -orbitals.^{87,101-103} The position of these functional groups with respect to the coordinating carbon of a cyclometalating ligand as well as ancillary bpy based ligands will strongly influence the LFSE.¹⁰⁴ For example, electron-withdrawing groups at *meta* position to the coordination site (and donating groups *ortho* or *para* to this position) enhance the field strength of the ligand and also enhance the d-orbital splitting. However in this study, the cyclometalating and ancillary ligands were separately substituted with several electron-withdrawing groups such as COOEt, Br, and $\text{CH}_2\text{PO}_3\text{Et}_2$ for the purpose of strongly binding to the surface of semiconductors. Surprisingly, the dpb ancillary ligand (emission wavelength for the Ir(III) complex is 554 nm) has the minimum electronic effect on the emission wavelength compared to the bpy ligand (emission wavelength for the Ir(III) complex is 540 nm). However, dceb as an ancillary ligand has maximum electronic effect on the emission wavelength (619 nm). This difference has been attributed to the better mesomeric and inductive ability of the carboxy ester groups compared to the other functional groups. Therefore, it is crucial to consider the total impact of a functional group when designing Ir(III) complexes.

The lifetime data obtained for the monomeric Ir(III) complexes containing carboxy ester groups have a maximum lifetime of 333 ns. Literature reports consistently suggest that heteroleptic Ir(III) complexes have a mixed triplet emissive

state.^{40,92,105-107} The lifetime data for $[\text{Ir}(\text{ppy-COOEt})_2(\text{bpy})](\text{PF}_6)$ (333 ns) measured is almost compared to the lifetime of $[\text{Ir}(\text{ppy})_2(\text{bpy})](\text{PF}_6)$ (337.5 ns)¹⁰⁸ at room temperature. Other iridium complexes have comparatively similar lifetimes (333 ns) to $[\text{Ir}(\text{ppy})_2(\text{bpy})](\text{PF}_6)$ unless $[\text{Ir}(\text{ppy-COOEt})_2(\text{dceb})](\text{PF}_6)$ (250 ns). The nature of the excited state for the ester containing heteroleptic bis-cyclometalated iridium(III) complexes presented in this chapter can not be understood properly only with the excited state lifetime data and the emission wavelengths, and need electrochemical data and computational investigations such as density functional theory (DFT) calculations. It is worth noting that the excited state lifetimes did not significantly differ with the carboxy derivatisation on the cyclometallated ppy ligands, or with different bpy based ancillary ligands. The lifetime decay curves and corresponding kinetic fit curves were obtained for the monomeric heteroleptic iridium complexes and are shown in **Appendix A**.

4.7. Conclusion

This chapter introduces ligands containing the carboxy ester group in the heteroleptic monomeric iridium complexes. A new reaction procedure for the synthesis of ppy-COOEt was developed. This synthetic procedure was found less complicated and was complete in 30 minutes. A high yield for ppy-COOEt was obtained using this modified synthetic procedure. A modified synthetic procedure for synthesising the chloro-bridged iridium precursor complex containing carboxy ester groups was also developed. Ethoxy ethanol was not a suitable reaction solvent for synthesising $[\text{Ir}(\text{ppy-COOEt})_2(\text{Cl})]_2$ as it resulted in decomposition of the compound. A reaction study revealed that ethanol was a good solvent for this reaction, and a high yield (93%) was obtained using ethanol. A series of monomeric iridium complexes were synthesised using the literature reaction procedure (DCM/ethanol). A number of bpy based ancillary ligands were attached to the iridium metal centre to prepare heteroleptic monomeric iridium complexes. The ultimate aim of this chapter was to synthesise Ir-Pd and Ir-Pt heterodinuclear catalysts for photocatalytic hydrogen production from water. But, due to the synthetic difficulties with the ester containing iridium complexes, synthesis of the heterodinuclear complexes could not be attempted within the limited period of time.

These iridium mononuclear complexes were characterised using NMR spectroscopy and CHN analysis. The NMR study revealed that the protons of the ester groups in ppy-COOEt have a similar chemical shift in the ^1H NMR spectra. H3 and H3' protons in the metal coordinated dceb ligand were found farthest downfield because of the electron withdrawing effect of the neighbouring carboxy ester groups. However, the H6 proton was observed slightly upfield in the case of metal coordinated dpb ligand. It was also observed that the carboxy and the phosphonate ester groups appeared at different chemical shifts while both the ligands are coordinated to the iridium metal. The ester groups in the dceb ligand are shifted further downfield (4.5 ppm) than the phosphonate ester groups (4.35 ppm). However, the chemical shifts of the carboxy ester group in the ppy-COOEt were similar with the introduction of the different bpy based ancillary ligands.

Absorption and emission data were also recorded to understand the different electronic transitions and the lowest emission state of the heteroleptic iridium complexes containing carboxy ester groups. The lifetime values did not change with the introduction of the carboxy groups. However, the emission wavelengths did vary with the introduction of different bpy based ancillary ligands. For example, $[\text{Ir}(\text{ppy-COOEt})_2(\text{dceb})](\text{PF}_6)$ has the lowest emission wavelength among all the heteroleptic iridium complexes reported in this chapter. Lifetime data (~340 ns) and the emission spectra suggested that the lowest emissive state was a mixed triplet state. The effect of the carboxy ester groups and the associated bpy based ancillary ligands on the photophysical properties of the iridium complexes were studied in this chapter. From the study it was concluded that the emission wavelength for $[\text{Ir}(\text{ppy-COOEt})_2(\text{N}^{\wedge}\text{N})](\text{PF}_6)$ complexes was red shifted with the introduction of carboxy ester groups to the peripheral ppy ligands and electron withdrawing groups to the bpy based ancillary ligands.

4.8. Experimental

4.8.1. Materials and instrumental

All the solvents used for spectroscopy were of spectroscopic grade. $\text{IrCl}_3 \cdot 3\text{H}_2\text{O}$ and 4-(2-pyridyl) benzaldehyde used for the reactions below were

obtained from Sigma-Aldrich and used without further purification. All other solvents and reagents used were reagent grade. 4,4'-dicarboxyethyl-2,2'-bipyridine(dceb), 5-bromo-2,2'-bipyridine(5Brbpy), 2,2':5',2''-terpyridine(bpp) and 4,4'-diphosphonate-2,2'-bipyridine(dpb) were synthesised in previous chapters. Purification of compounds was carried out using neutral alumina (Al_2O_3 , 150 mesh sizes). ^1H NMR (400 MHz) and 2D COSY were recorded in deuteriated solvents (d_3 -acetonitrile, CDCl_3) on a Bruker AC400 NMR and AC600 NMR Spectrometer with TMS or residual solvent peaks as reference. XWIN-NMR processor and ACDLABS 12.0 NMR processor software were employed to process the free induction decay (FID) profiles. The H-H 2-D COSY NMR involved the accumulation of 128 FIDs of 16 scans. Elemental analyses (CHN) were carried out using Exador Analytical CE440 by the Microanalytical Department, University College Dublin, Ireland. UV-Vis absorption spectra were recorded on a Shimadzu 3100 UV-Vis/NIR spectrophotometer with interfaced to an Elonex PC575 desktop computer using 1-cm path length quartz cells. The detection wavelength was 190-900 nm. The ASCII data for every UV-Vis spectra were further processed using Microcal Origin 8 pro software. Emission spectra were recorded on a Perkin-Elmer LS0B luminescence spectrophotometer, and the excitation wavelength was set at 350 nm. All emission spectra were initially generated by Perkin-Elmer FL Winlab custom built software and further the ASCII data were processed by Microcal Origin 8 pro software. The optical densities of all the sample solution for the emission spectra and lifetime studies were approximately 0.1-0.2 A.U. at the excitation wavelength 355 nm. The lifetime experiments were carried out with Dr. Mary Pryce in the School of Chemical Sciences, DCU.

4.8.2. Organic ligands

4-(2-pyridyl)benzoic acid (ppy-COOH)

4-(2-pyridyl)benzoic acid (ppy-COOH) was synthesised following a modified literature procedure.¹⁰⁹ 2.94 g (73.5 mmol) of NaOH was dissolved in 50 cm^3 of water and the brown suspension of silver oxide was prepared by adding a solution of 6.32 g (37.22 mmol) of AgNO_3 solution in 50 cm^3 of water. The solution was stirred continuously during the addition of silver nitrate solution to complete the reaction. The brown semisolid mixture was then cooled in an ice bath. 2 g (10.91 mmol) of 4-

(2-pyridyl)benzaldehyde was added to the cooled reaction mixture with stirring. The procedure was modified by adding 10 cm³ of THF to the reaction mixture for complete dissolution of 4-(2-pyridyl)benzaldehyde. After 30 minutes, no more reactant particle was left to dissolve and a silver mirror appeared on the side of the conical flask. The reaction was completed in 30 minutes as followed by TLC. The black silver suspension was removed by suction filtration. The black residue was further washed with hot water to obtain maximum amount of product. The combined filtrate was acidified with aqueous HCl solution to precipitate out the product from the aqueous solution. The product was then collected by filtration. Yield: 90% (1.95 g, 9.81 mmol). ¹H NMR (400 MHz, DMSO-*d*₆) δ ppm 7.43 (dd, *J* = 7.52, 4.74 Hz, 1 H), 7.94 (dd, *J* = 7.77, 7.77 Hz, 1 H), 8.01 - 8.10 (m, 3 H), 8.17 - 8.27 (m, 2 H), 8.72 (dd, *J* = 6.57, 1.01 Hz, 1 H).

Ethyl 4-(2-pyridyl)benzoate (ppy-COOEt)

Esterification of 4-(2-pyridyl)benzoic acid was performed using a literature procedure.^{69,80} 1 g (5.02 mmol) of 4-(2-pyridyl)benzoic acid was converted to ethyl 4-(2-pyridyl)benzoate. Yield: 93% (1.06 g, 4.66 mmol). ¹H NMR (400 MHz, DMSO-*d*₆) δ ppm 1.35 (t, *J* = 7.07 Hz, 3 H), 4.35 (q, *J* = 7.07 Hz, 2 H), 7.43 (dd, *J* = 7.45, 4.80, 0.88 Hz, 1 H), 7.94 (td, *J* = 7.77, 1.89 Hz, 1 H), 8.04 - 8.10 (m, 3 H), 8.21 - 8.28 (m, 2 H), 8.72 (dd, *J* = 4.80, 0.76 Hz, 1 H).

4.8.3. Metal complexes

[Ir(ppy-COOEt)(μ-Cl)]₂·2H₂O

788 mg (2.64 mmol) of IrCl₃·3H₂O and 1.2 g (5.28 mmol) of ppy-COOEt were added to 30 cm³ EtOH and refluxed for 24 hours. The reaction mixture turned from dark brown to orange. The reaction solution was reduced to 2-5 cm³ by rotary evaporation and 50 cm³ water was added. A yellow precipitate was collected by filtration. The product was washed with water and diethyl ether, and further recrystallised from DCM/ethanol solution. Yield: 1.67 g (1.24 mmol, 93%). ¹H NMR (400 MHz, DMSO-*d*₆) δ ppm 1.16 (td, *J* = 7.14, 1.64 Hz, 12 H), 4.03 - 4.15 (m, 8 H), 6.28 (s, 2 H), 6.85 (s, 2 H), 7.42 (dd, *J* = 8.08, 1.77 Hz, 2 H), 7.47 (dd, *J* = 8.08, 1.77 Hz, 2 H), 7.62 (dd, *J* = 7.33, 7.33 Hz, 2 H), 7.72 (t, *J* = 7.20 Hz, 2 H), 7.89 (d, *J* = 8.34 Hz, 2 H), 7.94 (d, *J* = 8.08 Hz, 2 H), 8.13 (t, *J* = 8.46 Hz, 2 H), 8.22 (td, *J* = 7.77, 1.39 Hz, 2 H), 8.33 (d,

$J = 7.83$ Hz, 2 H), 8.42 (d, $J = 8.34$ Hz, 2 H), 9.57 (d, $J = 4.55$ Hz, 2 H), 9.87 (d, $J = 6.06$ Hz, 2 H). Elemental analysis of $\text{C}_{56}\text{H}_{48}\text{Cl}_2\text{Ir}_2\text{N}_4\text{O}_8 \cdot 2\text{H}_2\text{O}$; M.W. = 1400.40; Calc: C 48.17, H 3.75, N 4.01. Found: C 48.33, H 3.61 and N 3.78%.

[Ir(ppy-COOEt)₂(bpp)](PF₆)

75.35 mg (0.32 mmol) 2,5-di(2-pyridyl)pyridine (bpp) was dissolved in 30 cm³ 4:1 (ethanol: dichloromethane). 200 mg (0.15 mmol) of $[\text{Ir}(\text{ppy-COOEt})_2(\mu\text{-Cl})_2]$ in 10 cm³ dichloromethane was added very slowly to the reaction mixture. The reaction mixture was further refluxed for another 6 hours in the dark. The solvent was completely removed by rotary evaporation. 30 cm³ of water was added and sonicated for 10 minutes. The aqueous solution was filtered twice. A saturated aqueous solution of KPF₆ was added to the filtrate and stirred for 30 minutes. The aqueous layer was extracted with DCM. The product was further washed with diethyl ether. The crude product was further purified by recrystallisation from DCM/ethanol solution. Yield: 184.5 mg (0.18 mmol, 60%). ¹H NMR (400 MHz, Acetonitrile-*d*₃) δ ppm 1.23 (td, $J = 7.14, 1.14$ Hz, 7 H), 4.15 - 4.22 (m, 4 H), 6.88 (d, $J = 1.26$ Hz, 1 H), 6.90 (d, $J = 1.26$ Hz, 1 H), 7.18 (m, 2 H), 7.38 (dd, $J = 7.58, 4.80$ Hz, 1 H), 7.53 (dd, $J = 7.64, 5.49$ Hz, 1 H), 7.66 (dt, $J = 8.08, 1.01$ Hz, 1 H), 7.70 (td, $J = 8.59, 1.77$ Hz, 2 H), 7.75 (dd, $J = 6.44, 1.39$ Hz, 1 H), 7.81 - 7.86 (m, 2 H), 7.90 - 8.03 (m, 5 H), 8.15 - 8.23 (m, 3 H), 8.55 (dd, $J = 5.68, 1.89$ Hz, 1 H), 8.60 (d, $J = 8.34$ Hz, 1 H), 8.62 - 8.67 (m, 2 H), 8.70 - 8.75 (m, 1 H). Elemental analysis for $\text{C}_{34}\text{H}_{35}\text{F}_6\text{IrN}_5\text{O}_4\text{P}$; M.W.: 1024.96; Calc: C 50.49, H 3.45, N 6.85. Found: C 50.37, H 3.33 and N 6.56%.

[Ir(ppy-COOEt)₂(bisbpy)](PF₆)

Synthesis $[\text{Ir}(\text{ppy-COOEt})_2(\text{bisbpy})](\text{PF}_6) \cdot \text{H}_2\text{O}$ was carried out using the synthetic procedure for $[\text{Ir}(\text{ppy-COOEt})_2(\text{bpp})](\text{PF}_6)$. 69 mg (0.22 mmol) of bisbpy and 120 mg (0.09 mmol) $[\text{Ir}(\text{ppy-COOEt})_2(\mu\text{-Cl})_2] \cdot 2\text{H}_2\text{O}$ were reacted in 30 cm³ 4:1 (ethanol: dichloromethane). The reaction was carried out for 12 hour. The product was then purified by column chromatography using 1:9 DCM/Ethanol as eluent. Yield: 6% (11.9 mg, 0.01 mmol). ¹H NMR (400 MHz, Acetonitrile-*d*₃) δ ppm 1.21 - 1.27 (m, 6 H), 4.13 - 4.23 (m, 4 H), 6.90 (d, $J = 1.52$ Hz, 1 H), 6.94 (d, $J = 1.52$ Hz, 1 H), 7.20-7.23 (m, 2 H), 7.44 (dd, $J = 7.58, 4.80$ Hz, 1 H), 7.57 (d, 1 H), 7.70 (dd, $J = 8.21, 5.05$ Hz, 2 H), 7.77 (dd, $J = 5.81, 0.76$ Hz, 1 H), 7.86 - 8.05 (m, 8 H), 8.17 - 8.24 (m, 4 H),

8.43 (d, $J = 8.08$ Hz, 1 H), 8.47 - 8.52 (m, 2 H), 8.59 - 8.64 (m, 2 H), 8.65 - 8.71 (m, 2 H). Elemental analysis: Insufficient material.

[Ir(ppy-COOEt)₂(bpy)](PF₆)

[Ir(ppy-COOEt)₂(bpy)](PF₆) was synthesised using the synthetic procedure for [Ir(ppy-COOEt)₂(bpy)](PF₆). 100 mg (0.07 mmol) of [Ir(ppy-COOEt)(μ-Cl)]₂ and 25.23 mg (0.16 mmol) of bpy were reacted in 30 cm³ 4:1 (ethanol: dichloromethane). Yield: 53% (66.34 mg, 0.07 mmol). ¹H NMR (400 MHz, Acetonitrile-*d*₃) δ ppm 1.23 (t, $J = 7.20$ Hz, 6 H), 4.18 (q, $J = 7.07$ Hz, 4 H), 6.87 (d, $J = 1.26$ Hz, 2 H), 7.18 (dd, $J = 7.45, 5.94, 1.52$ Hz, 2 H), 7.52 (dd, $J = 7.71, 5.43, 1.01$ Hz, 2 H), 7.68 (dd, $J = 8.21, 1.64$ Hz, 2 H), 7.72 (dd, $J = 5.81, 0.76$ Hz, 2 H), 7.93 (d, $J = 8.08$ Hz, 2 H), 7.95 - 8.03 (m, 4 H), 8.13 - 8.23 (m, 4 H), 8.56 (d, $J = 8.08$ Hz, 2 H). Elemental analysis for C₃₈H₃₂F₆IrN₄O₄P, M.W.: 947.88. Calc: C 48.25, H 3.34, N 5.92. Found: C 48.22, H 3.34 and N 5.89%.

[Ir(ppy-COOEt)₂(5Br bpy)](PF₆).H₂O

[Ir(ppy-COOEt)₂(5Brbpy)](PF₆) was synthesised using synthetic procedure of [Ir(ppy-COOEt)₂(bpy)](PF₆). 610.23 mg (0.44 mmol) of [Ir(ppy-COOEt)(μ-Cl)]₂ and 232 mg (0.98 mmol) of 5Brbpy were reacted in 30 cm³ 4:1 (ethanol: dichloromethane). Yield: 41% (370 mg, 0.36 mmol). ¹H NMR (400 MHz, Acetonitrile-*d*₃) δ ppm 1.23 (t, $J = 7.20$ Hz, 6 H), 4.18 (qd, $J = 7.07, 4.29$ Hz, 8 H), 6.82 (s, 2 H), 6.88 (s, 2 H), 7.16 - 7.23 (m, 4 H), 7.54 (ddd, $J = 7.64, 5.49, 1.26$ Hz, 2 H), 7.64 - 7.71 (m, 6 H), 7.81 (dd, $J = 6.57, 1.52$ Hz, 2 H), 7.87 - 8.02 (m, 12 H), 8.13 - 8.24 (m, 6 H), 8.34 (dd, $J = 8.84, 2.27$ Hz, 2 H), 8.47 (d, $J = 8.34$ Hz, 2 H), 8.54 (d, $J = 8.08$ Hz, 2 H). Elemental analysis for C₃₈H₃₁BrF₆IrN₄O₄P.H₂O. M.W.: 1044.79. Calc: C 44.68, H 3.38, N 5.36. Found: C 43.79, H 2.78 and N 5.30%.

[Ir(ppy-COOEt)₂(dpb)](PF₆)

[Ir(ppy-COOEt)₂(dpb)](PF₆) was synthesised using the synthetic procedure for [Ir(ppy-COOEt)₂(bpy)](PF₆). 100 mg (0.07 mmol) of [Ir(ppy-COOEt)(μ-Cl)]₂ and 73 mg (0.16 mmol) of dpb were reacted in 30 cm³ 4:1 (ethanol: dichloromethane). Yield: 6% (10 mg, 0.008 mmol). ¹H NMR (400 MHz, Acetonitrile-*d*₃) δ ppm 1.08 - 1.25 (m, 18 H), 3.42 - 3.62 (m, 4 H), 3.95 - 4.12 (m, 8 H), 4.16 (q, $J = 7.07$ Hz, 4 H), 6.87 (d, $J = 1.52$ Hz, 2 H), 7.19 (t, $J = 6.32$ Hz, 2 H), 7.46 (d, $J = 5.31$ Hz, 2 H), 7.63 (dd, $J =$

8.08, 1.77 Hz, 2 H), 7.75 (d, $J = 5.56$ Hz, 2 H), 7.86 - 7.92 (m, 4 H), 7.96 (t, $J = 7.33$ Hz, 2 H), 8.19 (d, $J = 8.08$ Hz, 2 H), 8.76 (br. s., 2 H). Elemental analysis: Insufficient material.

[Ir(ppy-COOEt)₂(dceb)](PF₆)

[Ir(ppy-COOEt)₂(dceb)](PF₆) was synthesised using the synthetic procedure for [Ir(ppy-COOEt)₂(bpp)](PF₆). 100 mg (0.07 mmol) of [Ir(ppy-COOEt)(μ-Cl)]₂ and 48.51 mg (0.16 mmol) of dceb were reacted in 30 cm³ 4:1 (ethanol: dichloromethane). Yield: 50% (76.44 mg, 0.07 mmol). ¹H NMR (400 MHz, Acetonitrile-*d*₃) δ ppm 1.23 (t, $J = 7.07$ Hz, 6 H), 1.43 (t, $J = 7.07$ Hz, 6 H), 4.19 (q, $J = 7.07$ Hz, 4 H), 4.49 (q, $J = 7.07$ Hz, 4 H), 6.85 (d, $J = 1.77$ Hz, 2 H), 7.17 (dd, $J = 7.52, 5.87$ Hz, 2 H), 7.63 - 7.76 (m, 4 H), 7.94 (d, $J = 8.08$ Hz, 2 H), 7.95 - 8.03 (m, 4 H), 8.19 (dd, $J = 5.56, 0.76$ Hz, 2 H), 8.21 (d, $J = 7.83$ Hz, 2 H), 9.10 (dd, $J = 1.64, 0.63$ Hz, 2 H). Elemental analysis for C₄₄H₄₀F₆IrN₄O₈P, M.W.: 1092. Calc: C 48.48, H 3.70, N 5.14. Found: C 48.03, H 3.48, and N 4.93%.

4.9. References

-
- (1) Cook, T. R.; Dogutan, D. K.; Reece, S. Y.; Surendranath, Y.; Teets, T. S.; Nocera, D. G. *Chem. Rev.* **2010**, *110*, 6474-6502.
 - (2) Cline, E. D.; Bernhard, S. *Chimia* **2009**, *63*, 709-713.
 - (3) Herrero, C.; Lassalle-Kaiser, B.; Leibl, W.; Rutherford, A. W.; Aukauloo, A. *Coord. Chem. Rev.* **2008**, *252*, 456-468.
 - (4) Dempsey, J. L.; Esswein, A. J.; Manke, D. R.; Rosenthal, J.; Soper, J. D.; Nocera, D. G. *Inorg. Chem.* **2005**, *44*, 6879-6892.
 - (5) Chow, J.; Kopp, R. J.; Portney, P. R. *Science* **2003**, *302*, 1528-1531.
 - (6) Nazeeruddin, M. K.; Baranoff, E.; Grätzel, M. *Solar Energy* **2011**, *85*, 1172-1178.
 - (7) O'Regan, B.; Gratzel, M. *Nature* **1991**, *353*, 737-740.
 - (8) Grätzel, M. *J. Photochem. Photobiol. C: Photochem. Rev.* **2003**, *4*, 145-153.
 - (9) Campbell, W. M.; Burrell, A. K.; Officer, D. L.; Jolley, K. W. *Coord. Chem. Rev.* **2004**, *248*, 1363-1379.
 - (10) Polo, A. S.; Itokazu, M. K.; Murakami Iha, N. Y. *Coord. Chem. Rev.* **2004**, *248*, 1343-1361.

- (11) Nazeeruddin, M. K.; Klein, C.; Liska, P.; Grätzel, M. *Coord. Chem. Rev.* **2005**, *249*, 1460-1467.
- (12) Hammes-Schiffer, S. *Acc. Chem. Res.* **2009**, *42*, 1881-1889.
- (13) Hammes-Schiffer, S.; Hatcher, E.; Ishikita, H.; Skone, J. H.; Soudackov, A. V. *Coord. Chem. Rev.* **2008**, *252*, 384-394.
- (14) McConnell, I.; Li, G.; Brudvig, G. W. *Chem. Biol.* **2010**, *17*, 434-447.
- (15) Wenger, O. S. *Coord. Chem. Rev.* **2009**, *253*, 1439-1457.
- (16) Alstrum-Acevedo, J. H.; Brennaman, M. K.; Meyer, T. J. *Inorg. Chem.* **2005**, *44*, 6802-6827.
- (17) Hammes-Schiffer, S. *Acc. Chem. Res.* **1982**, *42*, 1881-1889.
- (18) Inagaki, A.; Akita, M. *Coord. Chem. Rev.* **2009**, *254*, 1220-1239.
- (19) Fihri, A.; Artero, V.; Razavet, M.; Baffert, C.; Leibl, W.; Fontecave, M. *Angew. Chem. Int. Ed.* **2008**, *47*, 564-567.
- (20) Rau, S.; Schäfer, B.; Gleich, D.; Anders, E.; Rudolph, M.; Friedrich, M.; Görls, H.; Henry, W.; Vos, J. G. *Angew. Chem. Int. Ed.* **2006**, *45*, 6215-6218.
- (21) DiSalle, B. F.; Bernhard, S. *J. Am. Chem. Soc.* **2011**, *133*, 11819-11821.
- (22) Metz, S.; Bernhard, S. *Chem. Commun.* **2010**, *46*, 7551-7553.
- (23) Tinker, L. L.; Bernhard, S. *Inorg. Chem.* **2009**, *48*, 10507-10511.
- (24) Curtin, P. N.; Tinker, L. L.; Burgess, C. M.; Cline, E. D.; Bernhard, S. *Inorg. Chem.* **2009**, *48*, 10498-10506.
- (25) Cline, E. D.; Adamson, S. E.; Bernhard, S. *Inorg. Chem.* **2008**, *47*, 10378-10388.
- (26) Goldsmith, J. I.; Hudson, W. R.; Lowry, M. S.; Anderson, T. H.; Bernhard, S. *J. Am. Chem. Soc.* **2005**, *127*, 7502-7510.
- (27) Gärtner, F.; Cozzula, D.; Losse, S.; Boddien, A.; Anilkumar, G.; Junge, H.; Schulz, T.; Marquet, N.; Spannenberg, A.; Gladiali, S.; Beller, M. *Chem. Eur. J.* **2011**, *17*, 6998-7006.
- (28) Merrifield, B. *Science* **1986**, *232*, 341-347.
- (29) Balkenhohl, F.; von dem Bussche-Hunnefeld, C.; Lansky, A.; Zechel, C. *Angew. Chem., Int. Ed.* **1996**, *35*, 2288.
- (30) Kassel, D. B. *Chem. Rev.* **2001**, *101*, 255.
- (31) Lebl, M. *J. Comb. Chem.* **1999**, *1*, 3.
- (32) Yamazaki, H.; Shouji, A.; Kajita, M.; Yagi, M. *Coord. Chem. Rev.* **2010**, *254*, 2483-2491.

- (33) Lalrempuia, R.; McDaniel, N. D.; Mueller-Bunz, H.; Bernhard, S.; Albrecht, M. *Angew. Chem., Int. Ed.* **2011**, *49*, 9765-9768, S9765/1-S9765/5.
- (34) Houghten, R. A.; Pinilla, C.; Blondelle, S. E.; Appel, J. R.; Dooley, C. T.; Cuervo, J. H. *Nature* **1991**, *354*, 84-88.
- (35) Ott, I.; Scharwitz, M.; Scheffler, H.; Sheldrick, W. S.; Gust, R. *J. Pharm. Biomed. Anal.* **2008**, *47*, 938-942.
- (36) Cawse, J. N. *Acc. Chem. Res.* **2001**, *34*, 213-218.
- (37) Church, T. L.; Andersson, P. G. *Coord. Chem. Rev.* **2008**, *252*, 513-531.
- (38) Tandon, P. K.; Sahgal, S.; Singh, A. K.; Gayatri; Purwar, M. *J. Mol. Catal. A: Chem.* **2005**, *232*, 83-88.
- (39) Baranoff, E.; Suarez, S.; Bugnon, P.; Bolink, H. J.; Klein, C.; Scopelliti, R.; Zuppiroli, L.; Grätzel, M.; Nazeeruddin, M. K. *ChemSusChem* **2009**, *2*, 305-308.
- (40) Lowry, M. S.; Bernhard, S. *Chem. Eur. J.* **2006**, *12*, 7970-7977.
- (41) Baranoff, E.; Yum, J.-H.; Graetzel, M.; Nazeeruddin, M. K. *J. Organomet. Chem.* **2009**, *694*, 2661-2670.
- (42) Evans, R. C.; Douglas, P.; Winscom, C. J. *Coord. Chem. Rev.* **2006**, *250*, 2093-2126.
- (43) Slinker, J. D.; Gorodetsky, A. A.; Lowry, M. S.; Wang, J.; Parker, S.; Rohl, R.; Bernhard, S.; Malliaras, G. G. *J. Am. Chem. Soc.* **2004**, *126*, 2763-2767.
- (44) Lowry, M. S.; Goldsmith, J. I.; Slinker, J. D.; Rohl, R.; Pascal, R. A.; Malliaras, G. G.; Bernhard, S. *Chem. Mater.* **2005**, *17*, 5712-5719.
- (45) Slinker, J. D.; Koh, C. Y.; Malliaras, G. G.; Lowry, M. S.; Bernhard, S. *Appl. Phys. Lett.* **2005**, *86*, 173506/1-173506/3.
- (46) Ren, X.; Kondakova, M. E.; Giesen, D. J.; Rajeswaran, M.; Madaras, M.; Lenhart, W. C. *Inorg. Chem.* **2010**, *49*, 1301-1303.
- (47) Ge, G.; Zhang, G.; Guo, H.; Chuai, Y.; Zou, D. *Inorg. Chim. Acta* **2009**, *362*, 2231-2236.
- (48) Beeby, A.; Bettington, S.; Samuel, I. D. W.; Wang, Z. *J. Mat. Chem.* **2003**, *13*, 80-83.
- (49) Coppo, P.; Plummer, E. A.; De Cola, L. *Chem. Comm.* **2004**, 1774-1775.
- (50) You, Y.; Park, S. Y. *J. Am. Chem. Soc.* **2005**, *127*, 12438-12439.
- (51) Rudmann, H.; Shimada, S.; Rubner, M. F. *J. Am. Chem. Soc.* **2002**, *124*, 4918.

- (52) Slinker, J.; Gorodetsky, A.; Parker, S.; Bernards, D.; Flores-Torres, S.; Abruna, H. D.; Houston, P. A.; Bernhard, S.; Malliaras, G. G. *Polym. Prepr. (Am. Chem. Soc., Div. Polym. Chem.)* **2004**, *45*, 163-168.
- (53) Bernhard, S.; Barron, J. A.; Houston, P. L.; Abruna, H. D.; Ruglovksy, J. L.; Gao, X.; Malliaras, G. G. *J. Am. Chem. Soc.* **2002**, *124*, 13624-13628.
- (54) Adachi, C. *J. Appl. Phys.* **2001**, *90*, 5048-5053.
- (55) Tang, C. *Appl. Phys. Lett.* **1987**, *51*, 913-918.
- (56) Tinker, L. L.; McDaniel, N. D.; Bernhard, S. *J. Mater. Chem.* **2009**, *19*, 3328-3337.
- (57) Coughlin, F. J.; Westrol, M. S.; Oyler, K. D.; Byrne, N.; Kraml, C.; Zysman-Colman, E.; Lowry, M. S.; Bernhard, S. *Inorg. Chem. (Washington, DC, U. S.)* **2008**, *47*, 2039-2048.
- (58) Zysman-Colman, E.; Slinker, J. D.; Parker, J. B.; Malliaras, G. G.; Bernhard, S. *Chem. Mater.* **2008**, *20*, 388-396.
- (59) Parker, S. T.; Slinker, J. D.; Lowry, M. S.; Cox, M. P.; Bernhard, S.; Malliaras, G. G. *Chem. Mater.* **2005**, *17*, 3187-3190.
- (60) Coughlin, F. J.; Westrol, M. S.; Oyler, K. D.; Byrne, N.; Kraml, C.; Zysman-Colman, E.; Lowry, M. S.; Bernhard, S. *Inorg. Chem.* **2008**, *47*, 2039-2048.
- (61) Plummer, E. A.; Hofstraat, J. W.; De Cola, L. *Dalton Trans.* **2003**, 2080-2084.
- (62) Neve, F.; Crispini, A.; Campagna, S.; Serroni, S. *Inorg. Chem.* **1999**, *38*, 2250-2258.
- (63) Oro, L. A.; Ciriano, M. A.; Pérez-Torrente, J. J.; Villarroja, B. E. *Coord. Chem. Rev.* **1999**, *193-195*, 941-975.
- (64) Gallagher, L. A.; Serron, S. A.; Wen, X.; Hornstein, B. J.; Dattelbaum, D. M.; Schoonover, J. R.; Meyer, T. J. *Inorg. Chem.* **2005**, *44*, 2089-2097.
- (65) Gillaizeau-Gauthier, I.; Odobel, F.; Alebbi, M.; Argazzi, R.; Costa, E.; Bignozzi, C. A.; Qu, P.; Meyer, G. J. *Inorg. Chem.* **2001**, *40*, 6073-6079.
- (66) Arachchige, S. M.; Brown, J.; Brewer, K. J. *J. Photochem. Photobiol. A: Chem.* **2008**, *197*, 13-17.
- (67) Tschierlei, S.; Karnahl, M.; Presselt, M.; Dietzek, B.; Guthmuller, J.; González, L.; Schmitt, M.; Rau, S.; Popp, J. *Angew. Chem. Int. Ed.* **2010**, *49*, 3981-3984.
- (68) Rau, S.; Walther, D.; Vos, J. G. *Dalton Trans.* **2007**, 915-919.

- (69) Sprintschnik, G.; Sprintschnik, H. W.; Kirsch, P. P.; Whitten, D. G. *J. Am. Chem. Soc.* **1977**, *99*, 4947-4954.
- (70) Gosmini, C.; Bassene-Ernst, C.; Durandetti, M. *Tetrahedron* **2009**, *65*, 6141-6146.
- (71) Coleridge, B. M.; Bello, C. S.; Ellenberger, D. H.; Leitner, A. *Tetrahedron Lett.* **2010**, *51*, 357-359.
- (72) Bolliger, J. L.; Frech, C. M. *Chem. Eur. J.* **2010**, *16*, 11072-11081.
- (73) Ackermann, L.; Potukuchi, H. K.; Kapdi, A. R.; Schulzke, C. *Chem. Eur. J.* **2010**, *16*, 3300-3303.
- (74) Kowalczyk, J. J.; Agbossou, S. K.; Gladysz, J. A. *J. Organomet. Chem.* **1990**, *397*, 333-346.
- (75) Hirano, M.; Hirai, M.; Ito, Y.; Tsurumaki, T.; Baba, A.; Fukuoka, A.; Komiya, S. *J. Organomet. Chem.* **1998**, *569*, 3-14.
- (76) Padilla-Tosta, M. E.; Manuel Lloris, J.; Martínez-Máñez, R.; Pardo, T.; Soto, J. *Inorg. Chim. Acta* **1999**, *292*, 28-33.
- (77) Travis, B. R.; Sivakumar, M.; Hollist, G. O.; Borhan, B. *Organic Letts.* **2003**, *5*, 1031-1034.
- (78) Chatterjee, D.; Mitra, A.; Shepherd, R. E. *Inorg. Chim. Acta* **2004**, *357*, 980-990.
- (79) Kuwabara, K.; Itoh, A. *Synthesis* **2006**, *2006*, 1949-1952.
- (80) Greenway, G. M.; Greenwood, A.; Watts, P.; Wiles, C. *Chem. Comm.* **2006**, 85-87.
- (81) Dixon, I. M.; Collin, J.-P.; Sauvage, J.-P.; Flamigni, L.; Encinas, S.; Barigelletti, F. *Chem. Soc. Rev.* **2000**, *29*, 385-391.
- (82) Sie, W.-S.; Jian, J.-Y.; Su, T.-C.; Lee, G.-H.; Lee, H. M.; Shiu, K.-B. *J. Organomet. Chem.* **2008**, *693*, 1510-1517.
- (83) Sie, W.-S.; Lee, G.-H.; Tsai, K. Y.-D.; Chang, I. J.; Shiu, K.-B. *J. Mol. Struct.* **2008**, *890*, 198-202.
- (84) Lo, K. K.-W.; Chan, J. S.-W.; Chung, C.-K.; Tsang, V. W.-H.; Zhu, N. *Inorg. Chim. Acta* **2004**, *357*, 3109-3118.
- (85) Tang, H.; Li, Y.; Wei, C.; Chen, B.; Yang, W.; Wu, H.; Cao, Y. *Dyes and Pigments* **2011**, *91*, 413-421.
- (86) Tinker, L. L.; Bernhard, S. *Inorg. Chem.* **2009**, *48*, 10507-10511.

- (87) Tamayo, A. B.; Alleyne, B. D.; Djurovich, P. I.; Lamansky, S.; Tsyba, I.; Ho, N. N.; Bau, R.; Thompson, M. E. *J. Am. Chem. Soc.* **2003**, *125*, 7377-7387.
- (88) Sprouse, S.; King, K. A.; Spellane, P. J.; Watts, R. J. *J. Am. Chem. Soc.* **1984**, *106*, 6647-6653.
- (89) Coughlin, F. J.; Westrol, M. S.; Oyler, K. D.; Byrne, N.; Kraml, C.; Zysman-Colman, E.; Lowry, M. S.; Bernhard, S. *Inorg Chem* **2008**, *47*, 2039-2048.
- (90) Bolink, H. J.; Cappelli, L.; Cheylan, S.; Coronado, E.; Costa, R. D.; Lardies, N.; Nazeeruddin, M. K.; Orti, E. *J. Mat. Chem.* **2007**, *17*, 5032-5041.
- (91) Schmid, B.; Garces, F. O.; Watts, R. J. *Inorg. Chem.* **1994**, *33*, 9-14.
- (92) You, Y.; Park, S. Y. *Dalton Trans.* **2009**, 1267-1282.
- (93) Ohsawa, Y.; Sprouse, S.; King, K. A.; DeArmond, M. K.; Hanck, K. W.; Watts, R. J. *J. Phys. Chem.* **1987**, *91*, 1047-1054.
- (94) Costa, R. D.; Viruela, P. M.; Bolink, H. J.; Ortí, E. *J. Mol. Str.: THEOCHEM* **2009**, *912*, 21-26.
- (95) Kessler, F.; Costa, R. D.; Di Censo, D.; Scopelliti, R.; Orti, E.; Bolink, H. J.; Meier, S.; Sarfert, W.; Gratzel, M.; Nazeeruddin, M. K.; Baranoff, E. *Dalton Trans.* **2012**, *41*, 180-191.
- (96) Liu, S.-J.; Zhao, Q.; Fan, Q.-L.; Huang, W. *Eur. J. In. Chem.* **2008**, *2008*, 2177-2185.
- (97) Dedeian, K.; Shi, J.; Forsythe, E.; Morton, D. C.; Zavalij, P. Y. *Inorg. Chem.* **2006**, *46*, 1603-1611.
- (98) You, Y.; Kim, K. S.; Ahn, T. K.; Kim, D.; Park, S. Y. *J. Phys. Chem. C* **2007**, *111*, 4052-4060.
- (99) Duan, H.-S.; Chou, P.-T.; Hsu, C.-C.; Hung, J.-Y.; Chi, Y. *Inorg. Chem.* **2009**, *48*, 6501-6508.
- (100) You, Y.; Seo, J.; Kim, S. H.; Kim, K. S.; Ahn, T. K.; Kim, D.; Park, S. Y. *Inorg. Chem.* **2008**, *47*, 1476-1482.
- (101) Lowry, M. S.; Hudson, W. R.; Pascal, R. A.; Bernhard, S. *J. Am. Chem. Soc.* **2004**, *126*, 14129-14135.
- (102) Lamansky, S.; Djurovich, P.; Murphy, D.; Abdel-Razzaq, F.; Kwong, R.; Tsyba, I.; Bortz, M.; Mui, B.; Bau, R.; Thompson, M. E. *Inorg. Chem.* **2001**, *40*, 1704-1711.

- (103) Lamansky, S.; Djurovich, P.; Murphy, D.; Abdel-Razzaq, F.; Lee, H.-E.; Adachi, C.; Burrows, P. E.; Forrest, S. R.; Thompson, M. E. *J. Am. Chem. Soc.* **2001**, *123*, 4304-4312.
- (104) Tsuzuki, T.; Shirasawa, N.; Suzuki, T.; Tokito, S. *Adv. Mater.* **2003**, *15*, 1455-1458.
- (105) Passaniti, P.; Browne, W. R.; Lynch, F. C.; Hughes, D.; Nieuwenhuyzen, M.; James, P.; Maestri, M.; Vos, J. G. *J. Chem. Soc., Dalton Trans.* **2002**, 1740-1746.
- (106) D. Beer, P.; Timoshenko, V.; Maestri, M.; Passaniti, P.; Balzani, V. *Chem. Commun.* **1999**, 1755-1756.
- (107) Maestri, M.; Sandrini, D.; Balzani, V.; Maeder, U.; Von Zelewsky, A. *Inorg. Chem.* **1987**, *26*, 1323-1327.
- (108) Garces, F. O.; King, K. A.; Watts, R. J. *Inorg. Chem.* **1988**, *27*, 3464-3471.
- (109) Campaigne, E.; LeSuer, W. M. *J. Am. Chem. Soc.* **1948**, *70*, 1555-1558.

Chapter 5

The Effect of water during the quantitation of formate in photocatalytic studies on CO₂ reduction in dimethylformamide

Chapter 5 describes the use of ion-chromatography to quantify the reduction products of CO₂ reduction following photocatalysis. A series of time and water concentration dependent experiments were carried out to investigate the formation of formate from 5:1 dimethylformamide (DMF)/triethylamine (TEA) and 5:1 dimethylformamide (DMF)/triethanolamine (TEOA) solutions. The experimental results suggest that aqueous solutions of DMF formed a significant amount of formate in the presence of organic bases like triethylamine and triethanolamine. Production of formate was further confirmed by IR and ¹³C NMR spectroscopy.

5.1. Introduction

In a search for new environmentally friendly energy sources, there is increasing interest in the development of solar driven photocatalytic systems capable of producing hydrogen from water, and also for the reduction of CO₂ into chemical fuels.¹⁻⁷ A wide range of both homogeneous and heterogeneous systems have been developed and their efficiency in the presence of sacrificial electron donors have been studied as a function of molecular component, sensitizer and catalyst.⁸⁻¹⁷ These studies have shown that based on the conditions and photocatalyst used a range of products, such as CO, methanol, methane and formate can be obtained. While the first three can be determined by gas chromatography, formate is usually measured in aqueous environments using techniques such as conductivity, titrations and ion chromatography. However no attention has been paid to the potential affect that sacrificial agents may have on these measurements. Sacrificial agents are present in high concentrations and acts as a strong base. Investigations focussed on the photocatalytic reduction of CO₂ in the presence of transition metal complexes have identified formate as one of the reduction products. Workers in the area typically evaluate catalyst efficiency in terms of “turnover number”; defined as the number of product molecules that are formed per catalyst molecule. In these studies dimethylformamide is regularly used as a solvent. The stability of solvents in such systems is crucial. The effect of elevated temperature upon DMF stability has been previously reported¹⁸ but since the majority of photochemical reactions are carried out at ambient temperature this issue is of limited importance. However, triethylamine (TEA) and triethanolamine (TEOA) are routinely used as sacrificial agents in these type of photocatalytic systems. Against this background it is important to consider the effect of a base on aqueous DMF, a reaction reported as early as 1970 by Buncel *et al.* who observed that the addition of 20 mM NaOH to DMF-water mixtures resulted in the liberation of dimethylamine and formate depending upon the relative amounts of water present.¹⁹ Later in 1998 Kankaanpera *et al.* extended this study to, dimethylacetamide and selected ureas.²⁰ More recently, Opstad *et al.* investigated the formation of relatively long-lived radicals when DMF and DMSO were treated with small amounts of bases (MeOK and EtOK).²¹

The present study evaluates the hydrolysis of DMF in the solvent systems which are typically used in reactions involving photochemical reduction of CO₂ and/or conditions used for the quantitation of the amounts of formate formed. Both TEOA and TEA are typically used as electron donors, and 5:1 (v/v) DMF/amine mixtures were prepared as model solvent systems (in the absence of catalyst, typically present at 10⁻⁴ M). Ion exchange chromatography has previously been applied to the determination of anions in selected solvents and so was used herein to quantify formate production in the solvent system (see later sections).²²⁻²⁴ The results obtained indicate that great care needs to be taken in the determination of formate levels in DMF/sacrificial agent/H₂O mixtures.

5.2. Experimental

5.2.1. Materials and sample preparation

Anhydrous dimethylformamide (DMF), triethanolamine (TEOA), triethylamine (TEA), sodium formate (HPLC grade), sodium carbonate, sodium bicarbonate, potassium nitrate, potassium nitrite, sodium bromide, sodium fluoride, potassium chloride and potassium acetate were purchased from Sigma-Aldrich and used without further purification. Deionised water was used for each experiment wherever needed. Each solution was prepared using volumetric glassware (volumetric flasks and volumetric pipettes). A stock solution of 5:1 DMF/TEA(v/v) and DMF/TEOA(v/v) were freshly prepared. The same stock solution was used to prepare different diluted samples (1-90%, v/v) prior to injection. Further, the diluted samples were injected to carry out time dependent study over a period of 24 h. All glassware was washed with aqua-regia prior to use.

5.2.2. Instrumentation

The experiment was carried out using a ICS-1500 (DIONEX). The Column specification is RFICTM IonPac[®] AS22 Analytical 4 × 250 mm (DIONEX) and the suppressor specification is as ASRS[®] 300 4-mm (DIONEX). The instrumentation is illustrated in the DIONEX ICS 1500 manual.²⁵ Aqueous solutions containing 4.5 M of Na₂CO₃ and 1.3 M of NaHCO₃ was used as eluent. The experiment was carried out

with a flow rate of 1.2 ml/min with 25 μ L injection volume and 31mA suppressor current. The column temperature was maintained at 30 °C. Fourier transform infrared (FT-IR) spectra were obtained with a Perkin Elmer Spectrum 100 FT-ATR using attenuated total reflection. ^{13}C NMR spectra were recorded using a Bruker Advance 600 NMR Spectrometer.

5.3. Ion chromatography and method validation

Typically ion chromatographic determination of anions in solvents requires a sample dilution step in the mobile phase or water prior to injection to improve the chromatography, particularly for weakly retained anions such as formate. Conveniently, in this work the addition of water as a pre-injection dilution step permitted the facile study of DMF hydrolysis in DMF/water mixtures containing organic bases. Before a comprehensive study of DMF hydrolysis was performed, preliminary method validation studies showed the method to be precise (% RSD: 1.33 % and <0.01 % for peak area and retention time respectively, $n = 8$) (**Figure 5.1** and **Table 5.1**), sensitive (LOD: 1.2×10^{-7} M formate, S/N: 2) (See **Figure 5.2**) with a linear range of 1.2×10^{-7} to 2×10^{-2} M (See **Figure 5.3** and **Table 5.2**). Selectivity was confirmed by adequately resolving formate from potentially interfering anions as shown in **Figure 5.4**.

5.3.1. Precision

Table 5.1: Area, retention times of formate solutions and percentage relative standard deviation of the peak areas.

Area of 0.6×10^{-4} (M) formate solution (μS)	Retention time(min)	%Relative standard deviation = 1.33
0.0783	3.426667	
0.0797	3.426667	
0.0800	3.426667	
0.0816	3.426667	
0.0807	3.426667	
0.0814	3.426667	
0.0806	3.426667	
0.0811	3.426667	

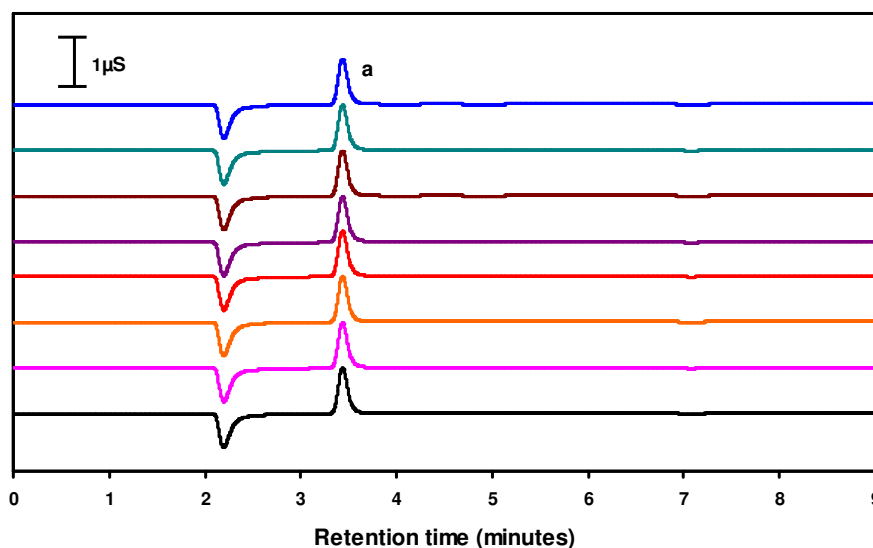


Figure 5.1: 6×10^{-5} (M) formate solution was injected for eight times to validate the reproducibility of the peak area of formate. a) formate (3.42 min).

The above experiment was carried out to verify the reproducibility of data. The retention time for formate in eight injections remained identical (3.42 min). The formate peak area for each injection was estimated. The relative standard deviation (1.33) of eight peak area is evident that the data are reproducible even at low concentrations of 6×10^{-5} M.

5.3.2. Sensitivity

Noise between 4.8-7 min: $N = 0.004245$, signal $S = 0.0213700$

Signal to noise ratio for 2×10^{-7} M formate solution is $S/N = 5$.

Sensitivity limit = 1.2×10^{-7} M formate solution. $S/N = 2$.

A sensitivity experiment was carried out to calculate the lowest limit of detection (LOD) of formate concentration. A standard solution of 2×10^{-7} M formate was injected. The noise was measured as 0.004245 (4.8-7 min) and response of formate peak was measured as 0.0213700. The signal to noise ratio (S/N) was 5 for 2×10^{-7} M formate solution. Therefore, the LOD was calculated as 1.2×10^{-7} M formate solution where the S/N is 2.

5.3.3. Linearity

Table 5.2: Area of formate peaks in different known aqueous formate solution.

Conc. (M)	Area (μSm)
2×10^{-7}	0.0022
1×10^{-6}	0.0031
2×10^{-6}	0.0043
1×10^{-5}	0.0238
2×10^{-5}	0.0491
1×10^{-4}	0.2553
2×10^{-4}	0.5256
1×10^{-3}	2.9983
1×10^{-2}	28.9993
2×10^{-2}	58.0001

Linear range is 1.2×10^{-7} M to 2×10^{-2} M.

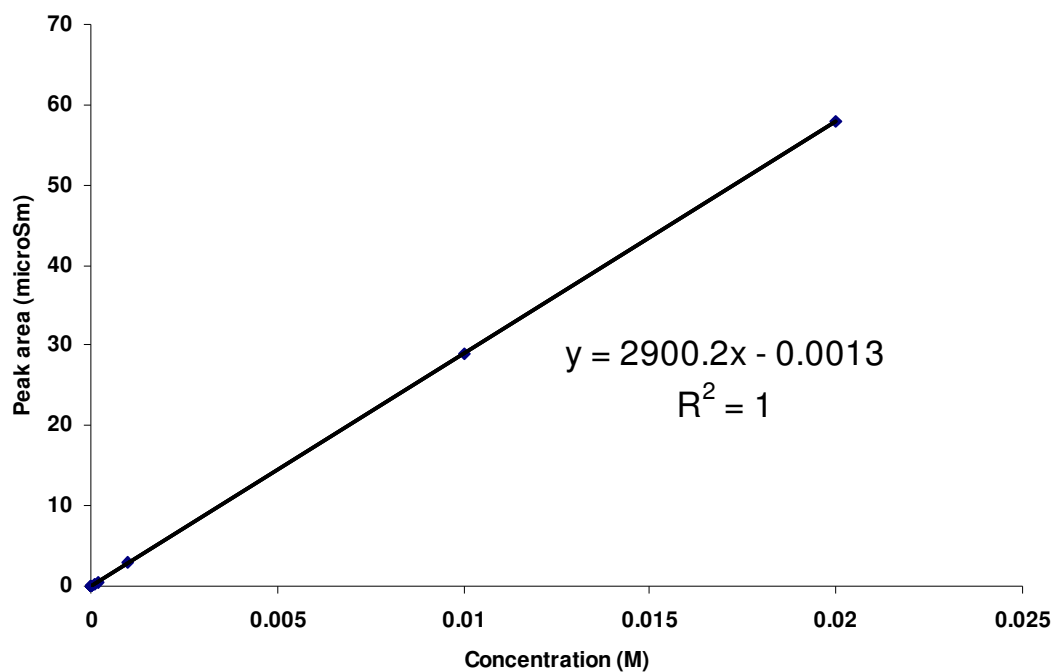


Figure 5.3: Linearity curve for standard formate concentrations.

Linear equation: $y = 2900.2x - 0.0013$; $R^2 = 1$. Concentration of formate in DMF/TEA/water and DMF/TEOA/water were calculated as peak area of formate divided by the slope of the calibration curve.

5.3.4 Selectivity

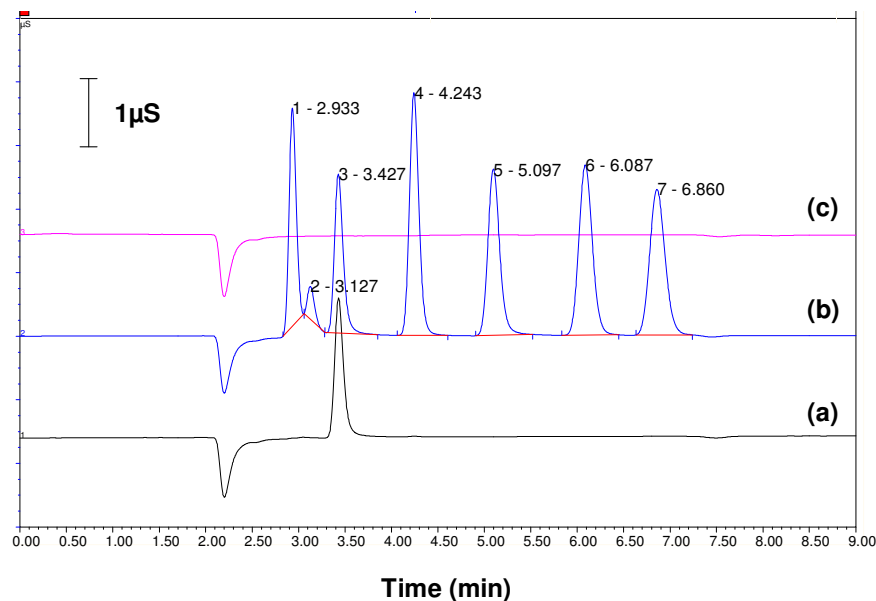


Figure 5.4: Comparison of chromatograms for selectivity study. a) formate b) mix anions c) water 1) fluoride (2.93 min) 2) acetate (3.12 min) 3) formate (3.42 min), 4) chloride (4.24 min) 5) nitrite (5.09 min), 6) nitrate (6.08 min) and 7) bromide (6.86 min). Concentration of all the ions are 10^{-4} M.

The above experiment (**Figure 5.4**) was carried out to identify the formate peak from other interfering anions. Seven other aqueous solutions containing seven different anions were injected separately, and a mixture of anions also. It was possible to assign all the peaks in the mixture by comparing the chromatogram of each anion separately. It was possible to distinguish the formate anion from the other anions present.

5.4. Results and discussion

5.4.1. Ion chromatography

Intuitively, a dilution of the sample with water would be expected to result in decreased response for the analyte anion proportional to the dilution factor however in this work the opposite was observed. Another important point is that sample preparation (typically a dilution step) was often performed several hours before injection, in instances where many samples are queued for injection in an autosampler. Water was added to individual 5:1 DMF/TEOA solvent mixtures prior to injection at levels of 0, 1, 2, 5, 10, 30, 50, 75, 85 and 90 % v/v. The resulting samples were injected after fixed periods of time of 0 minutes, 2, 5, 8 and 24 hours and levels of formate quantified against a calibration curve.

As illustrated in **Figure 5.5** and **Figure 5.6**, formate concentrations increased both with increasing concentration of water especially with water concentrations greater than 30 vol% and less than 80% with time (See **Figure 5.7**). Concentrations of water < 30 vol% resulted in relatively modest variations in formate levels (10^{-4} M) whereas >30 vol% resulted in significant increases with the rate of formate production generally increasing with water content and time. For example, after diluting a DMF/TEOA sample 50 % with water, formate levels increased from its baseline level of 10^{-5} M to 1.88×10^{-4} M after 2 hours and 4.29×10^{-4} M after 8 hours, representing a 10-fold increase in formate levels. The addition of 75 % water increased formate levels to 4.35×10^{-4} M after 2 hours and 1.16×10^{-3} M after 8 hours, representing a 40-fold increase.

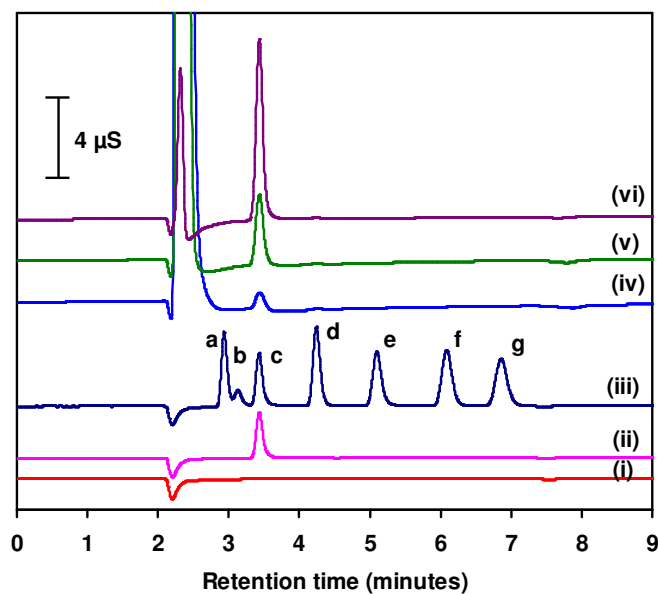


Figure 5.5: Increase in formate levels with water concentration for 5:1 DMF/TEOA solutions stored for 2 hours. (i) blank: water, (ii) 10^{-4} M formate, (iii) standard 10^{-4} M anion mix, (iv) DMF/TEOA + 30 vol% water, (v) DMF/TEOA + 50 vol% water, (vi) DMF/TEOA + 75 vol% water. Peak assignment: (a) fluoride, (b) acetate, (c) formate, (d) chloride, (e) nitrite, (f) nitrate, (g) bromide. The void peak corresponds to water and all un-retained cations (such as TEOA, TEA and analyte counter ions).

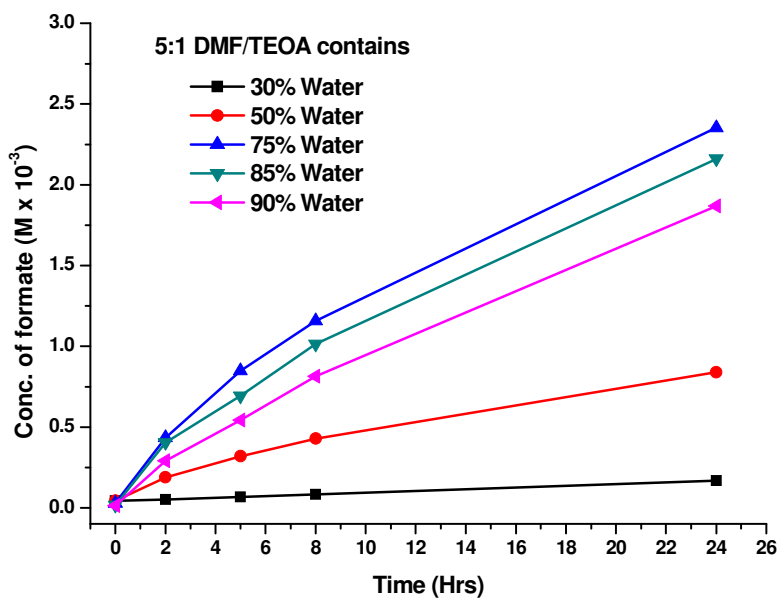


Figure 5.6: The effect of time and water concentration (30-90%)(v/v) on the formate concentration in a 5:1 DMF/TEOA solution.

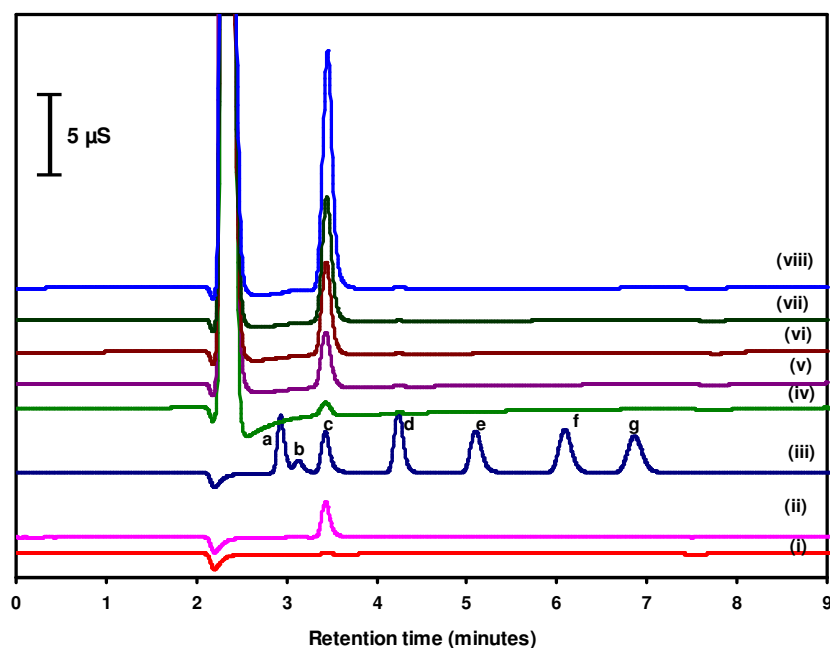


Figure 5.7: Increase in formate levels with time for 5:1 DMF/TEOA containing 50 vol% water. (i) blank: water, (ii) 10^{-4} M formate, (iii) standard 10^{-4} M anion mix, (iv) 0 hours, (v) 2 hours, (vi) 5 hour, (vii) 8 hour, (viii) 24 hour. The void peak corresponds to water and all un-retained cations (such as TEOA, TEA and analyte counter ions).

The formation of formate in DMF/water mixtures is mediated by the presence of the organic base which was confirmed by injecting 30:70 DMF/water in the absence of either TEOA or TEA at different times over a 24 hour period. The peak area for baseline levels of formate already present in the aqueous DMF remained constant as shown in **Figure 5.8**, most likely since a source of OH^- anions (organic base) was absent. It is highly unlikely that significant amounts of formate are formed on the column since the peak areas obtained are independent of the flow rate used. DMF and 5:1 DMF/TEOA were also injected directly, without dilution, to verify the presence of formate and baseline levels of up to 10^{-4} M of formate were found as shown in **Figure 5.8** and **5.9** under these conditions.

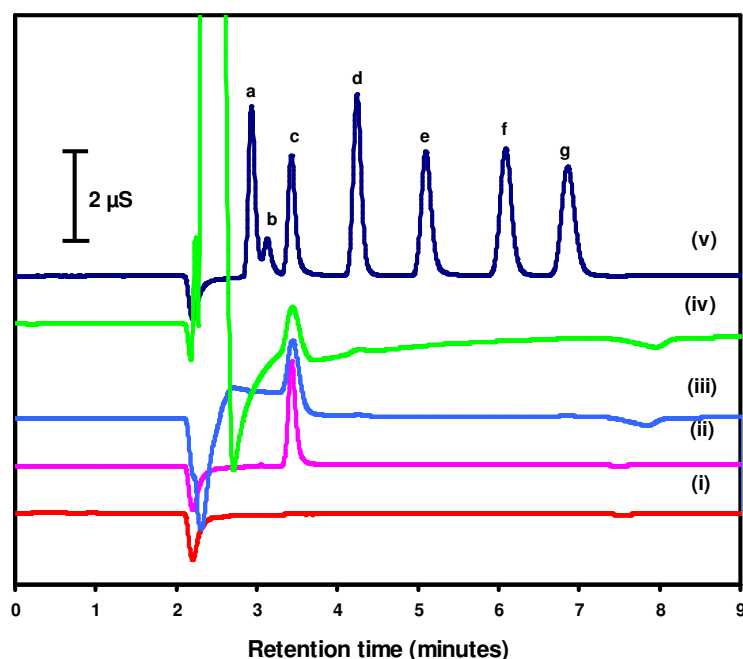


Figure 5.8: Determination of formate in undiluted DMF and undiluted 5:1 DMF/TEOA injected immediately after preparation (time = 0 min) (i) water, (ii) 10^{-4} M formate, (iii) DMF (iv) 5:1 DMF/TEOA, (v) anion standard solution in water. Peak assignments: (a) fluoride, (b) acetate, (c) formate, (d) chloride, (e) nitrite, (f) nitrate, (g) bromide. The void peak corresponds to water and all unretained cations (such as TEOA, TEA and analyte counter ions).

The shape (-ve and +ve) of the chromatogram in the region of 2-3 min retention time differs for the base line in chromatograms for pure DMF (iii) and DMF/TEOA mixture (iv). All the desorption/absorption at 2.2 min is the void peak (water), and this dip corresponds to the time taken for the required solutes to elute from the column.²²⁻²⁴ DMF which is an organic solvent which possibly creates an different aqueous environment for the detector. The increased positive shape in the region of ~2 minutes is apparently due to the solvent effect of DMF. In the case of DMF/TEOA mixture (iv), the peak shape for chromatogram at 2-3.3 min retention time is also possibly due to combined organic solvent effect (DMF and TEOA) in the conductivity detection. Chromatograms for DMF and DMF/TEOA indicate that the formate level is 10^{-4} M, which is present in the DMF or may be formed from the hydrolysis of DMF under basic conditions (The eluent is a aqueous $\text{NaCO}_3/\text{NaHCO}_3$ buffer), while passing through the column (3.4 min, retention time of formate). There

is a potential difficulty in the detection of such a trace level of formate concentration in organic solvents by ion chromatography without diluting the sample with water.²² Therefore, based on the above two predictions, 10^{-5} to 10^{-4} M formate can be considered as base line concentration in the quantitation of formate level in the samples.

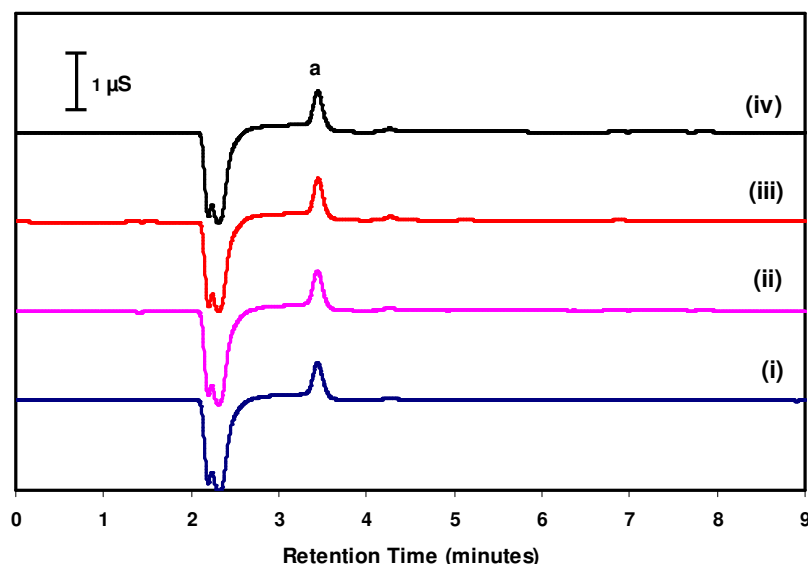


Figure 5.9: Effect of time on formate levels in DMF containing 70 % (v/v) water. (i) 0 hour (ii) 30 sec (iii) 3 hour (iv) 24 hour. Peak assignments: (a) formate. This figure demonstrates that formate (peak a) forms in the absence of base, and the amount of it remained consistent over the time period 0-24 hrs.

The above experiment (**Figure 5.9**) was performed to verify whether the hydrolysis of DMF takes place in the absence of organic base like triethanolamine or triethylamine. Aqueous solutions of DMF were injected at various time intervals (0, 30 min, 3 hours and 24 hours), and the amount of formate (a, 3.42 min) in the DMF/water mixture did not change with time. This indicates that the presence of base is a requisite for the formation of formate in these experiments.

Triethylamine has also been used as an electron donor in the photoreduction of CO_2 and therefore it is pertinent to study its role in the hydrolysis of DMF leading to erroneously high levels of formate being produced which affects turnover numbers values for the product. Quantitative determination of formate in DMF/TEA mixtures

incorporating < 30 vol% water was difficult due to broad chromatographic peaks and so concentrations of water were restricted to 50 vol% and higher.

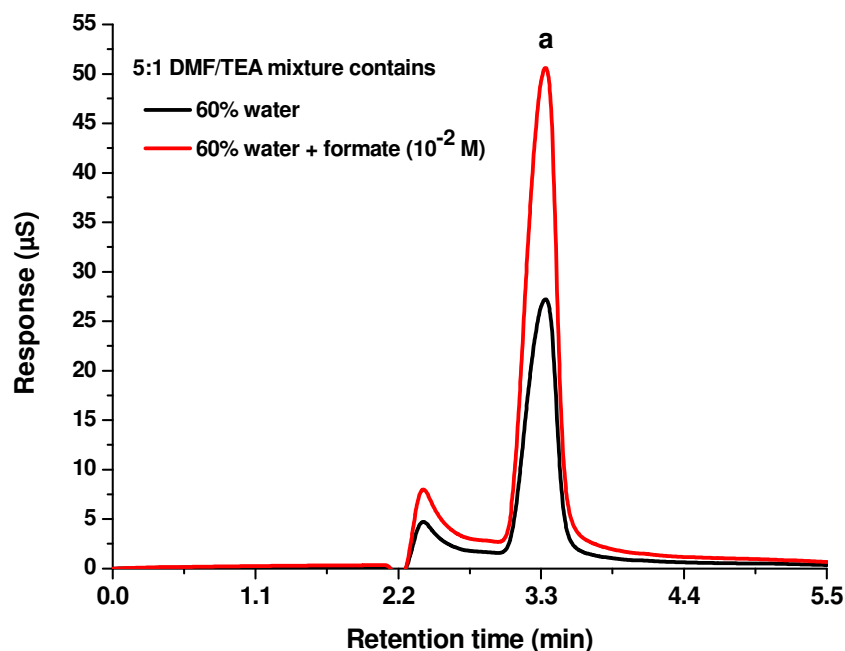


Figure 5.10: Spiking experiment for the confirmation of formate peak was recorded using 5:1 DMF/TEA mixture after 30 min of time. a) 3.33 min (formate).

Figure 5.10 shows a thirty minute old 5:1 DMF/TEA mixture including 60 vol% water, and spiked with formate. An increase in peak area after adding a known formate concentration (Spiking experiment) permitted subsequent unequivocal quantitation of formate from external calibration curves. The retention time of formate in DMF/TEA/water is shifted to 3.33 min as opposed to the standard formate solution where the peak was observed at 3.42 min. This spiking experiment was essential to verify whether the peak at 3.33 retention time is formate. The chromatograms (See **Figure 5.10**) clearly indicate that the peak at 3.33 min is formate in the DMF/TEA/water mixture. The reason for shifting the retention time of formate may be due to the combined solvent effect of DMF and TEA. DMF and TEA may facilitate the formate ion to elute at a faster rate from the column. The strange peak shape in the region between 2.2-3.2 min is also possibly due to combined solvent effect of DMF/TEA. Both TEOA and TEA have markedly different K_b values of 5.78×10^{-7} and 5.18×10^{-4} respectively. Equimolar concentrations of TEA relative to

TEOA should lead to greater OH^- production since TEA is the stronger base, resulting in increased DMF hydrolysis as described previously.

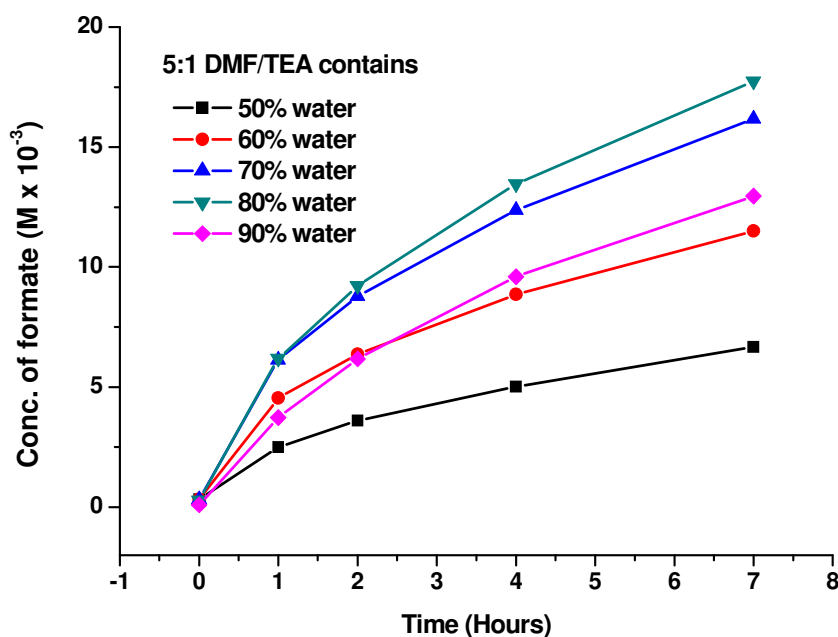


Figure 5.11: The effect of time and water concentration (50-90%)(v/v) on the formate concentration in a 5:1 DMF/TEA solution.

Figure 5.11 shows that formate levels increased both with increased water content (up to 80%) and also increased with time. As much as 10^{-2} M formate was produced from a 5:1 DMF/TEA /water mixture containing 80 vol% water prepared 7 hours prior to injection. It is possible to determine the relative rate of formate production (See **Figures 5.12** and **5.13**). For example, 1.88×10^{-4} M formate was formed in DMF/TEOA containing 50 vol% water after two hours whereas when the relatively weak organic base TEOA was replaced with the stronger base TEA, formate production increased to 3.61×10^{-3} M within two hours.

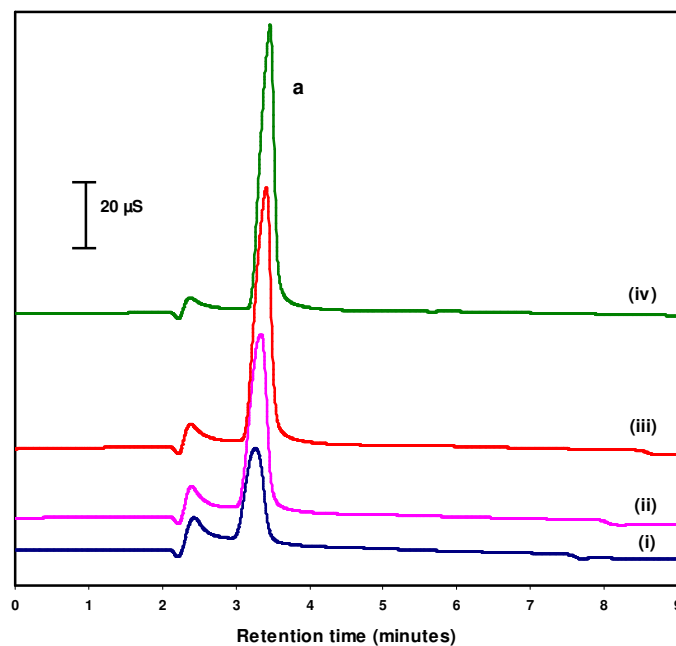


Figure 5.12: Formate levels with water concentration for 5:1 DMF/TEA solutions stored for 1 hour. (i) 50 vol% water (2.50×10^{-3} M), (ii) 60 vol% water (4.54×10^{-3} M), (iii) 70 vol% water (6.13×10^{-3} M), (iv) 80 vol% water (6.18×10^{-3} M). Peak assignment: (a) formate.

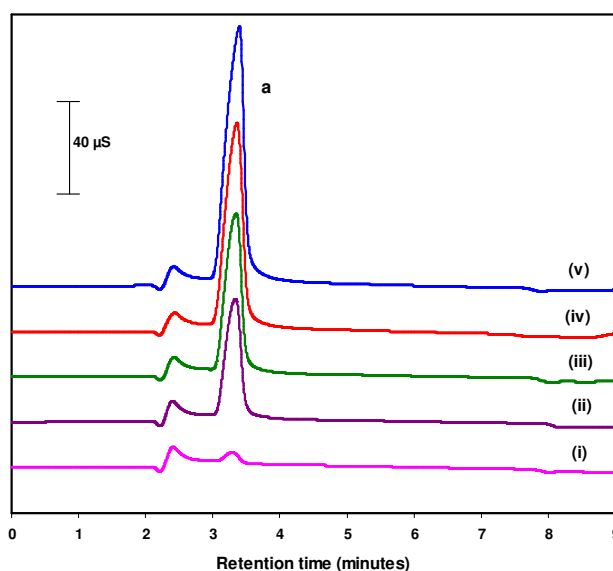


Figure 5.13: Increase in formate levels with time for 5:1 DMF/TEA solutions containing 60 vol% water. (i) 0 hours (0.32×10^{-3} M), (ii) 1 hour (4.54×10^{-3} M), (iii) 2 hours (6.36×10^{-3} M), (iv) 4 hours (8.86×10^{-3} M), (v) 7 hours (11.49×10^{-3} M). Peak assignment: (a) formate.

The conductivity response observed in the region 2.3-2.6 minutes might be due to the presence of TEA as no such response was observed for 70% water content in DMF (See **Figure 5.9**). Further, the concentration of TEA decreases with an increase in water content in the DMF/TEA mixture (see **Figure 5.12**) but remains identical with the increase in time (see **Figure 5.13**).

5.4.2. NMR spectroscopy

Further verification of the presence of formate in aqueous DMF mixtures incorporating an organic base was confirmed by ^{13}C NMR spectroscopy. The spectrum of DMF and a sample of 5:1 DMF/TEOA containing 75 % water is shown in **Figure 5.14** and in **Figure 5.15** respectively. Peaks for DMF, TEOA and both degradation products of DMF hydrolysis (formate and dimethylamine) are clearly visible. ^{13}C NMR was again used to confirm the presence of formate in an aqueous DMF/TEA mixture. **Figure 5.16** shows characteristic peaks for formate (170.6 ppm) and dimethylamine (35.5 ppm) as well as DMF (164.8 ppm, 36.9 ppm and 31.4 ppm) and TEA (46.0 ppm and 9.1 ppm).

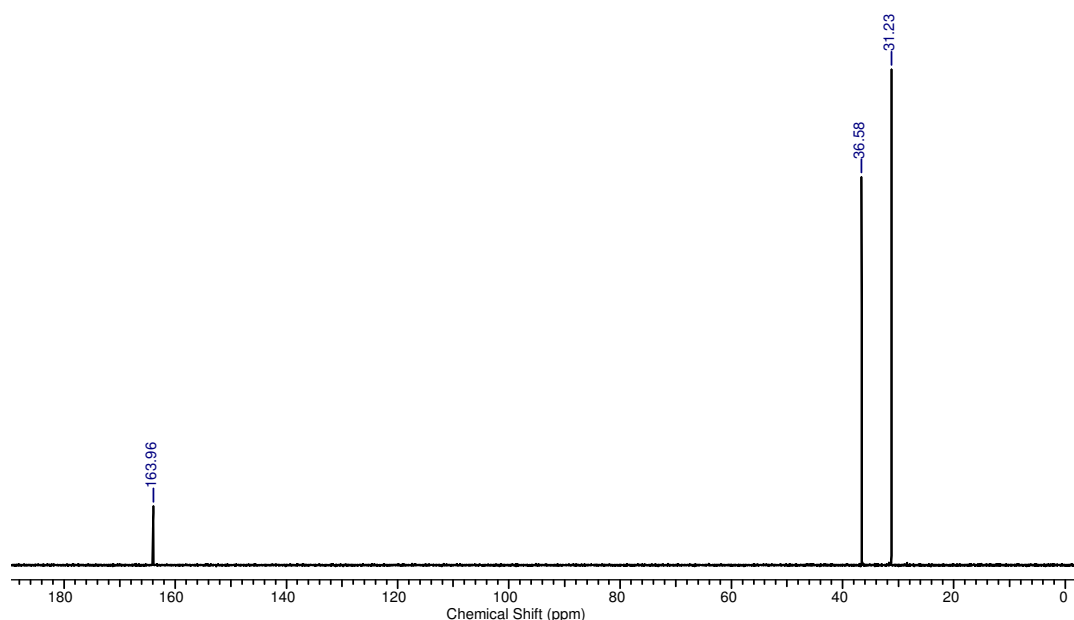


Figure 5.14: ^{13}C NMR (D_2O , 600 MHz) of commercially purchased DMF

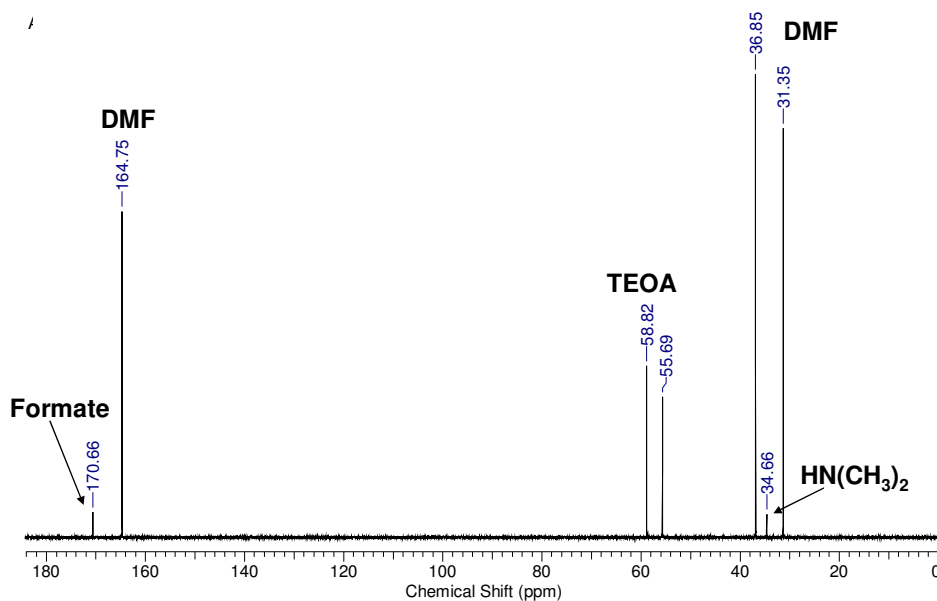


Figure 5.15: ^{13}C NMR (D_2O , 600 MHz) of 5:1 DMF/TEOA mixture containing 75% water.

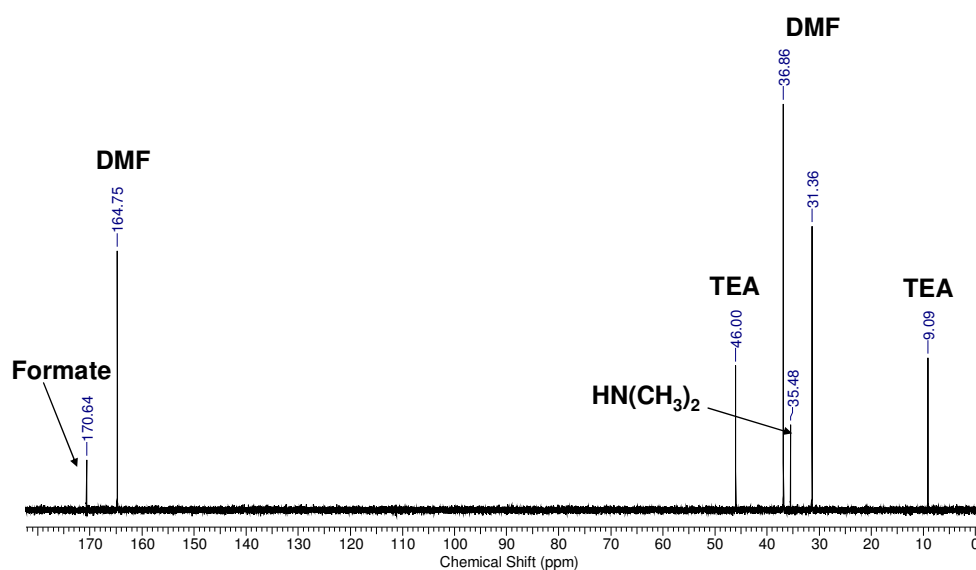


Figure 5.16: ^{13}C NMR (D_2O , 600 MHz) of 5:1 DMF/TEA mixture containing 80% water.

A controlled time dependent ^{13}C NMR study has been carried out to confirm that hydrolysis occurs with 70% D_2O . This study suggests that the hydrolysis of DMF

has also been taken place with 70% D₂O. The rate of formation of formate is faster for DMF/TEA/D₂O mixtures compared to DMF/TEOA/D₂O mixtures. The time depended ¹³C NMR spectra are displayed in **Figure 5.17** and **5.18**.

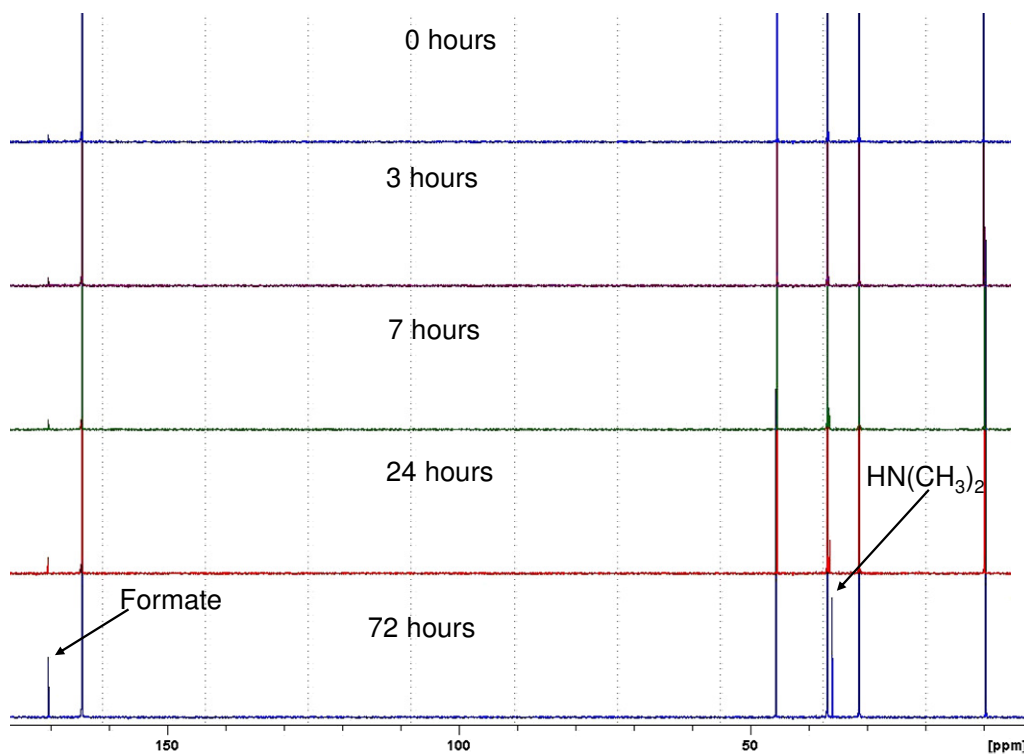


Figure 5.17: Time dependent NMR experiment on 5:1 DMF/TEA mixture contains 70% D₂O

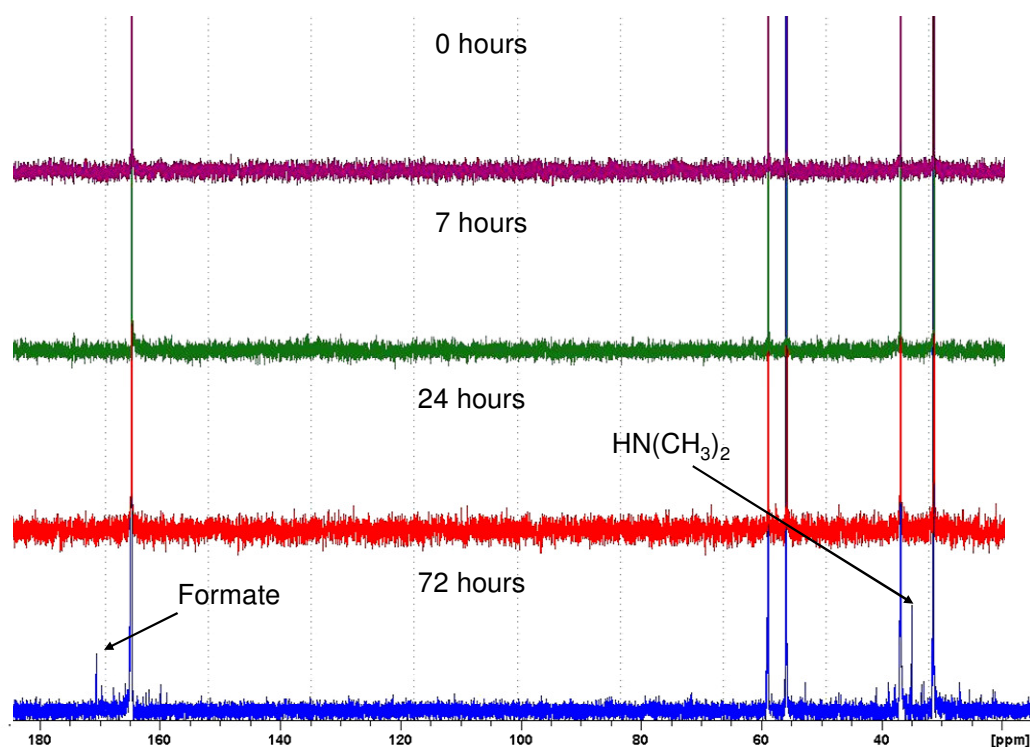


Figure 5.18: Time dependent NMR experiment on 5:1 DMF/TEOA mixture contains 70% D₂O

5.4.3. FTIR spectroscopy

FTIR spectroscopy also confirmed the presence of formate as illustrated in **Figure 5.19**. Overlaid FTIR spectra of DMF/water, formate, and DMF/TEA/water (See **Figure 5.19**) show that there are stretching vibrations for C = O at 1581 cm⁻¹ and a C-O band at 1351 cm⁻¹ (symmetric and asymmetric stretching frequencies of -COO⁻ group) which are indicative of the presence of formate in the DMF/TEA/water mixture. FTIR spectroscopy for DMF/TEOA/water mixtures were also recorded but IR stretching bands for C-O and C = O were not detected which may be due to the low concentration of formate in the DMF/TEOA/water mixture.

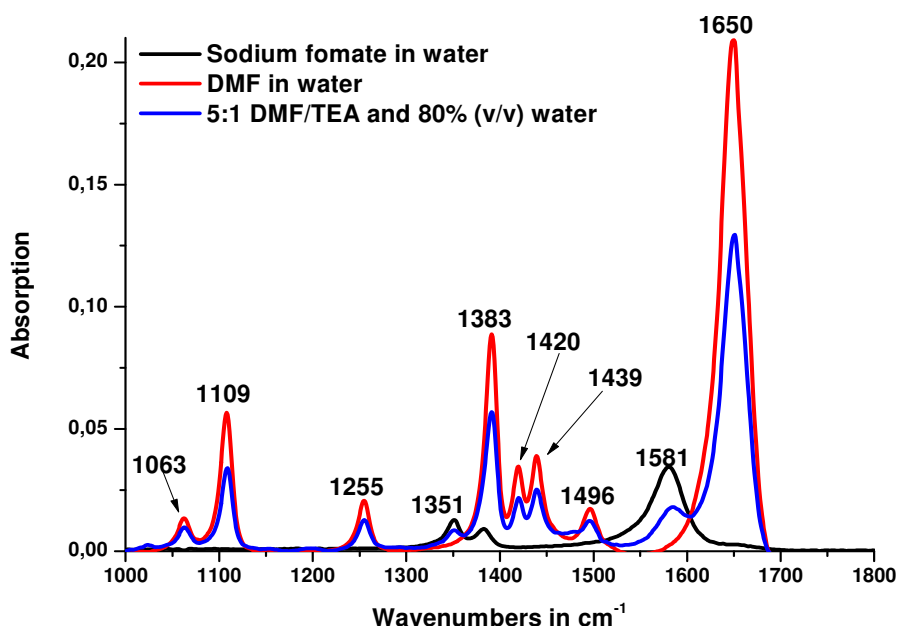
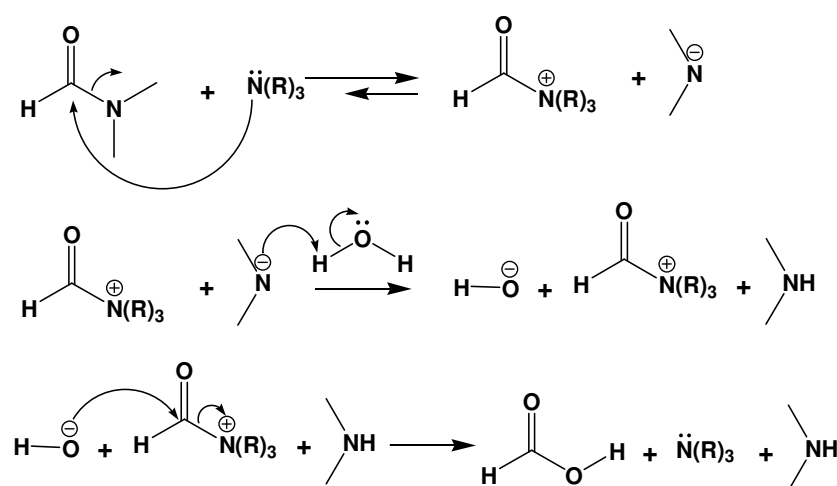


Figure 5.19: IR spectrum of 5:1 DMF/TEA mixture containing 80 vol% of water.

5.5. Possible mechanism for the formation of formate

No decomposition products for the tertiary amines (TEA and TEOA) were detected by ^{13}C NMR and FTIR spectroscopy which suggests that tertiary amines might act as the catalysts in the hydrolysis of DMF. This hydrolysis reaction can be described as a base (TEOA or TEA are organic bases and good nucleophiles) catalysed hydrolysis of DMF. A proposed reaction mechanism is as follows (See Scheme 5.1).



Scheme 5.1: Proposed reaction mechanism of $\text{N}(\text{R})_3$ ($\text{R} = -\text{CH}_2\text{CH}_3, -\text{CH}_2\text{CH}_2\text{OH}$) catalyzed formation of formate from aqueous solution of DMF.

As an explanation for the above proposed mechanism, triethylamine and triethanolamine are good nucleophiles and replace the amide group (>N^-) from the dimethylformamide. The tertiary amine is positively charged, when attached to carbonyl carbon, and the positive charge is stabilised with the positive inductive effect (+I effect) of three ethyl groups (TEA) (by three ethylalcohol groups in the case of TEOA). In the next step, the negative nitrogen atom in $\text{N}^-(\text{CH}_3)_2$ abstracts a proton from a water molecule and is neutralised. Another nucleophilic substitution occurs, replacing the tertiary amine cation by a hydroxyl ion which leads to the formation of formic acid and dimethylamine, as hydrolysed products of DMF. In this case, TEA and TEOA possibly acted as catalysts and enhance the rate of formation of formate from aqueous DMF mixture.

5.6. Conclusion

This study shows that caution should be exercised when determining catalyst turnover numbers for photocatalytic systems for CO_2 reduction based upon formate levels when DMF is used as a solvent. The results obtained show that when the water content is high, spontaneous formation of formate is observed. Since in photocatalytic experiments, in general low water concentrations are used i.e. < 30 % this observation is less critical for the actual photocatalytic process. However, during analysis of the samples obtained problems may occur. In the presence of the organic bases TEA and TEOA formate concentrations in the range 10^{-2} to 10^{-3} M were found. At lower water concentrations that process is much less prevalent. The results also show that the amount of formate increases with time, adding another measure of uncertainty. This indicates that when using DMF as a solvent in photocatalytic studies care should be taken about the amount of water present. The observations are most important for the choice of the analytical procedure used to analyse the photocatalytic mixtures. When aqueous analytical methods such as titrations, ion chromatography or conductivity are used the DMF/amine photocatalytic samples obtained after irradiation need to be diluted with water to allow accurate measurement. At that stage serious problems arise and the formate concentrations measured may be overestimated.

5.7. References

-
- (1) Morris, A. J.; Meyer, G. J.; Fujita, E. *Acc. Chem. Res.* **2009**, *42*, 1983-1994.
 - (2) Teets, T. S.; Nocera, D. G. *Chem. Commun.* **2011**, *47*, 9268-9274.
 - (3) McDaniel, N. D.; Bernhard, S. *Dalton trans.* **2010**, *39*, 10021-10030.
 - (4) Sakai, K.; Ozawa, H. *Coord. Chem. Rev.* **2007**, *251*, 2753-2766.
 - (5) Losse, S.; Vos, J. G.; Rau, S. *Coord. Chem. Rev.*, *254*, 2492-2504.
 - (6) Rau, S.; Walther, D.; Vos, J. G. *Dalton Trans.* **2007**, 915-919.
 - (7) Takeda, H.; Ishitani, O. *Coord. Chem. Rev.* **2009**, *254*, 346-354.
 - (8) Doherty, M. D.; Grills, D. C.; Muckerman, J. T.; Polyansky, D. E.; Fujita, E. *Coord. Chem. Rev.* **2009**, *254*, 2472-2482.
 - (9) Hayashi, Y.; Kita, S.; Brunschwig, B. S.; Fujita, E. *J. Am. Chem. Soc.* **2003**, *125*, 11976-11987.
 - (10) Fujita, E.; Wishart, J. F.; van Eldik, R. *Inorg. Chem.* **2002**, *41*, 1579-1583.
 - (11) Fujita, E. *Coord. Chem. Rev.* **1999**, *185-186*, 373-384.
 - (12) Behar, D.; Dhanasekaran, T.; Neta, P.; Hosten, C. M.; Ejeh, D.; Hambright, P.; Fujita, E. *J. Phys. Chem. A* **1998**, *102*, 2870-2877.
 - (13) Ogata, T.; Yanagida, S.; Brunschwig, B. S.; Fujita, E. *J. Am. Chem. Soc.* **1995**, *117*, 6708-6716.
 - (14) Tagata, T.; Nishida, M.; Nishida, A. *Tetrahedron Lett.* **2009**, *50*, 6176-6179.
 - (15) Matsuoka, S.; Kohzuki, T.; Pac, C.; Ishida, A.; Takamuku, S.; Kusaba, M.; Nakashima, N.; Yanagida, S. *J. Phys. Chem.* **1992**, *96*, 4437-4442.
 - (16) Ishida, H.; Terada, T.; Tanaka, K.; Tanaka, T. *Inorg. Chem.* **1990**, *29*, 905-911.
 - (17) Ishida, H.; Tanaka, K.; Tanaka, T. *Organometallics* **1987**, *6*, 181-186.
 - (18) Muzart, J. *Tetrahedron* **2009**, *65*, 8313-8323.
 - (19) Buncel, E.; Symons, E. A. *J. Chem. Soc. D: Chem. Commun.* **1970**, 164-165.
 - (20) Kankaanpera, A.; Scharlin, P.; Kuusisto, I.; Kallio, R.; Bernoulli, E. *J. Chem. Soc., Perkin Trans. 2* **1999**, 169-174.
 - (21) Øpstad, C. L.; Melø, T. B.; Sliwka, H.-R.; Partali, V. *Tetrahedron* **2009**, *65*, 7616-7619.
 - (22) "Determination of trace anions in organic solvents" Dionex application note 85.

- (23) *"Determination of sulfate and chloride in ethanol by ion chromatography"*
Dionex application note 175.
- (24) *"Determination of chloride and sulfate in methanol using ion chromatography"* *Dionex application note 201.*
- (25) *Dionex ICS-1500 ion chromatography system operator's manual* **2005**,
Document No. 031917.

Chapter 6

Future work

This chapter outlines the future work, based on the results presented in this thesis.

Chapter 2 describes different ruthenium mononuclear complexes, their synthetic procedures, characterisations and photophysical properties. A number of ruthenium complexes were derivatised to carboxy groups. Future work will involve synthesising heterodinuclear complexes and carrying out electrochemical studies. In addition, photocatalytic hydrogen production from water using these ruthenium photosensitisers in solution as well as to the surface of semiconductor should be carried out.

Chapter 3 reports a number of Ru(II)/Re(I) complexes. These complexes are characterised with different spectroscopic tools. Electrochemical studies for these heterodinuclear complexes should be carried out. Future work should also focus on studies for hydrogen production from water and the reduction of CO₂ in solution, and also on semiconductors surface. This chapter described a preliminary immobilisation study on the nickel oxide, however more characterisation data using IR spectroscopy, SEM and BET isotherm studies are essential to fully characterise the catalyst on the immobilised surface.

Chapter 4 discusses the synthetic procedures for carboxy derivatised Ir(III) complexes. A number of carboxy derivatised iridium complexes have been synthesised and characterised in this chapter. Electrochemical studies of these iridium complexes should be carried out. Future work also involves the photocatalytic hydrogen production in solution as well as in heterogeneous catalytic systems.

In **Chapter 5** the effect of water on the DMF/TEA and DMF/TEOA mixture was carried out and this study showed an increase in formate concentration with both time and water content (30-90%) (v/v). The formation of formate from DMF was explained as a base catalysed hydrolysis reaction. Future work involves an investigation of the same hydrolysis process in presence of inorganic acids and bases, and identifying various reaction products following photocatalytic studies.

Appendix A

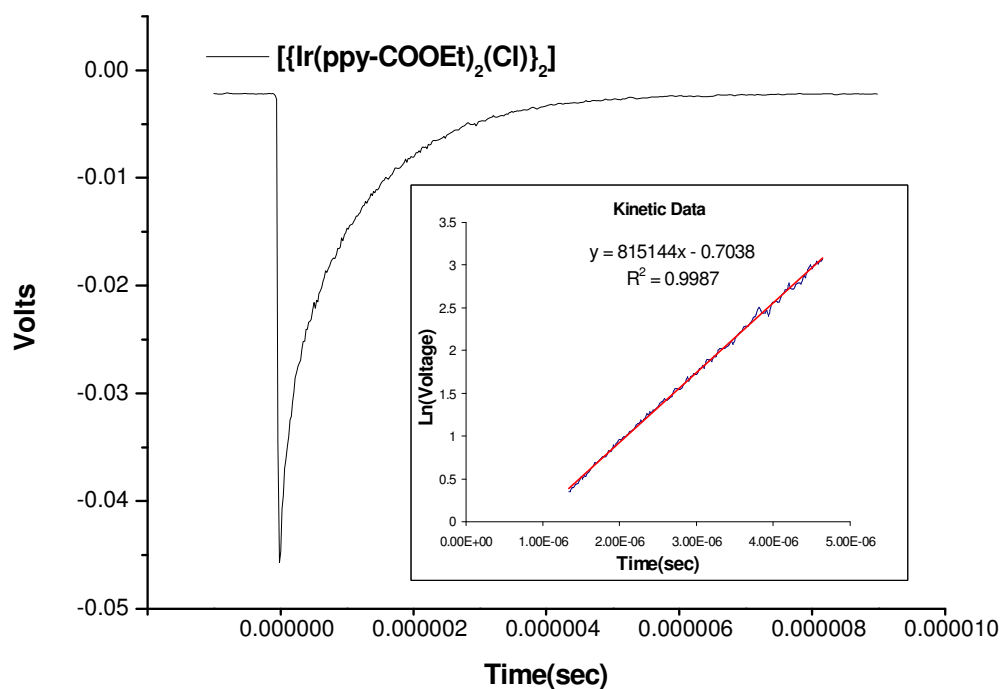


Figure A1: Life time experiment and kinetic fit graph of $[\text{Ir}(\text{ppy-COOEt})_2(\mu\text{-Cl})]_2$. Life time experiment was recorded in nitrogen purged DCM solution at room temperature.

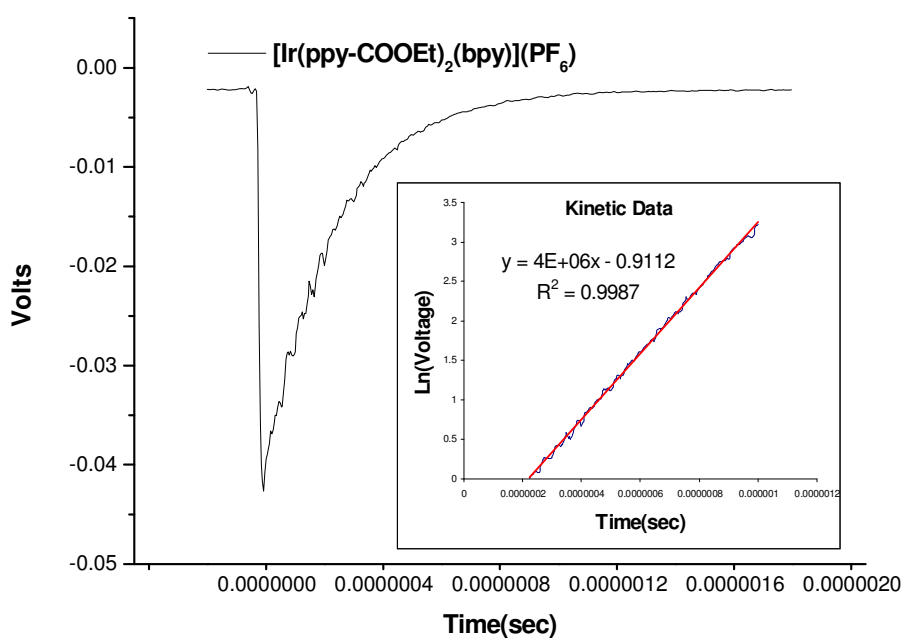


Figure A2: Life time experiment and kinetic fit graph of $[\text{Ir}(\text{ppy-COOEt})_2(\text{bpy})](\text{PF}_6)$. Life time experiment was recorded in nitrogen purged DCM solution at room temperature.

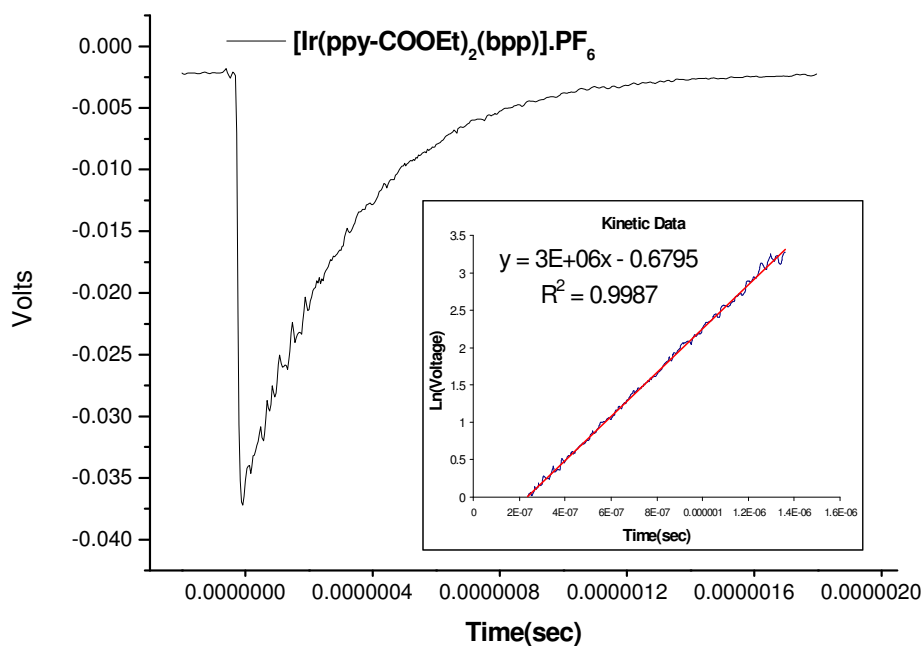


Figure A3: Life time experiment and kinetic fit graph of $[\text{Ir}(\text{ppy-COOEt})_2(\text{bpp})](\text{PF}_6)$. Life time experiment was recorded in nitrogen purged DCM solution at room temperature.

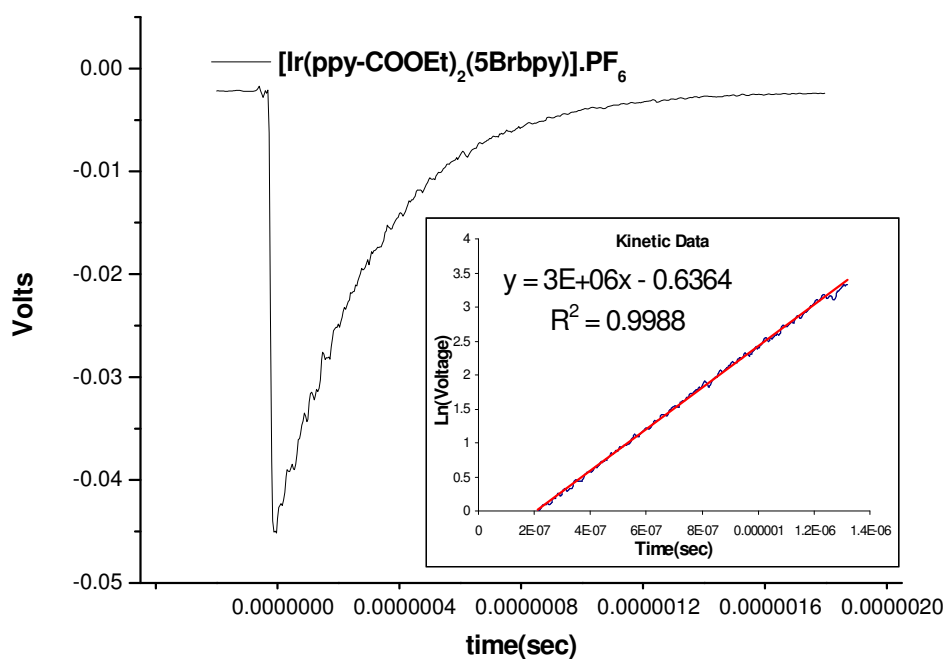


Figure A4: Life time experiment and kinetic fit graph of $[\text{Ir}(\text{ppy-COOEt})_2(5\text{Brbpy})](\text{PF}_6)$. Life time experiment was recorded in nitrogen purged DCM solution at room temperature.

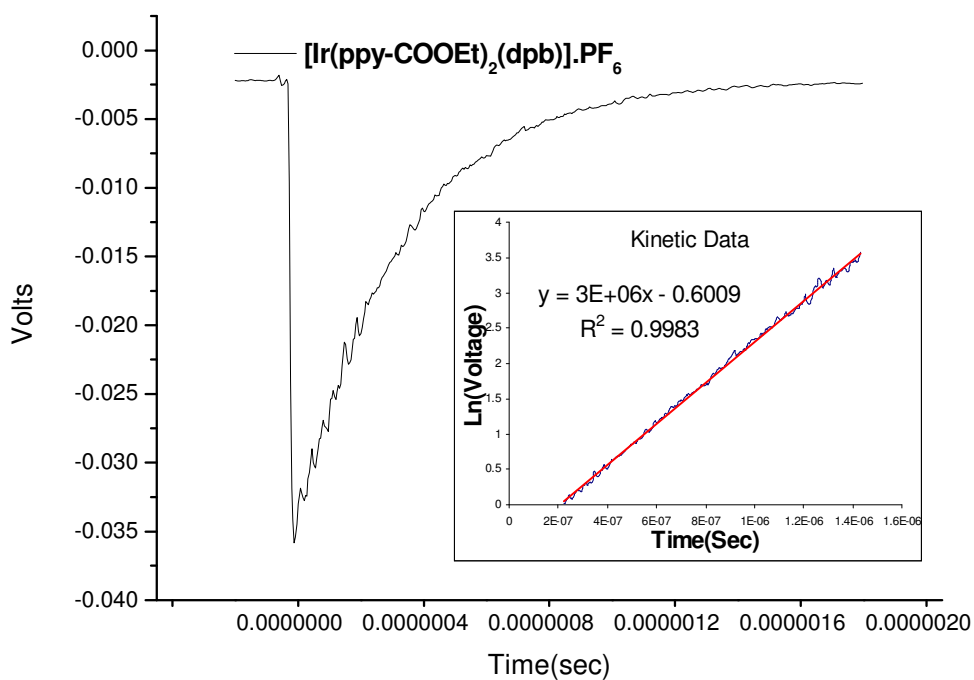


Figure A5: Life time experiment and kinetic fit graph of $[\text{Ir}(\text{ppy-COOEt})_2(\text{dpb})](\text{PF}_6)$. Life time experiment was recorded in nitrogen purged DCM solution at room temperature.

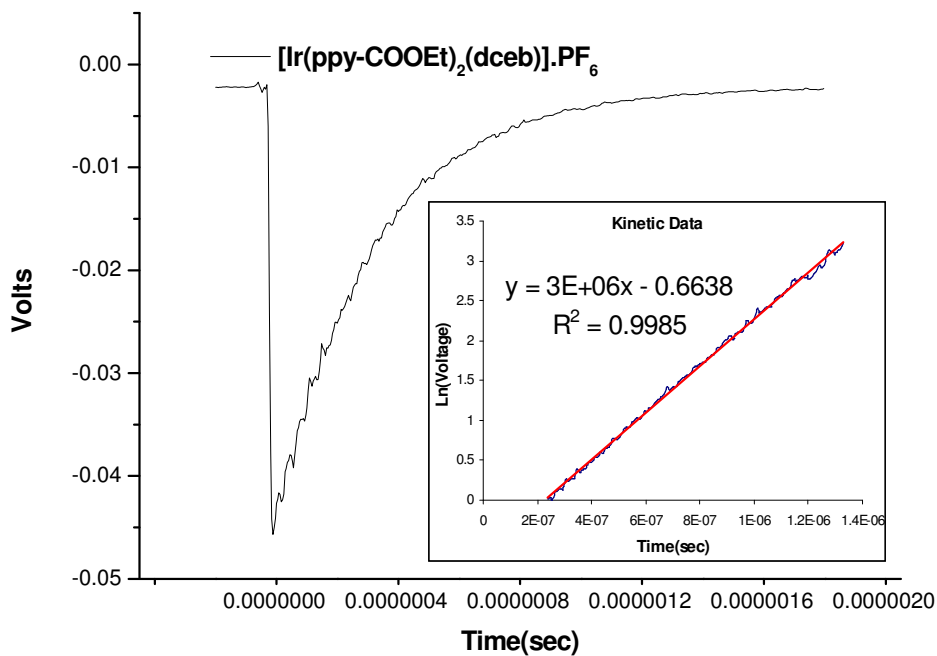


Figure A6: Life time experiment and kinetic fit graph of $[\text{Ir}(\text{ppy-COOEt})_2(\text{dceb})](\text{PF}_6)$. Life time experiment was recorded in nitrogen purged DCM solution at room temperature.

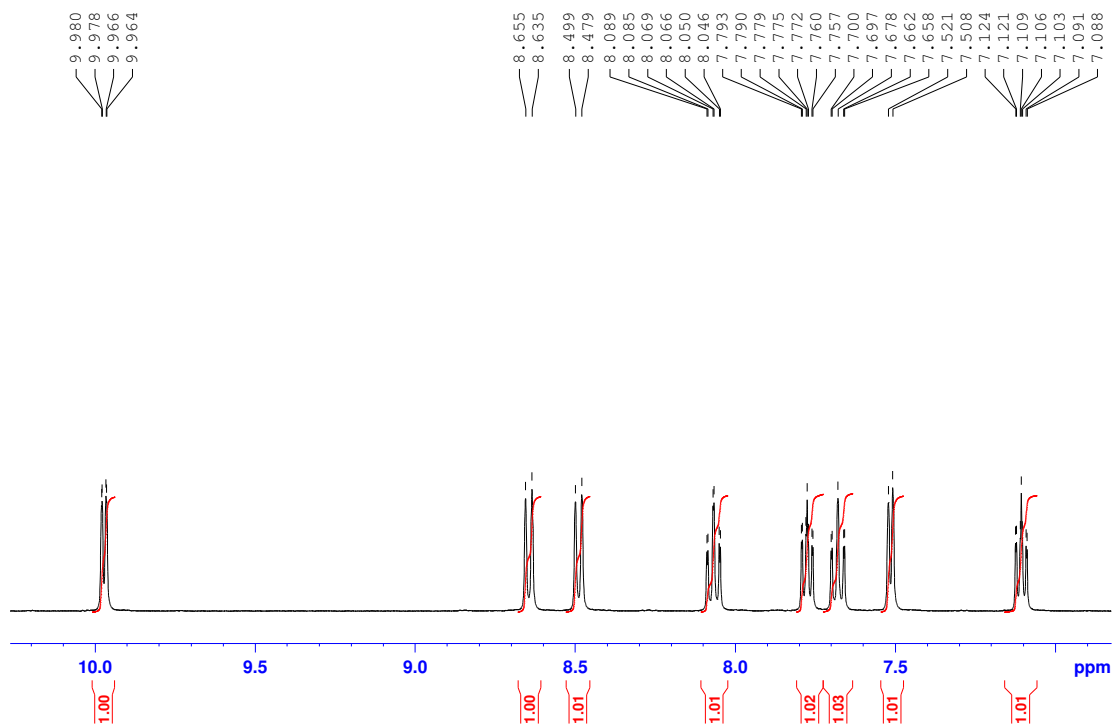


Figure A7: ^1H NMR (DMSO- d_6 , 400 MHz) of $[\text{Ru}(\text{bpy})_2\text{Cl}_2]$

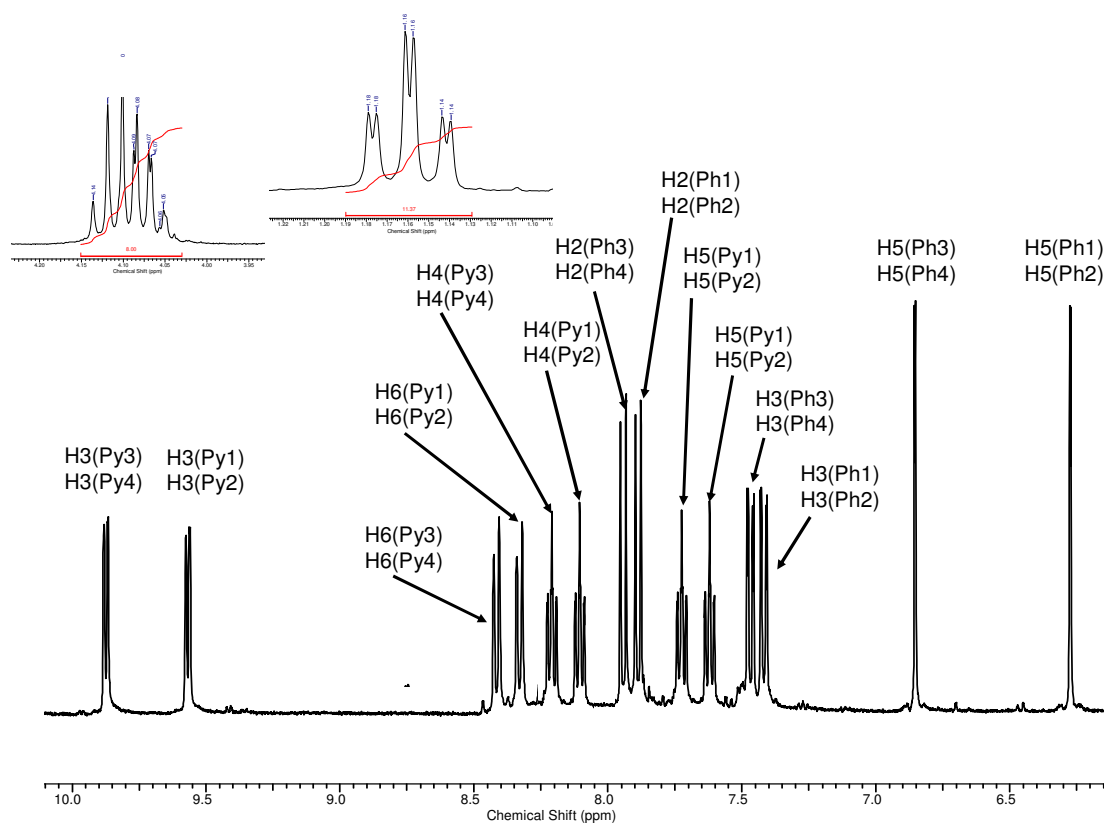


Figure A8: ^1H NMR (DMSO- d_6 , 400 MHz) of $[\text{Ir}(\text{ppy-COOEt})_2\text{Cl}]_2$

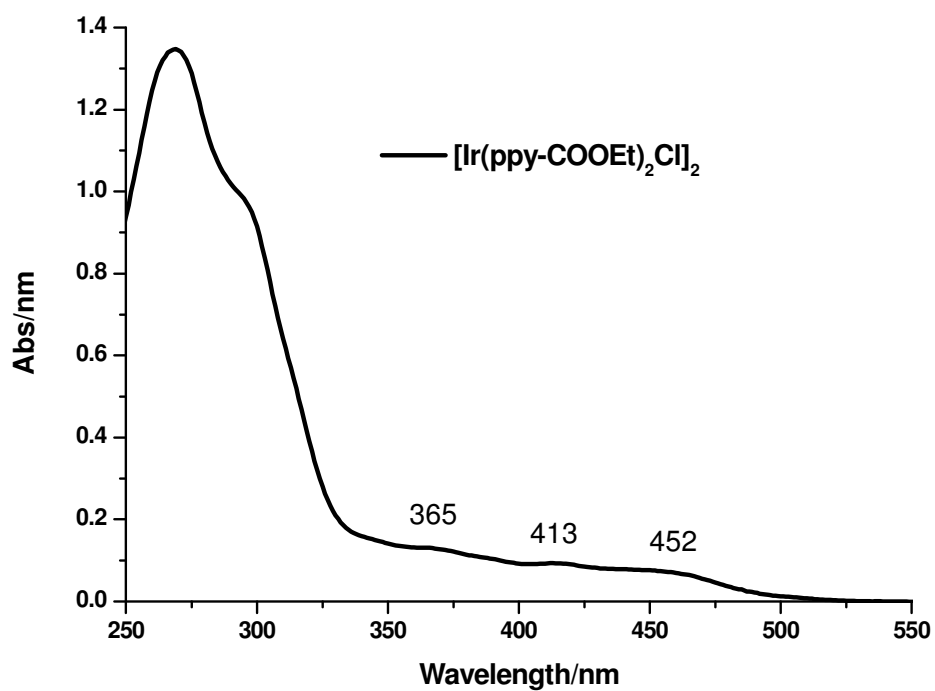


Figure A9: UV-Vis spectra of $[\text{Ir}(\text{ppy-COOEt})_2\text{Cl}]_2$ was recorded in acetonitrile at room temperature. Conentration of the solution is $\sim 10^{-5}$ M.

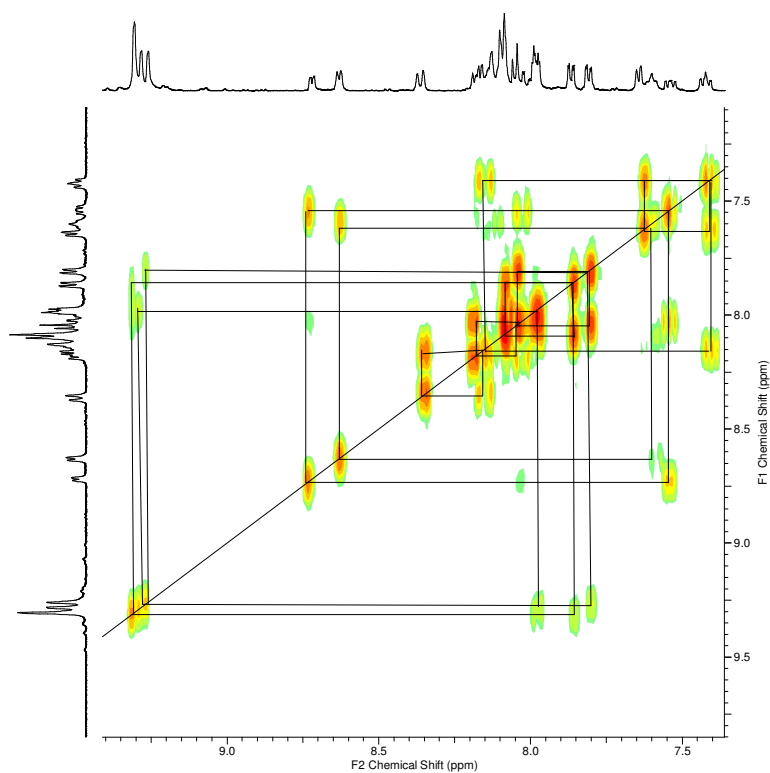


Figure A10: 2D COSY NMR (DMSO-d_6 , 400 MHz) of $[\text{Ru}(\text{dceb})_2(\text{Hbpt})\text{Re}(\text{CO})_3\text{Cl}]^{2+}$

1,10-phenanthroline-5,6-dione (phendione)

The product was synthesised by a modified literature procedure.¹

1 g (5.61 mmol) of 1,10-phenanthroline and 5.95 g (50 mmol) of KBr were added to a flask and kept in ice bath. Then 20 cm³ of conc. H₂SO₄ was added and stirred for 15 minutes. 10 cm³ of conc. HNO₃ was then added very slowly onto the reaction mixture. Brown fumes were coming out from the reaction mixture. Then the temperature of reaction mixture was raised to 100 °C by hot water bath. The reaction solution became brown. The reaction was stopped and poured in an ice water after the brown fumes were stopped and was neutralised with a NaOH solution. Orange coloured slurry was found which was extracted with DCM and dried over MgSO₄. The solution was concentrated by rotary evaporation and reprecipitated by adding ethyl acetate. The product was collected by filtration and further purified by washing with ethyl acetate. Yield: 1.14 g (5.48 mmol) (86%). ¹H NMR (d₆-DMSO, 400 MHz): δ (ppm) 8.98(d, 2H), 8.4(d, 2H), 7.68(dd, 2H).

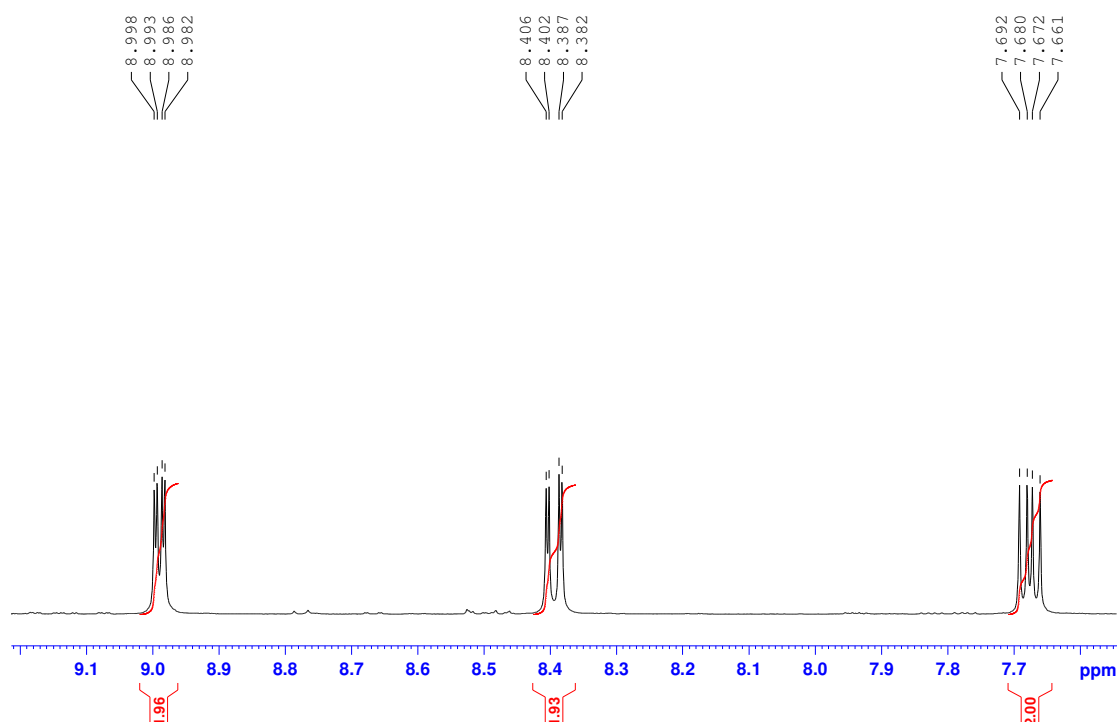


Figure A11: ¹H NMR (DMSO-*d*₆, 400 MHz) of 1,10-phenanthroline-5,6-dione

Phen bridging ligand (tpphz)

600 mg (2.85 mmol) of 1,10-phenanthroline-5,6-dione, 62 mg (0.359 mmol) of sodium hydrosulfite and 3.5 g (excess) of ammonium acetate were added to a round bottom flask and mixed thoroughly by shaking. Then the solid reaction mixture was melted under reflux condition and kept under nitrogen atmosphere for two hours at 180°C. 10 ml of water was added after the reaction cooled down at room temperature. The brown-orange precipitate was collected by filtration and washed with water, ethanol and then acetone. Yield: 396 mg (1.03 mmol). ^1H NMR (CDCl_3 , 400 MHz): δ (ppm) 9.61(dd, 4H, $J = 8.3$ Hz, $J' = 1.6$ Hz), 9.36(dd, 4H, $J = 5.1$ Hz, $J' = 1.4$ Hz), 7.86(dd, 4H, $J = 8.3$, $J' = 5.1$).

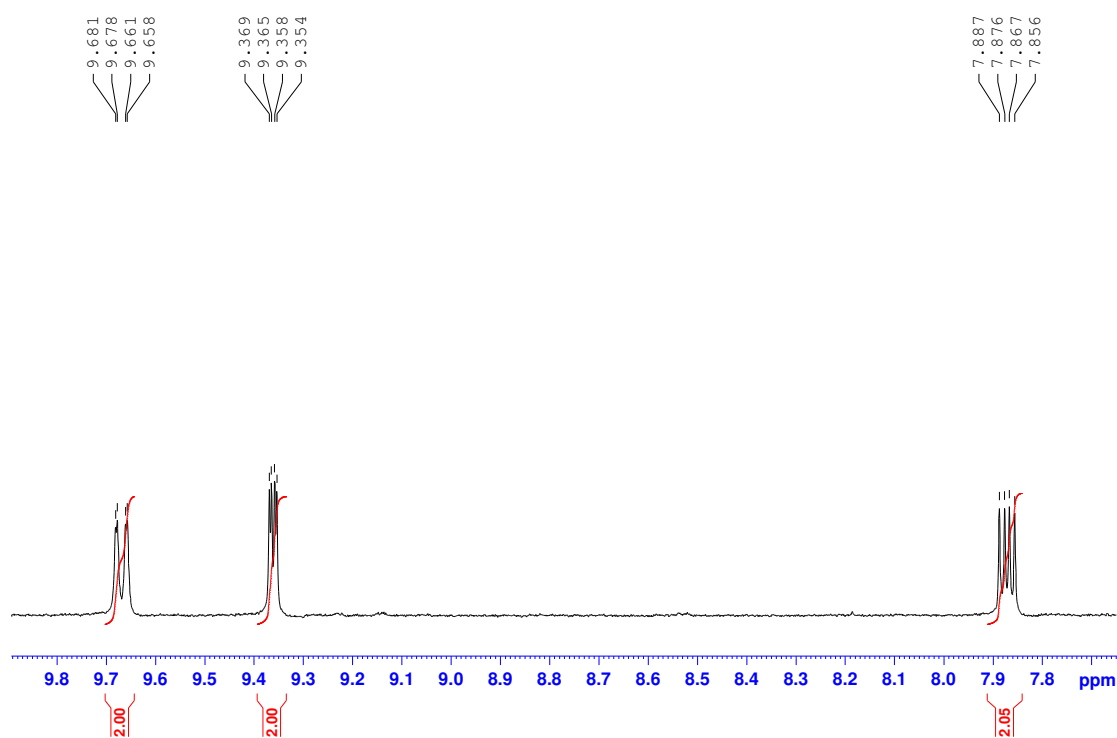


Figure A12: ^1H NMR (CDCl_3 , 400 MHz) of therapyridylphenazine(tpphz)

References

- (1) Rupesh, K. R.; Deepalatha, S.; Krishnaveni, M.; Venkatesan, R.; Jayachandran, S. *Eur. J. Med. Chem.* **2006**, *41*, 1494-1503.

Appendix B

Publications and poster presentations

Poster presentations

1. **Avishek Paul**, Gurmeet Singh Bindra, Suraj Soman, Martin Schulz, Jane Inglis, Mary T. Pryce, Johannes G. Vos and Sven Rau “Design of photocatalysts for solar driven hydrogen evolution.” Poster presentation, Challenges in Renewable Energy (ISACS4), **MIT Boston, USA, July 2011.**
2. Nadia Coburn, Declan Traynor, **Avishek Paul**, Danilo Dini, Johannes G. Vos, Muhammad Awais, Denis Dowling, and Don MacElroy, “Binuclear complexes of ruthenium and rhenium as dye-sensitizers of p-type semiconductors for CO₂ photo reduction.” Poster presentation, Solar Energy Conversion (SEC) conference, **University College Dublin, Ireland, April 2011.**
3. Suraj Soman, **Avishek Paul**, Gurmeet Singh Bindra, Mary T. Pryce, Johannes G. Vos. “Harvesting Of Solar Energy for the Generation of H₂.” Poster presentation, **EPA National Research Conference, Croke Park, Ireland, June 2010.**

Publications

1. **Avishek Paul**, Damian Connolly, Martin Schulz, Mary T. Pryce, Johannes G. Vos “The effect of water during the quantitation of formate in photocatalytic studies on CO₂ reduction in DMF” *Inorg. Chem.* **2012**, *51*, 1977–1979.
2. Singh Bindra, G.; Schulz, M.; **Paul, A.**; Soman, S.; Groarke, R.; Inglis, J.; Pryce, M. T.; Browne, W. R.; Rau, S.; Maclean, B. J.; Vos, J. G. “The effect of peripheral bipyridine ligands on the photocatalytic hydrogen production activity of Ru/Pd catalysts” *Dalton trans.* **2011**, *40*, 10812-10814.
3. Schulz, M.; Hirschmann, J.; Draksharapu, A.; Singh Bindra, G.; Soman, S.; **Paul, A.**; Groarke, R.; Pryce, M. T.; Rau, S.; Browne, W. R.; Vos, J. G. “Reinvestigating 2,5-di(pyridin-2-yl)pyrazine ruthenium complexes: selective deuteration and Raman spectroscopy as tools to probe ground and excited-state electronic structure in homo- and heterobimetallic complexes” *Dalton trans.* **2011**, *40*, 10545-10552.



Design of photocatalysts for solar driven hydrogen evolution

Avishek Paul,^a Gurmeet Singh Bindra,^a Suraj Soman,^a Martin Schulz,^a Jane Inglis,^a

Mary Pryce,^{*a} Johannes G. Vos,^{*a} and Sven Rau.^{*b}



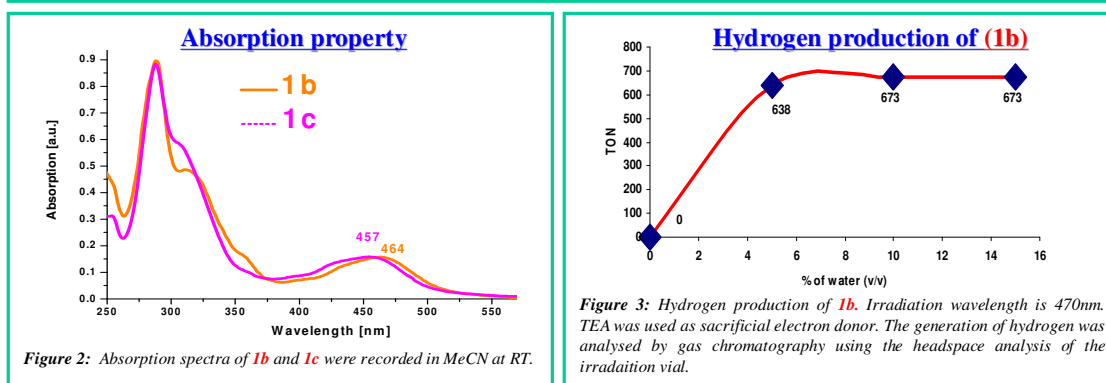
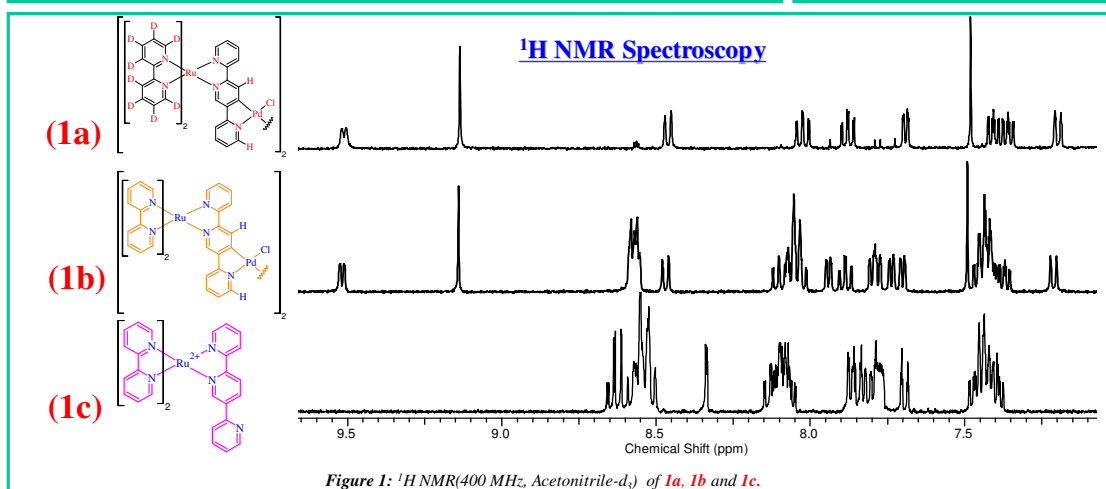
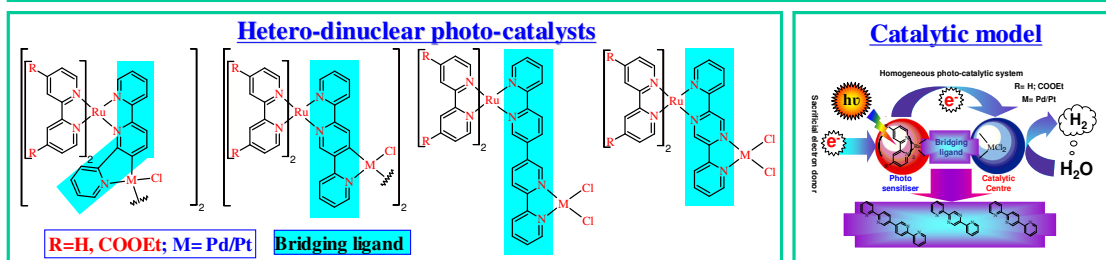
(a) SRC for Solar Energy Conversion, School of Chemical Sciences, Dublin City University, Dublin-9, Ireland.

(b) Department of Inorganic Chemistry, Friedrich-Alexander-Universität, Egerlandstraße 1, 91058 Erlangen, Germany

Email: apaul85@gmail.com



Abstract: Hydrogen is well considered as “The ultimate green fuel” for the solution of future energy needs and the prevention of global warming.^{1,2} Water is a vast source of hydrogen and sun is the universal energy source on the earth. Considering the above issues, the design and synthesis of few novel ruthenium-palladium or ruthenium-platinum hetero bimetallic complexes are reported for solar hydrogen evolution from water, where ruthenium polypyridyl precursors act as light harvesting units and Pd/Pt as active catalytic sites.^{3,4} The synthesis and characterisation of a series of bimetallic complexes are reported and results obtained show that the properties of the compounds such as catalytic efficiency can be optimised by tuning the peripheral polypyridine ligand and by using different bridging ligands.



Acknowledgement: We acknowledge and thank Environmental Protection Agency (EPA grant no. 2008-ET-MS-3-S2) and Science Foundation Ireland (SFI grant no. 08RFP-CHE1349) for supporting this project.

Reference: 1. T. P. Yoon, M. A. Ischay and J. Du, *Nature Chem.*, 2010, **2**, 527-532. 2. T. R. Cook, D. K. Dogutan, S. Y. Reece, Y. Surendranath, T. S. Teets and D. G. Nocera, *Chem. Rev.*, 2010, **110**, 6474-6502. 3. S. Rau, B. Schäfer, D. Gleich, E. Anders, M. Rudolph, M. Friedrich, H. Görls, W. Henry and J. G. Vos, *Angew. Chem. Int. Ed.*, 2006, **45**, 6215-6218. 4. M. G. Walter, E. L. Warren, J. R. McKone, S. W. Boettcher, Q. Mi, E. A. Santori and N. S. Lewis, *Chem. Rev.*, 2010, **110**, 6446-6473.



Binuclear complexes of ruthenium and rhenium as dye-sensitizers of *p*-type semiconductors for CO₂ photoreduction

Nadia Coburn,^a Declan Traynor,^a Avishek Paul,^a Danilo Dini,^a
Johannes G. Vos,^a Muhammad Awais,^b Denis Dowling,^b Don MacElroy^c

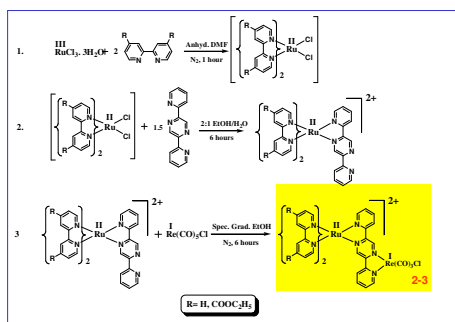
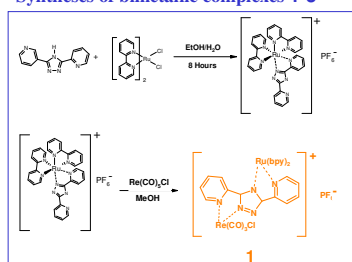
SRC for Solar Energy Conversion: (a) School of Chemical Sciences, Dublin City University, Dublin 9, Ireland;
(b) School of Electrical, Electronic and Mechanical Engineering (c) School of Chemical and Bioprocess Engineering, University College Dublin, Belfield, Dublin 4, Ireland



Abstract

The working principle of Graetzel's solar cell¹ has been applied for the definition of a new cell configuration that reduces CO₂ upon illumination of dye-sensitized *p*-type semiconductors with visible radiation. The syntheses of new bimetallic ruthenium/rhenium polypyridyl complexes as dye-sensitizers as well as the preliminary studies of their photocatalytic properties towards CO₂ reduction have been undertaken. The capability of these complexes to reduce CO₂ into formate, oxalate and carbon monoxide is proven by turnover numbers higher than 200. Design of these compounds took into account the photophysical properties of ruthenium-pyridyl complexes² with the catalytic properties of the rhenium centre³ for CO₂ reduction.⁴ Bridging ligands are constituted by conjugated pyridyl-based systems that allow excitation/electron transfer⁵ from the ruthenium-centred photoactive site to the rhenium-centred catalytic site.

Syntheses of bimetallic complexes 1-3



Spectral characterization of bimetallic complexes

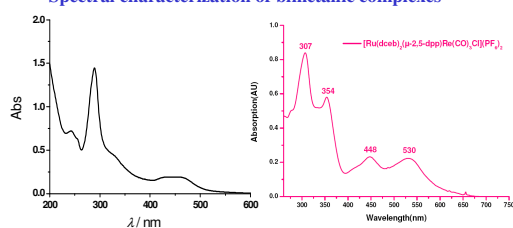


Figure 1: Optical spectra of **1** (left) and **3** ($R = COOC_2H_5$) (right).

Excited state and electrochemical properties of **1**

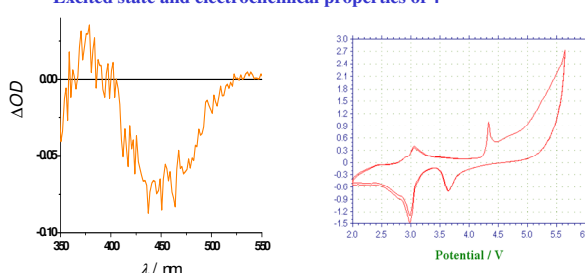


Figure 2: (Left) Transient optical spectrum of complex **1** upon excitation with 9 ns pulses at 532 nm. Spectrum is taken after 30 ns from excitation (excited state lifetime: 200 ns). (Right) Cyclic voltammetry of complex **1** on Pt electrode (reference electrode: Li⁺/Li; scan rate: 30 mV s⁻¹).

Photocatalytic properties of **1**

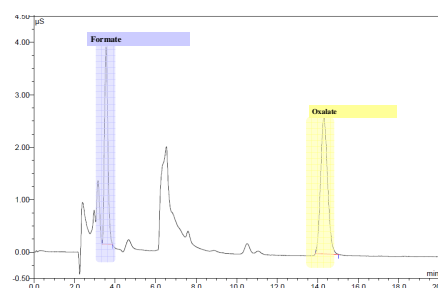


Figure 3: Ion chromatogram showing the presence of formate and oxalate anions as reaction products following the photocatalyzed reduction of CO₂ in the 10⁻² M solution of complex **1** after 24 hrs of irradiation at 470 nm.

References

- O'Regan, B.; Graetzel, M. *Nature* **1991**, 353, 737-739;
- Juris, A.; Balzani, V.; Barigelli, F.; Campagna, S.; Belser, P.; Von Zelewsky, A. *Coord. Chem. Rev.* **1988**, 84, 85-277;
- Hawecker, J.; Lehn, J.M.; Ziessel, R. *J. Chem. Soc. Chem. Comm.* **1983**, 536-538;
- (a) Morris, A.J.; Meyer, G.J.; Fujita, E. *Acc. Chem. Res.* **2009**, 42, 1983-1994; (b) Takeda, H.; Ishitani, O. *Coord. Chem. Rev.* **2010**, 254, 346-354;
- (a) Rau, S.; Schaefer, B.; Gleich, D.; Anders, E.; Rudolph, M.; Friedrich, M.; Goerls, H.; Henry, W.; Vos, J.G. *Angew. Chem. Int. Ed.* **2006**, 45, 6215-6218; (b) Halpin, Y.; Cleary, L.; Cassidy, L.; Horne, S.; Dini, D.; Browne, W.R.; Vos, J.G. *Dalton Trans.* **2009**, 4146-4153.



Acknowledgements

We acknowledge and thank Science Foundation Ireland for their funding of this Cluster Programme (07/SRC/B1160) and our Industry Partners for their support of this Programme



SOLARPRINT

CELTIC CATALYSTS

CHALLENGING CHIRAL SYNTHESIS





HARVESTING OF SOLAR ENERGY FOR THE GENERATION OF H₂



Suraj Soman, Avishek Paul, Gurmeet Singh Bindra, Mary T. Pryce, Johannes G. Vos
SRC for Solar Energy Conversion; School of Chemical Sciences, Dublin City University, Dublin 9, Ireland.



Abstract

Due to the current need for clean and sustainable sources of chemical fuels, the photolysis of water into dihydrogen and dioxygen has become an important area of active research. One approach in the development of a system capable of splitting water has been through the use of molecular catalysts powered by visible light. These systems typically utilise a photosensitiser (PS) for light absorption, an electron relay (ER) to create charge separation, and a sacrificial reductant (SR) to serve as an electron source that allows for the catalytic production of hydrogen without concurrent dioxygen evolution. Historically, ruthenium(II) complexes have been the most common PS choice, recently, iridium(III) PS have come under investigation as superior alternatives to Ru(II) PS species due to their higher turnover numbers (TON), even with solutions containing externally added catalyst. The first type of Ir-Pt mixed metal photocatalytic systems, [Ir(ppy)₂(BPP)Pt(H₂O)Cl].PF₆ (II) & [Ir(ppy)₂(BPP)Pd(H₂O)Cl].PF₆ (III) were developed by our group, and have showed promising results on gas chromatography (GC) with a higher turnover number for H₂ production.

Introduction

With the onset of global warming, combined with reducing reserves of fossil fuels, finding new ways of producing energy is becoming an increasingly urgent concern,¹ hence the utilisation of solar energy is an approach well worth pursuing. In our work we aim to develop a new technology for the production of hydrogen in an environmentally sustainable manner. One approach is through the use of molecular catalysts powered by visible light.²⁻⁴ In our studies we focus on the utilisation of iridium complexes. In this presentation our results obtained for the catalytic generation of hydrogen with the mononuclear iridium complexes and the hetero bimetallic Ir-Pt/Pd type complexes are reported. The first Ir-Pt mixed metal photocatalytic system developed & its mechanism for intramolecular hydrogen generation is shown in figure 1.

Structure, Mechanism and NMR

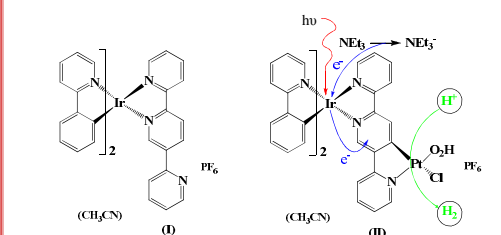


Figure 1: Structural representation of [Ir(ppy)₂(BPP)]PF₆ (I) & [Ir(ppy)₂(BPP)Pt(H₂O)Cl].PF₆ (II) and possible photocatalytic mechanism for H₂ production in II is shown.

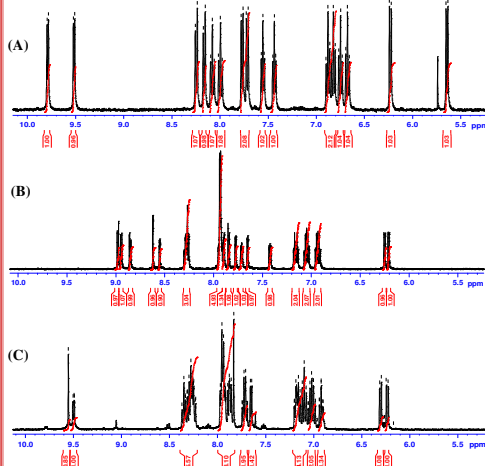


Figure 2: ¹H NMR spectra (A) cyclometallated chloro bridged Iridium starting material ([Ir(ppy)₂Cl]₂) (B) [Ir(ppy)₂(BPP)]PF₆ (I) (C) [Ir(ppy)₂(BPP)Pt(H₂O)Cl].PF₆ (II) carried out in d⁶-DMSO.

Conclusions

Iridium metal complexes have been extensively studied as chromophores for specific light to chemical energy conversion schemes since they have enhanced spin-orbit coupling which results in a long-lived triplet excited state. In our group, we have synthesised heterodinuclear Ir-Pt/Pd complexes, characterised using NMR, Mass-Spec, CHN, absorption, emission and lifetime measurements which showed promising results. More recently, expertise in this area has been applied to the design of photocatalytic systems which can efficiently harness solar energy for the production of hydrogen and the reduction of CO₂ in an environmentally sustainable manner. Detailed studies are at present on going in our group on the catalytic generation of hydrogen with the mononuclear iridium complexes for intermolecular photocatalytic systems and the hetero bimetallic Ir-Pt/Pd complexes for intramolecular photocatalytic systems using gas chromatography.

References

- (1) (a) Powering the planet: Chemical challenges in solar energy utilization N.S. Lewis, D.G. Nocera, *Proc. Natl. Acad. Sci. U.S.A.*, **2006**, *103*, 15729 (b) The future of energy supply: Challenges and opportunities, N. Armaroli, V. Balzani, *Angew. Chem., Int. Ed. Engl.* **2007**, *46*, 52; Lewis, N. S.; Nocera, D. G. *Proc. Natl. Acad. Sci. U.S.A.* **2006**, *103*, 15729–15735.
- (2) Meyer, T. J. *Acc. Chem. Res.* **1989**, *22*, 163–170.
- (3) Alstrum-Acevedo, J. H.; Brennaman, M. K.; Meyer, T. J. *Inorg. Chem.* **2005**, *44*, 6802–6827.
- (4) Esswein, A. J.; Nocera, D. G. *Chem. Rev.* **2007**, *107*, 4022–4047.

Absorption and Emission

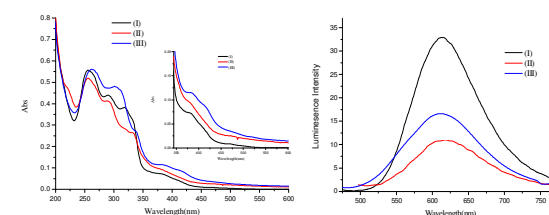


Figure 3: (A) UV-Vis spectra for complexes I, II & III in spectrometric grade CH₃CN (MLCT region enlarged inside) (Conc = 1*10⁻⁵M) (B) Emission spectra at 298K for complexes I, II & III, λ_{ex}=380nm for all the complexes, measured in spectrometric grade CH₃CN (Conc = 1*10⁻⁵).

Lifetime Measurements

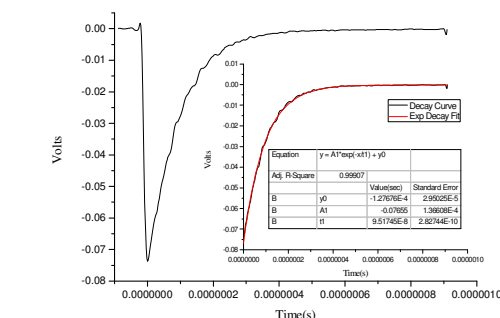


Figure 4: (A) Excited state decay curve obtained following excitation at emission maximum nm in CH₃CN for complex I

Table 1

Complex	Absorption λ _{abs} (nm) ε (LM ⁻¹ cm ⁻¹) x 10 ³	Emission(298K) λ _{em} (nm)	Lifetime (298K) (ns)
I	255(11.11), 292(8.75), 320(7.61), 380(1.46)	614	952
II	256(10.37), 290(8.24), 318(5.67), 334(5.22), 380(1.89)	612	809
III	262(11.23), 302(9.59), 338(5.40), 382(2.31), 415(1.72)	616	658

Table 1: Photophysical measurement values(absorption, emission & lifetime) for complexes I, II & III in spectrometric grade CH₃CN (Conc = 1*10⁻⁵M).

Acknowledgements

The authors would like to thank the EPA for financial support (EPA grant 2008-ET-MS-3-S2)

Effect of Water during the Quantitation of Formate in Photocatalytic Studies on CO₂ Reduction in Dimethylformamide

Avishek Paul,[†] Damian Connolly,[‡] Martin Schulz,[†] Mary T. Pryce,[†] and Johannes G. Vos*,[†]

[†]SRC for Solar Energy Conversion and [‡]Irish Separation Science Cluster, School of Chemical Sciences, Dublin City University, Dublin 9, Ireland

Supporting Information

This text redacted due to 3rd party copyright
This text redacted due to 3rd party copyright
This text redacted due to 3rd party copyright
This text redacted due to 3rd party copyright
This text redacted due to 3rd party copyright
This text redacted due to 3rd party copyright
This text redacted due to 3rd party copyright
This text redacted due to 3rd party copyright
This text redacted due to 3rd party copyright
This text redacted due to 3rd party copyright
This text redacted due to 3rd party copyright
This text redacted due to 3rd party copyright
This text redacted due to 3rd party copyright
This text redacted due to 3rd party copyright
This text redacted due to 3rd party copyright
This text redacted due to 3rd party copyright
This text redacted due to 3rd party copyright
This text redacted due to 3rd party copyright
This text redacted due to 3rd party copyright

[illegible]

[illegible]

Cite this: *Dalton Trans.*, 2011, **40**, 10812

www.rsc.org/dalton

COMMUNICATION

The effect of peripheral bipyridine ligands on the photocatalytic hydrogen production activity of Ru/Pd catalysts†

Gurmeet Singh Bindra,^a Martin Schulz,^a Avishek Paul,^a Suraj Soman,^a Robert Groarke,^a Jane Inglis,^a Mary T. Pryce,^a Wesley R. Browne,^b Sven Rau,^c Brian J. Maclean^d and Johannes G. Vos^{*a}

Received 29th June 2011, Accepted 23rd August 2011

DOI: 10.1039/c1dt11241d

This text redacted due to 3rd party copyright
This text redacted due to 3rd party copyright
This text redacted due to 3rd party copyright
This text redacted due to 3rd party copyright
This text redacted due to 3rd party copyright
This text redacted due to 3rd party copyright
This text redacted due to 3rd party copyright
This text redacted due to 3rd party copyright
This text redacted due to 3rd party copyright
This text redacted due to 3rd party copyright
This text redacted due to 3rd party copyright
This text redacted due to 3rd party copyright
This text redacted due to 3rd party copyright
This text redacted due to 3rd party copyright
This text redacted due to 3rd party copyright
This text redacted due to 3rd party copyright
This text redacted due to 3rd party copyright
This text redacted due to 3rd party copyright

[illegible]

[illegible]

[illegible]

[illegible]

[illegible]

[illegible]

[illegible]

[illegible]

[illegible]

[illegible]